

This thesis is the result of the author's original research. It has been composed by the author and has not been previously submitted for examination which has led to the award of a degree. The copyright of this thesis belongs to the author under the terms of the United Kingdom Copyright Acts as qualified by University of Strathclyde Regulation 3.50. Due acknowledgement must always be made of the use of any material contained in, or derived from, this thesis.'

Signed:

Date:

Acknowledgements

Firstly, I would like to thank my supervisors, Professor Paul Garside and Professor James Brewer, for their patience, support and guidance throughout my PhD. In particular I would like to thank Paul for encouraging me to remain focused and for all the time and effort he dedicated to the writing of this thesis.

I would also like to thank all members of Paul & Jim's lab group, past and present. The advice, support and technical expertise that they have offered me over the years have been invaluable and I have learned something from everyone. In particular, I would like to thank John Butcher for his help and advice with the molecular biology aspects of my project and all the physicists at the Centre for Biophotonics for their technical support with the microscopes and their back office banter!

Finally, I would like to thank my family for their support throughout my time at University.

Contents

Abstract	1
----------	---

Chapter 1

Introduction

1.1	Summary	3
1.2	Innate and Adaptive Immunity	4
1.3	T cells	4
1.4	The importance of T cell migration	6
1.5	Lymphocyte recirculation	7
1.6	Lymph node structure and organisation	8
1.7	Lymph node development	10
1.8	Dendritic cells	11
1.9	T cell activation	13
1.10	T cell differentiation	14
1.11	MPLSM of DC-T cell interactions in the lymph node	17
1.12	MPLSM studies of DC-T cell interactions in the tissue	21
1.13	Thesis objectives	23

Chapter 2

Materials and Methods

2.1	Materials and Methods	30
2.2	Animals	31
2.3	Antigens and Adjuvants	31
2.4	Cell culture	32
2.5	Cell labelling	33
2.6	Culture conditions for <i>in vitro</i> co-culture systems	33
2.7	Conjugation assay	34
2.8	<i>In vitro</i> imaging	34
2.9	Click-iT™ EdU Cell Proliferation Assay	34
2.10	Multiplex analysis of cytokines	35
2.11	Adoptive transfer of antigen specific lymphocytes	36
2.12	Lymph Node Transplant Model	37
2.13	Air pouch model	37
2.14	Histological evaluation	38
2.15	Haematoxylin and Eosin staining (H&E)	38
2.16	Delayed Type Hypersensitivity (DTH) Reaction	39
2.17	Flow cytometry	39

2.18	Immunohistochemistry (IHC)	40
2.19	Multi-photon laser scanning microscopy (MPLSM)	42
2.20	Statistics	42
2.21	FTY720 treatment	43
2.22	Anti-LFA-1 antibody (H68)	43
2.23	Fluorescent beads	43
2.24	Buffers	43
2.25	Transfection of HEK cells with Kaede	44
2.26	Cloning of Kaede	44
2.27	PCR primer design	45
2.28	PCR amplification of Kaede gene	45
2.29	Preparation of a 1% agarose gel	46
2.30	Sequencing of recombinant Topo Kaede constructs	47
2.31	Isolation of the PCR amplified products	47
2.32	Transformation of recombinant pET TOPO Kaede into BL21 Star One Shot Cells and Expression of Kaede	47
2.33	Transformation of recombinant pET TOPO Kaede into BL21 Star One Shot Cells and Expression of Kaede	47
2.34	Culture conditions for pilot expression	48
2.35	Sodium dodecyl sulfate-polyacrylamide gel electrophoresis (SDS-PAGE) and Western Blot	49
2.36	Purification of Kaede	50
2.37	Conjugating Kaede to beads	51
2.38	Photo-switching of Kaede by epi-fluorescence microscopy	51

Chapter 3

The effect of FTY720 and an LFA-1 blocking Ab on DC-T cell interactions *in vitro* and *in vivo*

3.1	Introduction	53
3.2	Results	57
3.3	The LFA-1 blocking Ab can bind to, and be detected on, the cell surface of T cells and DCs	57
3.4	Pre-treatment of DCs with FTY720 does not modulate their activation status	58
3.5	LFA-1 blocking antibody and FTY720 treatment fails to block DC-T cell clustering <i>in vitro</i> as assessed by flow cytometry	59
3.6	LFA-1 blocking antibody and FTY720 treatment reduces the number and duration of DC-T cell interactions <i>in vitro</i> when assessed dynamically	60
3.7	LFA-1 blocking antibody and FTY720 treatment significantly reduces DC capacity to stimulate T cell proliferation, <i>in vitro</i>	61
3.8	FTY720 treatment did not appear to affect DC-T cell interactions <i>in vivo</i>	64

3.9	An LFA-1 blocking Ab did not appear to modulate DC-T cell interactions <i>in vivo</i>	68
3.10	The effect of FTY720 and an LFA-1 blocking Ab on T cell differentiation and effector function <i>in vivo</i>	69
3.11	Discussion	73

Chapter 4

Developing and characterising a lymph node transplant model

4.1	Introduction	106
4.2	Results	109
4.3	A LN transplanted into the ear pinna can survive and is histologically normal	109
4.4	Age and type of LN transplanted can influence success rate of grafting procedure	110
4.5	Transplanting a neonatal LN under the ear pinna was not successful	110
4.6	The tLN maintains the cellular populations and organisation of a conventional LN	111
4.7	LN inducer cells of host mouse origin can be detected within the tLN	116
4.8	The tLN can participate in lymphocyte re-circulation with its new host in its location new anatomical	117
4.9	Adoptively transferred CFSE labelled lymphocytes can migrate into and be detected within the tLN	118
4.10	Antigen injected into the tip of the ear pinna can drain into and be detected within the tLN	118
4.11	The tLN can respond to immunisation at level comparable to a conventional LN	119
4.12	Lymphocytes migrate at a comparable speed in the transplanted and control LN	120
4.13	Discussion	122

Chapter 5

Developing an imageable tissue site of inflammation in the ear pinna

5.1	Introduction	145
5.2	Results	153
5.3	Histological analysis shows successful induction of the air pouch model in the rump but not the ear pinna	153
5.4	Granulocytes can be identified in the air pouch of the rump but not the ear pinna	154
5.5	Ear pinna thickness increases during a DTH reaction	155
5.6	Antigen specific T cells can be detected within the ear pinna	155
5.7	Macrophages and neutrophils are present in the DTH reaction in the ear pinna	157
5.8	Cytokine profile of the DTH reaction in the ear pinna	158
5.9	Antigen specific T cells can be imaged within the ear pinna during the DTH response	159
5.10	Antigen specific T cell can be imaged within the ear pinna in combination with fluorescent beads during the DTH response	161

5.11	Antigen specific T cells and DCs can be imaged within the ear pinna during the DTH response	162
5.12	HEK cells transfected with the Kaede expression vector express Kaede protein and can be photo-switched	163
5.13	Primers were designed to amplify the Kaede gene	164
5.14	Kaede gene was successfully cloned into pET-TOPO vector	165
5.15	BL21 Star TM were transformed with Kaede-pET-TOPO vector and expression of Kaede was induced using IPTG	165
5.16	Kaede protein was purified and quantified	166
5.17	Kaede protein was conjugated to beads and taken up by DCs <i>in vitro</i>	167
5.18	Kaede conjugated beads were taken up by DCs and visualised in the LN <i>in vivo</i>	168
5.19	Discussion	169

Chapter 6

6.1	Summary, Conclusions and Future Work	199
-----	--------------------------------------	-----

	References	206
--	------------	-----

List of tables and figures

Chapter 1

Figure 1.1	An illustration of LN architecture	26
Figure 1.2	An illustration of lymphocyte recirculation	27
Figure 1.3	Cell surface molecules and ligands involved in DC-T cell interactions	28

Chapter 2

Table 2.1	The sequence of solvents and stains used for Haematoxylin and Eosin staining	38
Table 2.2	Flow cytometry and IHC reagents	40
Table 2.3	Buffers	44
Table 2.4	Reaction cycles for the amplification of the Kaede gene	46
Table 2.5	Reaction components for the amplification of the Kaede gene	46

Chapter 3

Figure 3.1	LFA-1 blocking Ab can bind to, and be detected on, the cell surface of LFA-1 expressing DCs and T cells	80
Figure 3.2	FTY720 does not inhibit DC activation in response to LPS	81
Figure 3.3	FTY720 and an LFA-1 blocking Ab fail to block DC-T cell conjugates when investigated statically <i>in vitro</i>	82
Figure 3.4	Interactions between OVA pulsed DCs and DO11.10 T cells were imaged at 6 and 20 hours post co-culture following treatment with either FTY720 or an LFA-1 blocking Ab	83
Figure 3.5	FTY720 and an LFA-1 blocking Ab reduce the number of stable DC-T cell contacts at 20hours	84
Figure 3.6	Treatment of DCs with FTY720 or an LFA-1 blocking Ab significantly reduced antigen specific CD4 ⁺ T cell proliferation	85
Figure 3.7	FTY720 significantly inhibits the production of IL2 and IL12 from antigen stimulated DC-T cell co-cultures	86
Figure 3.8	LFA-1 blocking Ab significantly inhibits the antigen specific production of cytokines from DC-T cell co-cultures	87
Figure 3.9	Pre-treatment of T cells with FTY720 does not significantly affect DC-T cell interactions and T cell dynamics within the LN <i>in vivo</i>	88
Figure 3.10	Treatment with FTY720 ip does not significantly affect DC-T cell interactions and T cell dynamics within the LN <i>in vivo</i>	89
Figure 3.11	Pre-treatment of DCs with FTY720 does not significantly affect DC-T cell interactions and T cell dynamics within the LN <i>in vivo</i>	90
Figure 3.12	The effect of FTY720 treatment on antigen specific proliferation, the up-regulation of CD69 and down-regulation of CD62L	91
Figure 3.13	The effect of an LFA-1 blocking Ab on antigen specific T cell	

	proliferation and the up-regulation of CD69	92
Figure 3.14	Behaviour of DCs and DO11.10 T cells was imaged in the DLN following treatment with an LFA-1 blocking Ab	93
Figure 3.15	Treatment with FTY720 <i>in vivo</i> significantly increases the number CD4 ⁺ KJ ⁺ cells in the DLN but did not affect the differentiation of T follicular helper cells	94
Figure 3.16	Treatment with an LFA-1 blocking Ab <i>in vivo</i> reduced the number CD4 ⁺ KJ ⁺ cells in the DLN but did not affect the differentiation of T follicular helper cells	95
Figure 3.17	The effect of FTY720 treatment on the antigen specific production of Th1 cytokines	96
Figure 3.18	The effect of FTY720 treatment on the antigen specific production of Th2 cytokines	97
Figure 3.19	The effect of FTY720 treatment on the antigen specific production of pro-inflammatory chemokines	98
Figure 3.20	The effect of FTY720 treatment on the antigen specific production of growth and repair factors	99
Figure 3.21	The effect of an LFA-1 blocking Ab on the antigen specific production of Th1 cytokines	100
Figure 3.22	The effect of an LFA-1 blocking Ab on the antigen specific production of Th2 cytokines	101
Figure 3.23	The effect of an LFA-1 blocking Ab on the antigen specific production of pro-inflammatory	102
Figure 3.24	The effect of an LFA-1 blocking Ab on the antigen specific production of growth and repair factors	103
Table 3.1	Summary of cytokine production from <i>in vitro</i> antigen stimulated co-cultures	63
Table 3.2	Summary of cytokine/chemokine production from <i>ex vivo</i> re-stimulated LNs treated with FTY720 and an LFA-1 blocking Ab <i>in vivo</i>	72

Chapter 4

Figure 4.1	The tLN is histologically normal	127
Figure 4.2	Age of recipient and type of LN transplanted may impact success rate of engraftment procedure	128
Figure 4.3	Using neonatal LNs for the transplant procedure proved unsuccessful	129
Figure 4.4	T and B lymphocyte areas can be visualised within the tLN	130
Figure 4.5	CD11c expressing dendritic cells can be detected in the tLN	131
Figure 4.6	BP3 ⁺ stromal cells can be detected in the tLN	132
Figure 4.7	Gp38 ⁺ lymphatic endothelial cells can be detected in the tLN	133
Figure 4.8	The T cell attracting chemokine CCL21 can be detected within the tLN	134
Figure 4.9	Vascular cell adhesion molecule 1 (VCAM-1) can be detected in the tLN	135
Figure 4.10	A comparison of the populations of lymphocytes within the tLN to the populations in a control LN	136
Figure 4.11	LN inducer cells of host mouse origin can be detected within the tLN	137

Figure 4.12	Lymphocytes from the recipient mouse re-circulate into the tLN	138
Figure 4.13	Adoptively transferred CFSE labelled lymphocytes re-circulate into host LNs and the tLN	139
Figure 4.14	The tLN can drain antigen from its new anatomical location in the ear pinna	140
Figure 4.15	The tLN can respond to antigen challenge in a conventional manner	141
Figure 4.16	Multi-photon imaging of the tLN <i>in situ</i> reveals that lymphocytes migrate within the tLN at comparable velocities to lymphocytes within a control LN	143

Chapter 5

Figure 5.1	An air pouch lining can be created in the rump but not the ear pinna	179
Figure 5.2	Identification of cells infiltrating the air pouch of the rump	180
Figure 5.3	Identification of cells infiltrating the air pouch in the ear pinna	181
Figure 5.4	Measure of changes in ear thickness in response to the induction of a DTH reaction	182
Figure 5.5	Antigen specific T cells can be recovered from the ear pinna following the induction of a DTH reaction	183
Figure 5.6	Macrophages and neutrophils can be recovered from the ear pinna following the induction of a DTH reaction	184
Figure 5.7	The production of proinflammatory cytokines in the ear pinna following the induction of a DTH reaction	185
Figure 5.8	The production of chemokines in the ear pinna following the induction of a DTH reaction	186
Figure 5.9	The production of growth and repair factors in the ear pinna following the induction of a DTH reaction	187
Figure 5.10	Antigen specific T cells can be imaged in the ear pinna during the DTH reaction	188
Figure 5.11	Comparison of mean velocity, meandering index and displacement of T cells in a site of inflammation in the ear pinna and the DLN	189
Figure 5.12	Fluorescent beads injected with HAO are taken up by local APCs and can be imaged in the ear pinna	190
Figure 5.13	Antigen presenting DCs and antigen specific T cells interact in the ear pinna during the DTH reaction	191
Figure 5.14	HEK 293 cells were transfected with the Kaede expression vector	192
Figure 5.15	Primers were designed to amplify the Kaede gene from the mammalian expression vector into the pET-TOPO vector	193
Figure 5.16	Kaede gene was cloned into the pET-TOPO expression vector	194
Figure 5.17	BL21 Star <i>E.coli</i> were transfected with the Kaede-pET-TOPO expression vector	195
Figure 5.18	SDS-PAGE and Western Blot analysis of pilot expression of Kaede protein	196
Figure 5.19	DCs pulsed with Kaede beads were imaged <i>in vitro</i> and photo-converted using UV light	197
Figure 5.20	DCs pulsed with Kaede conjugated to beads were visualised	

	<i>in vivo</i> using MPLSM	198
Table 5.1	Summary of cytokines, chemokines and growth factors detected in split ear culture of DTH reaction	159

Abstract

The kinetics and dynamics of dendritic cell (DC)-T cell interactions in the lymph node (LN) are thought to be critical in initiating and regulating immune responses in both health and disease. DCs are localised in lymphoid and non-lymphoid tissues and effector and memory T cells continually migrate between both sites. However, the relationship and degree of interaction between the non-lymphoid site of tissue inflammation and the draining lymph node (DLN) remains relatively uncharacterised. This thesis aimed to develop novel *in vivo* model systems that would allow identifiable antigen specific T cells and DCs and their interactions in the tissue site of inflammation and DLN to be imaged and characterised using multi-photon laser scanning microscopy (MPLSM). This thesis describes the development of a novel model, in which a LN is transplanted into the murine ear pinna. Analysis of the structural organisation, cellular populations and functionality of the transplanted LN (tLN) revealed that the model provides a fully functional lymphoid organ, vascular and lymphatic supply in a convenient location for *in vivo* MPLSM. Moreover, this thesis describes the development of an imageable site of tissue inflammation in the ear pinna, that when combined with the tLN, should facilitate future studies of DC-T cell interactions in a non-lymphoid tissue site of inflammation and its DLN, by MPLSM. Thus, the systems developed in this thesis should allow some unanswered questions to be addressed, including whether T cells require to see antigen presented by DCs at the tissue site of inflammation or back in the DLN to initiate, maintain or regulate an immune response. A better understanding of the relationship between DC-T cell interactions at the tissue site of inflammation and the DLN, will hopefully provide novel therapeutic targets in circumstances of autoimmunity and inflammatory disease and facilitate improved targeting of current therapies.

Chapter 1

General Introduction

1.1 Summary

The mammalian immune system has evolved to provide defence against invading pathogens and cancer (1). A complex, yet integrated collection of molecules, cells and organs, encompass a dynamic system, consisting of both innate and adaptive components, which work in concert to provide a highly protective immune response capable of specifically recognising and eliminating almost any potential antigen it may encounter (2). The complex interactions that take place between antigen presenting dendritic cells (DCs) and CD4⁺ T cells in the secondary lymphoid organs are central to the adaptive immune system's ability to generate a protective immune response to foreign invaders and to maintain peripheral tolerance to self (2-8).

The introduction of the imaging technique, multi-photon laser scanning microscopy (MPLSM), has offered a wealth of knowledge as to how DCs and T cells interact in the lymph node (LN) *in vivo* and the frequency and duration of these interactions are thought to be critical in initiating and potentially regulating the course of an immune response (2, 4, 6, 8-14). However, while it is widely assumed that adaptive immune responses are initiated in the LN draining the site of tissue injury, this is not entirely clear as recent data has emerged to suggest a novel pathway of immune activation in the tissue, particularly in secondary immune responses (15-18). DCs are localised in lymphoid and non-lymphoid tissues and effector and memory T cells continually migrate between both sites (19-24). However, the relationship and degree of interaction between the tissue site of inflammation and the draining LN (DLN) during the course of an immune response remains poorly understood. Whether T cells interact with antigen presenting DCs at the tissue site of inflammation to initiate, maintain or regulate a response will have fundamental implications for the targeted treatment of chronic inflammatory diseases with pathology focused at tissue sites and for the generation of novel therapeutic targets. A lack of real time imaging of the tissue site of inflammation has slowed progress in this field and this thesis therefore aims to establish novel *in vivo* model systems that will allow DC-T cell interactions to be visualised and

characterised at and between the tissue site of inflammation and the DLN during the induction and maintenance of immune responses *in vivo* by MPLSM.

1.2 Innate and Adaptive Immunity

The mammalian immune response confers protection against invasive pathogens through a multi-layered system of non-specific (innate) and specific (adaptive) responses. The innate immune response is an evolutionarily ancient, highly conserved system that provides rapid, non-specific defence against infection, without the generation of immunological memory. The levels of innate defence include physical barriers, antimicrobial agents and inflammatory cells, such as neutrophils, macrophages and DCs (25). In contrast, the adaptive immune response, which is mediated by T and B lymphocytes, is characterised by its antigen specificity; diversity; self/non self recognition and immunological memory (26). Although slower to respond on primary encounter of an invading pathogen, the adaptive immune response generates immunological memory, which provides a more rapid and more effective response upon secondary infection (27). However, the innate and adaptive immune systems are not mutually exclusive, with many cells of the innate arm of the immune response acting to trigger and actively participate in the effector mechanisms of the adaptive response. For example, DCs that acquire antigen at the tissue site of inflammation in a non-specific manner and present it to antigen specific T cells, act as a bridge between the innate and adaptive arms of the immune response (24).

1.3 T cells

T lymphocytes are crucial for the development of almost all protective and pathological immune responses and as a result, have been described as the ‘conductors of the immunological orchestra’, due to their numerous roles in both regulating and actively participating in adaptive and cell mediated immune responses (28, 29). For T cells to carry out their functions effectively, they must respond specifically to foreign antigen in the form

of short peptides, which are presented in the context of self major histocompatibility complex (MHC) molecules on the surface of antigen presenting DCs (30, 31). T cells recognise and respond to antigen through the use of their highly diverse cell surface receptors, which are generated somatically by random gene rearrangement to provide each T cell with a structurally unique antigen receptor (32, 33). This process occurs during T cell development in the specialised microenvironment of the thymus, and can theoretically yield up to 10^{18} different specificities (34). However, due to the random nature of this process, auto-reactive specificities are often generated. Thus, to ensure that only T cells capable of recognising foreign peptides in the context of self MHC molecules are selected for survival, developing T cells expressing a newly rearranged TCR undergo a strict programme of positive and negative selection in the thymus (35, 36).

The TCR is a heterodimeric complex of integral membrane proteins and according to different forms of the TCR they express, T cells can be broadly characterised into two distinct lineages. The first of these is the gamma delta ($\gamma\delta$) T cell lineage, which represents only a small population of T cells and are the first to develop in the thymus (37). Secondly, the alpha beta ($\alpha\beta$) T cell lineage represents the majority T cells and can be further subdivided on the basis of cell surface expression of the co-receptors CD8 and CD4, which play key roles in T cell signalling and adhesion to the MHC molecule during peptide recognition (38). CD8⁺ and CD4⁺ T cells carry out distinct functions, CD8⁺ T cells recognise peptides in the context of MHC class I and offer protective immunity by killing pathogen infected or dysregulated host cells (39). In contrast, CD4⁺ T cells recognise peptides in the context of MHC class II and function as 'helper' cells by playing a central role in directing and actively participating in humoral and cell mediated immune responses. CD4⁺ T cells interact with B cells to facilitate their production of high affinity antibodies; induce macrophages to develop enhanced microbicidal and cell recruitment activity; support the generation of CD8⁺ T cell memory and produce cytokines and chemokines to enhance and direct immune responses (40-43).

1.4 The importance of T cell migration

LNs selectively localise and trap antigen and antigen presenting cells trafficked there via tissue draining afferent lymphatics and are thought to be the primary location in which DCs can introduce antigen to the adaptive immune system (44). Each specificity of antigen specific T cell is present at a low frequency (<1 per 100,000) and the immune system must ensure that rare lymphocytes, bearing the appropriate antigen receptor, are located in the right LN at the right time to encounter their requisite antigen and respond appropriately (45, 46). Lymphocyte recirculation helps overcome this issue by ensuring the continuous migration of naïve lymphocytes between the LNs, allowing them to scan the body for their cognate antigen in a process known as 'immune surveillance'. When T cells specifically recognise a pMHC complex in the context of co-stimulation (see below and figure 1.3), antigen recognition results in the clonal expansion and differentiation of antigen specific T cells. Following their activation in the LN, effector T cells migrate from the LN into sites of inflammation where they can mediate protective immunity (47). Moreover, memory T cells, which have been previously activated to clear an invading pathogen can also readily enter non-lymphoid sites and function to patrol the tissues in case of future attack (9, 48, 49). Thus, both effector and memory T cells have direct access to the tissues where tissue resident DCs or newly recruited monocyte derived DCs are present (50). However, while it is well established that both DCs and T cells can be found within inflamed and non inflamed tissues, the kinetics and dynamics of their interactions in non lymphoid tissue sites during a protective immune response or chronic inflammatory condition are poorly defined (18, 51-53). What is clear, is that cellular migration between the tissue site of inflammation and DLN is continuous. For example, an animal model of a chronic inflammatory disease with pathology focused at a non-lymphoid tissue site, can be transferred from one animal to another by transferring a suspension of CD4⁺ T cells isolated from the LN draining the site of pathology (54). This result serves to demonstrate the continual cellular communication between the LN and the local tissues. Moreover, immune responses already established at non-lymphoid tissue sites, can be significantly attenuated by blocking the exit of T cells from the LN using the immuno-modulatory agent, FTY720 (55-57). This high-affinity agonist of the sphingosine 1-phosphate receptor 1 is in phase III clinical trials in renal transplantation and has been shown to prolong graft survival by reducing CD4⁺ T cell infiltration into

transplanted organs and to inhibit disease progression in animal models of chronic inflammatory pathology (55-57). In conclusion, T cell migration is essential for the initiation of immune responses in the LN and for the targeted delivery of effector and memory T cells to the tissue site of inflammation or to a site of immune pathology. Moreover, cellular migration between the LN and the tissue site during an ongoing immune response appears to be continuous. However, to what extent T cells rely on this for their maintenance and regulation and what role DCs play in this either at the tissue site of inflammation or back in the DLN is not clear. Moreover, whether these events only occur in dysregulated, chronic inflammatory responses, is unknown.

1.5 Lymphocyte recirculation

Experiments in mice engineered to lack secondary lymphoid organs and the molecules regulating movement in and between them, have established their critical role in mammalian adaptive immunity and the dependence of almost every aspect of their function on cell migration (58-61). Mice deficient for IL-7R α or LT β R, critical receptors in the development of LNs (see below), display an absence of LNs and as a result an inability to generate protective immune responses (58, 59). Moreover, mice deficient in the chemokines or adhesion molecules required to mediate lymphocyte migration into the LN, such as CCL19/21 and ICAM-1/2 respectively, have a significant reduction in the number of lymphocytes within the LN and are compromised in their ability to initiate a protective immune response (60, 61). Furthermore, blocking the migration of activated effector T cells from the LN using the drug FTY720, which acts as an agonist of S1P₁ receptor, prevents their ability to mediate protective immunity (62). Consequently, defects in LN development and the ability of cells to migrate to and from them, result in severe immunodeficiency and serve to demonstrate the importance of migration for the initiation of protective immune responses in the LN and their delivery to inflamed tissue sites.

Classic experiments by Gowans and co-workers outlined the phenomenon of lymphocyte recirculation and its key role in the generation of a protective immune response. Their discovery followed a study in 1950 in which Mann and Higgins employed the use of a

technique, first described in 1948, for the collection of lymph and lymphocytes from the thoracic duct of un-anaesthetised rats (63). Their findings revealed that, although very large numbers of lymphocytes could initially be collected from a thoracic duct fistula, continuous drainage for several days resulted in a sharp decline in the output of cells (63). Moreover, if all the cells from the fistula were continuously reinfused into the blood, the output of lymphocytes would remain constant (64). As a result, Gowans questioned the fate of lymphocytes following their departure from the lymphatic circulation and began to re-examine the initial assumption that lymphocytes existed in a static system. Consequently, Gowans postulated that the recirculation of lymphocytes from the blood to the lymph was the most appropriate explanation, however, his proposals were first met with caution and his findings were not readily accepted until a collaboration with Knight on an elegant experiment in 1964. Their key contribution was to re-infuse lymphocytes labelled with tritiated compounds back into the blood, in an attempt to trace the elusive pathway of the 'disappearing' lymphocytes (65). Determining their location by autoradiography at various time points after intravenous infusion, the labelled cells behaved as predicted by migrating from the blood into the cortex of the LNs, while later reappearing in large numbers in the thoracic duct lymph. Thus, in 1964, the recirculation pathway was delineated and lymphocytes did not disappear, but instead continually reappeared in the lymph as they followed a circular route of migration in a highly dynamic process, crucial for the generation and dispersal of effector and memory lymphocyte populations (see figure 1.2) (65).

1.6 LN structure and organisation

LNs are highly evolved, structurally complex organs consisting of a variety of cell types, which together function as a surveillance system to collect and present antigens from local tissues in an appropriate manner to lymphocytes of the immune system. LNs are surrounded by a capsule and the complex micro-architecture and cellular populations of the LN are supported by a network of endothelial and stromal cells, see figure 1.1 for diagram (66-69). Immediately beneath the LN capsule is the subcapsular sinus, into which tissue draining afferent lymphatic vessels empty their content, delivering molecules, antigens and antigen presenting cells from the local tissue. A population of macrophages line the subcapsular

sinus and function to filter infiltrating debris (70-72). Broadly a LN can be divided into 2 principal regions of cellular activity, which are guided and maintained by a set of specific chemo-attractant factors, known as chemokines. The chemokine CXCL13 maintains the B cell follicular region on the outer edge of the LN. The follicles contains B220⁺ B cells and a network of stromal follicular dendritic cells (FDCs) (73-75). The chemokines CCL19 and CCL21 organise the inner T cell area, known as the paracortex, which contains CD4⁺ and CD8⁺ T cells and subsets of DCs anchored to a network of stromal fibroblastic reticular cells (FRCs). The efficient generation of an antigen specific immune response is directly dependent on the organisation and segregation of the T and B cell populations within the LN (76-78). The site-specific expression of homeostatic chemokines by distinct stromal cell populations also controls the movement of B and T cells within secondary lymphoid tissue (60, 79, 80).

The non-haematopoietic cell types of the LN can be divided into subsets on the basis of their location, function and phenotype. The stromal cell subsets that make up the parenchyma of LN, include FRCs and FDCs, while the endothelial subsets that supply blood and lymph flow through the LN, include vascular endothelial cells and lymphatic endothelial cells. Reticular networks have been observed in LNs for more than 100 years, however, the cellular components of these only began to be characterised in the 1960s (81-84). FRCs produce and surround collagen-rich reticular fibres, forming an enclosed conduit structure that is separate and distinct from the parenchyma of the lymphoid tissue. Small molecules, such as chemokines and antigens, can enter the conduit network in LNs from the tissue draining afferent lymph and are delivered rapidly to T cell zones and HEVs (67). Molecules of high molecular mass cannot enter the conduit lumen and instead are trapped by subcapsular sinus macrophages. This functional exclusion of large molecules and particles restricts and filters the types of signal delivered by the FRC conduits. LN resident DCs form a stable organised network by adhering to and extending their dendrites between FRCs in the T cell zone (85, 86). This allows the DCs to sample antigens, transported though the conduit system from tissue derived lymph, and present them to T cells (87, 88). FRCs, can be differentiated from other lymphoid stromal cells by their expression of the glyco-protein, podoplanin (also known as gp38) and can be readily identified by their production of the chemokines CCL19 and CCL21, which are crucial for maintaining the organisation of the T

cell zones (60, 89). FDCs were confusingly named after DCs on the basis of their morphology; however, these cells are non-haematopoietic in origin and form the principal stromal cell type of the B cell region. FDCs form a dense network and function to capture and present antigens to B cells (90, 91). Moreover, they are responsible for the production of the chemokine CXCL13, critical to maintaining the integrity of the B cell follicles (75, 92).

Vascular and lymphatic endothelial cells are the other non-haematopoietic cell types that are abundant in the LN. The vascular endothelial cells of the blood vessels that supply the LN are referred to as high endothelial venules (HEVs) and differ from conventional endothelial cells by their specific expression of several proteins, which increase their adhesive properties for recirculating lymphocytes, such as the vascular cell adhesion molecule (VCAM-1) and the chemokine CCL21 (93, 94). Lymphocytes enter the LN from the blood through these HEVs, which are often positioned in regions between T and B cell areas of the LN (83, 95). Similarly, lymphatic endothelial cells express various adhesion molecules and the chemokine CCL21, which are involved in cell entry into the lymphatics and function to drain antigen and cells from the local tissue as previously discussed (96). Altogether the distinct cellular organisation and stromal support network of a LN provide an environment critical for the development of adaptive immune responses and for the homeostatic maintenance of lymphocyte populations (97, 98).

1.7 LN development

LNs form sequentially in a complex process during the embryonic stages of development in the mouse. At day 10.5–11.5 of embryonic development, cells from the anterior cardinal vein start to bud and sprout, forming lymph endothelial cells under the guidance of the homeobox gene, *Prox-1* (99-102). The newly formed lymph endothelial cells then separate from the anterior cardinal vein and form a lymph sac at approximately day 11.5–12.5 of embryonic development. From the lymph sac, the LN and lymphatic vasculature develop, following independent pathways of development, guided by distinct transcription factors. LNs develop through recruitment and interaction of lymphoid tissue inducer (LTi) cells, from fetal liver progenitors, and mesenchymal organiser cells, which congregate in the LN

anlagen (103). The LT α cells express lymphotoxin $\alpha_1\beta_2$ (LT $\alpha_1\beta_2$), which allows them to specifically interact with the corresponding lymphotoxin β receptor (LT β R) of the mesenchymal organiser cells (101, 104). This key cellular interaction activates a signalling cascade resulting in the expression of adhesion molecules and homeostatic chemokines, such as the B and T cell chemo-attractants CXCL13 and CCL21 (104, 105). This stimulating microenvironment initiates a positive feedback loop, leading to further cell recruitment and clustering and to the development of characteristic lymphoid structures such as high endothelial venules (HEVs) (105). As a result, the LN acquires the cellular components and structural features characteristic of a developed LN and defects of the molecules involved in the recruitment and signalling cascades of these cells, such as the LT β R, lead to a failure in the development of peripheral LNs (58).

1.8 Dendritic cells

The activation of a protective and highly specific adaptive immune response, requires a system that can survey, decipher and quickly respond to insults, such as infection, in an appropriate manner (106). DCs participate in all of these important activities and are specialised in the uptake, processing and presentation of antigens to T cells. DCs continually sample their environment for antigens in peripheral tissues and periodically migrate from non lymphoid tissue sites to the LNs via tissue draining afferent lymphatics under the guidance of the chemokines CCL19/21, which bind to and stimulate their migration through the CCR7 receptor (107, 108). Once in the LN, DCs can present tissue acquired antigens in the form of pMHC complexes to re-circulating T cells (109). The maturation status of the DC is thought to be influential in determining the outcome of antigen encounter by a T cell on the surface of a DC in the LN (110). DCs express germline encoded, pattern recognition receptors that are capable of recognising and sensing highly conserved molecular patterns of infectious agents, such as molecules important in microbial survival known as 'danger signals' in the tissue (25). For example, a family of transmembrane proteins, known as the Toll like receptors bind directly to ligands such as lipopolysaccharide (LPS) of gram negative bacteria and double stranded DNA of viruses (111-113). Stimulation of these receptors triggers intracellular signaling and gene transcription through the NF-KB pathway, which

results in the maturation of the DC. Mature DCs downregulate endocytosis and stop sampling their environment for antigens (114). They transiently increase their synthesis and transport of MHC class II molecules and increase their efficiency of antigen processing, which gives rise to the rapid accumulation of a high number of pMHC II complexes at the cell surface (109, 114, 115). Moreover, their expression of co-stimulatory molecules (see below) is enhanced and their production of cytokines, such as IL12 is upregulated (24, 109). Consequently, mature DCs are highly efficient at stimulating and activating T cells in the LN. In contrast, antigen presentation by immature DCs, which have not encountered a 'danger signal' in the tissue and have therefore not undergone the maturation process, do not have the capacity to effectively prime T cell responses. Instead, antigen presentation by immature DCs has been implicated in the induction of T cell tolerance, either by inducing T cell unresponsiveness/'anergy' or the induction of regulatory type T cells. However, DCs stimulated by a 'danger signal' up-regulate the co-stimulatory molecules required for effective T cell activation such as CD40 and CD80/86 (see figure 1.3), and can therefore induce the activation and differentiation of antigen specific T cells. Thus, through their ability to present antigen in a variety of contexts, DCs can induce the clonal expansion and differentiation of CD4⁺ T cells or their clonal anergy and are therefore key initiators and crucial regulators of the adaptive immune response (22, 116, 117).

The key role of DCs in the initiation of immune responses, was conclusively demonstrated using the diphtheria toxin experimental system, in which the expression of the diphtheria toxin receptor (DTR) in mouse DCs was induced under the control of the CD11c promoter (118, 119). This system allowed the specific depletion of DCs *in vivo*, by injection of diphtheria toxin, which would bind to and kill DTR expressing CD11c⁺ DCs. This model was first used to link DCs to the priming of immunity to *Listeria monocytogenes* and liver-stage *Plasmodium yoelii* and showed that in their absence, protective immune responses were not efficiently generated (119). Subsequent studies extended this approach to emphasise the role of DCs in the initiation of immunity and the generation of secondary immune responses (120-127).

DCs were first observed in skin sections in the late 1800s, and were initially mistaken for cells of neurological activity and not fully characterised until the 1970s (116). Since their

discovery, DCs have emerged as a complex group, consisting of a number of unique subsets, with distinct and overlapping functionalities (23, 128). Broadly DCs can be categorised into four major subgroups, the plasmacytoid DCs (pDCs), the monocyte-derived inflammatory DCs, the CD11b⁺ DCs and the CD11b⁻ DCs. Several DCs fall into the CD11b⁺ DC group, including the CD4⁺ and CD4⁻CD8⁻ lymphoid tissue resident DCs; skin resident CD11b⁺ and Langerhans DCs; and CD11b⁺CD103⁺ DCs of the gut. The CD11b⁻ DC group includes lymphoid resident CD8 α ⁺ DCs and the CD103⁺ langerin-positive DCs of the skin, lungs and other tissues. Broadly, these four subgroups can be characterised on the basis of function, with pDCs being associated with the production of type I interferon, anti-viral responses and the balance between tolerance and immunity (129-131). Monocyte derived inflammatory DCs are thought to play an important role in the control of events in inflamed non lymphoid tissues, including antigen presentation and the initiation of local secondary responses (18). Finally, CD11b⁺ DCs stimulate CD4⁺ T cell responses while CD11b⁻ DCs cross present antigens to and prime cytotoxic CD8⁺ T cells (132-134).

1.9 T cell activation

T cell activation requires two signals generated from the DC, the first of which is specific recognition of pMHC complex by the TCR (signal 1), and the second is co-stimulation provided by cell surface molecules expressed on the activated DC (signal 2). The T cell receptor (TCR) complex has 6 transmembrane protein subunits, including the $\alpha\beta$ heterodimer of the TCR and the ϵ δ ζ γ chains of the associated CD3 molecule (33, 135). The $\alpha\beta$ subunit is responsible for the specific recognition of the pMHCII complex while the CD3 molecule is responsible for the transmission of the signal into the cell via specialised tyrosine phosphorylation motifs, known as ITAMs (Immunoreceptor Tyrosine-based Activation Motifs) on the intracellular portion of the ϵ δ ζ γ chains (135). Upon specific engagement of the TCR by a pMHCII complex presented on the surface of a DC, the Src family kinase Lck becomes activated and proceeds to phosphorylate the ITAMs on the ϵ δ ζ γ subunits of the TCR (136). Phosphorylated ITAMs promote the recruitment and subsequent activation of another tyrosine kinase, ZAP-70, which phosphorylates and activates numerous downstream signalling pathways which contribute to the activation of

transcription factors, calcium mobilisation and cytoskeletal reorganisation and ultimately result in cellular proliferation, differentiation, cytokine production (3). However, T cell activation is regulated by various co-stimulatory receptors expressed on the surface of activated DCs and signaling through the TCR alone results in a non-responsive state (anergy) in which T cells are refractory to re-stimulation (137, 138). Engagement of such co-stimulatory molecules augments intracellular signaling pathways initiated by TCR stimulation and triggers distinct signaling pathways critical, critical to ensuring T cell activation, proliferation and differentiation (see figure 1.3) (3). CD28, which engages CD80/86 on activated DCs, is considered to be the most important co-stimulatory receptor expressed on naïve T cells and its stimulation provides essential signals that enhance the production of the proliferation and survival cytokine, IL-2 and prevents the induction of anergy and cell death (25, 139-141). In addition, stimulation of CD28 promotes expression of several other co-stimulatory molecules including OX40 and ICOS which play an important role in memory T cell formation and in the regulation of T cell dependant antibody responses in the germinal center reaction, respectively (142). Co-stimulatory molecule expressed on T cells, such as CD40L, can stimulate and enhance DCs in their ability to fully stimulate T cell activation. Following TCR stimulation, T cells upregulate CD40L which stimulates signaling through CD40 on the surface of DCs and leads to their enhanced expression of MHC molecules, CD80/CD86 and to their production of cytokines, such as IL12, all of which contribute to the induction of T cell proliferation and cytokine production (143). Thus, T cell signaling and activation by DCs is a two-step process that requires the recognition of a specific pMHCII complex and reciprocal signaling via co-stimulatory molecules, which ensure the full functional activation of the T cell.

1.10 T cell differentiation

Following engagement of the TCR by the appropriate pMHCII complex, CD4⁺ T cells proliferate and differentiate into a wide variety of effector subtypes, characterised on the basis of cytokine secretion (144). CD4⁺ T cells can differentiate into at least two functional classes of cell during an immune response: Th1 cells, which secrete IFN γ and Th2 cells which secrete IL-4 (145, 146). Th1 cells mediate immune responses against intracellular

pathogens and in humans play a particularly important role in resistance to mycobacterial infections. In contrast, Th2 cells mediate host defense against extracellular parasites including helminths. However, both subsets have been implicated in pathological responses, such as autoimmunity and allergy, respectively (147). A number of models have been proposed to explain how naïve T cells differentiate and many factors are thought to influence the generation of the Th1 and Th2 subsets (148, 149). The T-box transcription factor (T-bet) has been identified as the master regulator of Th1 differentiation (150). STAT1 is the major transducer of IFN γ signalling and plays a critical role in the IFN γ mediated induction of T-bet expression (151). Moreover, STAT4, which is stimulated by IL-12, plays a key role in amplifying the Th1 response (152). In contrast, Th2 development is mediated through the transcription factor STAT6, which is activated by IL-4 and acts to stimulate the expression of the Th2 master regulator gene, GATA-3 (153, 154).

IL-17 producing CD4⁺ T cells (Th17 cells) have been identified as a unique subset of T helper cells that develops along a pathway that is distinct from Th1/Th2 differentiation. The mechanism of Th-17 development has been shown to be dependent on the cytokine, IL-23 and to be independent of STAT-1, 4, 6 and T-bet (155, 156). The hallmark effector cytokines of Th1 and Th2 cells, IFN γ and IL-4, have both been shown to negatively regulate the generation of Th17 cells (155, 156). This third subset of effector T cells has been implicated in the promotion of immune mediated tissue damage and inflammatory conditions such as the autoimmune disease, multiple sclerosis (157-159). Thus, while naïve CD4⁺ T cells are distinct in their antigen recognition specificity, they have substantial plasticity for development of a variety of effector phenotypes.

A key role of activated CD4⁺ T cells is their ability to migrate towards B cell follicles and provide cognate help to antigen-specific B cells to promote their production of high-affinity class switched antibodies and their differentiation into memory B cells, thereby ensuring long-term humoral immunity (160-162). Germinal centers are specialized structures that develop within B cell follicles and are the principle site for processes such as somatic hypermutation, class switch recombination, and selection of high-affinity B cells (163). Initially it was presumed that only Th2 cells migrated into B cell follicles to participate in the germinal centre reaction, however, Th1 cells were also shown to migrate and provide 'T cell

help' (164). More recently, the roles of follicular migration and the delivery of B cell help have been assigned to a novel distinct subset of CD4⁺ T cells, known as the T follicular helper cells (Tfh). The differentiation pathway of Tfh cells has been shown to be distinct from the Th1/2/17 pathways, being regulated by ICOS ligand (ICOSL) expressed on B cells and dependent on the cytokines IL-21, IL-6 and the transcription factor STAT3 (165). These cells are characterized by their expression of CXCR5, which enables their homing to B cell follicles, and their expression of IL-21, which directly regulates B cell proliferation and class switching as demonstrated by IL-21R deficient mice which display defective antibody responses and impaired germinal-center formation (165-167).

An additional subset of CD4⁺ T cells, are the regulatory T cells, which make up a diverse group of cells which function to actively suppress self reactive T cells to maintain immunological self tolerance (168). Naturally arising CD25⁺CD4⁺ regulatory T cells develop in the thymus and represent approximately 10% of CD4⁺ T cells. These cells are characterised by their expression of a high affinity TCR specific for self antigens and their expression of the transcription factor Foxp3. CD25⁺CD4⁺ regulatory T cells have been reported to mediate their suppressive effects via a cell contact dependent mechanism, such as CTLA-4, which binds directly to CD80/86 on DCs to prevents their co-stimulation and activation of auto-reactive T cells and by the release of suppressive cytokines, such as IL10 and TGFβ (169, 170). Deficiency in, or dysfunction of, this cell type results in the development of multi-organ autoimmune disease, which serves to underlie their importance in maintaining a state of self tolerance (171). In addition to naturally arising CD25⁺CD4⁺ regulatory T cells which develop in the thymus, a subpopulation of CD4⁺ T cells has been shown to develop a regulatory phenotype in the periphery following stimulation with antigen presenting immature or tolerogenic DCs and/or exposure to the anti-inflammatory cytokine IL-10 (172, 173). This induces the differentiation of a unique subset of T cells, known as Tr1 cells, which secrete IL10 and TGFβ and display immunoregulatory properties (174).

1.11 MPLSM of DC-T cell interactions in the LN

The nature of the dynamic interactions that take place between CD4⁺ T cells and DCs in the LN are critical in initiating, maintaining and regulating immune responses. The duration, stability, and number of DC-T cell contacts required to achieve full T cell activation are factors of key importance when attempting to understand how immune responses are generated and how to manipulate them for the development of vaccines and novel therapeutics. Historically, the study of antigen specific T cells *in vivo* has been associated with considerable technical difficulty due to the low frequency (<1 per 100,000) of each specificity, which is below the limits of detection using techniques such as, flow cytometry and immunohistochemistry (175). However, the advent of the adoptive transfer model, in which the size of the antigen specific population can be artificially increased by transferring TCR-transgenic T cells into a syngenic non-transgenic recipient, overcame these technical difficulties. The system therefore provides a population of T cells, specific for a model antigen, large enough (0.2–1%) to be detected *in vitro* or *in vivo* using an anti-TCR monoclonal antibody, MHC-II tetramer or fluorescent labeling prior to transfer (176, 177).

The bulk of experimental data as to how DCs and T cell interact, was initially derived from *in vitro* model systems (175). Observations using cell culture systems allowed antigen specific T cells to be easily manipulated, monitored and assessed by assays of function, such as cytokine secretion and proliferation, following their *in vitro* co-culture with antigen loaded DCs. In addition, *in situ* analysis using cell transfer models and imaging techniques provided a wealth of molecular detail as to how DCs and T cells interact (5, 178). Initially, *in vitro* experimentation suggested that the formation of a stable point of cell-cell contact, with an antigen presenting DC, was essential to ensure T cell activation (179-183). This specialised and highly organised junction between the cells was referred to as the immunological synapse, and was shown to consist of two distinct regions. A central region, of 1-3 μm diameter, was termed the central supramolecular activation cluster (c-SMAC) and was shown to contain the TCR and the co-stimulatory molecule, CD28. This structure was surrounded by a peripheral (p-SMAC) region of adhesion molecules, including LFA-1 and the cytoskeletal molecule talin (see figure 1.4) (183, 184). *In vitro* studies, in which lipid bilayers containing pMHC complexes and ICAM-1 were used to model antigen presenting cells, outlined the key role of the adhesion molecule LFA-1 on the surface of T cells in mediating

the formation of the synapse. Moreover, these studies revealed that the synapse was formed initially by a central zone of LFA-1 with a peripheral ring of TCRs at the contact site with the DC, but within minutes this distribution was reversed (183, 184). Initially, it was assumed that this reorganisation of cell surface molecules and formation of the immunological synapse, which can remain stable for more than 1 hour, was essential to ensure TCR triggering and T cell activation (179). Observations of fixed LN tissue sections and of conjugate DC-T cell clusters isolated from dissociated LNs also supported this view (185-188). However, in contrast, three-dimensional collagen-matrix videomicroscopy found that DC-T cell interactions were relatively brief and that serial and short-lived contacts with DCs were sufficient to activate CD4⁺ T cells (189). Moreover, it was observed that TCR-mediated signalling through the tyrosine kinases, Lck and ZAP-70, can precede the formation of a mature immunological synapse (190). Thus, *in vitro* and *in vivo* analysis of DC-T cell interactions suggested that the formation of a stable and organised point of cell-cell contact was a necessary prerequisite to T cell activation, however, not all studies supported this theory and some proposed the immunological synapse to be more important in functions such as polarised secretion, endocytosis and recycling of various receptors, such as the TCR (191).

More recently, the development of multi-photon imaging technology has enabled DC-T cell interactions to be visualised and tracked in real time in intact explanted LNs or in surgically exposed LNs in live anaesthetised mice (192, 193). Such observations had previously been limited to *in vitro* and *in situ* systems, which were either non-physiological or representative of only a single snapshot in time. In contrast, MPLSM allows DCs and T cells to be imaged in a four-dimensional, spatiotemporal manner in the complex and physiological environment of organised lymphoid tissue and therefore provides a more representative view of how these cells interact *in vivo*. The concept of MPLSM is based upon the absorption of two or more photons of low energy, which synchronously excite a fluorophore in a quantum event, resulting in the emission of a fluorescence signal within the visible spectrum (194). The technique was introduced in live cell imaging of the LN as an alternative to single photon confocal microscopy due to its superior qualities of depth penetration, reduced photodamage and lack of out-of-focus bleaching (195).

During MPLSM of the LN, typically a volume of approximately $200 \times 200 \times 50 \mu\text{m}$ is imaged every 10–30 s for 30 to 120 minutes. The data generated is analysed using specialised software, such as Volocity, to extract parameters including cell velocity, trajectories and cell contact duration. The majority of imaging experiments carried out to date have employed *ex vivo* or endogenously labeled TCR transgenic T cells to control the specificity of the T cells being imaged. DCs have been visualised either directly *in vivo* using transgenic mice expressing the yellow fluorescent protein under the control of the CD11c promoter or following the transfer of *ex vivo* labeled bone marrow derived DCs (196). This experimental setup has been the favoured approach to dissect the features of DC-T cell interactions during the initiation of adaptive immune responses in the LN, with a few variations regarding the type of T cells (CD4^+ versus CD8^+ T cells, TCR specificity) and antigen used (type, mode of delivery, and dose), and the subset of DCs visualised (endogenously labeled DCs versus transferred bone marrow derived DCs). Nonetheless, common themes have emerged from the results of these studies and the introduction of MPLSM has offered much insight into how DCs and T cells interact during the initiation of an immune response within the LN.

T cell behaviour within the LN during the initiation of an adaptive immune response is thought to progress through distinct stages. Initially, naïve T cells display robust motility and migrate through the LN with an average velocity of approximately $11\mu\text{m}/\text{min}$, in a manner that has been described as a ‘random walk’, due to a lack of directional migration (193, 197, 198). During this phase, highly motile T cells have been shown to scan multiple DCs for their cognate antigen, making only short-lived interactions, which dominate this early stage of the activation process (6, 8, 14, 189). Prolonged interactions between antigen bearing DCs and antigen specific T cells are seen after 6-12 hours but are not thought to involve the formation of the stable synapse observed *in vitro*, as extensive changes in DC shape and T-cell crawling on the DC surface are characteristic features of long-lived DC-T cell conjugates *in vivo* (6, 8, 14, 199). After approximately 24 hours, T cells begin to dissociate from stable clusters and adopt a ‘swarming’ behavior. During this time T cells begin to proliferate and differentiate into activated effector cells, which migrate from the LN to the tissue site of inflammation to resolve any ongoing infection (200). Following re-exposure to antigen, imaging studies have revealed that primed T cells display inherently slower migration and

increase the intensity of their interactions with DCs in the LN and while it was initially assumed that primed T cells have a reduced requirement for co-stimulation, recent studies have shown that CD28 stimulation is critical for secondary T cell responses (201-205).

Multi-photon studies have revealed that the number and duration of DC-T cell interactions in the LN, can shape the outcome of the T-cell response. In particular, the transition from a phase of transient interactions to a phase of long-lasting contact, has been shown to be of critical importance in determining the outcome of T cell priming. Moreover, it is thought that this decision is made during the initial phase of transient contacts, during which time changes occur at the level of the DC or the T cell, which account for the modification of DC-T cell dynamics to more stable and prolonged contacts (11, 206). Direct *in vivo* assessment using MPLSM has confirmed the importance of prolonged DC-T cell interactions for efficient T cell activation and proliferation by introducing agents that block the presentation of antigen to T cells, such as an MHCII blocking antibody and interrupting the formation of long lived DC-T cell clusters (4). Moreover, when OVA peptide antigen was administered in the absence of an adjuvant, a format that favours the induction of tolerance, DC-T cell interactions remained brief and transient and failed to progress to the long lived stable contacts observed when OVA peptide antigen was administered in combination with an adjuvant (8). Consistent with these findings long lived clusters failed to form in models of oral tolerance in mesenteric LNs of the gut (207). Thus, stable DC-T cell interactions are thought to be critical for the induction of T cell priming, while brief contacts which fail to progress to stable more prolonged interactions are associated with the induction of T cell tolerance. In addition, regulatory T cells have been shown to dampen T cell responses by reducing the stability of DC-T cell contacts and when T cells are negatively regulated in the LN through stimulation of CTLA-4, their motility is increased, reducing their ability to form stable contacts and decreasing their cytokine production and proliferation (12, 13, 208). Thus, by modulating the ability of T cells to form stable interactions with DCs, the threshold for T cell activation is increased and can provide an effective method for regulating T cell activation and controlling aberrant immune responses.

1.12 MPLSM studies of DC-T cell interactions in the tissue

Studies employing MPLSM have revealed DC-T cell interactions in the LN to be highly dynamic and variation in the reciprocal communication taking place between these interacting cell types can give rise to very different outcomes, such as priming versus tolerance (209). Thus, the nature of the dynamic interactions taking place between CD4⁺ T cells and DCs in the relevant LN draining a site of pathology, inflammation or vaccination, are likely to be critical in initiating, maintaining and regulating immune responses. However, effector T cells carry out their functions in inflamed non-lymphoid tissues and it is therefore critical that imaging studies of secondary immune responses progress to characterising the dynamics of effector T cells at the tissue site of inflammation, as well as in the LN. Thus far, few attempts have been made to visualise effector T cells and their interactions within non-lymphoid tissue sites of inflammation due to the technical difficulties associated with such experiments. However, CD8⁺ cytotoxic T cells have been imaged using MPLSM infiltrating solid tumours and brain tissue in mouse models of cancer and experimental autoimmune encephalomyelitis, respectively. These studies have focused on tracking CD8⁺ cytotoxic T cell interacting with and killing target cells in the inflamed tissue site (210-214). A more recent imaging study of the brain of mice chronically infected with *Toxoplasma gondii*, revealed that antigen specific CD8⁺ T cells were recruited to the infected brain tissue and persisted there in the presence of ongoing antigen recognition, forming transient interactions with CD11b⁺ antigen presenting cells (215). In addition, CD4⁺ effector memory T cells have been imaged migrating within the ear pinna during a delayed type hypersensitivity (DTH) response and their behaviour characterised in the presence and absence of a calcium channel blocking molecule (211, 212). CD4⁺ effector memory T cells stably attached to and interacted with antigen presenting cells during the DTH reaction and blocking calcium signalling could inhibit the migration of these cells through the tissue, suggesting a requirement for continued stimulation of activated effector T cells during an inflammatory response in non-lymphoid tissues and a potential therapeutic target for the treatment of chronic inflammatory disease (211, 212). These studies have provided key insights into effector T cell dynamics at the tissue site of inflammation, however, in comparison to imaging studies of naïve T cell migration and DC-T cell interactions in the LN, progress to characterise effector T cells and their interactions with DCs in non-lymphoid tissues has been slow.

More recently, the role of DCs in stimulating T cells within local sites of inflammation have been examined (18, 216-218). CD11b⁺ DCs were shown to stimulate inflammatory cytokine production by both regulatory and effector memory T cells in inflamed skin, although the exact origin of these cells was left undefined (18, 120, 216, 219). In addition, DCs have been linked to local T cell stimulation during influenza infection, in which they appeared to promote T cell proliferation and survival directly in the lung (217, 218). McGill *et al.* used clodronate-based DC ablation to demonstrate that the DCs involved in local stimulation were a population recruited by the infection. However, they were able to exclude the involvement of CD103⁺ tissue resident alveolar DCs, as they were unable to restore T cell proliferation when directly re-introduced into the lung following the DC ablation (217). Monocyte-derived DCs have also been shown to promote expansion of memory T cells in response to Herpes Simplex Virus-1 reactivation in sensory ganglia (18). Thus, memory T cells can interact with and be activated directly in the tissues by monocyte derived DCs (18).

The aforementioned studies of DC-T cell interactions in non lymphoid tissue sites have involved the use and characterisation of previously activated effector memory T cells, with almost no studies examining the behaviour of newly activated effector T cells at the tissue site of inflammation during a primary immune response. Moreover, while it is widely assumed that immune responses are initiated in the LN, recent studies have suggested a novel pathway of immune activation in non lymphoid tissues, involving skin resident $\gamma\delta$ TCR expressing epidermal T cells. These tissue associated T cells, which are situated in the basal dermis forming a network with keratinocytes and local Langerhans DCs, respond to ligands upregulated on the surface of stressed, transformed or virus infected keratinocytes, such as NKG2D. Transgenic mice were generated in which an NKG2D-ligand, Rae-1, could only be upregulated on keratinocytes and within 72 hours, tissue resident T cells had become activated and appeared to appose Langerhans DCs (17). Given that Langerhans DCs do not express NKG2D, their results implied a novel flow of information, in which stressed, transformed or infected epithelial cells directly activate local T cells which in turn activate tissue resident DCs (17). Moreover, recent studies have strongly implicated this NKG2D-ligand interaction pathway in transplant graft rejection and in the generation of antigen specific antibodies to epicutaneous OVA that was greater in mice in which Rae-1 was acutely upregulated during antigen administration (15, 16). Thus, many outstanding questions

remain, in particular, whether effector T cells proliferate in non-lymphoid tissues in response to re-encounter with antigen loaded DCs or whether they simply carry out effector functions such as cytokine production is contentious. Furthermore, whether newly activated effector T cells are maintained at the tissue site of inflammation or are required to migrate back to the DLN is unclear. A more detailed knowledge of the dynamic migration and cellular interactions of effector T cells will have important consequences for the development and improved targeting of immuno-therapeutics.

1.13 Thesis Objectives

As highlighted above, the kinetics and dynamics of DC-T cell interactions are thought to be critical in initiating, maintaining and regulating immune responses in both health and disease (7, 9). However, the relationship and degree of interaction between the DLN and tissue site of inflammation remains relatively uncharacterised. Whether T cells require to see antigen presented by DCs at the tissue site of inflammation to initiate or maintain a response is thought to have fundamental implications for the targeted treatment of autoimmune disease, such as rheumatoid arthritis. This thesis aims to develop novel *in vivo* model systems that will allow identifiable antigen specific T cells and DCs and their interactions in the tissue site of inflammation and DLN to be imaged and characterised using MPLSM. A better understanding of the relationship between DC-T cell interactions in the tissue site of inflammation and DLN, will hopefully provide novel therapeutic targets in circumstances of autoimmunity and inflammatory disease and facilitate improved targeting of current therapies.

The objectives of this thesis are therefore to:

- 1. To create an *in vitro* model system in which the effects of modulating DC-T cell interactions can be assessed and characterised**

To establish *in vitro* model systems in which DC-T cell interactions and the effects of modulating these interactions can be assessed and characterised. First assessing these

interactions *in vitro* should allow the establishment of the parameters to test in the study of DC-T cell interactions *in vivo*. Moreover, developing methods to block or modulate DC-T cell interactions *in vitro*, could provide a useful tool to assess and analyse the relative requirement for these cellular interactions at both the tissue site of inflammation and the DLN in future studies *in vivo*. As proof of principle, the immunosuppressive drug FTY720, which blocks T cell egress from the LN and the integrin blocking LFA-1 binding antibody (Ab) were employed to target distinct aspects of T cell function, namely adhesion and migration, in an attempt to modulate DC-T cell interactions.

2. To establish and characterise a LN transplant model in the murine ear pinna

To establish and characterise a novel LN transplantation model, in which the inguinal LN is transplanted into the ear pinna of the mouse. This model will provide a lymphoid organ, vascular and lymphatic supply in a convenient location for *in vivo* MPLSM without the need for surgical procedures to expose a native LN.

3. To establish and characterise an imageable site of tissue inflammation in the murine ear pinna

To establish and characterise the air pouch model in the ear pinna, in which specific and non specific inflammation can be induced, allowing DC-T cell interactions to be imaged in the a tissue site of inflammation by MPLSM.

4. To create an *in vivo* model system that provides a tissue site of inflammation and DLN within close proximity to allow DC-T cell interactions to be imaged at and between both sites

The aims of this thesis were to combine the LN transplant model with the model of tissue inflammation in the ear pinna to provide a novel system in which both site are located in a convenient location for *in vivo* imaging of DC-T cell interactions at and between both sites. The LN and tissue site have never been assessed in parallel and by creating a LN and tissue

site of inflammation in the ear pinna, it should be possible to contrast and compare DC-T cell interactions between each site and to determine whether they differ in aberrant immune responses.

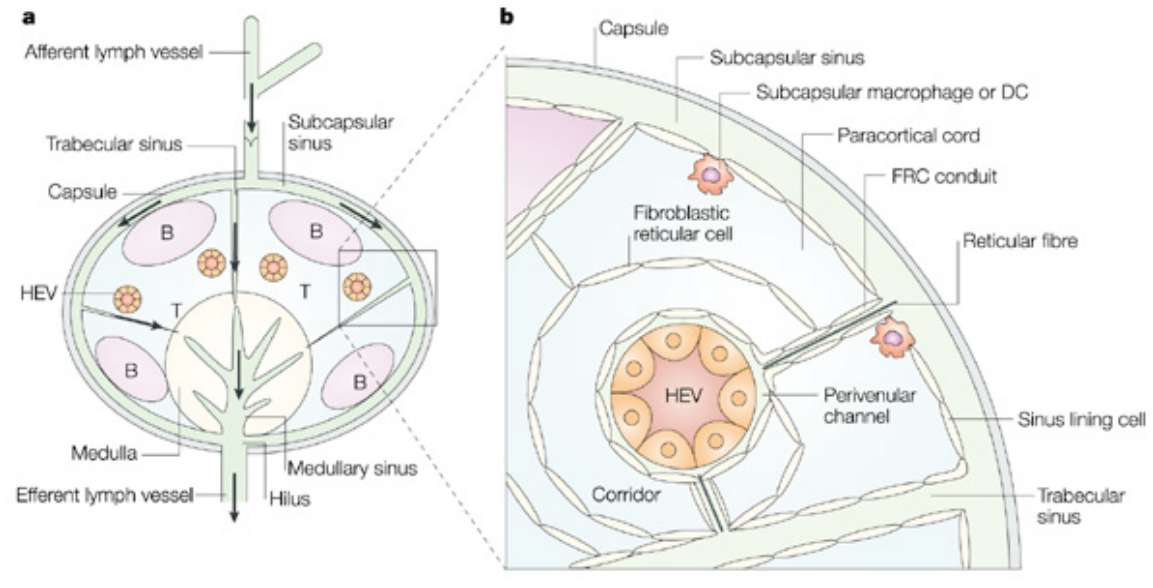


Figure 1.1 An illustration of LN architecture (A) The schematic diagram shows the major structural components of a LN. Afferent lymphatic vessels drain the local tissue and supply the LN with antigen and antigen presenting cells. Arrows indicate the main routes of lymph flow into and within the LN. Blunt ending afferent lymph vessels collect and channel interstitial fluid into the subcapsular sinus. From here, the lymph is drained towards the medulla through fibroblastic reticular cell (FRC) conduits that connect to the medullary sinus. (B) Schematic depiction of a paracortical cord/area of the LN. The T cell area can be seen in light blue and is shown adjacent to a B-cell follicle in pink. The B and T cell areas of the LN are guided and maintained by specific chemokines, CXCL13 and CCL19/21, respectively. Fibroblastic reticular cells and conduit forming collagen and laminin fibres penetrate the paracortex and provide essential structural support to the LN. At the centre of each paracortical area is a high endothelial venule (HEV) through which, recirculating lymphocytes enter the LN from the vascular supply. Image adapted from (44)

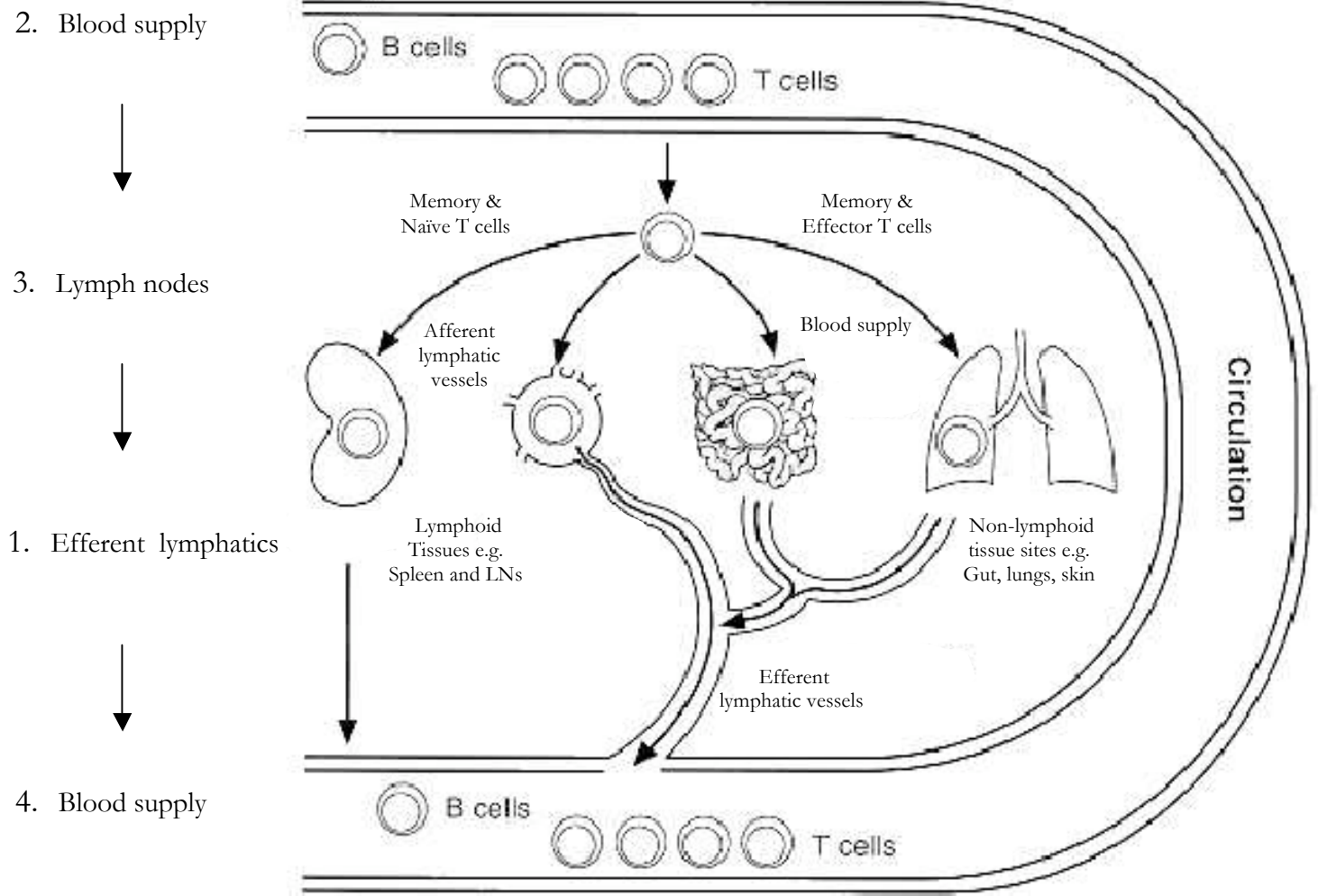


Figure 1.2 An illustration of lymphocyte recirculation. Intrinsically mobile naïve, effector and memory T cells follow a circular path of migration, traveling from the blood into the LNs and back to the blood via efferent lymphatic vessels and the thoracic duct (65). Memory and effector lymphocytes can migrate from the circulation into non-lymphoid tissue sites where they perform a surveillance function or mediate protective immunity (19, 220). To exit the tissue, memory and effector T cells drain to local LNs via afferent lymphatic vessels and re-enter the circulation via the efferent lymphatics and thoracic duct (221).

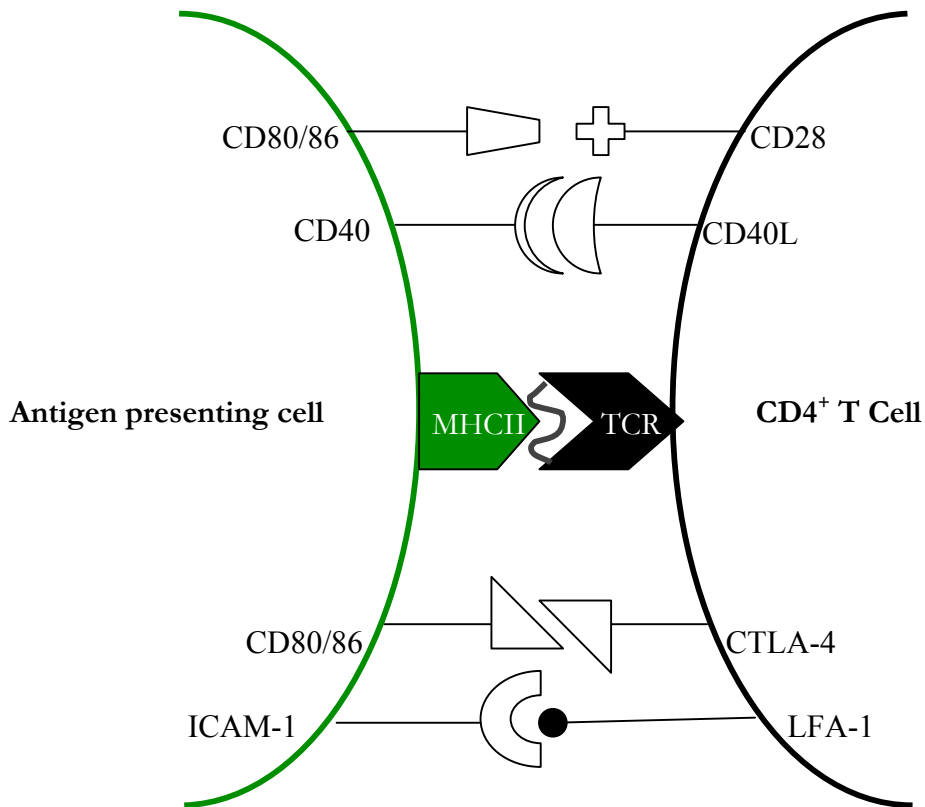


Figure 1.3 Cell surface molecules and ligands involved in DC-T cell interactions and the activation of CD4⁺ T cells. Abbreviations: Cytotoxic T lymphocyte associated protein 4 (CTLA-4); Lymphocyte function associated antigen (LFA-1); Intercellular adhesion molecule-1 (ICAM-1). CD28 is present on mature CD4⁺ T cells and binds CD80 and CD86 on DCs. CD28 is important for CD4⁺ T cell activation, clonal expansion and effector cell differentiation (140). CTLA-4 on CD4⁺ T cells also binds CD80/86 on the DC, however, this cell surface molecule acts to negatively regulate the T cell, inhibiting their proliferation and survival (222, 223). The engagement of CTLA-4 has been implicated as a key regulatory mechanism of T cell activation and is being harnessed for therapeutic purposes. CD40L is expressed on activated T cells following the stimulation of the TCR and CD28 and is important in the production of IL-12 and IFN γ in Th1 differentiation and in T cell help for B cell differentiation (139).

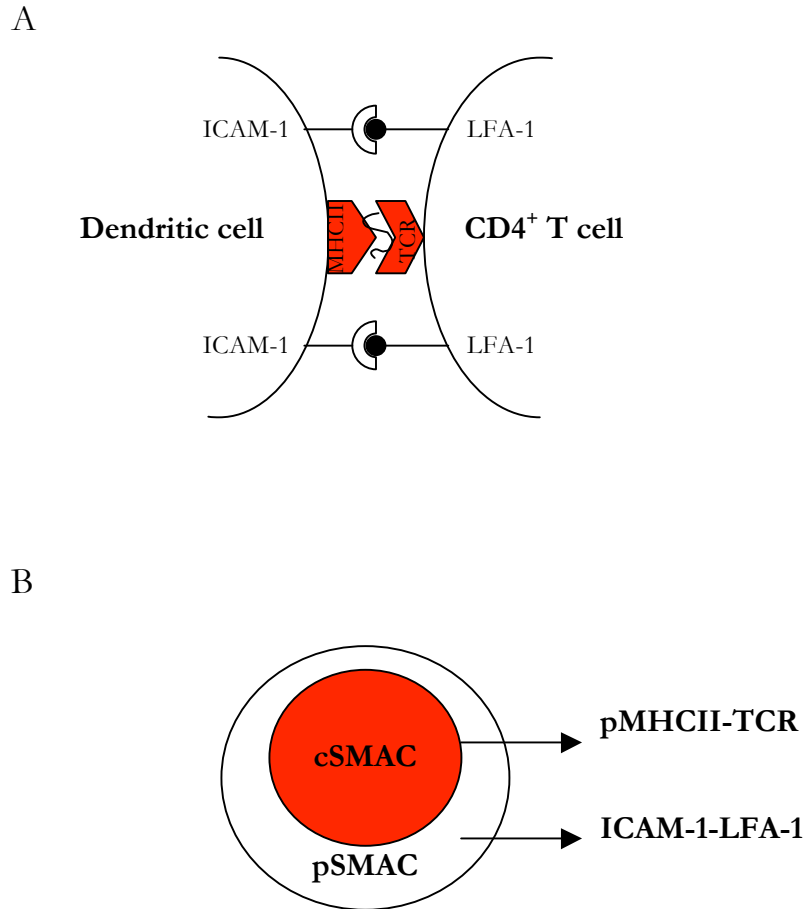


Figure 1.4 An illustration of the immunological synapse. A. Schematic of antigen specific DC-T cell interaction. Following pMHCII recognition and stimulation of the TCR, cell surface molecules re-arrange and organise into distinct regions. B. Schematic of the concentric rings of the immunological synapse. The central region, of 1-3 μm diameter, was termed the central supramolecular activation cluster (c-SMAC) and was shown to contain the TCR and the co-stimulatory molecule, CD28. This structure was surrounded by a peripheral (p-SMAC) region of adhesion molecules, including LFA-1 and the cytoskeletal molecule talin (183, 184).

Chapter 2

Materials and Methods

2.1 Animals

BALB/c (H-2^d) mice were used as a source of bone marrow cells for DC preparation. DO11.10 T cell receptor (TCR) transgenic (Tg) mice on a BALB/c background were used for all co-culture experiments, with the exception of *in vitro/vivo* imaging, in which DO11.10/SCID TCR Tg mice on a BALB/c background were used (224). These TCR Tg T cells recognise OVA₃₂₃₋₃₃₉ in the context of I-A^d MHCII and are detectable using the KJ1-26 clonotypic Ab (224). Like DO11.10 mice, OTII C57BL/6J mice express an OVA specific Tg TCR. However, the V α 2V β 5 TCR of OTII mice specifically recognises OVA₃₂₃₋₃₃₉ in the context of I-A^b MHCII (225). OTII C57BL/6J mice were employed in split ear experiments. In lymph node transplant experiments BALB/c, C57BL/6J mice and Ly5.1/C57BL/6J were used. In split ear DTH experiments (see below), DO11.10, BALB/c, CD2-GFP, CD2-OTII-GFP and C57BL/6J mice were used. In imaging studies of the joint, CD2-GFP, CD2-OTII-GFP and C57BL/6J mice were used (226). hCD2-GFP transgenic mice express the green fluorescent protein (GFP) under the control of the human CD2 promoter, a cell surface molecule expressed on T cells (226). More specifically, hCD2-OTII-GFP mice express GFP under the control of the hCD2 promoter in cells that express a V α 2V β 5 TCR that specifically recognises OVA₃₂₃₋₃₃₉ in the context of I-A^b MHCII. All animals were specified pathogen free and maintained under standard animal house conditions at Strathclyde University in accordance with Home Office Regulations.

2.2 Antigens and Adjuvants

OVA/CFA immunisation

Mice were immunised with ovalbumin protein at a concentration of 100 μ g OVA (Worthington Biochemical Corporation, Lakewood, NJ, USA) at a ratio of 1:1 OVA:complete Freund's adjuvant (CFA) (Sigma-Aldrich, Poole, UK).

HAO preparation and immunisation

Heat aggregated ovalbumin (HAO) was prepared by re-suspending OVA at 20mg/ml in PBS. The mixture was heated at 56°C for 2 hours until aggregated. Sterile PBS (Invitrogen, Paisley, UK) was added to the mixture and the sample was then centrifuged at 450 x g for 5 minutes. Supernatant was discarded and aggregated OVA was re-suspended at 20mg/ml in sterile PBS and frozen at -20°C until required. Prior to use, HAO was sonicated for 5 minutes on ice until clumps were broken down and the mixture could pass through a 27G needle. HAO was administered subcutaneously at a concentration of 100µg/mouse.

2.3 Cell Culture

Bone marrow derived DCs:

DCs were prepared from bone marrow (of BALB/c or C57BL/6J mice) as previously described (227). Bone marrow derived DCs were generated by using complete RPMI (RPMI 1640, 10% FCS (Harlan Sera labs), 2 mM L-glutamine, 100 U/ml penicillin, 100 mg/ml streptomycin, 1.25 mg/ml fungizone; all obtained from Invitrogen, Paisley, UK) in a syringe to flush out bone marrow from the femur and tibia. Cells were passed through nitex mesh (Cadisch & Sons Ltd. London, UK) to filter any bone particles and cells were washed in complete RPMI, centrifuged and counted. Bone marrow cells were plated at 0.5×10^6 cells/well in 6 well plates (Corning Costar, Sigma-Aldrich) and cultured with complete RPMI (RPMI 1640, 10% FCS (Harlan Sera labs), 2 mM L-glutamine, 100 U/ml penicillin, 100 mg/ml streptomycin, 1.25 mg/ml fungizone; all obtained from Invitrogen, Paisley, UK) supplemented with 10% GM-CSF obtained from the supernatant of X63 myeloma cells transfected with mouse GM-CSF cDNA (Luta).

Preparation of LN suspension to provide a source of T cells:

Peripheral and mesenteric lymph nodes were removed from the relevant strain of mouse and single cell suspensions were prepared by rubbing through Nitex mesh in complete medium.

Cells were washed in complete RPMI, centrifuged at 450 x g, counted and prepared for staining (see below).

2.4 Cell Labelling

The orange and red-fluorescent CellTrackers CMTPX and CFSE, (Molecular Probes Inc., Invitrogen, Paisley, UK) are colourless products that freely diffuse into cells. Intracellular cytosolic esterases cleave acetate groups to yield a highly fluorescent red or green product, respectively, which is retained within the cell.

CMTPX labelling of DCs:

Cells were incubated with (0.5 µl 20mM) CMTPX at 10^7 cells per ml CO₂ independent media (Invitrogen, Paisley, UK) for 40 minutes at 37°C. Unlike RPMI, CO₂ independent media is capable of maintaining long term pH stability under atmospheric levels of CO₂. Cells were washed twice in 20ml of CO₂ independent media, centrifuged at 450 x g and re-suspended in complete media.

CFSE labelling of T cells:

Cells were incubated with CFSE at 10^7 cells per ml HBSS (Invitrogen) + 0.5 µl of 10mM CFSE stock solution in DMSO for 12 min at 37°C. Cells were then washed twice in 20ml HBSS, centrifuged at 450 x g and re-suspended in complete media.

2.4 Culture conditions for *in vitro* co-culture systems

On day 7 of culture, DCs were pulsed for 6 hours with OVA (1mg/ml) and then activated with 1µg/ml lipopolysaccharide (LPS) from *Escherichia coli* 0111:B4 (Sigma-Aldrich, Poole, UK) for 24 hours. DCs in FTY720 (Cayman Chemical, Ann Arbor, MI, USA) treatment groups were incubated with the drug (or the DMSO control) at 1mg/ml in conjunction with LPS. Subsequently, DCs were harvested from the 6 well plates using cell scrapers (Greiner,

BioOne, Germany) and labelled following the outlined method. T cells were also acquired and labelled on day 8 and added to DCs in culture. For co-cultures treated with the LFA-1 binding Ab (or isotype control), cultures were incubated with 1mg/ml of either Ab upon co-culture of the cell types.

2.5 Conjugation Assay

Co-cultures were set up in 6 well plates, with each co-culture containing 0.5×10^6 DCs: 0.25×10^6 DO11.10 T cells + 0.25×10^6 BALB/c T cells. At 20 hours following the addition of T cells to the DCs, supernatant was removed and discarded. 1ml of 4% paraformaldehyde (Sigma-Aldrich, Poole, UK) was then added to each well and incubated for 20 minutes at 4°C (to fix co-clusters). 4ml of PBS was added containing 1ml of 0.06% gly-gly (Sigma-Aldrich, Poole, UK) and briefly incubated for 1 minute to neutralise any residual paraformaldehyde. Cells were harvested and prepared for flow cytometric analysis (see below).

2.5 *In Vitro* Imaging

Chamber slides (Nalge Nunc International, Hereford, UK) were prepared containing 0.5×10^5 DCs: 0.25×10^5 DO11.10 T cells + 0.25×10^5 BALB/c T cells in 400µl complete media. Slides were imaged for 2 hours using an inverted Nikon TE200 epi-fluorescent microscope using a x20 air lens and Metamorph software (Molecular Devices). The microscope is fitted with a Solent Scientific environmental chamber to allow an imaging temperature of 37°C to be maintained. Time-lapse movies were created by acquiring a series of fluorescent images at different emission wavelengths of 457/22nm and 530/20nm.

2.6 Click-iT™ EdU Cell Proliferation Assay

A proliferation assay was set up in a 96 well plate containing cells at a density of 2×10^5 in 200µl per well. Cells were cultured at 37°C for 48 hours, pulsed with 5µM of Edu and harvested after an additional 24 hours in culture. Edu (5-ethynyl-2'-deoxyuridine) is a nucleoside analog containing an alkyne and is incorporated into the newly formed DNA of

the proliferating cells. Proliferation measurements with Click-iT™ EdU (Invitrogen) were made following a copper-catalyzed reaction, in which the alkyne of Edu reacted with an azide-Alexa Fluor® 488, forming a stable covalent bond. Measurements of proliferation were then made by flow cytometry and were calculated on the basis of number of CD4 cells positive for Alexa Fluor® 488.

2.7 Multiplex analysis of cytokines

In some experiments, cytokines were analysed by multiplex analysis. This method involves the use of biotinylated detection Abs specific for different cytokines and chemokines, each of which is conjugated to a bead of defined spectral properties. This allows different cytokines/chemokines to be identified in the same sample. Moreover, the biotinylated aspect of the Ab allows the amount of cytokine/chemokine present in the sample to be quantified, by the addition of streptavidin conjugated to the fluorescent protein, R-phycoerythrin (RPE). Thus, laser excitation from the luminex instrument excites the sample and detects the type and amount of cytokine/chemokine on the basis of the spectral properties of the beads and the fluorescence intensity of RPE on each bead, respectively. The advantage of this system is that several analytes can be analysed in a small volume of sample.

Biosource Multiplex kits LMC0002 (Th1/Th2 6-plex) and LMC0001 (10-plex) (Invitrogen), were used according to the manufacturer's instructions. All reagents and buffers were sourced from the kits. Briefly, the supplied 96 well filter plate was pre-wetted with Working Wash solution before aspiration of well contents using vacuum apparatus. Beads were resuspended and 25µl bead mixture added per well and washed twice by the addition and aspiration of Working Wash solution from the wells. 50µl/well Incubation Buffer was added followed by 100µl/well standard or 50µl Assay Diluent plus 50µl sample. Plates were covered in aluminium foil and incubated on shaking apparatus at room temperature for 2 hours. The wells were then washed twice and 100µl/well biotinylated detection Ab added and incubated for 1 hour as above. Following two more washes, 100µl/well Streptavidin-RPE was added and incubated for 30 minutes as above. The wells were washed three final times before resuspending the beads in 100µl/well Working Wash solution and acquiring data on a Luminex 100™. Data was analysed using Luminex software and provided standard curves and sample data for each analyte.

2.8 Adoptive transfer of antigen specific lymphocytes

Peripheral lymph nodes, mesenteric lymph nodes, and spleens from DO11.10 BALB/c mice were pooled and forced through Nitex (Cadisch Precision Meshes, London, UK) using a syringe plunger. The suspensions were washed in sterile RPMI 1640 (Invitrogen) and counted using a Neubauer hemocytometer (Fisher Scientific, Leicestershire, UK). Lymphoid cells were analysed for the percentage of DO11.10 Tg T cells by staining for surface expression of CD4 and the Tg TCR (164). A sample of the cells were washed by adding 1 ml of FACS buffer (See table 2.3) before the suspensions were centrifuged at 450 x g for 5 min and the supernatant discarded. Cells were re-suspended in 50µl of purified anti-mouse CD16/CD32 (Fc block; 2.4G2 hybridoma supernatant) and incubated for 10 minutes at 4°C to prevent non-specific binding via Fc receptors. 1µl each of PE-labelled anti-CD4 mAb and FITC-labelled KJ1-26 mAb (recognising the transgenic TCR) or appropriately-labelled isotype controls (all Abs from BD Pharmingen unless otherwise stated, see table 2.2) was added to each sample which was then incubated for 20 minutes at 4°C. Cells were washed by addition of 1ml FACS buffer followed by centrifugation at 450 x g for 5 minutes at 4°C. The cell pellets were resuspended in 300µl FACS flow (see table 2.3) and analysed using a BD FACS Canto. Data was obtained using FACS DIVA (BD Bioscience) and analysis was performed using FlowJo software (Tree Star Incorporated, CA, USA). Cell suspensions containing 1×10^6 transgenic OVA specific T cells in 200 µl were injected intravenously, via the tail vein, into age-matched BALB/c recipients. In some experiments, cells were labeled with the fluorescent dye CFSE or CMTPX (Molecular Probes) immediately before use (see 2.4 for further details).

2.9 *In vivo* challenge

24 hours following the adoptive transfer of 1×10^6 naïve antigen specific DO11.10 or OTII T cells, recipient BALB/c or C57BL/6J mice were challenged in the footpad with 100µl of OVA/CFA or PBS as a control (as previously described). Alternatively, recipients were challenged with 3×10^6 fluorescently labelled DCs pulsed with 1mg/ml OVA (Worthington Biochemical Corporation) for 6 hours followed by overnight 1µg/ml LPS stimulation

(Sigma-Aldrich) (see 2.3 and 2.5 for further details of DC preparation and treatment). Popliteal LNs were excised at 20 hours post challenge for multi-photon imaging or after 3 days for proliferation by CFSE dilution or *in vitro* antigen re-stimulation.

2.10 *In vitro* re-stimulation of lymph node cells

72 hours following *in vivo* challenge, a single cell suspension from the popliteal LN was made and cells were plated at 200,000 per well in a 96 well plate format. Cells were incubated with 100µg/ml of OVA₃₂₃₋₃₃₉ peptide (Sigma-Genosys). Following 72 hours *in vitro* culture, cells were analysed by flow cytometry and supernatants were sampled for cytokine analysis by Luminex.

2.11 Lymph Node Transplant Model

3 week old and neonatal lymph node transplants

Inguinal lymph nodes were removed from either, newly weaned 3 week old mice or 2 day old neonatal mice and were inserted into a skin flap created in the ear pinna of the recipient mouse. Veterinary glue, (Vetbond; 3M, Loughborough, UK) was used to seal the skin flap and the transplanted lymph nodes were dissected for analysis after either 2 or 3 weeks.

2.12 Air Pouch Model

Air pouches were generated in BALB/c mice according to the methods of Sedgewick et al. (228). An area of the dorsal skin (2 cm²) was cleaned with alcohol and shaved to provide the pouch site. 1ml or 25µl of air was injected subcutaneously in the rump or ear pinna, with a 25-gauge or 30-gauge needle, respectively. In the rump, air pouches were injected with a further 1 ml of air on day 3, while in the ear pinna they were injected with a further 25µl to establish a definitive air pouch. On day 7, the mice were sacrificed and pouches were lavaged with sterile PBS (Invitrogen). Lavage fluid was analysed by flow cytometry to identify infiltrating cell types. The pouches were then dissected free from the surrounding tissue and fixed in formalin for histological evaluation by H&E staining (see below).

2.13 Histological evaluation

Tissue samples were fixed, dehydrated, and embedded in paraffin blocks with particular care to preserve the original shape of the pouch tissue. Sections were cut along a longitudinal axis at approximately the pouch midline, mounted and stained with hematoxylin and eosin (H&E). After staining, the slides were permanently bonded with coverslips (VWR, International, Leighton Buzzard, UK).

2.14 Haematoxylin and Eosin staining (H&E)

Tissues mounted onto non-APES-coated slides were placed in a Varistain 24-4 auto-staining processor (ThermoShandon, Essex, UK) to undergo haematoxylin and eosin (Sigma-Aldrich) staining in the sequence shown in Table 2.1. Tissue samples were then mounted in DPX mounting fluid (VWR International) and light microscopy (x10 magnification) was used to determine the presence of an air pouch cavity.

Solvent	Duration (minutes)
1. HistoClear	2
2. 100% Ethanol	3
3. Distilled Water	1
4. Haematoxylin	6
5. Distilled Water	1
6. 1% Acid alcohol	1
7. Distilled Water	1
8. Scott's Tap Water Substitute (STWS)	2
9. Distilled Water	1
10. 2% Eosin	5
11. 100% Ethanol	2
12. HistoClear	4

Table 2.1. The sequence of solvents and stains used for Haematoxylin and Eosin staining.

2.15 Delayed Type Hypersensitivity (DTH) Reaction

3×10^6 LN cells from either DO11.10 mice or HCD2-OTII-GFP mice were adoptively transferred intravenously via the tail vein into BALB/c or C57BL/6J recipients, respectively (see 2.10 for further details of adoptive transfer). Following 24 hours, mice were primed subcutaneously in the nape of the neck with 100 μ l of OVA/CFA (see 2.2 for details). After 10 days mice were challenged in the ear pinna with either 50 μ l of HAO (see 2.2 for details) to induce a DTH reaction or 50 μ l of PBS as a control.

2.16 Flow Cytometry

Single cell suspensions were prepared from lymphoid organs as described above, resuspended in 50 μ l Fc block and incubated for 10 minutes at 4°C. Abs or appropriately-labelled isotype controls were added to each sample at a dilution of 1:100 in Fc block. Cells were then incubated with the ab for 20 minutes at 4°C, see table 2.2 for full list of all Abs used. Cells were washed by addition of 1ml FACS buffer followed by centrifugation at 450 x g for 5 minutes at 4°C. For cells incubated with biotin labelled abs, the cell pellets were then re-suspended in 50 μ l FACS buffer with 1 μ l streptavidin-conjugated FITC/PE/APC (see table 2.2 for details) and incubated for a further 10 minutes at 4°C. The cells were washed FACS buffer, followed by FACS flow as above. Cell suspensions were resuspended in 300 μ l FACSflow and passed through nitex to remove cell clumps. Data was obtained using FACSCanto (BD Bioscience) and analysis was performed using FlowJo software (Tree Star Incorporated). Abs used for flow cytometry are summarised in Table 2.2.

Antigen	Isotype	Supplier	Label
CD4	Rat IgG2a	BD	FITC, PE, PerCP, Pacific blue
B220	Rat IgG2a	BD	FITC, Pacific Blue, APC

CD62L	Rat IgG2a	BD	PE
OVA-TCR (KJ1.26)	Mouse IgG2a	BD	Biotin, FITC
CD69	Ham IgG1	BD	APC
CD45.1	Mouse IgG2a	BD	Biotin
CD45.2	Mouse IgG2a	BD	Biotin/FITC
CD8	Rat IgG2a	ebioscience	APC
CD11c	Ham IgG1	BD	FITC/PerCp
CD11b	Rat IgG2b	BD	PE
CD40	Rat IgG2a	ebioscience	APC
CD86	Rat IgG2a	BD	APC
F4/80	Rat IgG2b	AbD serotec	FITC
Ly6G/Gr1	Rat IgG2b	Biologend	FITC
LFA-1	Rat IgG2a	ebioscience	Biotin/PE
PD1	Ham IgG2	ebioscience	PE
CXCR5	Rat IgG2a	BD	APC
ICOS	Rat IgG2b	BD	PE
Streptavidin-FITC		BD	
Streptavidin-PE		BD	
Streptavidin-APC		BD	
CCL21	Goat IgG	R&D	FITC
BP3		Gift from G.Anderson	bio
Gp38		Gift from G.Anderson	bio
VCAM-1	Mouse IgG1	Abcam	bio
CD3	Ham IgG1	BD	bio
Anti-FITC	Rabbit IgG	Invitrogen	FITC
Anti-mouse 594		Invitrogen	PE

Table 2.2 Flow cytometry and IHC reagents

2.17 Immunohistochemistry (IHC)

Tissue samples (e.g. ears containing a transplanted lymph node) were frozen in liquid nitrogen in tissue freezing media OCT (Optimum Cutting Temperature, Tissue-Tek) in

cryomoulds and stored at -70°C . Tissue sections ($8\ \mu\text{m}$) were cut on a cryostat (ThermoShandon, Cheshire, UK) at -20°C . Sections were mounted onto SuperFrost slides (BHD, Poole, UK) before being allowed to air-dry and stored at -20°C until further processing. Slides were brought to room temperature and fixed in acetone and the sections outlined with a wax pen to allow addition of solutions without cross contamination. The remainder of the staining process was carried out in a humidified darkened chamber. Sections were rehydrated in PBS for 10 minutes before incubating in 0.1% azide/2% H_2O_2 for 45 minutes, changing the solution three times. After washing in PBS, endogenous biotin was blocked by sequential 15 minute incubations with Avidin then Biotin solutions (Avidin-Biotin blocking kit from Vector Laboratories), each followed by washes in TNT buffer (see table 2.3 for details). Biotinylated Abs were diluted 1:250 in 1% blocking reagent (BR, from TSATM Biotin system, Perkin Elmer Life Sciences, Boston, USA) and added to sections for 40 minutes. Control sections were incubated with 1% blocking reagent (BR) only. Sections were washed three times in TNT buffer between the remainder of the steps. Streptavidin-horseradish peroxidase (HRP, from TSATM kit, Invitrogen Ltd) was diluted 1:100 in 1% BR and added to sections which were incubated for 30 minutes. Sections were then incubated in biotinylated tyramide diluted 1:50 in amplification diluent (both from TSATM kit) for 10 minutes. Sections were washed three times in TNT buffer. Streptavidin-AF-647 or AF-cascade blue (Molecular Probes) diluted 1:500 in BR was added to sections stained with primary biotinylated Abs for 30min. Sections were then washed three times in TNT buffer. Finally, any directly conjugated Abs were added at this stage and incubated for 30 minutes before being washed three times in TNT. The slides were left to dry briefly and mounted in either Vectashield or Vectashield containing DAPI to highlight the nuclei (Vector Laboratories). A glass coverslip followed that was sealed with nail varnish.

Confocal images of the sections were captured using the Leica SP5 confocal system. The appropriate laser lines and emission channels were selected using the Leica Application Suite. Colour levels of the acquired images were subsequently optimised using Volocity software (Improvision, Coventry, UK) using the “Auto contrast” function.

2.18 Multiphoton Laser Scanning Microscopy (MPLSM)

To image cellular behaviour in LNs, excised LNs were transferred into CO₂ independent medium (Invitrogen) at room temperature. The LN was bound with Vetbond glue (3M) onto a plastic coverslip that was then adhered with grease to the bottom of the imaging chamber continuously supplied with warmed (36.5 °C) and gassed (95% O₂ and 5% CO₂) RPMI before and throughout the period of microscopy. Excised LNs were imaged as previously described (12, 207). The two-photon excitation source was a solid-state, tuneable Titanium: sapphire laser system (Chameleon, Coherent Laser Group). The laser beam was routed into a multi-photon excitation laser scanning system (Radiance, Bio-Rad Laboratories). The objective lens used for all imaging investigations was the CFI-60 Fluo-W 40X/0.8 water-dipping objective lens (Nikon). The sample was illuminated with 780-830 nm, ~210 fs pulse duration and 76 MHz repetition frequency laser light. The emitted light was separated with a 550 nm dichroic mirror (Chroma Technologies). The scans were acquired with 500 lps and 512x512-pixel boxes, for a frame rate of 1.95 fps. Each imaged volume consisted of between 11 to 18 planes 1.95 μm apart. Volumes were acquired every 18 to 38 s.

The location (centroid) of individual T cells within each three-dimensional image stack were determined by intensity threshold-based object detection. Objects were tracked for at least 8 time points and the mean velocity, displacement and meandering index calculated for each. The interaction between DCs and T cells was measured by quantifying the co-localisation of green voxels with red as a fraction of the DC volume to generate the co-localisation coefficient – a measure of the proportion of DC volume in contact with T cells.

2.19 Statistics

Results are expressed as mean ± standard deviation. To test significance Student's unpaired T test was performed. A value of $p < 0.05$ was regarded as significant.

2.20 FTY720 treatment

FTY720 (Cayman Chemical, Ann Arbor, MI, USA) is a structural analogue of sphingosine. Once phosphorylated, FTY720 binds to and induces the down-regulation of sphingosine receptors. Used as an immuno-suppressive drug, FTY720 blocks the egress of lymphocytes from the LN. *In vitro*, FTY720 was added to cell cultures at a concentration of 1µg/ml for 24 hours prior to the use of the cells for either adoptive transfer or *in vitro* experimentation (229). *In vivo*, FTY720 was administered via the intra-peritoneal cavity at a concentration of 1mg/kg (230).

2.21 Anti-LFA-1 Ab (H68)

The LFA-1 binding ab was kindly supplied by Nancy Hogg (Cancer Research Institute, London). LFA-1 ab was used *in vitro* at 1µg/ml and used *in vivo* at 100µg/mouse. The isotype control ab, Rat-IgG2a (SouthernBiotech, Cambridge, UK) was used at the same concentration as the LFA-1 ab.

2.22 Fluorescent beads

Dark red fluorescent (660/680 excitation/emission maxima) FluoSpheres®, carboxylate-modified microspheres, of 0.04µm diameter (Invitrogen) were used in lymph node transplant experiments to test its ability to drain antigen from the local tissue. Beads were diluted 1/50 in HAO or PBS where indicated and approximately 50ul of the HAO/PBS/bead mixture was injected subcutaneously into the ear pinna.

2.23 Buffers

Buffer	Constituents
PBS	8g NaCl, 1.16g Na ₂ HPO ₄ , 0.2g KCl, 0.2g KH ₂ PO ₄ in 1 litre distilled water, pH 7.4
FACS buffer	2% FCS, 0.05% sodium azide in PBS
TNT wash buffer	10ml 0.1M Trizma base, 10ml 0.15M NaCl, 50µl Tween-20, 80ml distilled

	water
Incomplete RPMI	RPMI-1640 medium
Complete RPMI	RPMI-1640 medium, 10% FCS, 2mM L-glutamine, 100IU/ml penicillin, 100µg/ml streptomycin
Buffer NPI-10	50 mM NaH ₂ PO ₄ , 300 mM NaCl, 0.34 g imidazole (Adjust pH to 8.0 using NaOH)
Buffer NPI-20	50 mM NaH ₂ PO ₄ , 300 mM NaCl, 20 mM imidazole (Adjust pH to 8.0 using NaOH)
Buffer NPI-250	50 mM NaH ₂ PO ₄ , 300 mM NaCl, 250 mM imidazole (Adjust pH to 8.0 using NaOH)

Table 2.3 Buffers

2.24 Transfection of HEK cells with Kaede

Kaede is a naturally occurring photo-switchable fluorescent protein, derived from the stony coral, *Trachyphyllia geoffroyi*. Kaede expresses green fluorescence when excited with 488nm light. However, the unique feature of this protein is that following exposure to UV light, Kaede is irreversibly converted to a red fluorescence emitting protein when excited with 488nm light (231). The only commercially available format of the photo-switchable probe Kaede, is as a mammalian expression vector. Thus, a mammalian expression vector, pKaede-MC1, containing the Kaede sequence was purchased from MBL International. Lipofectamine™ 2000 (Invitrogen) was used according to the manufacturers guidelines to facilitate the entry of the mammalian expression vector into cells whereupon the Kaede protein was expressed.

2.25 Cloning of Kaede

Champion™ pET100 Directional TOPO® Expression Kit with BL21 Star™ One Shot® Chemically Competent *E. coli* (Invitrogen) was used to clone and express the Kaede gene. Champion™ pET Directional TOPO® vectors are powerful *E. coli* expression vectors that use the highly efficient T7 RNA polymerase to achieve strong transcription levels and high protein yields. T7 RNA polymerase is expressed by host *E. coli* under the control of the IPTG-inducible lacUV5 promoter, which allows transcription to be regulated with IPTG (Thermo Scientific). The key to TOPO® cloning is the enzyme DNA topoisomerase I, which functions both as a restriction enzyme and as a ligase. Its biological role is to cleave and rejoin DNA during replication. Vaccinia virus topoisomerase I specifically recognizes

the pentameric sequence 5'-(C/T)CCTT-3' and forms a covalent bond with the phosphate group attached to the 3' thymidine. It cleaves one DNA strand, enabling the DNA to unwind. The enzyme then re-ligates the ends of the cleaved strand and releases itself from the DNA. TOPO® vectors are provided linearised with topoisomerase I covalently bound to each 3' phosphate, which enables the vector to ligate DNA sequences with compatible ends. To ensure the Kaede gene sequence had compatible ends, PCR primers were designed to contain a short sequence at the 5' end of the forward primer that would allow the gene to be readily ligated into the TOPO® vector.

2.26 PCR primer design

Primers were designed based on the Kaede gene sequence and manufactured by the primer design service at Invitrogen. The Topo sequence necessary for directional cloning into pET100 vector, CACC, was added onto the 5' end of the forward primer. PCR primer sequences were as follows:

5' to 3' Forward Primer: CACC AT GGT GAG TCT GAT TAA ACC AGA AA
3' to 5' Reverse Primer: CTA CTT GAC GTT GTC CGG CAA T

2.27 PCR amplification of Kaede gene

For the amplification of the Kaede gene (677bp), 1.1X Ready-mix™ PCR Master Mix with 1.5mM MgCl₂ (Abgene) was used following the manufacturers instructions. This mixture is suitable for high fidelity standard PCR reactions. PCR primers were designed on the basis of the Kaede gene sequence using Invitrogen primer design service and were added to a final concentration of 0.5µM along with template DNA. The reaction cycles for the amplification are shown in table 2.4 Reaction volumes of 10µl were loaded onto a 1% agarose gel immersed in TAE buffer. Hyperladder 1 (Bioline), a DNA marker ranging between 200bp and 10,00bp, was loaded (5µl) to provide a size comparison for amplified products then electrophoresis was carried out. Subsequently the gel was visualised under UV light and

photographed using a Gel Doc 2000 system (Bio-Rad). See table 2.5 for full details of PCR reaction mixture.

Reaction step	Temperature °C	Time (mins)
Denaturing	95	5
Denaturing	95	1
Annealing	48-52	1
Extension	72	1
Final extension	72	10

Table 2.4 Reaction cycles for the amplification of the Kaede gene

Reaction components	Volume (µl)
Extensor Hi Fidelity PCR enzyme (1unit)	0.25
Extensor buffer 1 (10X) (2.25mM Mg)	5
dNTPs	0.2
Template DNA (100ng)	1
Fwd Primer (0.5µM)	0.5
Rev primer (0.5µM)	0.5
Ultra pure H ₂ O	42.55
Total volume	50

Table 2.5 Reaction components for the amplification of the Kaede gene

2.28 Preparation of a 1% agarose gel

In a plastic conical flask, molten agarose gel was prepared by dissolving agarose powder (MultiABgarose, Abgene) to a 1% w/v ratio in 1X Tris-acetate buffer made up from a 10X stock; 0.4M Tris base, 0.2M acetic acid, 0.01M EDTA, diluted in distilled water (TAE buffer). The solution was heated, until dissolved. Ethidium bromide (Sigma-Aldrich) was

added to the solution to a final concentration of 0.5µg/ml. The liquid gel was poured slowly into the gel casting chamber and a well comb was placed into the molten agar and the gel was left to set for 30 minutes. The set gel was placed into the electrophoresis tank and submerged in 1X TAE buffer. Samples were loaded into the wells using a pipette prior to electrophoresis at 120 volts.

2.29 Sequencing of recombinant Topo Kaede constructs

Topo-Kaede plasmids were sent for sequencing to Ninewells Hospital Sequencing service, Dundee, where they were analysed using the ABI 3730 capillary DNA sequencer. Sequences were then examined to ensure the Kaede gene had been inserted in the correct orientation and without any base pair errors.

2.30 Isolation of the PCR amplified products

Following PCR all of the reactions were loaded onto a 1% agarose gel and electrophoresed using hyperladder I (Biolone, London, UK) as a marker. The gel was placed on a UV light table and the fragments were cut out using a clean scalpel. The DNA was isolated from the gel using a Nucleospin Extract II kit (Machery & Nagel, Abgene, Epsom, UK) following the manufacturers instructions.

2.31 Transformation of recombinant pET TOPO Kaede into BL21 Star One Shot Cells and Expression of Kaede

Transformation of BL21 star *E.coli* with the pET TOPO Kaede construct was carried out chemically by 'heat shock' at 42°C. The chemically competent cells (50µl) were thawed on wet ice and 1 µl of the ligation mix was added by pipetting. The mixture was returned to ice for 30 minutes and then incubated at 42°C for 30 seconds. Immediately, cells were returned to ice and 250µl of room temperature S.O.C medium (Invitrogen) was added to the mixture. The sample was incubated for 1 hour at 37°C accompanied with shaking at 200rpm. The transformation culture was then plated out (100µl of each dilution spread per plate) onto

Agar plates supplemented with ampicillin (100µg/ml) and incubated overnight at 37°C. Using a sterile 200µl pipette tip, colonies were picked and mixed into 5ml L-Broth supplemented with ampicillin (100µg/ml) and incubated with shaking at 200rpm overnight at 37°C. The resulting cultures were then transferred into 1L flasks of L-Broth supplemented with ampicillin (100µg/ml) and grown to OD of 0.4-0.6 before adding Isopropyl-β-D-thiogalactopyranoside (IPTG) at 1uM, the chemical which induces expression from the T7 promoter. Cultures were grown for a further 6 hours before purification of the Kaede protein. To lyse the bacterial cells and release the Kaede protein, pellets freeze thawed twice and then re-suspended in lysis buffer (Invitrogen) and incubated for 20 minutes at room temperature on a rocking platform. Cells were checked for complete lysis using phase contrast microscopy. To remove cell debris, the cell lysates were centrifuged at 13,000g for 20 minutes leaving the soluble protein in the supernatant (lysate), which was transferred to a fresh eppendorff tube. Both fractions were stored at -20°C until analysis by sodium dodecyl sulfate-polyacrylamide gel electrophoresis (SDS-PAGE) or purification over a Ni-NTA column.

2.32 Culture conditions for pilot expression

Pilot expression studies were carried out to determine the optimal conditions for expression of the recombinant peptide. Overnight cultures of each clone were inoculated into fresh SOB broth (25ml) to an optical density at 600nm of 0.1 and were grown at 37°C until early / mid-log phase (O.D₆₀₀ of 0.4-0.6). IPTG was then added to final concentrations of 1mM and 10mM in order to determine the optimum concentration of IPTG for expression. The culture was then incubated at 37°C overnight, at 0hr, 3hr and 6hr timepoints 1ml samples were removed and the OD₆₀₀ was taken before centrifugation in eppendorf tubes at 13,000 rpm for 5 minutes. The supernatants were then aspirated and the pellets were stored at -20°C.

2.33 Sodium dodecyl sulfate-polyacrylamide gel electrophoresis (SDS-PAGE) and Western Blot

For the lysate samples, a 20 μ l volume was added to 5 μ l of 5X SDS sample buffer (250mM Tris pH6.8, 10% SDS, 50% glycerol, 0.02% bromophenol blue, 10% β -mercaptoethanol) and then boiled for 5 minutes prior to being loaded onto the gel. A 7 μ l volume of prestained protein ladder (Promega, Hampshire, UK) was added to a well alongside the samples to provide an estimation of peptide size and to indicate when the peptide of interest had resolved sufficiently for visualisation. His-tagged proteins were detected by western blot using an anti-his Ab (Invitrogen). Following electrophoresis of the samples on the polyacrylamide gel, proteins were transferred onto a nitrocellulose membrane following the manufacturers instructions. Gels were carefully removed from their plastic case and immersed in western blot running buffer (Invitrogen) alongside the nitrocellulose membrane and two pieces of filter paper that were cut to the size of the gel. These were equilibrated in the buffer for 15 minutes before being assembled and immersed in transfer buffer within a Bio-Rad electrophoresis tank (Bio-Rad, Hertfordshire, UK). The tank was situated in a cold room (4°C) and transfer of proteins from the gel onto the nitrocellulose membrane was carried out by electrophoresis at 20 volts overnight. A monoclonal ab specific to the polyhistidine tag and conjugated to the enzyme horse radish peroxidase (HRP) (Sigma-Aldrich) was used for the detection of Kaede after transfer onto the nitrocellulose membrane. Following transfer, using the Ab protocol as a guide, the membrane was immersed in PBS + 5% semi-skimmed milk powder to block non-specific ab binding to the membrane by saturating the membrane with proteins contained within the semi-skimmed milk. The blocking stage was performed for 1 hour on a rocking platform at room temperature. The membrane was washed twice in PBS and then incubated in Ab solution containing anti-his HRP conjugated Ab diluted 1/4000 in 25ml of PBS + 5% semi skimmed milk powder. The membrane was immersed in PBS and gently rocked for 5 minutes to remove any unbound ab. This step was repeated twice prior to detection of specifically bound Ab by incubating the membrane in SIGMA *FAST*TM DAB (3, 3'-diaminobenzidine) peroxidase substrate (Sigma-Aldrich) following the manufacturers instructions. One tablet set was dissolved in 15ml of deionized water and the solution poured over the nitrocellulose

membrane (Sigma-Aldrich). The membrane was then observed for the colourimetric reaction caused by the action of HRP on DAB and photographed using a digital camera.

2.34 Purification of Kaede

Following the expression of Kaede in BL21 star *E.coli* (Invitrogen) the protein was purified over Ni-NTA columns (Qiagen, West Sussex, UK), using the following protocol. Cultures were split between centrifuge flasks for Beckman and spun at 4000rpm, 20mins, 4°C. Pellets were frozen for at least 1 hour, thawed and refrozen twice to optimise lysis of *E.coli*. Pellets from each 1L culture were re-suspended in 10ml NPI-10 buffer, with 1ml of 10mg/ml Hen egg lysozyme (Biozyme laboratories, Gwent, UK) and a pinch each of DNase (Sigma-Aldrich) and Benzamidine (Sigma-Aldrich) (see table 2.3 for full ingredients of buffers). The mixture was incubated for 30min at room temperature and then transferred to Beckman centrifuge tubes and spun at 15,000g, 4°C for 30 minutes. Supernatants were collected and passed through a syringe filter of 0.2µm (Millipore, Watford, UK). Ni-NTA columns (Qiagen) were prepared by removing storage buffer & equilibrated with 10ml NPI-10 buffer by allowing to drain through. Filtered supernatants were added to the columns and allowed to drain through (Kaede protein should remain within the column). Columns were washed with 2x10ml NPI-20 buffer. Columns were then washed with 3ml NPI-250 to elute the protein. The majority of protein comes off in 2nd and 3rd ml, so each was collected separately. To concentrate the Kaede protein in PBS and to remove imidazole, the mixture was centrifuged in PBS at 400g for 10 minutes using an Amicon Ultra-15 Centrifugal Filter Unit with Ultracel-10 membrane (Millipore). This system retains proteins greater than 10kDa, allowing buffer components to be washed through and the protein to become concentrated. Once purified Kaede was stored at 4°C. The concentration of the Kaede protein was established using the BCA kit (Thermo Scientific) following manufactures guidelines. All purification steps were carried out in the dark to prevent exposure of Kaede to any naturally occurring UV light.

2.35 Conjugating Kaede to beads

Carboxylate-modified polystyrene latex beads of 2 μ m diameter were covalently conjugated to the Kaede protein (Sigma-Aldrich). Beads were washed three times in sterile PBS. Conjugation of Kaede to beads was conducted in 25mM MES, 1mM 1-ethyl-3-(3-dimethylaminopropyl) carbodiimide (Sigma-Aldrich), with beads at 5×10^{10} beads/ml and 300 μ g/ml Kaede. Conjugation reactions were rotated overnight at 200rpm in the dark at room temperature. The mixture was then washed twice in 25mM MES and centrifuged at 400g. Immediately before use, beads were washed twice in sterile PBS, centrifuged at 400g and re-suspended at $\sim 7.5 \times 10^{10}$ particles/ml.

2.36 Photo-switching of Kaede by epi-fluorescence microscopy

Kaede was photoswitched with a 1 second pulse of 405nm UV light from a Nikon TE200 epi-fluorescent microscope.

Chapter 3

The effect of FTY720 and an LFA-1 blocking Ab on DC-T cell interactions *in vitro* and *in vivo*

3.1 Introduction

As outlined in chapter 1, the overall aim of this PhD was to investigate the relationship between DC-T cell interactions taking place within a tissue site of inflammation and its DLN. In this chapter, a series of *in vitro* systems were developed to investigate DC-T cell interactions and to establish the effect of modulating such interactions using the immunosuppressive drug, FTY720 and an LFA-1 blocking Ab. While the ultimate objective was to develop *in vivo* model systems that would allow these cellular interactions to be examined in the context of a tissue site of inflammation and its DLN, first modulating these interactions *in vitro* allowed establishment of the parameters to test in the study of DC-T cell interactions. Moreover, developing methods to block or modulate DC-T cell interactions *in vitro*, could provide a useful tool to assess and analyse the relative requirement of these cellular interactions at both the tissue site of inflammation and the DLN in future studies *in vivo*. FTY720 is an immuno-suppressive drug known to modulate T cell migration, while LFA-1 plays a dual role on the surface of T cells, acting to both facilitate T cell migration and to decrease the threshold of T cell activation by triggering key signalling pathways (190, 232, 233). Thus, by employing FTY720 and an LFA-1 blocking Ab in the *in vitro* systems, distinct aspects of T cell function, namely adhesion and migration, were targeted in an attempt to block DC-T cell interactions. Furthermore, the results obtained from the *in vitro* systems provided preliminary data that informed the subsequent study of these molecules in an *in vivo* experimental setup.

Through their ability to present antigen and provide co-stimulation to CD4⁺ T cells, DCs are widely recognised as being key initiators and crucial regulators of the adaptive immune response. Early studies by Steinman *et al.* concluded that *in vitro* co-cultured DCs and T cells form multi-cellular aggregates that appeared important for the induction of T-cell proliferation (234). More recently, direct *in vivo* assessment using MPLSM has confirmed the importance of prolonged DC-T cell interactions for efficient T cell activation and proliferation by introducing agents that block the presentation of antigen to T cells and interrupting the formation of such multi-cellular aggregates (4). Moreover, the application of MPLSM has provided a wealth of information regarding the kinetics and dynamics of DC-T cell interactions *in vivo* during the induction of antigen specific immune responses (4, 7, 176,

209, 235-237). Consequently, there is a growing consensus that T-cell priming by DCs occurs in three successive stages, in which the initial and final stages are characterised by T cells undergoing a series of transient interactions with multiple DCs (235). However, it is the intervening stage, in which these interacting cell types establish a prolonged and stable interaction, that appears to be crucial for both the onset of clonal expansion and differentiation into effector lymphocytes (235). Moreover, it has also been suggested that by altering the nature of DC-T cell interactions, the reciprocal communication taking place between these interacting cell types can give rise to very different outcomes, such as priming versus tolerance (238). Thus, the finer details of how these cells interact is critical to maintaining the health of the immune system and being able to modulate them would be an invaluable tool in both understanding the relationship between the cellular interactions at the tissue site of inflammation and its DLN and in providing novel therapeutic targets for the intervention in disease.

LFA-1 is a cell surface molecule that belongs to a family of leukocyte integrins that are characterised by their common β -chain (CD18) (239). The hetero-dimeric molecule is completed by a distinct α -chain (CD11a) and together they function as a key adhesion receptor and signal-transducing molecule for the ligand ICAM-1 expressed on the surface of antigen presenting cells (240). LFA-1 plays a well documented role in mediating T cell migration and entry into the LN and tissue sites of inflammation (232, 241-244). Furthermore, LFA-1 plays a critical role in mediating adhesion to antigen-presenting DCs to facilitate a stable platform in which T cell activation and differentiation can take place (183, 184). This stable interface between the cells is referred to as the immunological synapse and is formed initially by a central zone of LFA-1, which is surrounded by a peripheral ring of TCRs at the contact site with the DC (see figure 1.4) (183). However, within minutes this distribution is reversed and the central area becomes occupied by TCRs that associate with internal signalling molecules, while LFA-1 becomes clustered as a peripheral ring co-localised with cytoskeletal proteins (183, 184). Thus, LFA-1 was considered to play a key role in maintaining stability of the synapse. However, work by Miller *et al.* suggest LFA-1 also functioned as a signalling molecule (232). By transfecting cells with MHC II molecules (peptide presenting) with or without the co-expression of ICAM-1, Miller *et al.* designed a set of artificial antigen presenting cells that expressed 100-fold more peptide-MHCII complexes

than normally expressed on DCs. Critically, engagement of the TCR with high amounts of antigen in the absence of ICAM-1, could not overcome a requirement for LFA-1 dependent interactions in the activation of naive CD4⁺ T cells (232). This finding was substantiated when subsequent studies demonstrated the activation of a signalling cascade, distinct to that mediated through the TCR, following the engagement of LFA-1 (245). In addition, experiments in which LFA-1 was mutated into a constitutively active form, demonstrated that an inability of LFA-1 to function normally *in vivo* severely attenuated the generation of an immune response (243). As a result, modulating LFA-1 *in vivo* using a humanised monoclonal (Efalizumab), has recently become a novel therapeutic (246-253). Efalizumab specifically blocks LFA-1 and had been successfully employed in the treatment of the auto-immune skin disorder, psoriasis, by inhibiting the migration of T cells into the skin tissue and preventing their re-activation and interaction with keratinocytes (253). However, in April 2009, Efalizumab was withdrawn from the market for the treatment of psoriasis following reports of an association between long-term therapy and the development of the viral brain disease, progressive multifocal leukoencephalopathy (PML), which occurs almost exclusively in immuno-suppressed patients (248). In conclusion, the role of LFA-1 on the surface of T cells is multifunctional, ranging from contributions to the adhesion and signalling cascades required to activate individual cells to the migration of T cell populations into secondary lymphoid organs and tissue sites of inflammation. Moreover, disorder or attenuation of its function can cause or alleviate serious autoimmune and inflammatory diseases, respectively.

In addition to an LFA-1 blocking Ab, the *in vitro* systems developed in this chapter were also used to investigate the effect of FTY720 on the interactions between DCs and CD4⁺ T cells. FTY720 is a homologue of the serum borne lipid, sphingosine-1-phosphate (S1P) and can modulate signalling through S1P G protein coupled receptors (S1PRs) (254). S1P mediated signalling plays an important role in the promotion and regulation of a variety of biological processes and has diverse effects on T cells and DCs ranging from migration, proliferation and endocytosis, respectively (255-258).

FTY720 is most commonly known for its application in transplant therapy due to its ability to induce lymphopenia by blocking the exit of lymphocytes from LNs and in turn inhibiting their influx into tissue sites of inflammation (233, 257). FTY720 is thought to block the

migration of lymphocytes from secondary lymphoid organs in a combination of ways. Following its phosphorylation *in vivo*, FTY720 binds to, and induces the down-regulation of, the S1PRs on the cell surface of T lymphocytes. This is thought to render T cells unable to migrate up the S1P gradient that exists between the LN and the efferent lymphatic vessels, blocking their exit the lymph node (233, 257). In addition, S1PRs are involved in the assembly of vascular endothelial cell–cell junctions and FTY720 has been reported to inhibit their permeability, causing the sinus-lining endothelium of the LN to present a physical barrier to exiting lymphocytes (259).

The ability to modulate S1P mediated signalling using FTY720 has a well established impact on T cell migration, however, it is also thought to impact a variety of functions of murine DCs. Pretreatment of bone marrow derived DCs with FTY720-P at 0.1 μ M or higher has been shown to significantly inhibit S1P-induced migration and endocytosis (255). Moreover, FTY720 has been shown to interfere with the levels and activation of the Rho family of small GTPases, which regulate cytoskeletal proteins and are involved in the formation of dendrites and stable interactions between T cells and DCs (260). Idzko *et al.* reported that contact between antigen loaded DCs and antigen specific T cells co-cultured *in vitro*, was reduced when DCs were pre-treated with FTY720 (229). Moreover, this observation was not related to an FTY720 enforced reduction in antigen processing and presentation, since DCs formed less stable interactions when pulsed with either OVA protein or OVA-peptide.

LFA-1 is a key adhesion and signalling molecule known to play an important role in DC-T cell interactions. In contrast, while FTY720 is known to have a significant impact on T cell migration, its role in DC-T cell interactions is less well characterised. In this chapter, a set of *in vitro* systems were developed to investigate DC-T cell interactions and the effect of blocking such interactions using an LFA-1 blocking Ab and FTY720 on downstream proliferation and differentiation of T cells. Moreover, the impact of both an LFA-1 blocking Ab and FTY720 on the dynamic interactions between DCs and T cell has never been directly visualised in the physiological environment of the lymph node. As outlined in the introduction, the kinetics and dynamics of DC-T cell interactions *in vivo* are critical parameters in determining the outcome of an immune response. Thus, since preliminary data

from *in vitro* systems revealed their ability to modulate DC-T cell interactions and downstream T cell proliferation and differentiation, the effects of FTY720 and an LFA-1 blocking Ab *in vivo*, were also investigated in this chapter.

3.2 Results

It was first of all necessary to establish some important parameters in the *in vitro* systems. Firstly, before employing the LFA-1 blocking Ab in the *in vitro* systems, it was prudent to confirm that the LFA-1 blocking Ab could bind to cell surface LFA-1. Secondly, since S1P mediated signalling is known to effect DC function, it was important to check that modulating S1P signalling using FTY720 did not alter the activation status or the survival of the DC following *in vitro* treatment with the drug. This also allowed a suitable concentration of the drug to be selected and ensured that the DCs used in the *in vitro* assays were viable and not impaired in their functional status.

3.3 The LFA-1 blocking Ab can bind to, and be detected on, the cell surface of T cells and DCs

LFA-1 is expressed on both DCs and T cells and to confirm whether the LFA-1 blocking Ab could bind specifically to cell surface LFA-1, a secondary Ab which targets the Fc portion of the LFA-1 blocking Ab, was employed. A lymphocyte suspension was produced from homogenised LNs while DCs were derived from *in vitro* bone marrow culture, as detailed in Materials and Methods. Cells were incubated with either the LFA-1 blocking Ab or an isotype control. Specific binding of the LFA-1 blocking Ab (RatIgG2a mAb) to cell surface LFA-1 was established using an anti-ratIgG-FITC Ab. In figure 3.1 A + D, T cells and DCs were first identified on the basis of size and granularity, with the T cell population being gated to reflect their smaller less granular characteristics in comparison to DCs. The cells were next gated on the basis of co-expression of CD4 or CD11c and anti-rat-IgG-FITC, to test for specific binding of the LFA-1 blocking Ab to T cells and DCs respectively. Following their incubation with the isotype control, only 5.87% of CD4⁺ T cells and 11.9%

of CD11c⁺ DCs stained positively with the anti-rat-IgG-FITC, figure 3.1 B + E. However, following incubation with the LFA-1 blocking Ab, 60.1% of CD4⁺ T cells and 87.4% of CD11c⁺ DCs stained positively with the anti-rat-IgG-FITC, figure 3.1 C + F, signifying specific binding of the LFA-1 blocking Ab to cell surface LFA-1. In addition, 35.6% of the lymphocytes incubated with the LFA-1 blocking Ab failed to express CD4⁺ but stained positively with the anti-rat-IgG-FITC Ab. This population most likely represented the CD8⁺ T cells and B cells present in the lymphocyte suspension, which are also known to express LFA-1, figure 3.1 C (261, 262).

3.4 Pre-treatment of DCs with FTY720 does not modulate their activation status

In the resting state, prior to their activation with a microbial and/or inflammatory product, DCs are considered to be poor stimulators of T cell activation with the expression of few MHC molecules and co-stimulatory molecules, such as CD40 and CD86, on their cell surface (263, 264). However, following stimulation of cell surface pathogen recognition receptors, such as Toll like receptors (TLRs), this phenotype can rapidly transform from an 'immature' to an 'activated' state, allowing DCs to become powerful stimulators of immunity (265-267). This process can be mimicked *in vitro* using the TLR4 stimulating microbial product LPS and can be observed using flow cytometric analysis to monitor the upregulation of T cell stimulatory cell surface markers (268). Previous studies revealed that FTY720 did not affect the ability of DCs to present antigen and thus signal 1 (as outlined in the introduction) remains intact (229). However, the effect of FTY720 on the ability of DCs to provide signal 2 to T cells is not well characterised and it was therefore important to establish whether incubating DCs with FTY720 prior to their stimulation with LPS would affect their upregulation of co-stimulatory molecules. DCs were incubated with 3 different concentrations of FTY720, ranging from 10ng/ml to 1µg/ml or the DMSO carrier control for 24 hours at day 7 of their *in vitro* culture. DCs were then incubated with LPS or medium alone (control) for a further 24 hours, to induce their activation and up-regulation of co-stimulatory molecules. Following flow cytometric analysis, DCs were gated on the basis of their size and granularity and their expression of CD11c, with dead cells being excluded on

the basis of propidium iodide positive staining, figure 3.2 A-C. Representative flow cytometric plots illustrate the expression of the co-stimulatory molecules, CD40 and CD86, both of which were substantially increased when DCs were pre-treated with the DMSO carrier control and stimulated with LPS figure 3.2 D + E. Summarised in figure 3.2 F + G, pre-treatment of DCs with FTY720 failed to prevent this increase at all concentrations.

3.5 LFA-1 blocking antibody and FTY720 treatment fails to block DC-T cell clustering *in vitro* as assessed by flow cytometry

The first assay developed to investigate the ability of co-cultured DCs and T cells to form stable conjugates under priming conditions, was a flow cytometric based system in which DCs and T cells were differentially labelled using fluorescent dyes and DC-T cell conjugates were represented by the presence both colours. In this system, DCs were labelled with CMTPX (red) and incubated with CFSE (green) labelled DO11.10 CD4⁺ T cells following pre-treatment of DCs with FTY720 or treatment with an LFA-1 blocking Ab (see chapter 2, Materials and Methods for further detail). After 20 hours in co-culture, cells were fixed using para-formaldehyde and analysed using flow cytometry to establish the proportion of stable red and green double positive conjugates. Figure 3.3 A-D, provides a series of representative flow cytometric plots that outline how each population of cells, including DC-T cell conjugates, were identified. Figure 3.3 A, the plot identifies CFSE labelled DO11.10 T cells and a population of unlabelled T cells of irrelevant specificities while figure 3.3 B, shows CMTPX labelled bone marrow derived DCs. In figure 3.3 C, gates identify the 3 populations highlighted in plots A + B and the arrow indicates double positive DC-T cell conjugates detected in the absence of antigen. Consistent with published results, the addition of OVA to the co-cultures gave rise to an increase in the proportion of antigen specific DC-T cell conjugates, indicated by the arrow in figure 3.3 D (269). Summarised in figure 3.3 E, FTY720 pulsed DCs did not appear impaired in their ability to form stable DC-T cell conjugates. In the absence of antigen, 1.72% of cells formed stable conjugates in DMSO treated control cultures compared to 1.54% in FTY720 treated cultures. FTY720 did not impair the ability of the cells to form stable antigen specific conjugates, with 6.7% cells

forming stable conjugates in DMSO treated control cultures compared with 7.01% in FTY720 treated cultures. Summarised in figure 3.3 F, the results show that after 20 hours, in the absence of antigen, the proportion of DCs and T cells forming stable conjugates in isotype control treated cultures was 1.29% compared to a slightly lower 0.75% in LFA-1 treated cultures. Moreover, in the presence of antigen the proportion of stable conjugates detected in isotype control treated cultures was slightly higher at 5.9%, in comparison with LFA-1 treated cultures at 5.69%.

3.6 LFA-1 blocking antibody and FTY720 treatment reduces the number and duration of DC-T cell interactions *in vitro* when assessed dynamically

Treatment with FTY720, failed to reduce the number of antigen specific DC-T cell conjugates formed between these co-cultured cell types when investigated statically by flow cytometric analysis, while treatment with an LFA-1 blocking Ab induced a slight reduction. However, this assay assessed DC-T cell interactions at a single snap shot in time and offered little information as to how the cells were interacting in the moments prior to and following their fixation with para-formaldehyde. Thus, the results obtained may not have been an accurate reflection of events in the co-culture systems. Consequently, it became necessary to develop a system that would allow cell-cell interactions to be directly visualised, contrasted and compared, in a dynamic format. Moreover, as well as examining DC-T cell interactions at 20 hours, a further time point was introduced at 6 hours. Published data has shown that DC-T cell interactions at this time point are often unstable and short lived and these results were therefore contrasted and compared with the number and duration of DC-T cell contacts at 20 hours, at which time the cells are thought to interact for more prolonged periods (4).

The interactions taking place between CMTPIX labelled DCs (red) and CFSE labelled DO11.10 CD4⁺ T cells (green), were imaged in an environmental chamber at 37°C over time using epi-fluorescence microscopy. Imaged at both 6 and 20 hours for a period of approximately 30 minutes, still images of the resulting QuickTime movies can be seen in

figure 3.4 (see enclosed CD for complete movies). At 6 hours DCs co-cultured with T cells in the presence of antigen in control cultures, appeared to form small conjugates. While at 20 hours, representative images of each movie shows the presence of large DC-T cell clusters, which appeared to remain intact for the entire imaging period, figure 3.4. These results were reflected in the co-cultures treated with FTY720 and an LFA-1 blocking Ab, figure 3.4. However, differences were revealed upon detailed analysis of DC-T cells interactions by measuring the number and duration of intersecting fluorescent green (T cells) and red (DCs) objects using Volocity software (Improvision). More specifically, Volocity software allows cells to be identified on the basis of colour and converted to objects. It can then measure how frequently objects interact and calculate the duration of each interaction. Firstly, the overall duration (time-frames) of DC-T cell contacts observed at 6 hours was substantially less than the duration of those observed at 20 hours. Secondly, at 6 hours control cultures revealed that co-cultured DCs and T cells made large numbers of short lived contacts. Both treatment with FTY720 and an LFA-1 blocking Ab resulted in a similar outcome, with the overall duration of contacts at 6 hours less than at 20 hours and contacts being short lived at 6 hours, figure 3.5 A. However, by 20 hours DCs and T cells made a higher number of more stable, long term contacts in the presence of antigen, figure 3.5 B. Treatment with FTY720 reduced the number of long term DC-T cell contacts in comparison with the control. Moreover, treatment with LFA-1 blocking Ab, also reduced the number of stable long term contacts in comparison with the control. Thus, assessing cells dynamically using time lapse microscopy revealed an impaired capacity of DO11.10 CD4⁺ T cells to form stable, long term antigen specific interactions with DCs *in vitro*, both in the presence of an LFA-1 blocking Ab and following treatment of DCs with FTY720.

3.7 LFA-1 blocking antibody and FTY720 treatment significantly reduces DC capacity to stimulate T cell proliferation, *in vitro*

The ability of DCs and T cells to make long-term stable interactions has been proposed to be a crucial parameter in determining both the fate of the T cell and the outcome of the subsequent immune response (4, 236). Thus, visualising and assessing differences in these

interactions is of immunological relevance since the activation, clonal expansion and differentiation of T cells can be directly affected (9). It was therefore important to devise an *in vitro* system that would offer a functional read out of DC-T cell interactions and allow the consequences of their modulation to be assessed. *In vivo*, each individual antigen specific T cell is present at an extremely low frequency and thus, the rapid expansion of a particular T cell specificity is a critical step in allowing the immune system to generate a response capable of eliminating an invading pathogen (176). Moreover, a key feature of T cell differentiation is their ability to release pro-inflammatory cytokines that stimulate and drive the adaptive immune response (270, 271). Thus, proliferation and cytokine production were assessed to determine whether the treatment of DCs with FTY720 or the blockade of the integrin LFA-1 on T cells, would have any effect on the ability of DCs to stimulate the antigen specific clonal expansion of T cells *in vitro*. T cell proliferation was assessed by flow cytometry using a Click-iT Edu Cell Proliferation Assay as described in Materials and Methods. Briefly, proliferation was measured by calculating the level of Edu incorporation by CD4⁺ T cells. Figure 3.6 A, outlines a representative flow cytometric plot used to measure the proportion of proliferating T cells which correspond to the cells double positive for the expression of CD4⁺ and Edu-Alexa-fluor 488. Consistent with expected results, the data illustrated in figure 3.6 B + C, demonstrate that the level of T cell proliferation induced by DCs in control cultures was substantially increased in the presence of antigen. Similarly, in FTY720 treated cultures the addition of antigen to the system increased the level of T cell proliferation. However, in comparison with DMSO treated control cultures, the level of antigen specific T cell proliferation observed was significantly less when DCs were pre-treated with FTY720 ($p=0.0004$). Likewise, in cultures treated with the LFA-1 blocking Ab, the addition of antigen to the system increased the level of T cell proliferation. However, in comparison with the isotype control treated cultures, the level of antigen specific T cell proliferation induced was also significantly less when cultures were treated with an LFA-1 blocking Ab ($p=0.0073$).

In the absence of antigen the output of cytokines from all control and treated cultures was negligible, therefore the results described here refer to the production of cytokines following antigen specific stimulation of the co-cultures, summarised below in table 3.1. Pre-treatment of DCs with FTY720 significantly reduced their production of the pro-inflammatory mediator IL12 ($p=0.0042$) and their ability to induce IL2 production by T cells ($p=0.0016$) in

comparison with DMSO treated control cultures, figure 3.7. In contrast, production of IL10, IL5 and IFN γ was not significantly reduced by FTY720 treatment in comparison with the DMSO treated controls. Figure 3.8 outlines the results of treating co-cultures with an LFA-1 blocking Ab and in comparison with isotype control treated cultures, production of IL12 ($p=0.0002$), IL2 ($p=0.0002$) and the anti-inflammatory cytokine IL10 ($p=0.0003$) were all significantly reduced. However, the production of IFN γ was not significantly altered by treatment with an LFA-1 blocking Ab. In contrast, treatment with an LFA-1 blocking Ab resulted in significantly higher levels of IL5 production in comparison with isotype control treated cultures ($p=0.0001$), figure 3.8.

Cytokine	FTY720 compared to DMSO control	LFA-1 Ab compared to isotype control Ab
IL2	significantly reduced ($p=0.0016$)	significantly reduced ($p=0.0002$)
IL12	significantly reduced ($p=0.0042$)	significantly reduced ($p=0.0002$)
IL10	not significant	significantly reduced ($p=0.0003$)
IL5	not significant	significantly increased ($p=0.0001$)
IFN γ	not significant	not significant

Table 3.1 Summary of cytokine production from *in vitro* antigen stimulated DC-T cell co-cultures treated with FTY720 and an LFA-1 blocking Ab *in vivo*

In the first section of this chapter, a set of *in vitro* assays were developed to study DC-T cell interactions and to establish which parameters were best measured when investigating these cellular interactions and their outcome. Moreover, the preliminary data collected from these *in vitro* systems showed an ability of FTY720 and an LFA-1 blocking Ab to modulate DC-T cell interactions. However, an immune response is the sum of many complex and dynamic individual cellular interactions, that are shaped by many environmental factors (176, 235). *In vivo* experiments that maintain the natural environment of the LN are crucial to acquire an accurate and detailed picture of how cells coordinate the initiation, maintenance and regulation of an immune response. Thus, in this next section of this chapter MPLSM was used to image the effect of FTY720 and blocking LFA-1 on the interactions taking place between DCs and T cells in the four-dimensional, physiological environment of an organised

LN (194). Furthermore, to examine the impact of interfering with DC-T cell interactions *in vivo*, the proliferation and differentiation of the antigen specific T cells were investigated.

3.8 FTY720 treatment did not appear to affect DC-T cell interactions *in vivo*

When imaged dynamically *in vitro*, pre-treatment of DCs with FTY720 reduced the number and duration of DC-T cell contacts. To assess the impact of FTY720 treatment on DC-T cell interactions *in vivo*, DO11.10 CD4⁺ T cells were labelled with CFSE (green) and adoptively transferred into a BALB/c recipient 24 hours before the subcutaneous transfer of CMTPX (red) labelled DCs into the footpad. 20 hours after the delivery of DCs, the DLN was removed for multi-photon imaging and the migration of T cells and their interaction with DCs were visualised and assessed. Throughout the *in vitro* experiments, DCs were pre-treated with FTY720, however, FTY720 is known to have diverse effects on DCs and T cells and to dissect the effect of FTY720 on DC-T cell interactions *in vivo*, 3 treatment groups were established, either DCs or T cells were pre-treated with FTY720 for 24 hours *in vitro* or the drug was delivered systemically via the intraperitoneal cavity (229, 233, 255, 256, 272, 273). Figures 3.9-11 A-D, detail representative images of each imaged DLN (see attached CD for full movies) from each FTY720 treatment group.

As discussed in the introduction, T cells are thought to migrate through the LN scanning for their specific antigen on the surface of DCs. Initially T cells migrate at relatively high speed, making only short lived contacts with DCs. However, in the later stages of antigen recognition, T cells are thought to alter their pattern of motility by slowing down to make stable long term contacts with DCs (7, 8, 235). In all FTY720 treated groups, T cell velocities were assessed to determine whether a drug known to block T cell migration and exit from the LN, would have any effect on T cell migration and slowing within the LN in response to antigen challenge. In the treatment group in which FTY720 was delivered systemically, T cell velocity decreased with the addition of antigen pulsed DCs in both control DMSO treated mice and drug treated mice. When comparing DMSO treated mice to FTY720 treated mice, there was no significant difference in T cell velocity in either the presence or absence of antigen, Figure 3.10 E. In the group in which T cells were pre-treated with FTY720, T cell

velocity decreased with the addition of antigen pulsed DCs following both pre-treatment of the T cells with DMSO and FTY720. When comparing velocities of DMSO treated T cells to FTY720 treated T cells, there was no significant difference in either the presence or absence of antigen, Figure 3.9 E. Similarly, when DCs were pre-treated with FTY720, T cell velocity decreased when DCs were pulsed with antigen and treated with both DMSO or FTY720. Furthermore, the antigen specific reduction in T velocity was not significantly altered following the treatment of DCs with FTY720, Figure 3.11 E. Thus overall, the speed at which T cells migrated within the LN was reduced in the presence of antigen and treatment with FTY720 failed to significantly alter this antigen specific slowing of T cell migration.

In addition to analysing T cell velocity, DC-T cell co-localisation was measured and assessed to determine the proportion of T cells interacting with DCs over the duration of the imaging period. In the treatment group in which FTY720 was delivered systemically, the co-localisation of DCs with T cells increased in the presence of antigen to represent antigen specific contacts between the cells in both DMSO treated control and drug treated mice. In addition, there was no significant difference in the level of antigen specific co-localisation when comparing DMSO treated to FTY720 treated mice, Figure 3.10 F. In the treatment group in which T cells were pre-treated with FTY720, their co-localisation with DCs increased in the presence of antigen when T cells were both pre-treated with DMSO and FTY720. Furthermore, there was no significant difference in the level of antigen specific co-localisation when comparing DMSO pre-treated T cells with FTY720 pre-treated T cells, Figure 3.9 F. In the treatment group in which DCs were pre-treated with FTY720, their co-localisation with T cells increased in the presence of antigen in both DMSO treated control and drug treated DC conditions. Moreover, there was no significant difference in the level of antigen specific co-localisation when comparing DMSO pre-treated DCs with FTY720 pre-treated DCs, Figure 3.11 F.

Multiphoton imaging and 'Volocity' analysis of T cell migration and their interactions with DCs, did not reveal any significant ability of FTY720 treatment to modulate cellular interactions and migration *in vivo*. CD4⁺KJ⁺ cells were next analysed for their up-regulation of CD69 and their down-regulation of CD62L, both of which are used as early markers of T

cell activation. Thus, assessing the expression of these molecules was used to further confirm the inability of FTY720 treatment to modulate DC-T cell interactions *in vivo*. CD69 is a cell surface glycoprotein and is one of the earliest inducible markers expressed during T cell activation. It can be up-regulated within an hour of T cell stimulation, with peak expression reached at 24 hours and this has been shown to be directly important for the retention of newly activated T cells within the LN, to facilitate their proliferation and differentiation (274-276). As described previously, naïve lymphocytes egress from the LN via stimulation of cell surface S1P₁ receptors, in response to the increasing S1P gradient that exists between the LN and afferent lymphatics (233). The up-regulation of CD69 on newly activated T cells results in the rapid down-regulation of cell surface S1P₁ receptors and therefore prevents their immediate exit from the LN (276). Thus, like FTY720, CD69 down-regulates S1P₁, however, while FTY720 down-regulates S1P₁ on all T cells, CD69 modulation of S1P₁ only occurs on antigen stimulated T cells. CD62L is a homing receptor that mediates the entry of naïve T cells to peripheral lymph nodes (277, 278). Following the antigen specific activation of T cells, CD62L is rapidly down-regulated to redirect newly activated T cells away from the LNs, increasing their potential recruitment to tissue sites of inflammation (279). In mice treated with either FTY720 or DMSO control systemically, expression of CD69 increased when DCs were pulsed with antigen prior to their transfer. When comparing antigen specific expression levels of CD69 in DMSO treated mice to FTY720 treated mice there was no significant difference, Figure 3.12 C. In contrast, the expression of CD62L on CD4⁺KJ⁺ cells was decreased when DCs were pulsed with antigen prior to their transfer. Treatment with FTY720 systemically did not significantly alter the antigen specific down-regulation of CD62L when compared to DMSO treated control mice, Figure 3.12 D. When compared to the DMSO treated control, FTY720 treatment showed no significant difference in the antigen specific reduction of CD62L expression, Figure 3.12 D. When T cells were pre-treated with FTY720 systemically, expression of CD69 increased when DCs were pulsed with antigen prior to their transfer in both DMSO and FTY720 treatment groups. Moreover, when comparing antigen specific expression levels of CD69 on CD4⁺KJ⁺ cells pre-treated with DMSO to T cells pre-treated with FTY720, there was no significant difference, Figure 3.12 C. The expression of CD62L on CD4⁺KJ⁺ T cells pre-treated with DMSO was decreased when DCs were pulsed with antigen prior to their transfer and pre-treatment of the T cells with FTY720 did not significantly alter this antigen specific effect. In addition,

when compared to T cell pre-treated with DMSO, FTY720 pre-treatment of T cells showed no ability to significantly alter the level of the antigen specific reduction in CD62L expression Figure 3.12 D. When DCs were pre-treated with FTY720 systemically, expression of CD69 increased when they were pulsed with antigen prior to their transfer following either DMSO or FTY720 treatment. Furthermore, when comparing antigen specific expression levels of CD69 on CD4⁺KJ⁺ cells following their interaction with DMSO treated DCs to FTY720 treated DCs, there was no significant difference, Figure 3.12 B. The expression of CD62L on CD4⁺KJ⁺ cells was decreased when DCs were pulsed with antigen prior to their transfer and pre-treatment of DCs with FTY720 did not significantly alter this antigen specific down-regulation nor did it show any ability to significantly alter the level of the antigen specific reduction, when compared to DMSO control, Figure 3.12 C. In summary, the expression levels of CD69 and CD62L on the surface of CD4⁺KJ⁺ cells were significantly increased and decreased in the presence of antigen, respectively, and treatment with FTY720 failed to significantly alter this.

The first set of multi-photon imaging experiments to investigate the effect of FTY720 treatment on the ability of DCs and T cells to interact *in vivo* revealed few differences, with early markers of activation, CD69 and CD62L, being expressed at levels comparable with DMSO treated controls. Expansion of the CD4⁺KJ⁺ cell population in response to OVA challenge was next investigated and consistent with the expected result, the absolute number of CD4⁺KJ⁺ cells within the DLN increased in response to antigen challenge. In comparison to the DMSO control, treatment of mice with FTY720 systemically, resulted in a significant increase in the absolute number of CD4⁺KJ⁺ cells in the DLN following immunisation with OVA pulsed DCs ($p=0.002$) Figure 3.12 A. In contrast, pre-treatment of T cells with FTY720 in comparison to DMSO, gave rise to a significant reduction in the absolute number of CD4⁺KJ⁺ cells in the DLN following stimulation with OVA pulsed DCs ($p=0.0355$), Figure 3.12 A. Pre-treatment of DCs with either the DMSO control or FTY720 prior to their transfer, failed to give rise to a significant difference in the absolute number of CD4⁺KJ⁺ cells within the DLN in response to OVA challenge. However, in each treatment group the proportion of CD4⁺KJ⁺ cells that had undergone cell division in response to OVA

challenge was not significantly altered in comparison to the proportion in DMSO control treated groups, Figure 3.12 B.

3.9 An LFA-1 blocking Ab did not appear to modulate DC-T cell interactions *in vivo*

When examined *in vitro*, treatment of co-cultures with the LFA-1 blocking Ab significantly reduced antigen specific T cell proliferation when compared with results obtained using an isotype control Ab (see above). To investigate the effect of LFA-1 blocking Ab on T cell division *in vivo*, mice were immunised with OVA/CFA and DLNs were removed after 72 hours for analysis. Consistent with the expected results, the absolute number of CD4⁺KJ⁺ cells in the DLN was significantly increased when mice were challenged with OVA/CFA in comparison to PBS, in both mice treated with the isotype control Ab ($p=0.0034$) and the LFA-1 blocking Ab ($p=0.001$), Figure 3.13 A. However, the absolute number of CD4⁺KJ⁺ cells in the DLN following immunisation with OVA/CFA was significantly less ($p=0.0097$) in mice treated with the LFA-1 blocking Ab compared with the isotype control, Figure 3.12 A. However, the proportion of CD4⁺KJ⁺ cells that had undergone cell division following treatment with an LFA-1 blocking Ab was not significantly reduced in comparison with isotype control treated mice Figure 3.12 B. Thus, while there were fewer CD4⁺KJ⁺ cells within the DLN, their capacity to respond to antigenic challenge by undergoing cell division did not appear to be impaired by the LFA-1 blocking Ab.

When imaged dynamically *in vitro*, the LFA-1 blocking Ab reduced the number and duration of DC-T cell contacts. To assess the impact of the LFA-1 blocking Ab on DC-T cell interactions *in vivo*, DO11.10 CD4⁺ T cells were labelled with CMTPX (red) and adoptively transferred into a BALB/c recipient 24 hours before the subcutaneous transfer of CFSE (green) labelled DCs into the footpad. 20 hours after the delivery of DCs, the DLN was removed for multi-photon imaging. Figure 3.14 A-D, details representative images of multi-photon movies acquired of the DLN (see attached CD for full movies) from each condition. However, the capacity of the LFA-1 blocking Ab to significantly reduce the absolute number of CD4⁺KJ⁺ cells within the DLN, had a major impact on the ability of the transferred

CMTPX labelled T cells to be imaged using multi-photon microscopy. As a result, visualising T cells and their interactions with DCs was not technically feasible and detailed analysis of T cell velocity and co-localisation with DCs was therefore not possible.

Analysis of the proportion of CD4⁺KJ⁺ cells that had proliferated in response to antigen challenge following treatment with an LFA-1 blocking Ab compared with an isotype control were similar and suggested that DC-T cell interactions were not impaired. However, since it was not possible to carefully visualise and assess whether the LFA-1 blocking Ab altered DC-T cell interactions using multi-photon microscopy, DLNs were homogenised and CD4⁺KJ⁺ cells were analysed for their up-regulation of the early activation marker, CD69. This was carried out to establish whether DC-T cell interactions had been modulated or whether they were sufficient to induce T-cell activation. In isotype control treated mice, the expression of CD69 was significantly up-regulated on CD4⁺KJ⁺ cells in response to antigen challenge ($p=0.0058$) Figure 3.12 C. Treatment of the mice with an LFA-1 blocking Ab, failed to inhibit this antigen specific up-regulation of CD69. Moreover, there was no significant difference in the expression levels of CD69 on antigen stimulated CD4⁺KJ⁺ cells in mice treated with the LFA-1 blocking Ab compared to the isotype control, Figure 3.12 C.

3.10 The effect of FTY720 and an LFA-1 blocking Ab on T cell differentiation and effector function *in vivo*

The first series of *in vivo* studies into the effect of FTY720 drug treatment did not reveal any significant differences in the ability of cells to interact, up-regulate the early activation marker, CD69 or undergo antigen specific proliferation, despite the number of cells within the LN being significantly altered. Moreover, while it was not possible to study the effect of an LFA-1 blocking Ab on antigen specific interactions, the ability to up-regulate the early activation marker, CD69 or undergo antigen specific proliferation was unchanged. It is thought that the ability of DCs and T cells to make long term stable interactions is crucial to determining both the fate of the T cell and the outcome of the subsequent immune response with respect to priming versus tolerance (8, 236, 237, 280). However, while no significant differences in the duration of DC-T cell interactions were reported here, the contribution of

contact duration and frequency alone to the functional outcome of a T cell, remains a matter of debate. Moreover, in tolerogenic conditions, T cell activation and proliferation have been reported to occur, thus often the true fate of the T cell is not revealed until their capacity to differentiate and function as effector cells is tested (280). Therefore, the next series of experiments in this chapter were performed to establish what effect if any, FTY720 and the LFA-1 blocking Ab have on T cell differentiation and effector function *in vivo*. DO11.10 T cells were adoptively transferred into a BALB/c recipient 24 hours before immunisation with OVA/CFA in the footpad. After 72 hours, DLNs were removed for flow cytometric analysis of antigen specific T cell clonal expansion and differentiation. In addition, cells were re-stimulated *in vitro* with antigen to assess pro-inflammatory cytokine output as a measure of T cell effector function. Since there had been no observed difference in the ability of DCs and T cells to interact, the FTY720 treatment groups were reduced to the ip route of administration only to minimise animal numbers.

Once activated, CD4⁺ T cells differentiate into effector cells that perform a variety of functions to direct the adaptive immune response (271, 281). In particular, CD4⁺ T cells play a crucial role in the development and enhancement of the antibody response, by differentiating into a subpopulation of T follicular helper (Tfh) cells that regulate and promote B cell proliferation, class switching and somatic hypermutation (282, 283). Phenotypically Tfh cells are characterised by the expression of CXCR5, which allows them to localise to B cell follicles in response to the B cell chemokine CXCL13, the inducible co-stimulatory receptor ICOS and the inhibitory receptor, PD-1 (41, 165). Thus, to test whether treatment with FTY720 or an LFA-1 blocking Ab had any impact on the ability of T cells to differentiate into effective helper cells, their expression of Tfh cell type molecules was assessed. In the absence of antigen stimulation, the proportions of CD4⁺KJ⁺ cells expressing the Tfh phenotypes, CXCR5⁺ICOS1⁺ and CXCR5⁺PD1⁺, was negligible (results not shown). In mice immunised with OVA/CFA and treated with FTY720, the proportion of CD4⁺KJ⁺ cells that up-regulated the expression of CXCR5 with ICOS and PD1, was not significantly different to the proportion expressed in DMSO treated control mice figure 3.15 B + C. Moreover, in mice immunised with OVA/CFA and treated with an LFA-1 blocking ab, the proportion of CD4⁺KJ⁺ cells that up-regulated the expression of CXCR5 with ICOS and

PD1 was increased, but not significantly, in comparison to isotype control Ab treated mice figure 3.16 B + C.

In addition to the differentiation of CD4⁺ T cells into Tfh cells, a measure of T cell effector function is their ability to produce a host of pro-inflammatory mediators that instruct and direct the activation and function of leukocytes involved in mediating the adaptive immune response (270, 271). As discussed in the introduction, CD4⁺ T cells can be characterised into different subsets on the basis of their cytokine output, which is of particular interest since different subsets are required to modulate and tailor the immune response towards the nature of the antigen challenge. Thus, to test whether FTY720 treatment or an LFA-1 blocking Ab had any ability to modulate the cytokine profiles induced by OVA/CFA immunisation, supernatants from re-stimulated cells were sampled and analysed for the presence of cytokines, chemokines and growth factors using the luminex system, as described in Materials and Methods. In the absence of antigen, cytokine production was negligible therefore all the results described below and summarised in table 3.2, refer to antigen stimulated cell cultures. In comparison to the results obtained from cultures of DMSO control treated mice, administration of FTY720 *in vivo*, did not significantly alter the production of pro-inflammatory Th1 type cytokines, Th2 type cytokines, chemokines and growth factors figures 3.17-.20. Similarly, the production of pro-inflammatory Th1 cytokines, Th2 cytokines, chemokines and growth factors was not significantly impaired by treatment with an LFA-1 blocking Ab in comparison to treatment with an isotype control Ab figures 3.21-24. However, a significantly higher ($p=0.0067$) concentration of macrophage inflammatory protein-1 α (MIP1 α) was detected in cell cultures from LFA-1 blocking Ab treated mice in comparison to isotype control treated mice.

Cytokine/Chemokine	FTY720 compared to DMSO control	LFA-1 Ab compared to isotype control Ab
IL2	Not significant	Not significant
IL1 β	Not significant	Not significant
IL4	Not significant	Not significant
IL5	Not significant	Not significant
IL6	Not significant	Not significant
IL10	Not significant	Not significant
IL12	Not significant	Not significant
IL13	Not significant	Not significant
IL17	Not significant	Not significant
IFN γ	Not significant	Not significant
MIG	Not significant	Not significant
KC	Not significant	Not significant
MIP-1 α	Not significant	Significantly increased (p=0.0067)
FGF	Not significant	Not significant
VGEF	Not significant	Not significant
TNF α	Not significant	Not significant
MCP-1	Not significant	Not significant
GM-CSF	Not significant	Not significant

Table 3.2. Summary of cytokine/chemokine production from *ex vivo* re-stimulated LNs treated with FTY720 and an LFA-1 blocking Ab *in vivo*

In addition to the flow cytometric analysis of the Tfh phenotype and the *in vitro* re-stimulation for cytokine analysis, the absolute number of CD4⁺KJ⁺ cells in the DLN was calculated. In comparison with DMSO control treatment, following immunisation, treatment with FTY720 gave rise to a significant increase (p=0.0001) in the absolute number of CD4⁺KJ⁺ cells in the DLN, figure 3.15 A. In contrast, following immunisation, treatment with an LFA-1 blocking Ab caused a marked reduction in the absolute number of CD4⁺KJ⁺ cells in the DLN in comparison to isotype control treated mice figure 3.16 A, reflecting results obtained in previous experiments Figure 3.12 A.

3.11 Discussion

DCs are potent, professional antigen-presenting cells (APC) conventionally identified *in vitro* by their ability to activate naive T cells (284). An appropriate antigen specific interaction between these cell types is an essential step in the process of priming and regulating an antigen specific immune response (8). The aim of this PhD was to investigate the relationship between DC-T cell interactions taking place within a tissue site of inflammation and its DLN. This chapter set out to develop a series of *in vitro* systems, in which DC-T cell interactions and the outcome of their modulation using FTY720 and an LFA-1 blocking Ab, could be measured and assessed. The ultimate objective was to develop *in vivo* model systems that would allow these cellular interactions to be examined in the context of a tissue site of inflammation and its DLN. However, by first developing systems to investigate and modulate these interactions *in vitro*, which parameters to test in the study of DC-T cell interactions were explored and established. Moreover, the potential use of FTY720 and an LFA-1 blocking Ab, in future *in vivo* studies, as tools to assess and analyse the relative requirement of these cellular interactions at both the tissue site of inflammation and the DLN was investigated using MPLSM. The results showed that while DC-T cell interactions were modulated by FTY720 and an LFA-1 blocking Ab *in vitro*, giving rise to an impairment in T cell proliferation and differentiation, the drug and Ab appeared to have little effect on DC-T cell interactions and the generation of T cell mediated immunity in the LN *in vivo*.

DC-T cell interactions were examined *in vitro* both statically and dynamically, which revealed contrasting results. When examined statically by flow cytometry, the proportion of DCs and T cells forming stable contacts were not affected by the pre-treatment of DCs with FTY720, however they were slightly reduced by treatment with an LFA-1 blocking Ab. While this assay offered a relatively quick and easy method for measuring DC-T cell interactions, it provided only a single snap shot in time and did not indicate the proportion of cells in clusters prior to, and following the addition of, the fixative, paraformaldehyde. Moreover, since other studies have shown that DC-T cell interactions are fluid and dynamic, it was important to design an assay that allowed these interacting cell types to be visualised and

analysed over a period of time (7, 8, 236, 285). Using epi-fluorescent microscopy, DCs and T cells imaged 6 hours following their co-culture made a high number of short-lived interactions and treatment with FTY720 or LFA-1 blocking Ab did not appear to alter this. However, the number and duration of antigen specific DC-T cell contacts observed in the various cultures at 20 hours differed substantially. In control cultures, DCs and T cells made a high number of stable interactions, while treatment with FTY720 and anti-LFA-1 blocking Ab resulted in a reduction in the number and duration of DC-T cell contacts. This observation at the 20 hour time point was of particular significance since it is thought that the ability of DCs and T cells to make long term stable interactions at this stage is crucial in determining both the fate of the T cell and the outcome of the subsequent immune response with respect to priming versus tolerance (7, 8, 237). The results observed here were consistent with previous findings, which reported that contact between antigen loaded DCs and antigen specific T cells co-cultured *in vitro*, was reduced when DCs were pre-treated with FTY720 (229). Moreover, *in vitro* analysis of T cells from both CD11a^{-/-} and CD18^{-/-} mice have shown that these cells are defective in their ability to undergo activation under conditions requiring cell-cell interactions with an APC (286, 287).

Central to the induction of protective immunity against infection is the fundamental ability of DCs to functionally activate and induce the clonal expansion and differentiation of antigen specific CD4⁺ T cells *in vivo*. However, prolonged DC-T cell contact is thought to precede productive T cell activation and to be necessary for the induction of clonal expansion and differentiation (209, 235). Thus, what effect a reduction in long-term stable contacts between DCs and T cells had on the ability of DCs to induce T cell priming was next investigated by designing an *in vitro* assay to assess T cell proliferation and cytokine production. Previous studies demonstrated that by mutating LFA-1 into a constitutively active form and preventing its normal function, CD4⁺ T cell expansion and subsequent function were impaired *in vivo* (243). Thus, the data presented in this chapter was consistent with the literature, since interfering with LFA-1 function using an LFA-1 blocking Ab, compared to an isotype control Ab, significantly reduced antigen specific T cell proliferation *in vitro*. Moreover, this was further reflected in a significant reduction in pro-inflammatory cytokine output following treatment with an LFA-1 blocking Ab. In contrast, the production

of the Th2 cytokine, IL5, was significantly increased and this was consistent with previous reports that blocking LFA-1 can give rise to a significant increase in the production of Th2 type cytokines (288). However, unlike LFA-1, published data on the effect of FTY720 treatment on DC-T cell interactions is limited and how this drug modulates their ability to interact is not yet characterised. Pre-treatment of DCs with FTY720, compared to the DMSO control, also significantly impaired their ability to induce antigen specific T cell proliferation and production of the proliferation enhancing cytokine, IL2. Moreover, pre-treatment of DCs with FTY720 impaired their production of the pro-inflammatory cytokine IL12. FTY720 has been previously shown not to modulate antigen presentation by DCs and in this chapter the activation status of the DC was shown to be unaffected by the drug (229). However, FTY720 treatment of DCs is known to modulate their migration, endocytosis and regulation of their cytoskeletal proteins (255, 260), yet *in vivo* studies have suggested that FTY720 does not have an ability to modulate the activation of an adaptive immune response (230, 273). Thus, how modulating S1P signalling using FTY720 in turn modulated DC-T cell interactions and T cell proliferation and differentiation *in vitro* was not clear.

A wealth of knowledge of the molecular and physiological aspects of the immune system has been acquired through the use of *in vitro* experimental systems. However, an immune response is the sum of many complex and dynamic cellular interactions that are shaped by environmental factors and *in vivo* experiments that maintain this natural environment were the next logical step to assess and determine the effect of FTY720 and an LFA-1 blocking Ab on DC-T cell interactions (176, 209, 235). Moreover, the impact of FTY720 and an LFA-1 blocking Ab on DC-T cell interactions had never been previously visualised in the physiological environment of the LN. As outlined in chapter 1, the kinetics and dynamics of DC-T cell interactions *in vivo* are critical parameters in determining the outcome of an immune response. In this chapter, MPLSM was the tool used to facilitate these studies by allowing cells and their interactions to be imaged dynamically *in vivo* (194).

FTY720 is an immunosuppressive drug well characterised for its ability to modulate S1P mediated signalling and to block T cell migration from the LN (233, 254, 273). In this chapter the ability of FTY720 to modulate T cell recirculation was observed when mice were either treated systemically with the drug or when T cells were pre-treated with the drug *in*

vitro. A significantly increased number of antigen specific T cells were detected within the DLN when mice were treated systemically, while a significantly decreased number were detected when T cells were pre-treated with the drug *in vitro* prior to their adoptive transfer. However, while the number of T cells within the LN was altered, the proportion of cells that had divided in response to antigen challenge did not differ from controls. FTY720 is a structural analogue of S1P and functions by binding to S1P1 receptors on the surface of T cells, inducing their down-regulation and preventing T cells from exiting the LN in response to S1P signals (233, 254, 259, 289). It is therefore most likely that a significant reduction in the absolute number of CD4⁺KJ⁺ cells within the DLN was observed since T cells pre-treated with FTY720 may have lost their ability to re-circulate evenly between the LNs following their adoptive transfer, by blocking their exit from the first LN they re-circulate in to. Moreover, this may have given rise to an uneven distribution of CD4⁺KJ⁺ cells between the LNs and resulted in a less than control level of CD4⁺KJ⁺ cells in the LN prior to antigen challenge. However, the opposite effect was observed when mice were treated systemically with FTY720 as the absolute number of CD4⁺KJ⁺ cells was significantly increased in comparison with DMSO treated mice. Since the adoptively transferred cells had already had 24 hours to equilibrate between the LNs, FTY720 treatment after immunisation may have prevented the potential exit of any CD4⁺KJ⁺ cells from the LN thus, giving rise to an increase in the overall number of antigen specific cells within the DLN. This explanation is consistent with published reports that show FTY720 treatment accelerates the exit of lymphocytes from the blood to the LNs where they are retained (273, 289).

Pinschewer *et al.* demonstrated that while FTY720 blocked the migration of T cells from the LN, treatment with the drug had no measurable effect on the activation and expansion of cytotoxic CD8⁺ T cells or CD4⁺ T cells in response to viral infection. Moreover, they reported that the humoral immune response was also unimpaired (230, 273). However, more recently it was reported that treatment with FTY720 can impair the humoral response, with the production of high affinity class switched antibodies being significantly reduced in response to T cell dependent antigens (290). Thus, while published data has consistently reported the role of FTY720 in blocking the egress of T cells from the LN, the effect of the drug on cellular interactions within the LN has remained ambiguous. In this chapter, the impact of FTY720 treatment on the interactions between DCs and T cells was imaged

dynamically in the LN. While the migration of T cells out of the LN was affected by treatment with FTY720, the migration of T cells within the LN and their co-localisation with DCs did not appear to be altered following treatment with the drug. The up-regulation of the early activation marker CD69 and down-regulation of CD62L in response to antigen specific stimulation were also both unaltered by treatment with FTY720. Moreover, the inability of FTY720 to alter T cell activation and function was further demonstrated in the cytokine output and differentiation of the cells into Tfh cells, both of which were unchanged. Thus, this data contributes new information to the field by demonstrating a failure of FTY720 to modulate the dynamic DC-T cell interactions within the LN and lends support to previously published data that details a failure of FTY720 to interfere with the generation of an immune response (230, 273).

While the impact of blocking DC-T cell interactions *in vivo* using an LFA-1 blocking Ab has never been directly visualised and assessed using MPLSM, the adoptive transfer of antigen specific LFA-1 defective T cells into wild type recipients revealed a defect in antigen specific T cell priming, cytokine and IgG2a production (291). Moreover, LFA-1 also plays a key role in mediating the migration of T cells and facilitating their re-circulation between secondary lymphoid organs (242, 244). In this chapter, treatment with an LFA-1 blocking Ab *in vivo*, significantly reduced the number of antigen specific T cells within the LN following immunisation (242, 244). It was therefore not possible to separate the effects of the LFA-1 blocking Ab on T cells outwith the LN from its effects on DC-T cell interactions within the LN since the significantly reduced number of T cells within the LN had a substantial impact on the *in vivo* multiphoton imaging studies (244, 292). When imaging an intact LN with MPLSM, the maximal imaging depth of penetration is approximately 200 μm , thus, fluorescently labelled cells must be in abundance throughout the LN to ensure as many as possible can be imaged.

In this chapter, analysis of T cell velocity and their ability to interact with DCs was not possible following treatment with the LFA-1 blocking Ab. However, more sensitive techniques such as flow cytometry were able to establish the effects of the LFA-1 blocking Ab on T cell activation and differentiation. Since prolonged and stable DC-T cell

interactions are thought to be necessary for and to precede these events, measuring T cell responses following treatment with the LFA-1 blocking Ab was used as an indication as to how much of an impact the antibody had had on DC-T cell interactions within the LN. Firstly, the expression of the early activation marker, CD69, on the surface of antigen specific T cells, was unaffected. Secondly, the proportion of cells that had divided in response to antigen challenge was comparable with the proportion of cells that had divided in the isotype control Ab treated mice. Moreover, T cell function did not appear to be impaired following treatment with the LFA-1 blocking Ab *in vivo*. The production of pro-inflammatory cytokines was not significantly affected and there was no increase in the production of the Th2 type cytokine, IL5, as observed in the *in vitro* systems. T cells differentiated and adopted the Tfh cell phenotype to levels comparable with controls. Thus, the results were consistent with the literature with respect to the effect of blocking LFA-1 on T cell re-circulation and entry into LN, however, they were not consistent with respect to the effect of blocking LFA-1 on T cell activation, proliferation and differentiation (242-244, 291, 292). It therefore appeared from the data presented here, that the LFA-1 blocking Ab failed to have any impact on the interactions between DCs and T cells within the LN and it is therefore possible to question whether the Ab penetrated and distributed throughout the LN effectively.

LFA-1 is a key adhesion and signalling molecule known to play an important role in DC-T cell interactions. In contrast, while FTY720 is known to have a significant impact on T cell migration, its role in DC-T cell interactions is less well characterised. This chapter has described the design of novel *in vitro* systems for analysis of DC-T cell interactions and has outlined the ability of FTY720 and an LFA-1 blocking Ab to reduce stable DC-T cell interactions and to modulate T cell proliferation and differentiation. In addition, the impact of FTY720 and the LFA-1 blocking Ab on DC-T cells interactions in the physiological environment of the LN *in vivo*, had never been directly visualised previously. Thus, the next step was to progress the *in vitro* studies to an *in vivo* experimental set up. However, the results did not mirror those obtained from the *in vitro* systems and the results of this chapter revealed an inability of these molecules to modulate DC-T cell interactions *in vivo* or to alter T cell proliferation and differentiation. Moreover, this contrasting set of results served to emphasise the importance of *in vivo* experimentation. While *in vitro* work offers a cheaper,

faster and easier alternative to *in vivo* work, it does not accurately represent the physiological environment of the immune system and results are therefore often misleading.

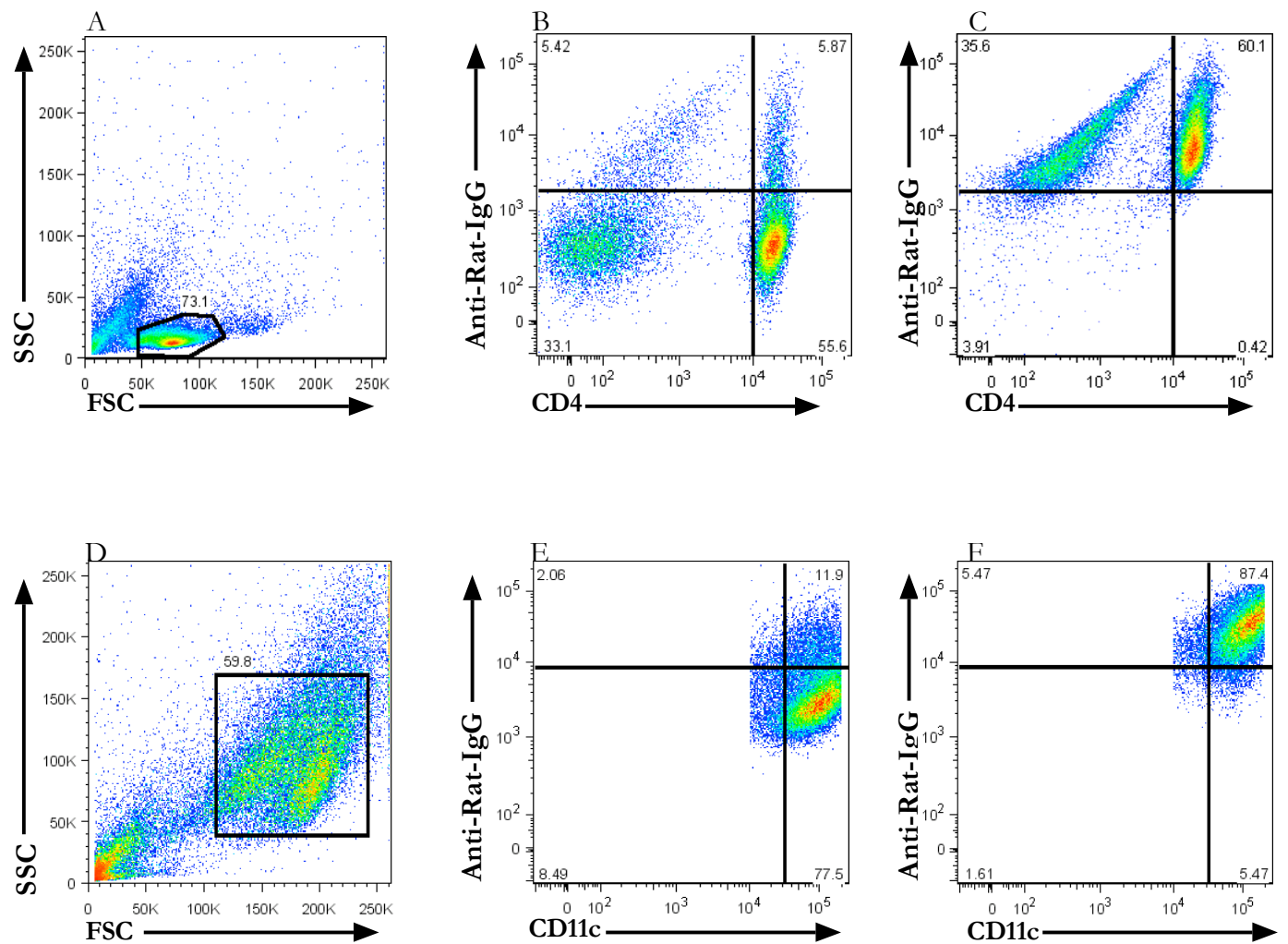


Figure 3.1. LFA-1 blocking Ab can bind to, and be detected on, the cell surface of LFA-1 expressing DCs and T cells

CD11c⁺ DCs and CD4⁺ T cells were incubated with the LFA-1 blocking Ab or with an isotype control Ab, followed by an anti-rat-IgG-FITC secondary Ab to detect specific binding of the LFA-1 blocking Ab to cell surface LFA-1. (A) Lymphocytes identified on basis of size and granularity (B) CD4⁺ T cells incubated with an isotype control Ab followed by anti-rat-IgG-FITC (C) CD4⁺ T cells incubated with the LFA-1 blocking Ab followed by anti-rat IgG FITC (D) Dendritic cells identified on basis of size and granularity (E) CD11c⁺ DCs incubated with an isotype control Ab followed by anti-rat-IgG-FITC (F) CD11⁺ DCs incubated with an LFA-1 blocking Ab followed by anti-rat-IgG-FITC

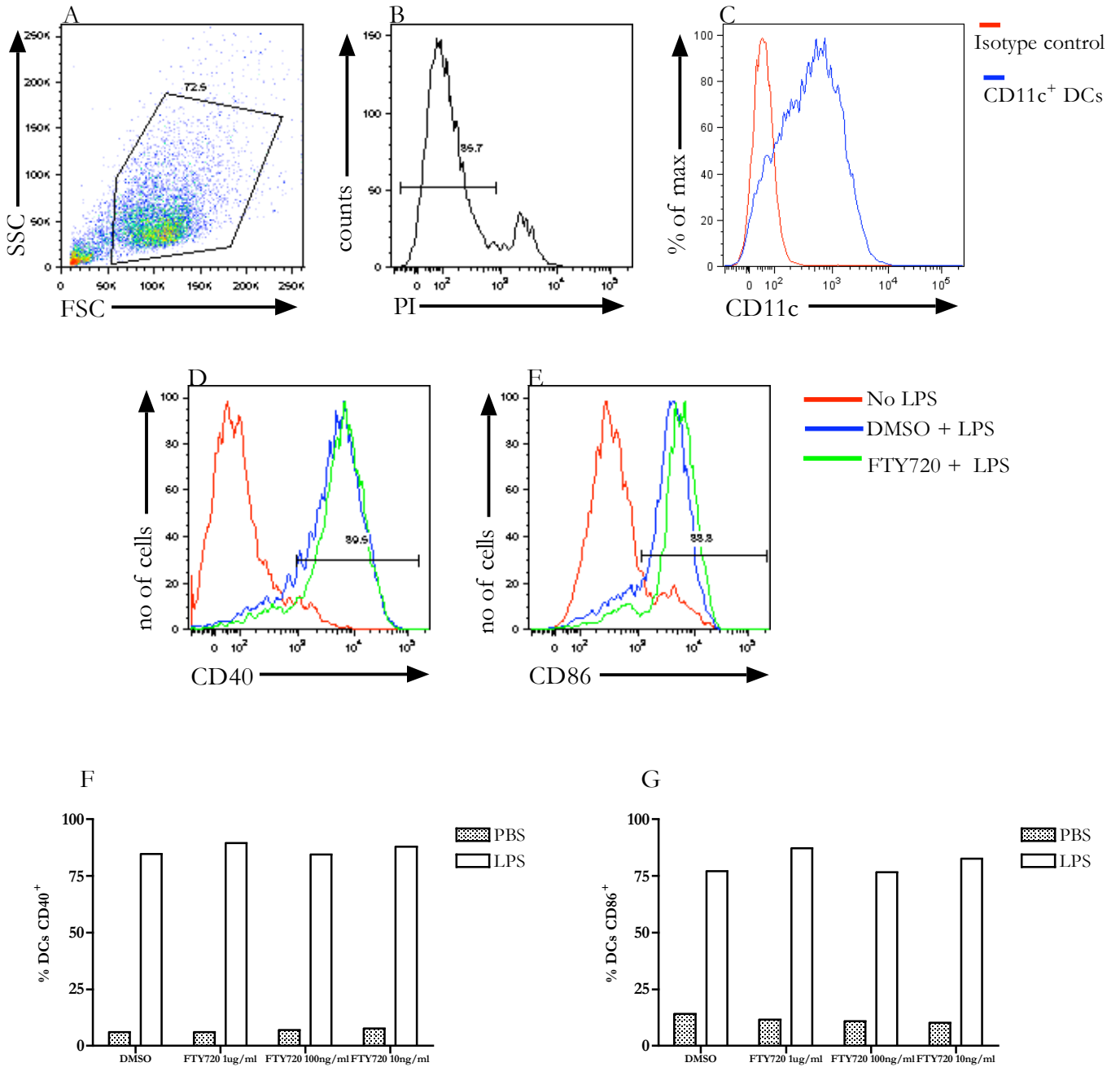


Figure 3.2. FTY720 does not inhibit DC activation in response to LPS

Bone marrow derived DCs were incubated with LPS following 24 hours pre-treatment with increasing concentrations of FTY720. DCs were gated on basis of (A) size and granularity (B) live cells/propidium iodide -ve (C) CD11c expression. (D) Representative plot demonstrates CD40 expression on CD11c⁺ DCs following treatment with FTY720 or the DMSO carrier control and stimulation with LPS (E) Representative plot demonstrates CD86 expression on CD11c⁺ DCs following treatment with FTY720 or the DMSO carrier control and stimulation with LPS (F) Graph summaries the fraction of CD11c DCs which were positive for the expression of the activation marker CD40 following pretreatment with FTY720, followed by LPS stimulation (G) Graph summarises the fraction of CD11c DCs which were positive for the expression of the activation marker CD86 following pretreatment with FTY720, followed by LPS stimulation

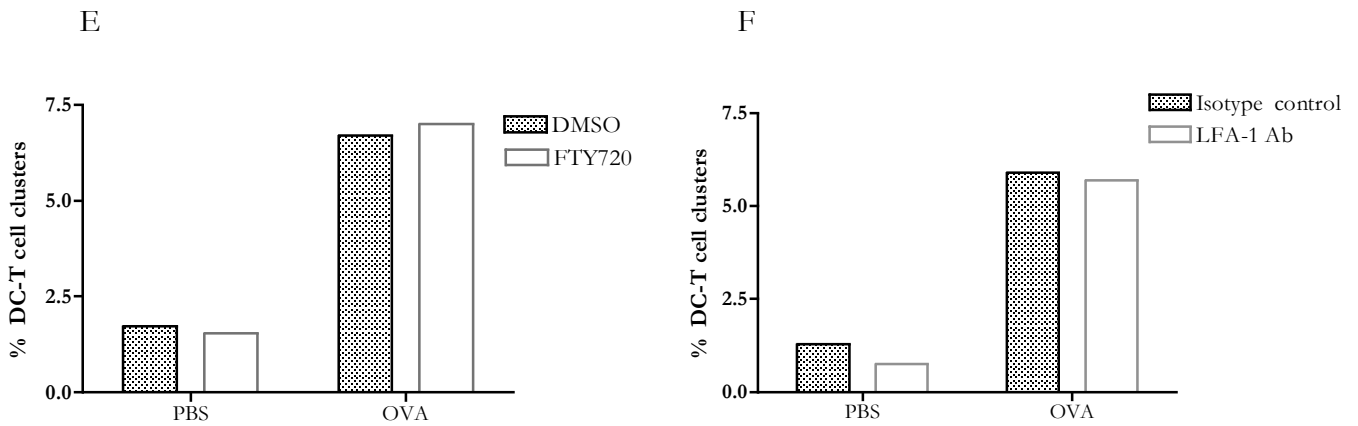
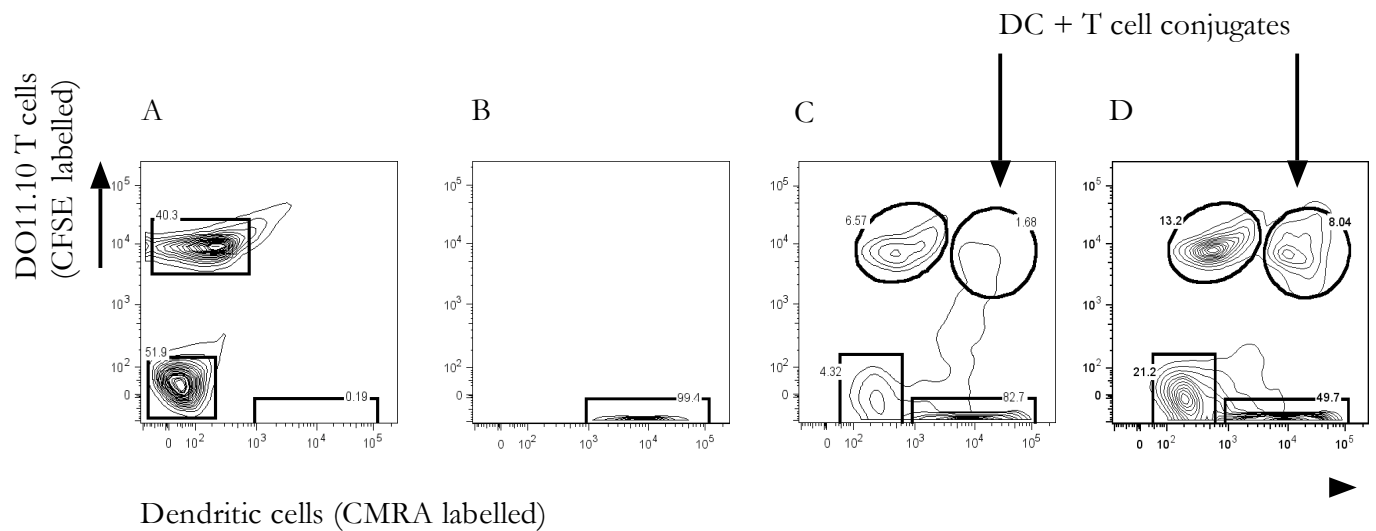


Figure 3.3. FTY720 and an LFA-1 blocking Ab fail to block DC-T cell conjugates when investigated statically *in vitro*

Representative plots identify (A) CFSE labelled DO11.10 T cells and a population of unlabelled T cells of irrelevant specificities. (B) CMRA labelled bone marrow derived DCs (C) Gates identify the 3 populations highlighted in plots A + B and the arrow indicates the double positive DC-T cell conjugates detected in the absence of antigen (D) Arrow identifies double positive DC-T cell conjugates in the presence of antigen. Graphs summarise the results of conjugation assay in which (E) FTY720 or an (F) LFA-1 blocking Ab were used to block DC-T cell clusters. Neither FTY720 pre-treatment of DCs nor the LFA-1 blocking Ab substantially reduced the % of DC-T cell clusters at 20 hours

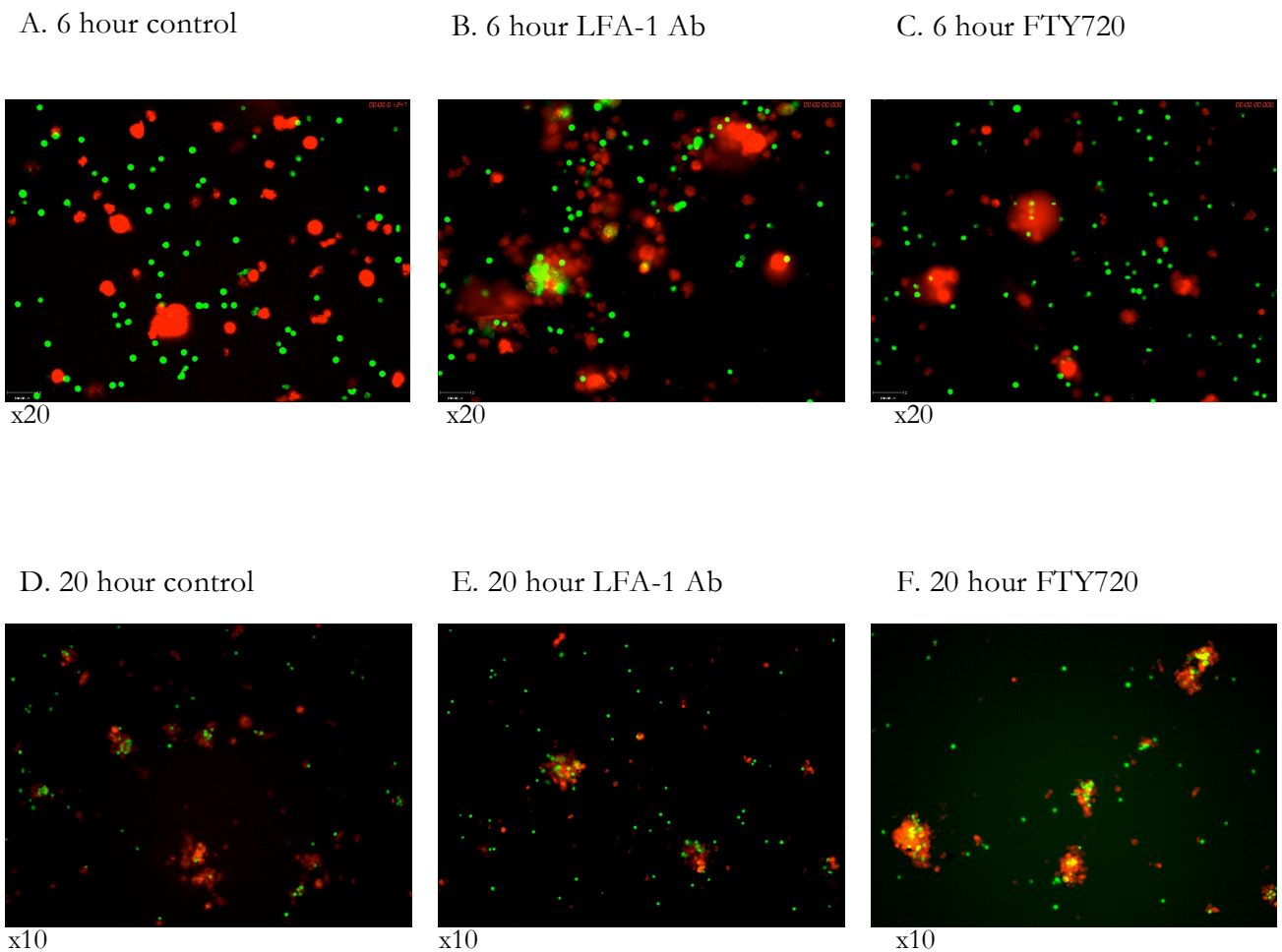


Figure 3.4 Interactions between OVA pulsed DCs (red) and DO11.10 T cells (green) were imaged at 6 and 20 hours post co-culture following treatment with either FTY720 or an LFA-1 blocking Ab

Red CMTPX labelled DCs and green CFSE labelled DO11.10 T cells were co-cultured *in vitro* for a period of 6 or 20 hours. Interactions between the cells were imaged for 30 minute periods using epi-fluorescence microscopy. Snapshots of the resulting *in vitro* movies are shown above. The effect of using an LFA-1 blocking Ab and FTY720 pre-treatment of DCs on the ability of cells to interact was examined. (A) 6 hour control culture (B) 6 hour LFA-1 blocking Ab treated culture (C) 6 hour FTY720 treated culture (D) 20 hour control culture (E) 20 hour LFA-1 blocking Ab treated culture (F) 20 hour FTY720 treated culture

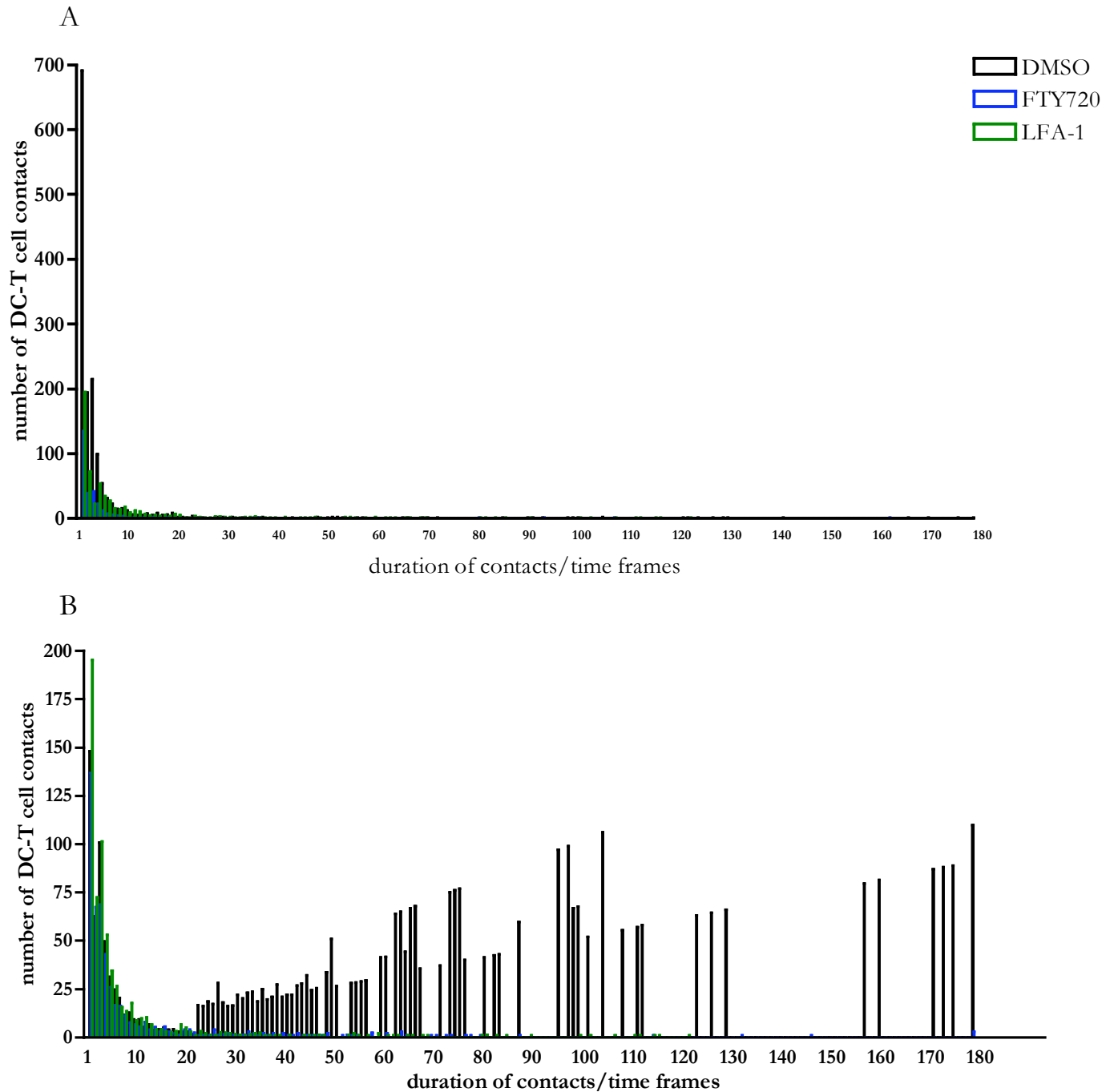


Figure 3.5 FTY720 and an LFA-1 blocking Ab reduce the number of stable DC-T cell contacts at 20hours

Interactions between OVA pulsed DCs and DO11.10 T cells were imaged using epi-fluorescent microscopy at 6 and 20 hours post co-culture of the cells for a period of 30 minutes. Interactions were measured by calculating the number and duration of intersecting fluorescent green (T cells) and red (DCs) fluorescent objects as described in Materials and Methods.(A) Number and duration of DC-T cell interactions at 6 hours post co-culture (B) Number and duration of DC-T cell interactions at 20 hours post co-culture.

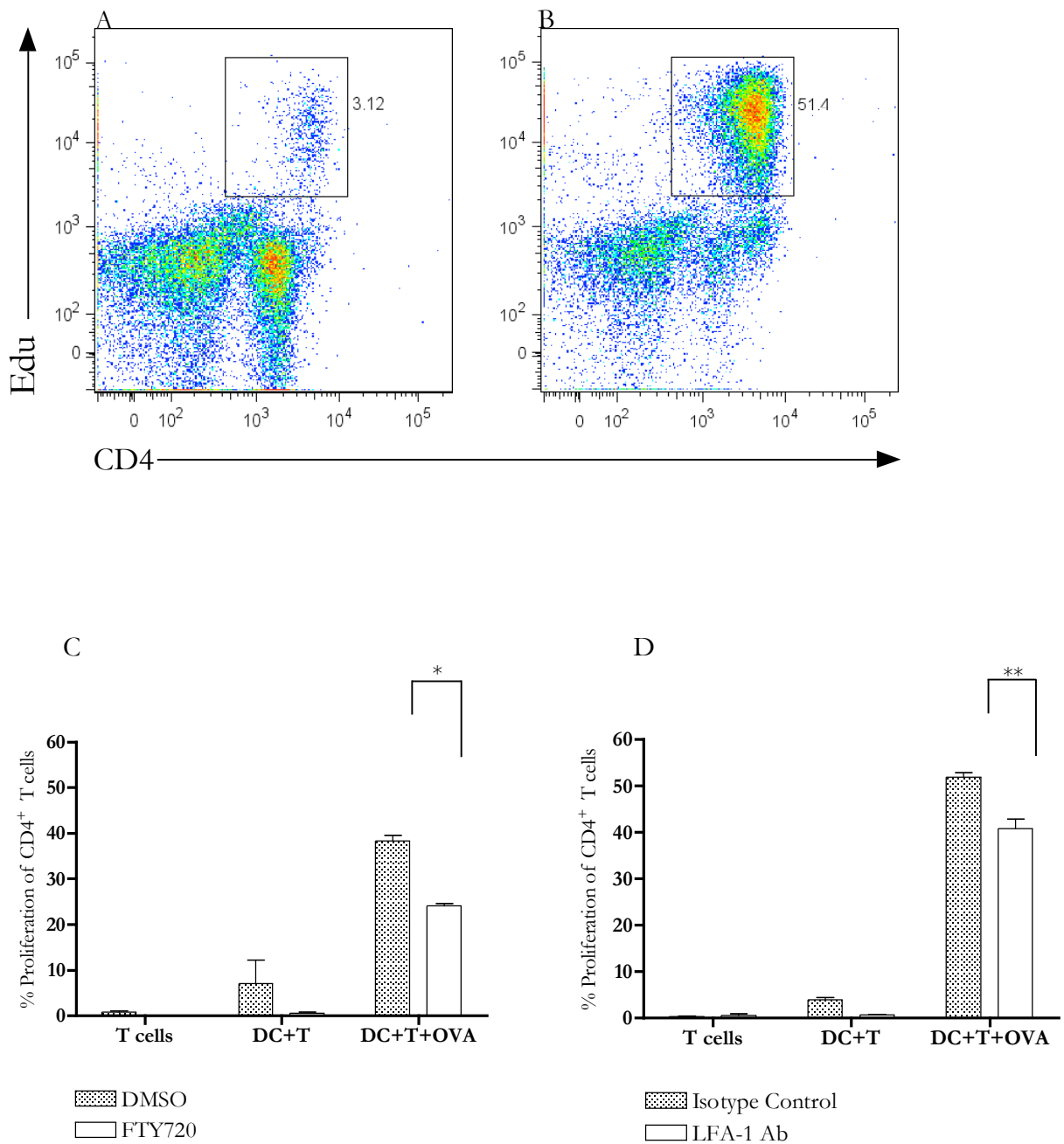


Figure 3.6. Treatment of DCs with FTY720 or an LFA-1 blocking Ab significantly reduced antigen specific CD4⁺ T cell proliferation

CD4⁺ T cell proliferation was measured as a level of Edu incorporation. Representative flow cytometric plots identify a population of (A) CD4⁺ cells stained for Edu following stimulation with non antigen pulsed control DCs (B) CD4⁺ cells stained for Edu following stimulation with antigen pulsed DCs (C) FTY720 significantly reduces antigen specific CD4⁺ T cell proliferation (*p=0.0004) (D) An LFA-1 blocking Ab significantly reduced antigen specific CD4⁺ T cell proliferation (**p=0.0073).

Results show the mean of triplicate samples \pm s.d.

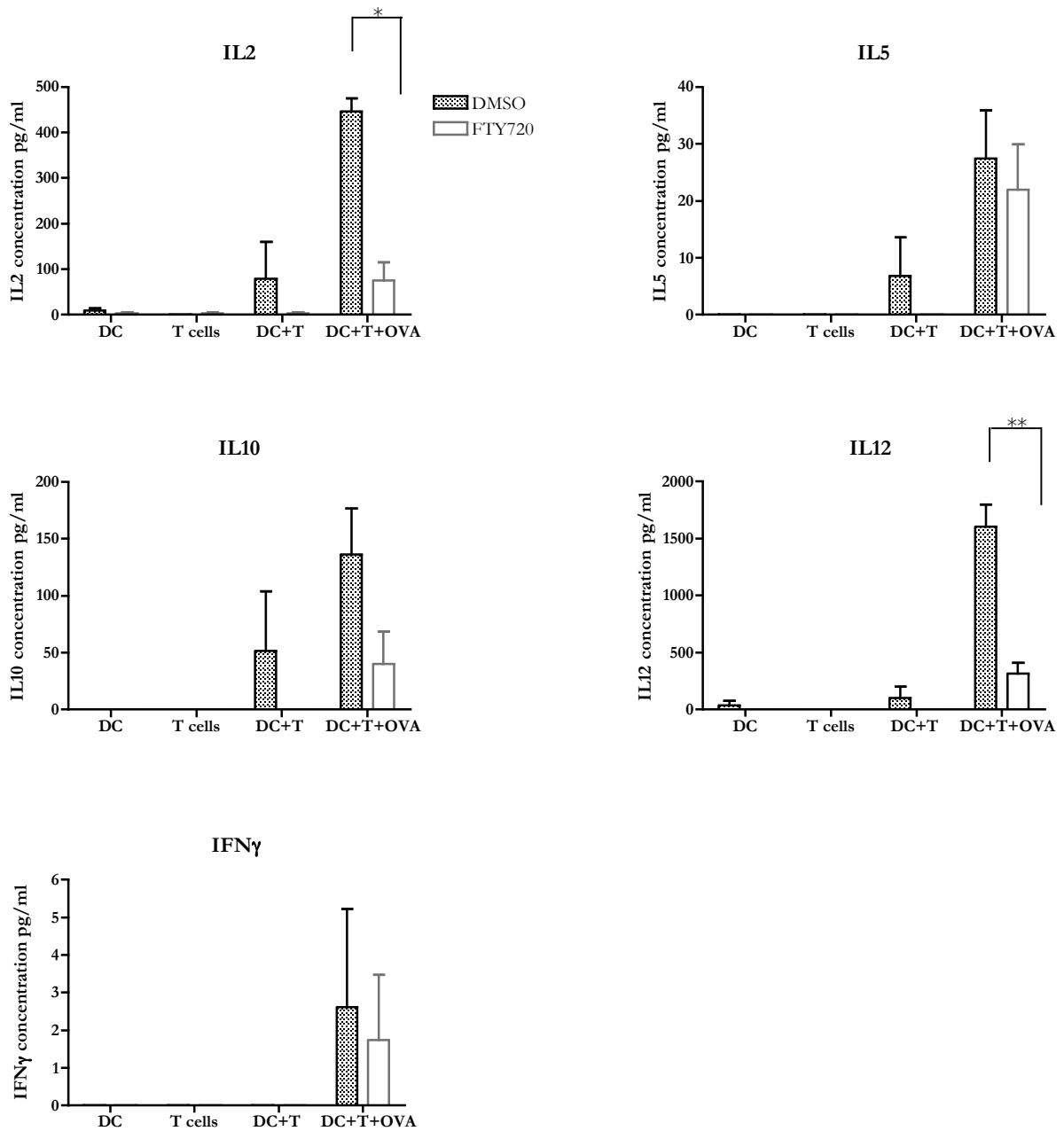


Figure 3.7. FTY720 significantly inhibits the production of IL2 and IL12 from antigen stimulated DC-T cell co-cultures

72 hours following the co-culture of DO11.10 T cells with OVA pulsed DCs that had been either treated with DMSO carrier control or FTY720, supernatants were analysed for the presence of the pro-inflammatory cytokines. Pre-treatment of DCs with FTY720 compared to DMSO did not significantly impair the production of IL5, IL10 and IFN γ , but did significantly reduce the production of IL2 (* $p=0.0016$) by T cells and IL12 (** $p=0.0042$) by DCs.

Results show the mean of triplicate samples \pm s.d.

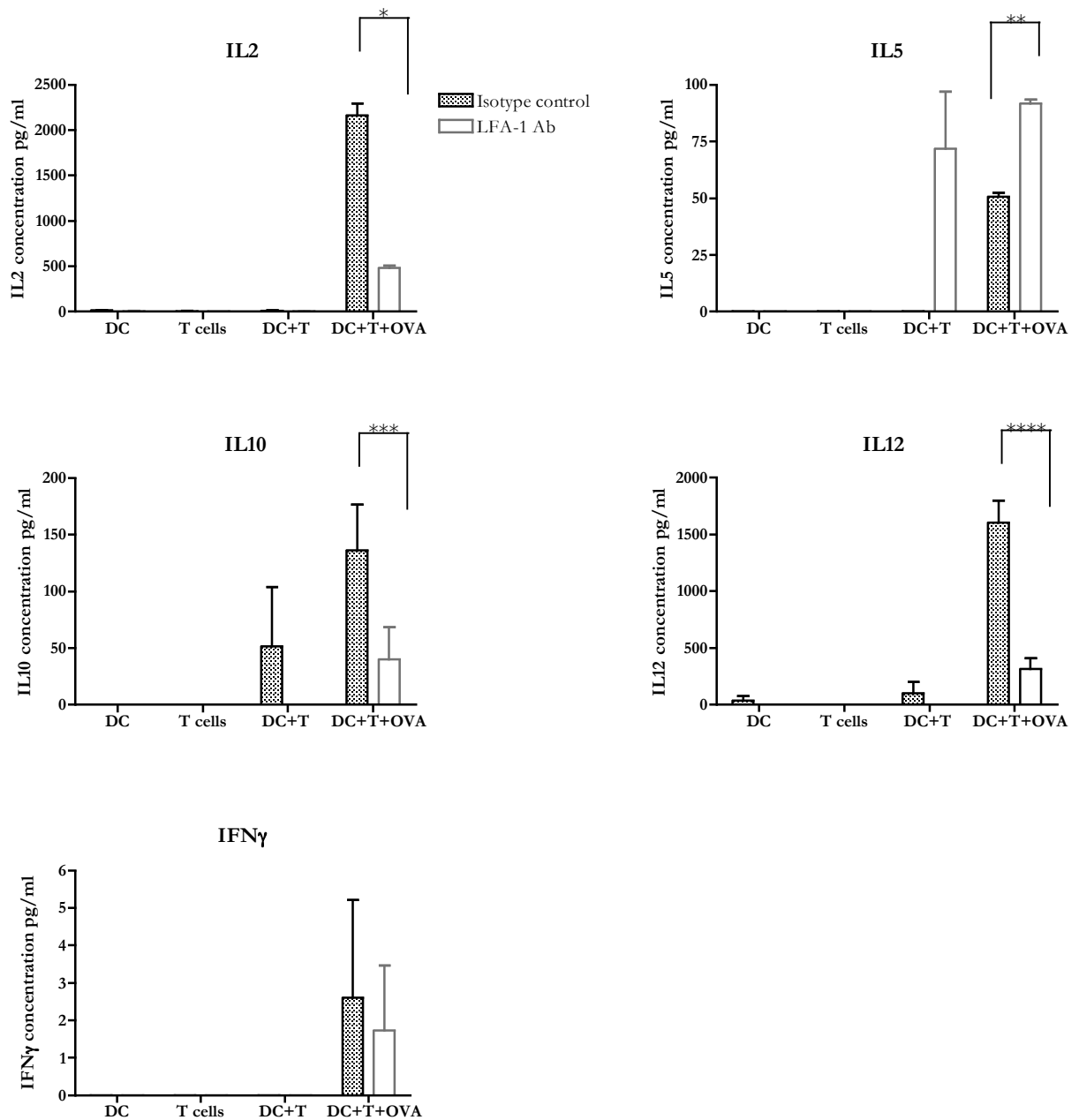


Figure 3.8 LFA-1 blocking Ab significantly inhibits the antigen specific production of cytokines from DC- T cell co-cultures

72 hours following the co-culture of DO11.10 T cells with OVA pulsed DCs in the presence of either an LFA-1 blocking Ab or an isotype control ab, supernatants were analysed for the presence of the pro-inflammatory cytokines. In comparison to isotype control treated cultures, production of IL5 was significantly increased by the presence of the LFA-1 blocking Ab (**p=0.0001). The production of IL2 (*p=0.0002) and IL10 (***p=0.0003) by T cells and IL12 (****p=0.0002) by DCs was significantly impaired following treatment with an LFA-1 blocking ab, while the production of IFN γ was not significantly affected. Results show the mean of triplicate samples \pm s.d.

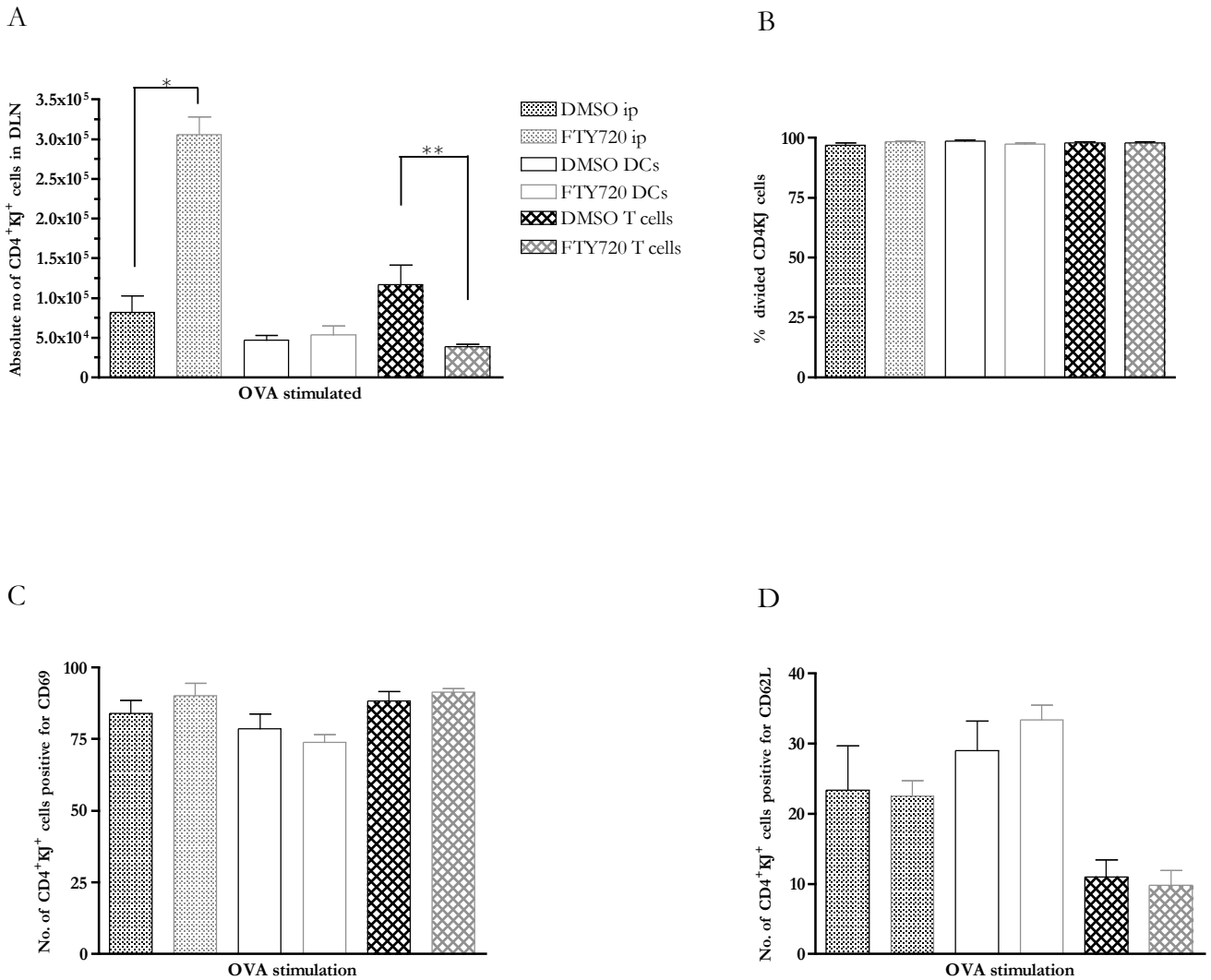


Figure 3.12 The effect of FTY720 treatment on antigen specific proliferation, the up-regulation of CD69 and down-regulation of CD62L

The DO11.10 adoptive transfer model was used to assess the effect of FTY720 treatment on the ability of DCs and T cells to interact *in vivo*, undergo clonal expansion and upregulation markers of activation (A) 72 hours post immunisation with OVA pulsed DCs, the absolute number of CD4⁺KJ⁺ cells was assessed in the draining popliteal LN. In comparison with control DCs, OVA pulsed DCs significantly increased the number of CD4⁺KJ⁺ cells in the DLN (results not shown). In mice treated with FTY720 systemically compared with DMSO, the absolute number of CD4⁺KJ⁺ cells was significantly increased in response to OVA stimulation (*p=0.002). Pre-treatment of T cells with FTY720 in comparison with DMSO, significantly reduced the absolute number of CD4⁺KJ⁺ cells in response to OVA stimulation (**p=0.0355). (B) Graph summarises the % of CD4⁺KJ⁺ cells that divided in response to OVA stimulation following treatment with FTY720 or DMSO control. CD4⁺KJ⁺ cells were analysed at 20 hours post antigen challenge for (C) % of cells positive for CD69 expression. (D) % of cells positive for CD62L expression. Results show the mean of triplicate samples ± s.d.

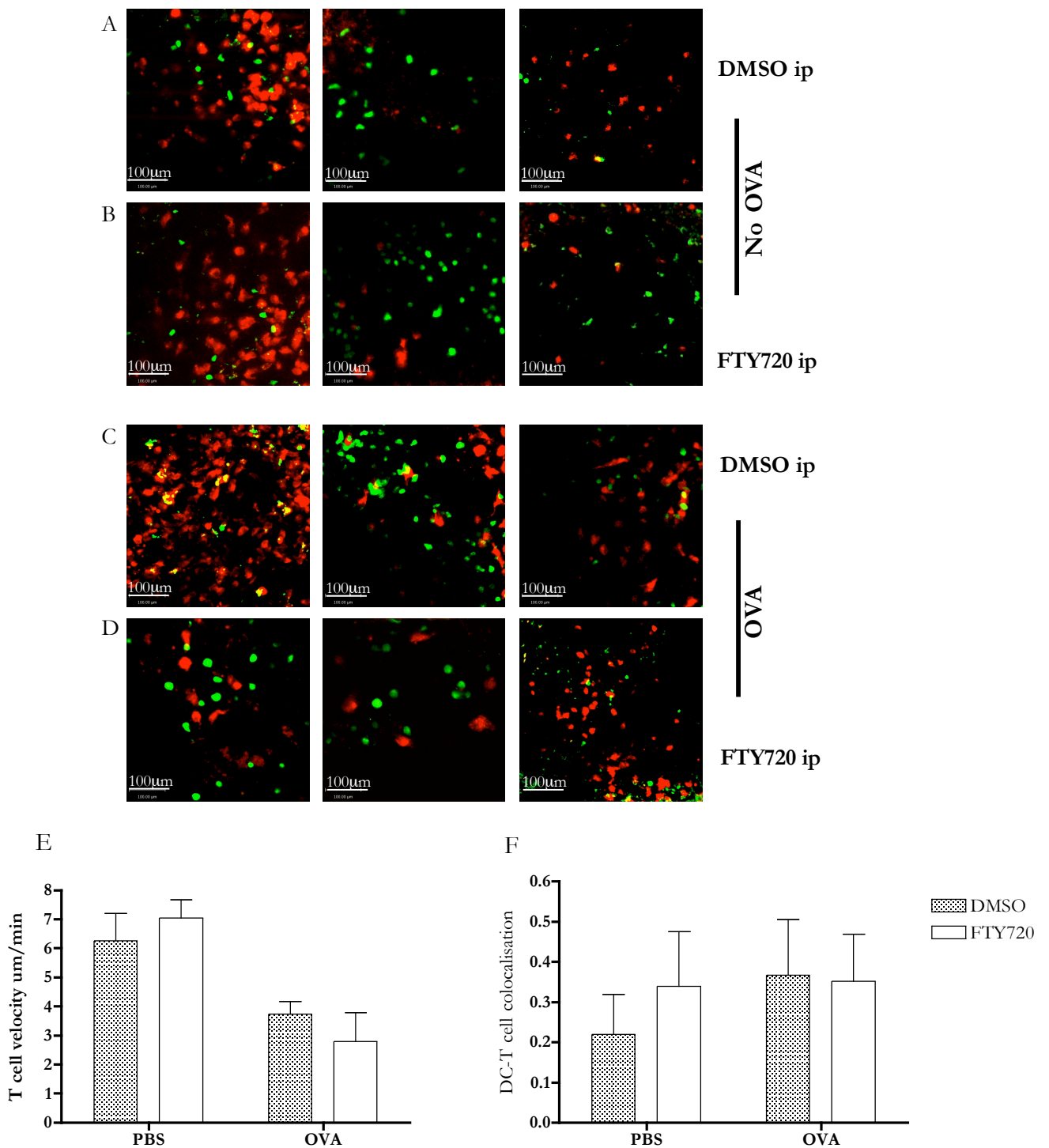


Figure 3.10. Treatment with FTY720 ip does not significantly affect DC-T cell interactions and T cell dynamics within the LN *in vivo*

BALB/c mice were injected with CFSE-labelled DO11.10 T cells (green) and CMTPX-labelled DCs (red) which had been, untreated (A+B) or pulsed with OVA (C+D). Mice were treated with DMSO (A+C) or FTY720 (B+D) ip. Cellular interactions in the draining popliteal LNs were imaged by multiphoton microscopy 20 hours later. Images represent a z-compressed 30 μm stack from a single time point (full sequences available as movies on attached CD. T cell movement was analysed using Volocity software (Improvision) and the (E) mean velocity of T cells calculated (F) DC-T cell interactions were measured by quantifying the colocalisation of green voxels with red to determine the proportion of DC volume in contact with T cells. Data shown are representative of triplicate samples for 2 similar experiments.

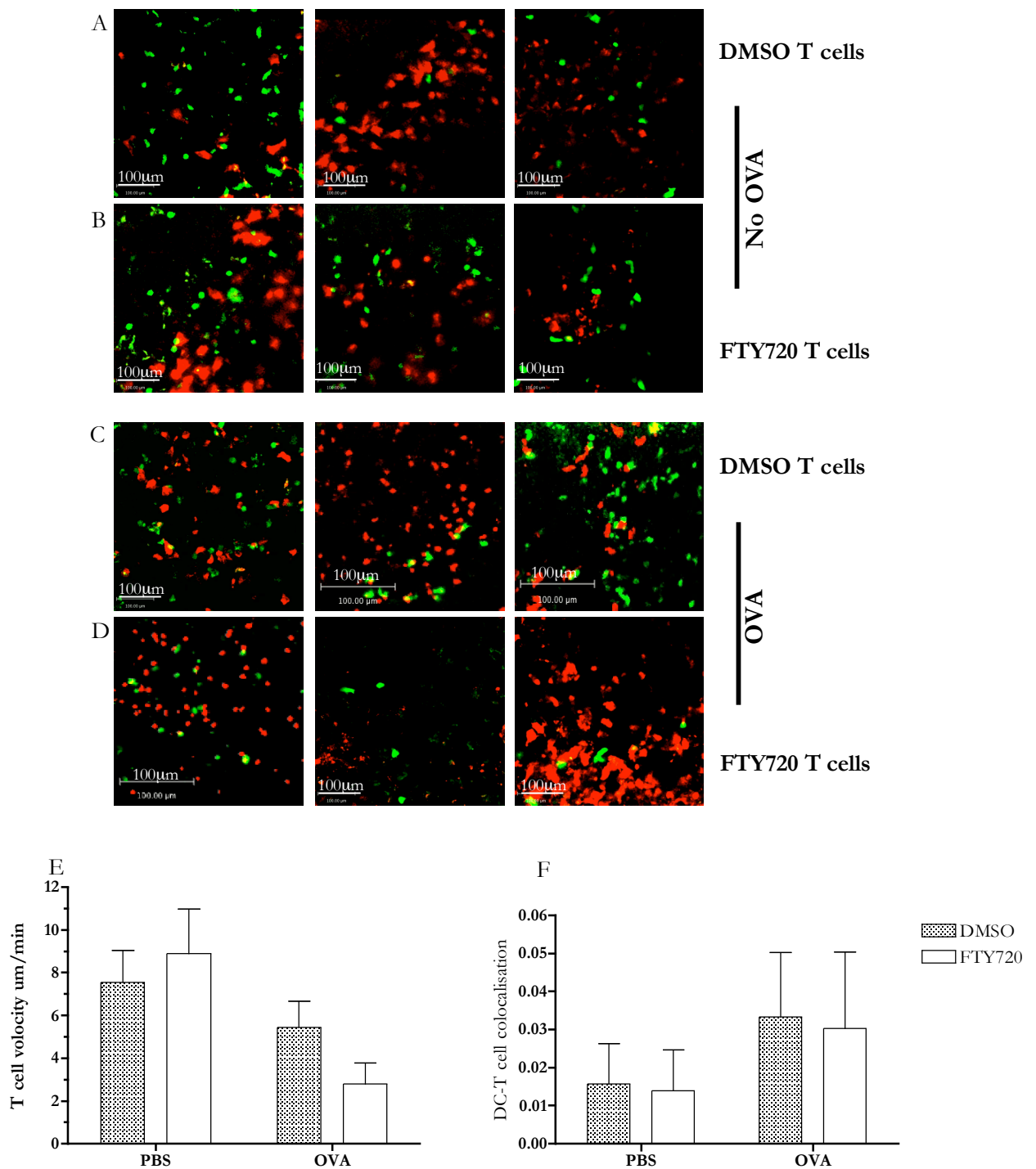


Figure 3.9 Pre-treatment of T cells with FTY720 does not significantly affect DC-T cell interactions and T cell dynamics within the LN *in vivo*

BALB/c mice were injected with CMTPX-labelled DO11.10 T cells (red), which had been treated with DMSO (A+C), treated with FTY720 (B+D) and CFSE-labelled DCs (green) which had been, untreated (A+B) or pulsed with OVA (C+D). Cellular interactions in the draining popliteal LNs were imaged by multiphoton microscopy 20 hours later at x40 magnification. Images represent a z-compressed 300 μm stack from a single time point (full sequences available as movies on attached CD). T cell movement was analysed using Volocity software (Improvision) and the (E) mean velocity of T cells calculated (F) DC-T cell interactions were measured by quantifying the colocalisation of green voxels with red to determine the proportion of DC volume in contact with T cells. Data shown are representative of triplicate samples for 2 similar experiments.

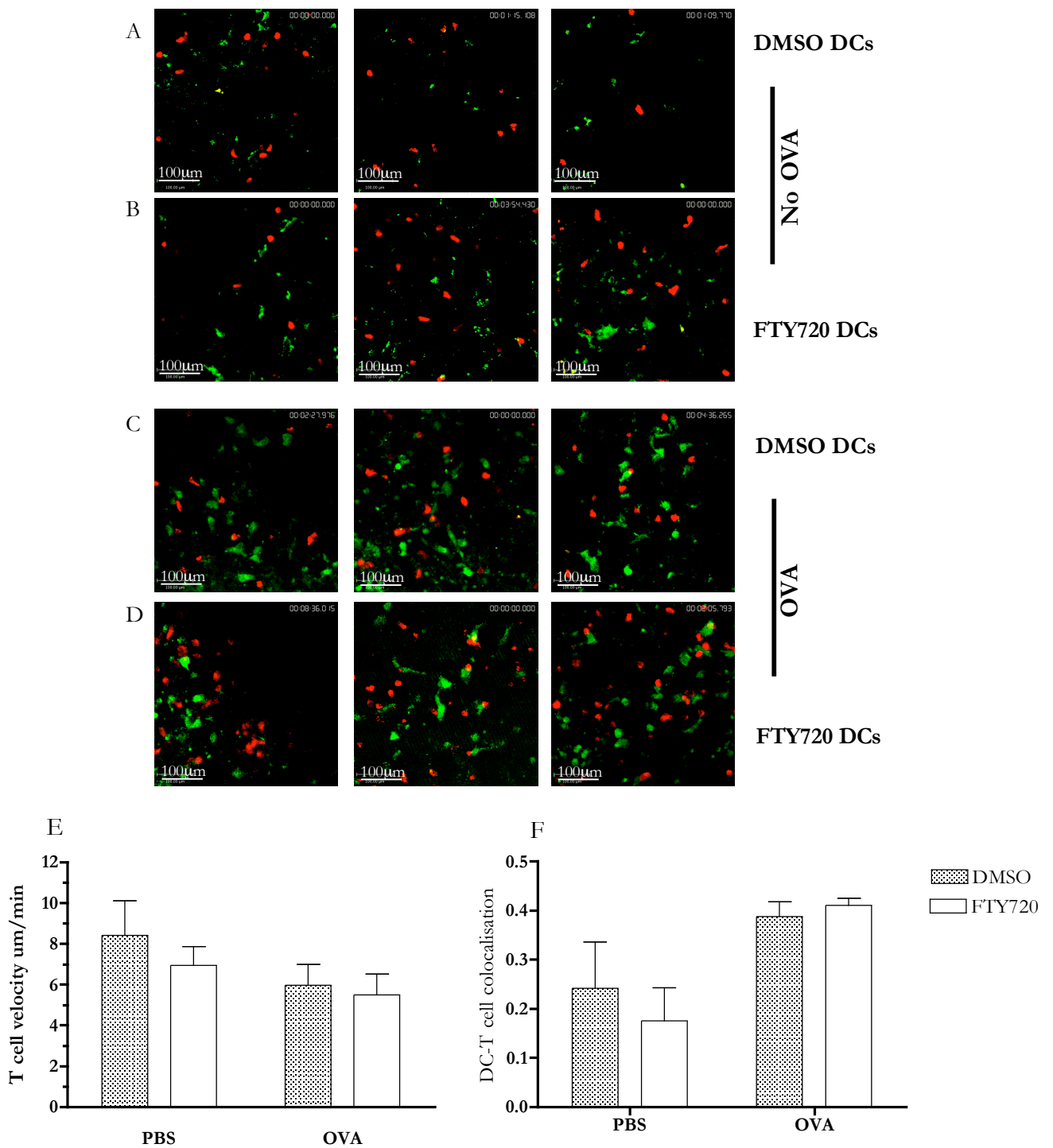


Figure 3.11. Pre-treatment of DCs with FTY720 does not significantly affect DC-T cell interactions and T cell dynamics within the LN in vivo

BALB/c mice were injected with CFSE-labelled DO11.10 T cells (green) and CMTPX-labelled DCs (red) which had been treated with DMSO (A), treated with FTY720 (B), treated with DMSO prior to OVA pulse (C) or treated with FTY720 prior to OVA pulse (D). Cellular interactions in the draining popliteal LNs were imaged by multiphoton microscopy 20 hours later at x40 magnification. Images represent a z-compressed 30µm stack from a single time point (full sequences available as movies on enclosed CD). T cell movement was analysed using Velocity software (Improvision) and the (E) mean velocity of T cells calculated (F) DC-T cell interactions were measured by quantifying the colocalisation of green voxels with red to determine the proportion of DC volume in contact with T cells. Data shown are representative of triplicate samples for 2 similar experiments.

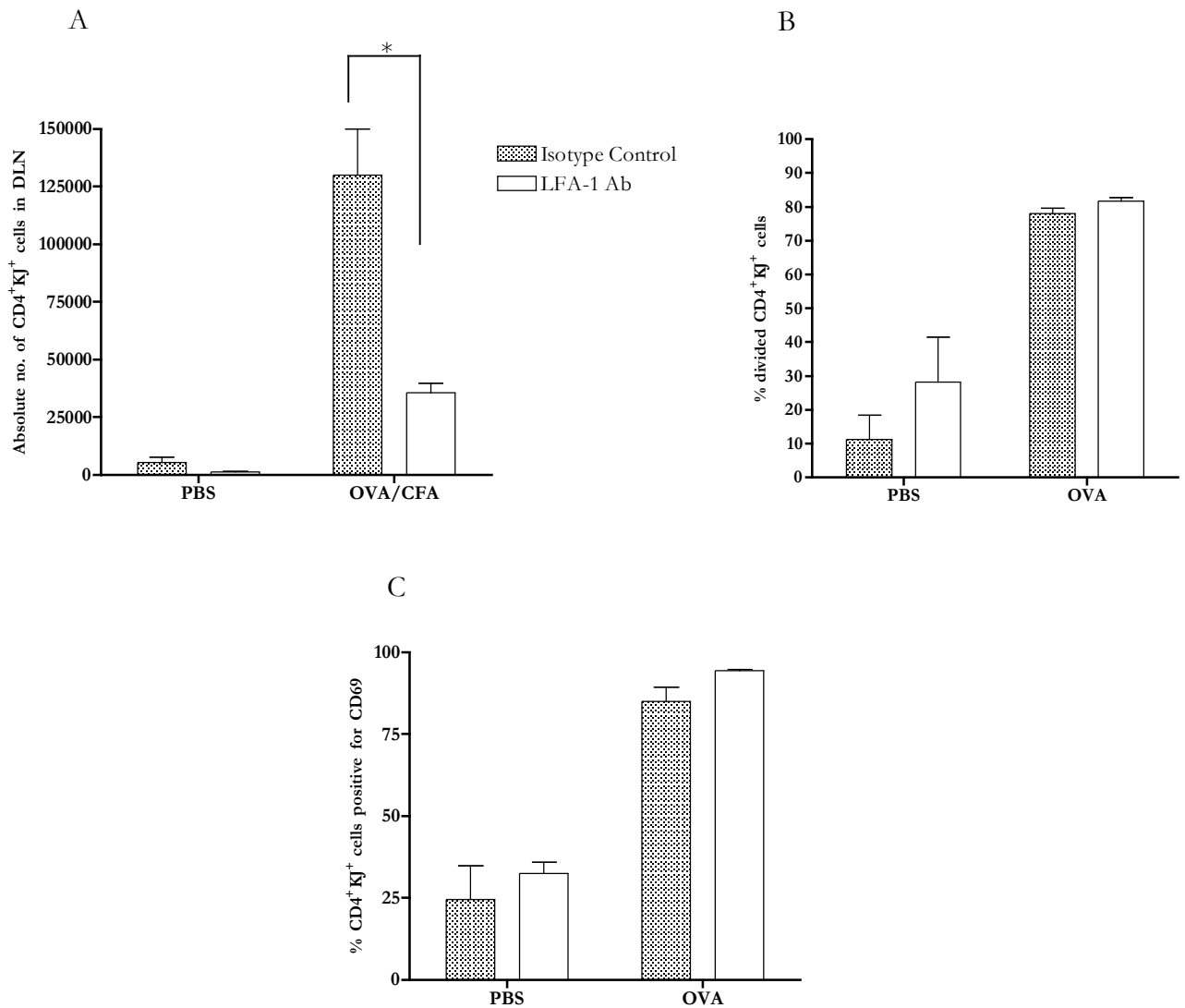


Figure 3.13 The effect of an LFA-1 blocking Ab on antigen specific T cell proliferation and the up-regulation of CD69

Following the adoptive transfer of OVA specific DO11.10 T cells, mice were immunised in the footpad with OVA/CFA and treated with either the LFA-1 blocking Ab or the isotype control ab. DLNs were removed after 72 hours (A) The absolute number of CD4⁺KJ⁺ cells was significantly reduced following treatment with an LFA-1 blocking Ab compared to the isotype control ab (*p=0.0097) (B) The % of CD4⁺KJ⁺ cells in the DLN that divided in response to antigen challenge was not impaired by treatment with an LFA-1 blocking Ab (C) 20 hours post immunisation with OVA pulsed DCs the % of CD4⁺KJ⁺ cells positive for the expression of CD69 was not significantly altered following treatment with an LFA-1 blocking Ab Results show the mean of triplicate samples \pm s.d.

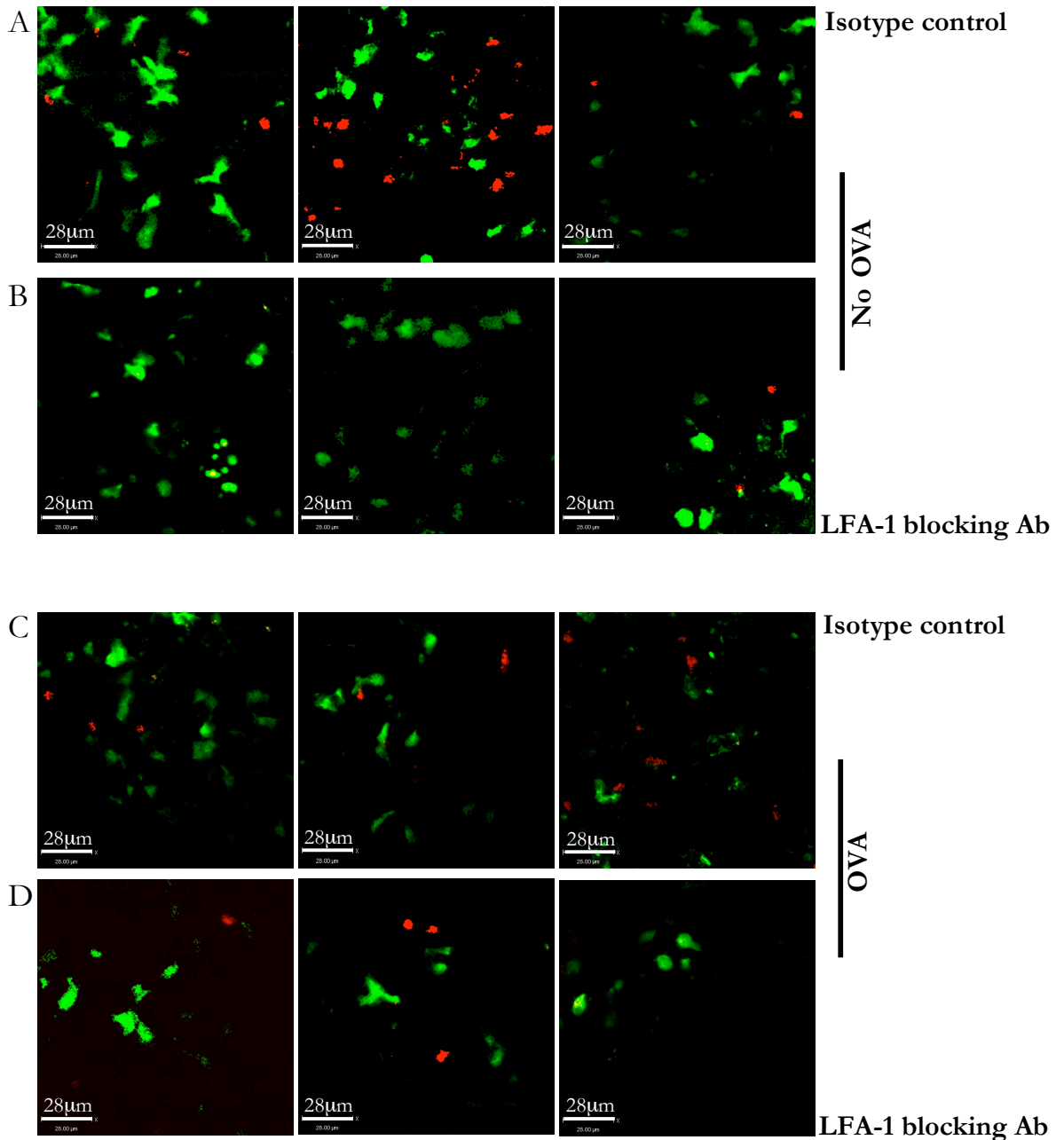
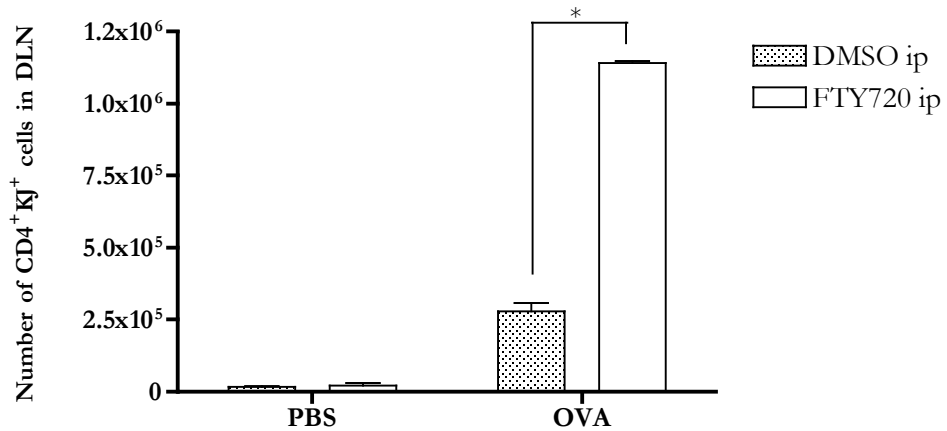


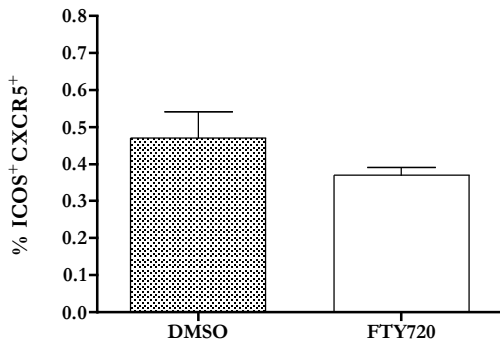
Figure 3.14 Behaviour of DCs (green) and DO11.10 T cells (red) was imaged in the DLN following treatment with an LFA-1 blocking Ab

BALB/c mice were injected with CMTPX-labelled DO11.10 T cells (red) and CFSE-labelled DCs (green) which had been untreated (A+B) or pulsed with OVA (C+D). Mice were treated with an isotype control ab (A+C) or an LFA-1 blocking ab (B+D). Cellular interactions in the draining popliteal LNs were imaged by MPLSM 20 h later at x40 magnification for approximately 30 minutes. Images represent a z-compressed 30-um stack from a single time point (full sequences available as movies on attached CD). Data shown are representative of triplicate samples.

A



B



C

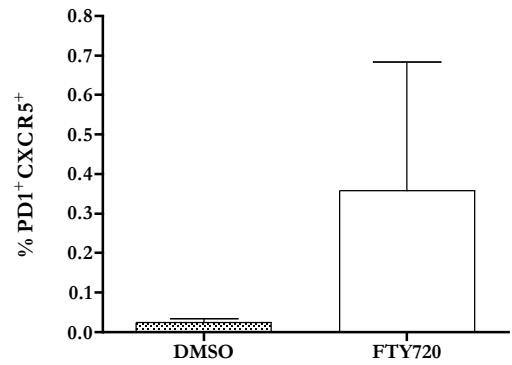


Figure 3.15. Treatment with FTY720 *in vivo* significantly increases the number CD4⁺KJ⁺ cells in the DLN but did not affect the differentiation of T follicular helper cells.

BALB/c mice were injected with DO11.10 T cells, immunised in the footpad with OVA/CFA and treated with either the DMSO or FTY720. After 72 hrs DLNs were removed for flow cytometric analysis of the absolute number of CD4⁺KJ⁺ cells. (A) Compared to DMSO control treatment, FTY720 significantly increased the absolute number of CD4⁺KJ⁺ cells in the DLN following antigen challenge (*p=0.0001). (B) The % of CD4⁺KJ⁺ cells positive for the expression of CXCR5⁺ICOS⁺ (C) The % of CD4⁺KJ⁺ cells positive for the expression of CXCR5⁺PD1⁺ Results show the mean of triplicate samples ± s.d.

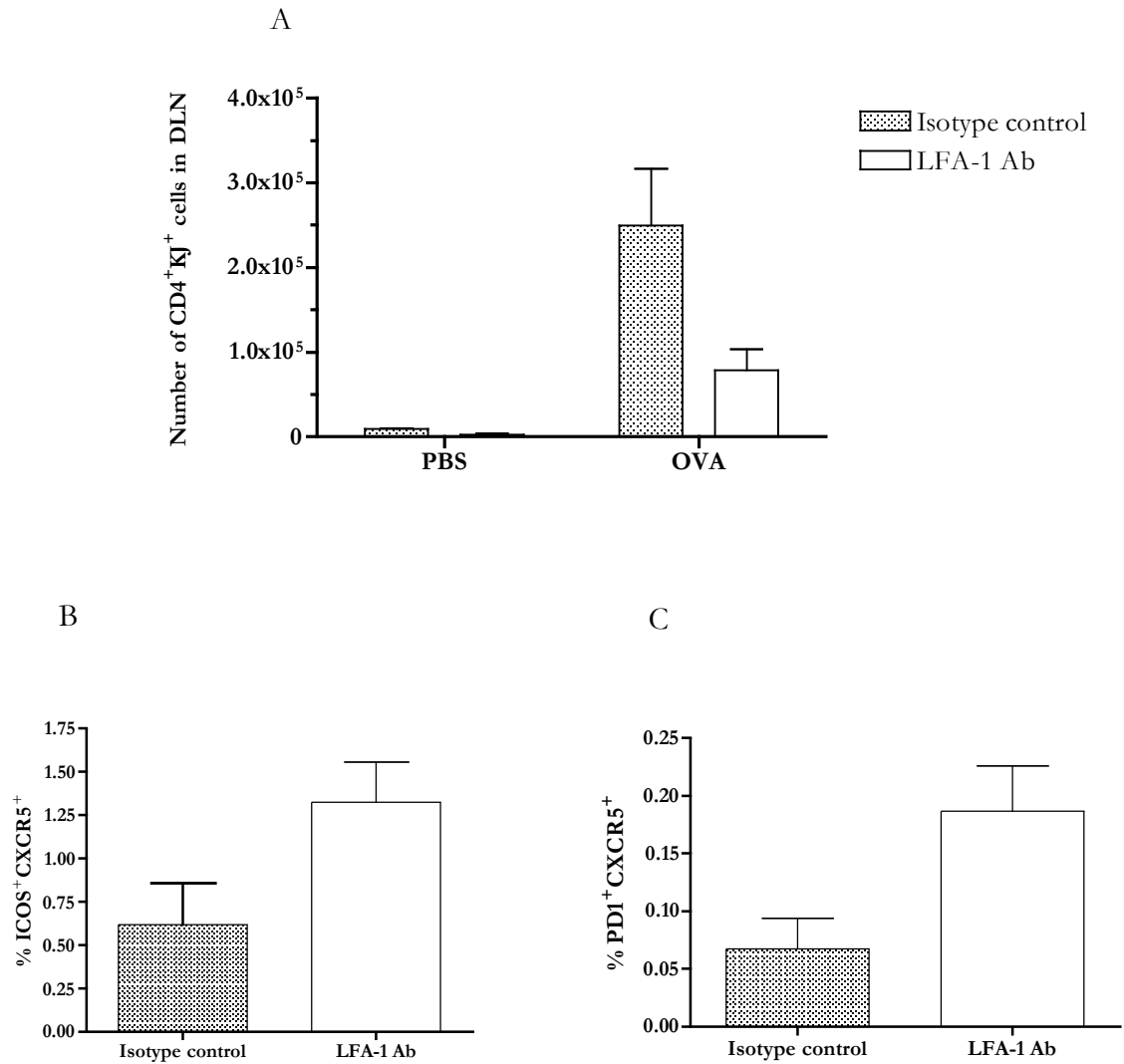


Figure 3.16. Treatment with an LFA-1 blocking Ab *in vivo* reduced the number CD4⁺KJ⁺ cells in the DLN but did not affect the differentiation of T follicular helper cells.

BALB/c mice were injected with DO11.10 T cells, immunised in the footpad with OVA/CFA and treated with either an isotype control ab or an LFA-1 blocking Ab. After 72 hrs DLNs were removed for flow cytometric analysis of the absolute number of (A) CD4⁺KJ⁺ cells (B) The % of CD4⁺KJ⁺ cells positive for the expression of CXCR5⁺ICOS⁺ (C) The % of CD4⁺KJ⁺ cells positive for the expression of CXCR5⁺PD1⁺ Results show the mean of triplicate samples ± s.d.

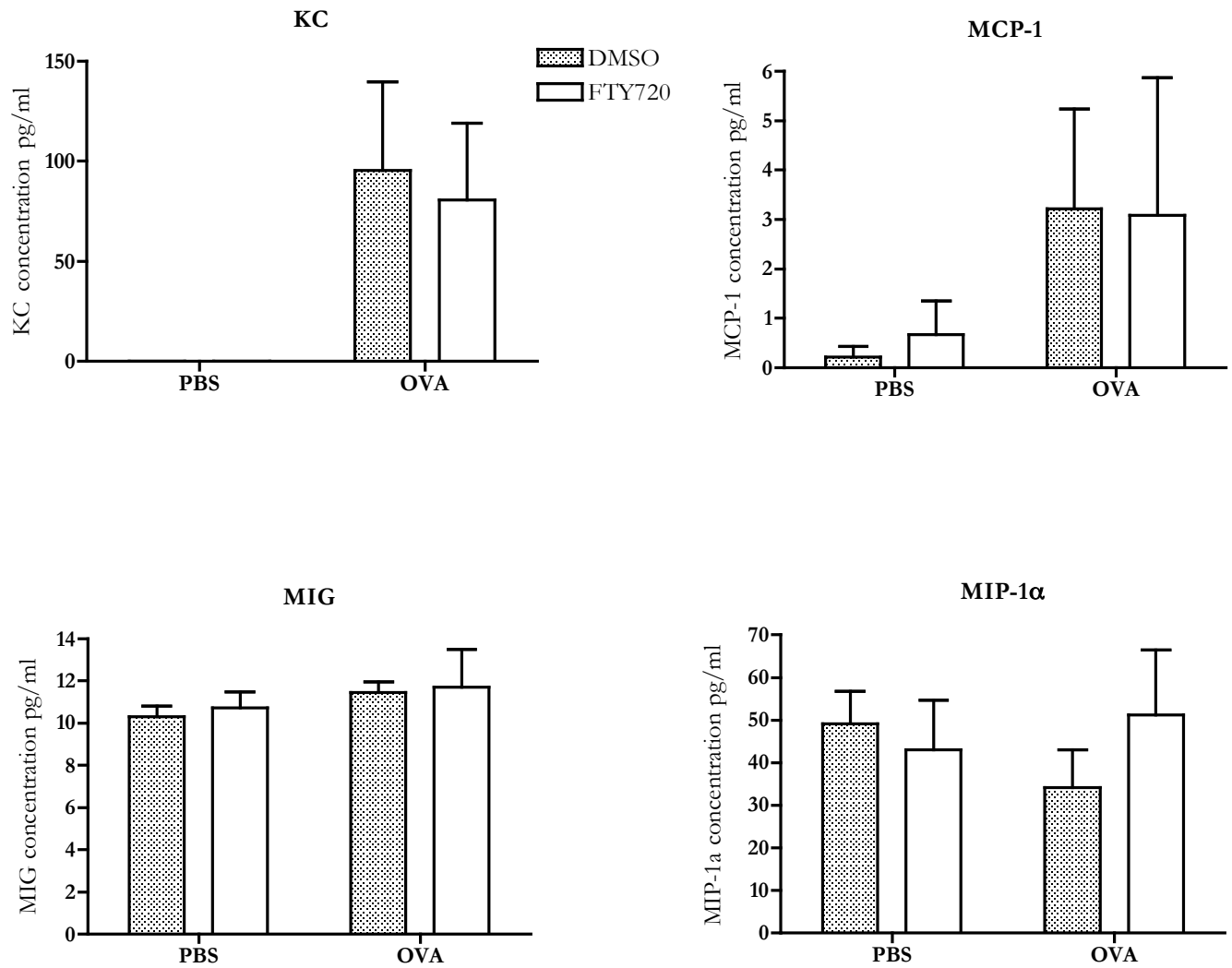


Figure 3.19 The effect of FTY720 treatment on the antigen specific production of pro-inflammatory chemokines

BALB/c mice were injected with DO11.10 T cells, immunised in the footpad with OVA/CFA and treated with either FTY720 or the DMSO control. After 72 hrs DLNs were removed and re-stimulated with antigen *in vitro* for a further 72 hours. Supernatants were analysed for the presence of the pro-inflammatory chemokines, KC, MCP-1, MIG, MIP-1α and treatment with FTY720 failed to significantly alter their production. Results show the mean of triplicate samples \pm s.d.

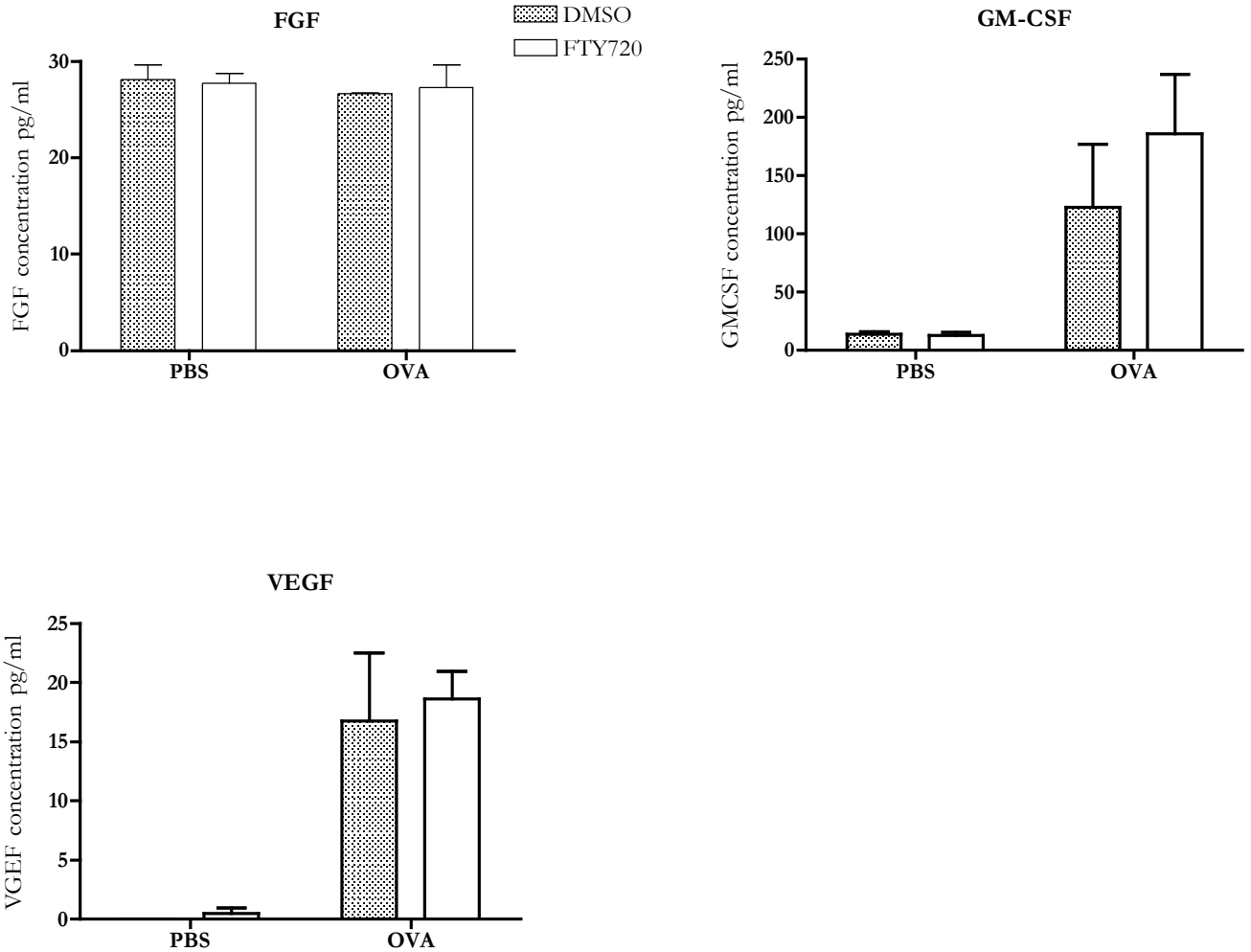


Figure 3.20 The effect of FTY720 treatment on the antigen specific production of growth and repair factors

BALB/c mice were injected with DO11.10 T cells, immunised in the footpad with OVA/CFA and treated with either FTY720 or the DMSO control. After 72 hrs DLNs were removed and re-stimulated with antigen *in vitro* for a further 72 hours. Supernatants were analysed for the presence of the growth and repair factors. Treatment with FTY720 *in vivo* did not result significantly alter the production of FGF, GMCSF or VEGF. Results show the mean of triplicate samples \pm s.d.

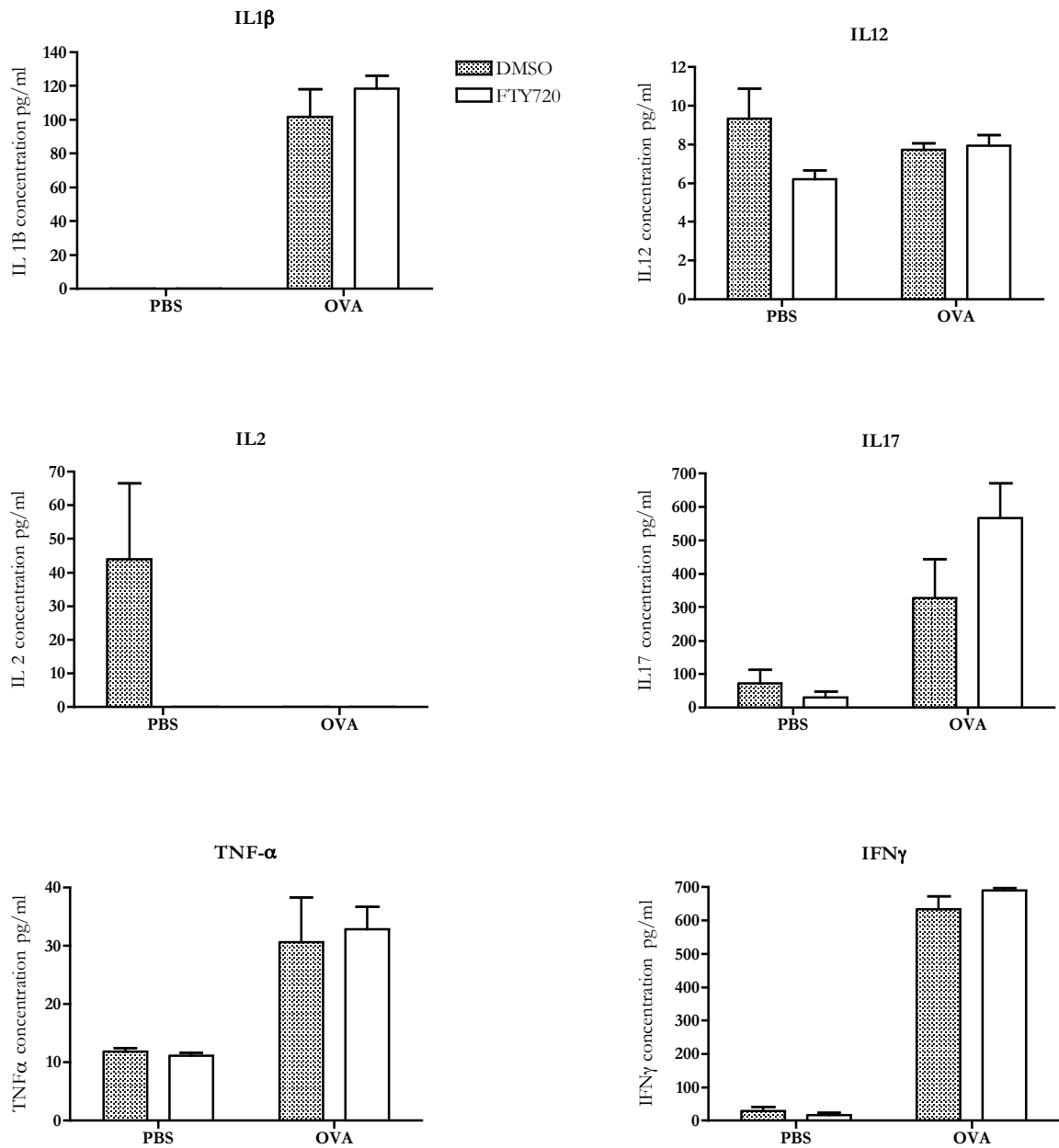


Figure 3.17 The effect of FTY720 treatment on the antigen specific production of Th1 cytokines

BALB/c mice were injected with DO11.10 T cells, immunised in the footpad with OVA/CFA and treated with either FTY720 or the DMSO control. After 72 hrs DLNs were removed and re-stimulated with antigen *in vitro* for a further 72 hours. Supernatants were analysed for the presence of the pro-inflammatory cytokines. Treatment with FTY720 *in vivo* did not significantly alter the production of IL1 β , IL12, IL2, IL17, TNF α , IFN γ .

Results show the mean of triplicate samples \pm s.d.

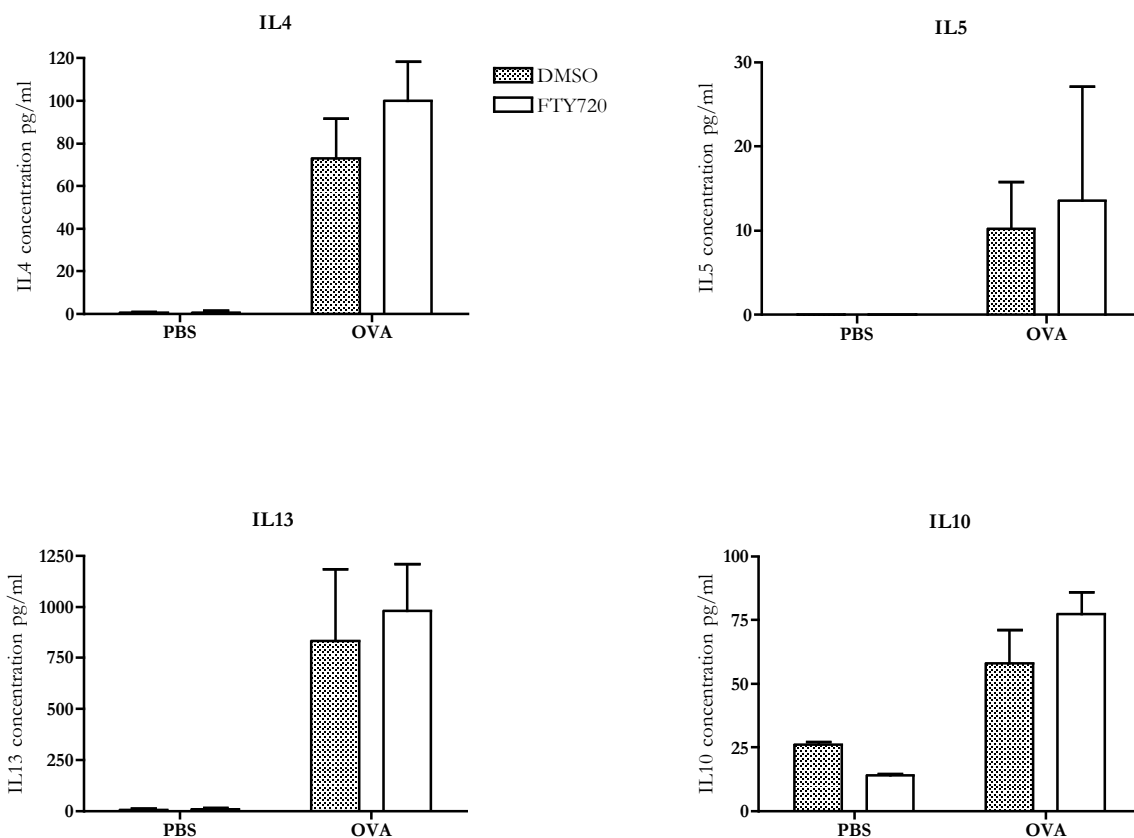


Figure 3.18. The effect of FTY720 treatment on the antigen specific production of Th2 cytokines

BALB/c mice were injected with DO11.10 T cells, immunised in the footpad with OVA/CFA and treated with either FTY720 or the DMSO control. After 72 hrs DLNs were removed and re-stimulated with antigen *in vitro* for a further 72 hours. Supernatants were analysed for the presence of the pro-inflammatory cytokines. Treatment with FTY720 *in vivo* did not significantly alter the production of IL4, IL5, IL13 or IL10. Results show the mean of triplicate samples \pm s.d.

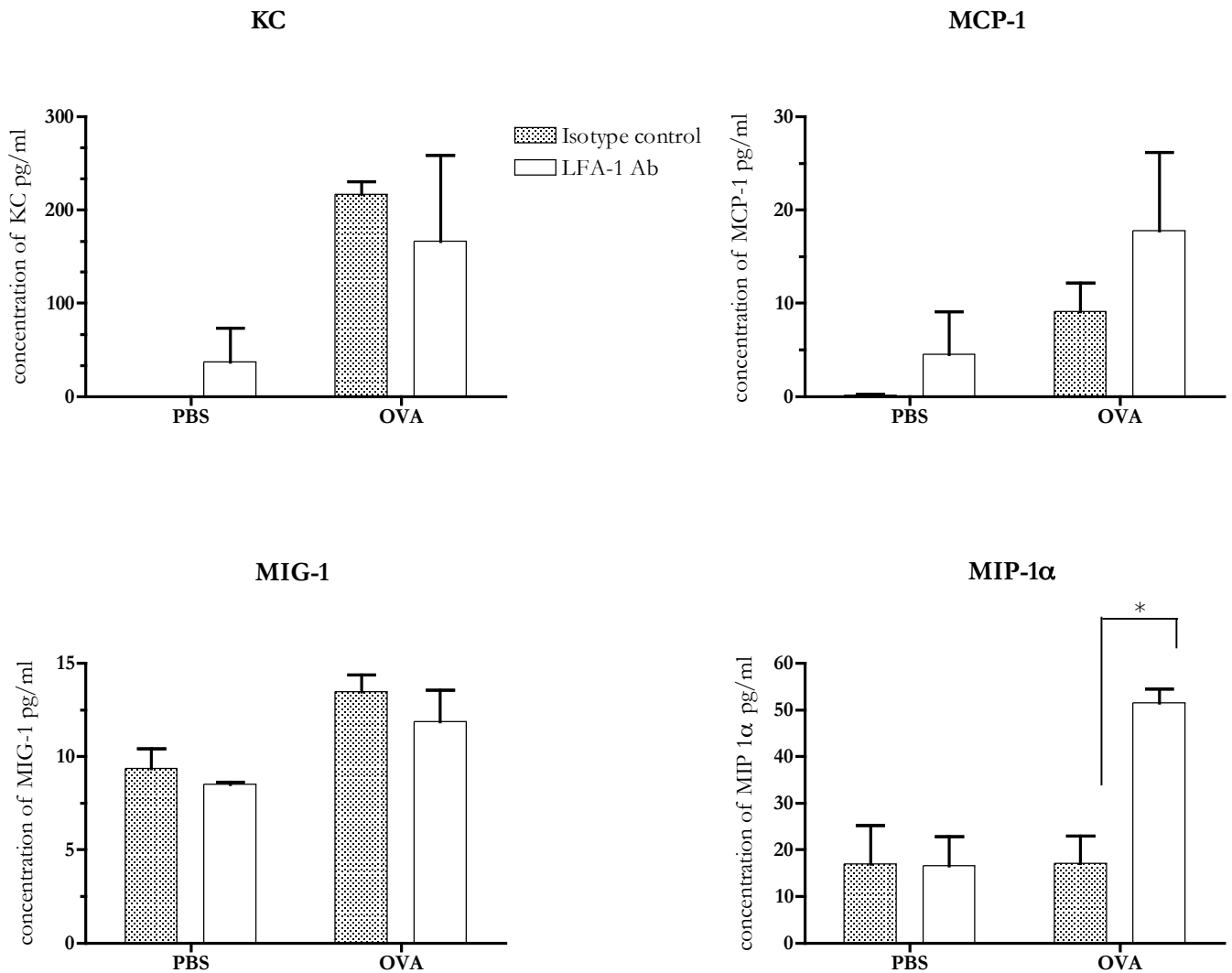


Figure 3.23 The effect of an LFA-1 blocking Ab on the antigen specific production of pro-inflammatory

BALB/c mice were injected with DO11.10 T cells, immunised in the footpad with OVA/CFA and treated with either an isotype control Ab or an LFA-1 blocking Ab. After 72 hrs DLNs were removed and re-stimulated with antigen *in vitro* for a further 72 hours. Supernatants were analysed for the presence of the pro-inflammatory chemokines. Treatment with an LFA-1 blocking Ab did not result in a significant reduction of KC, MCP-1, MIG, however, it did result in a significant increase of MIP-1a ($p=0.0067$).

Results show the mean of triplicate samples \pm s.d.

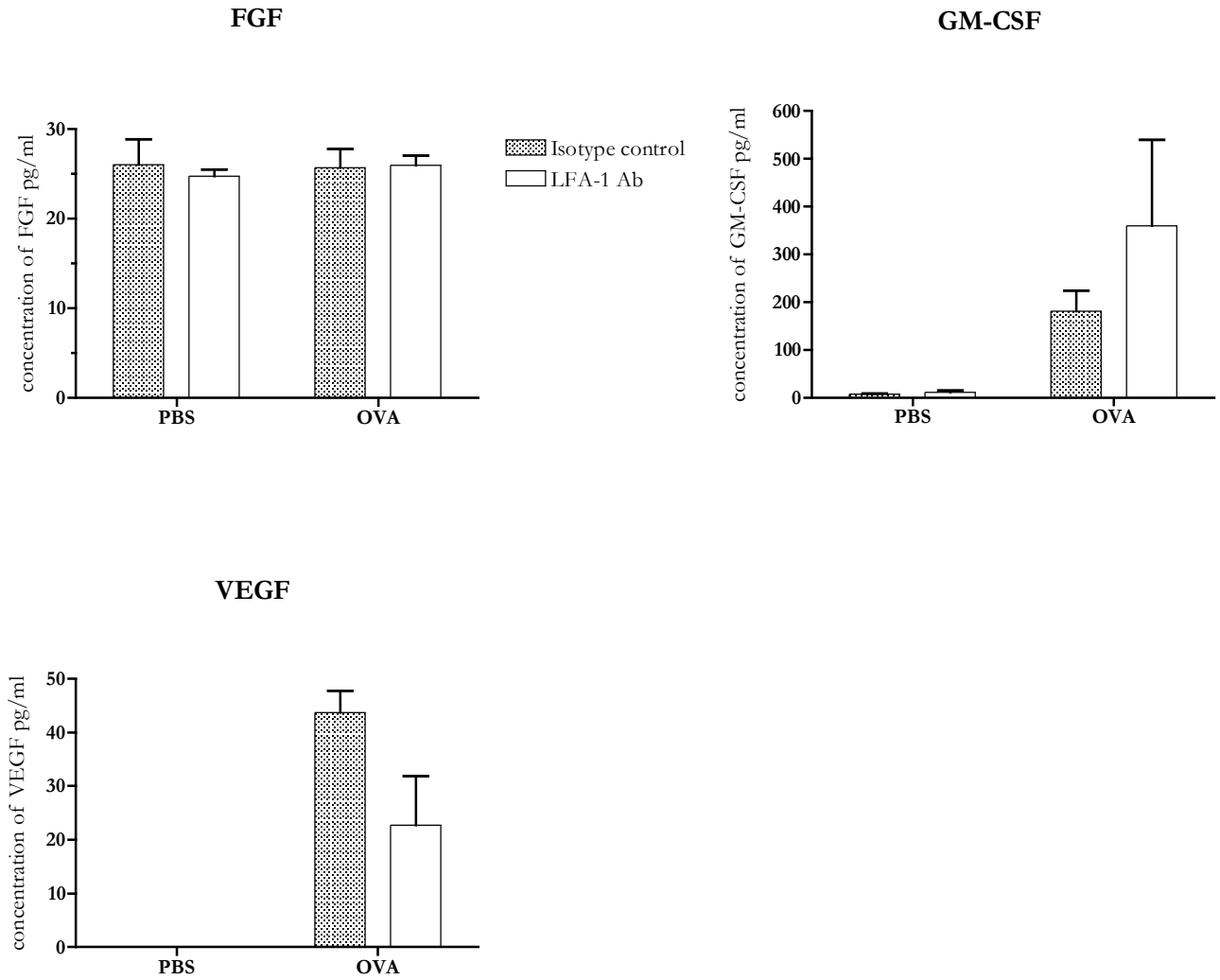


Figure 3.24 The effect of an LFA-1 blocking Ab on the antigen specific production of growth and repair factors

BALB/c mice were injected with DO11.10 T cells, immunised in the footpad with OVA/CFA and treated with either an isotype control Ab or an LFA-1 blocking Ab. After 72 hrs DLNs were removed and re-stimulated with antigen *in vitro* for a further 72 hours. Supernatants were analysed for the presence of the growth and repair factors. Treatment with an LFA-1 blocking Ab did not result in a significant reduction of FGF, GMCSF or VEGF. Results show the mean of triplicate samples \pm s.d.

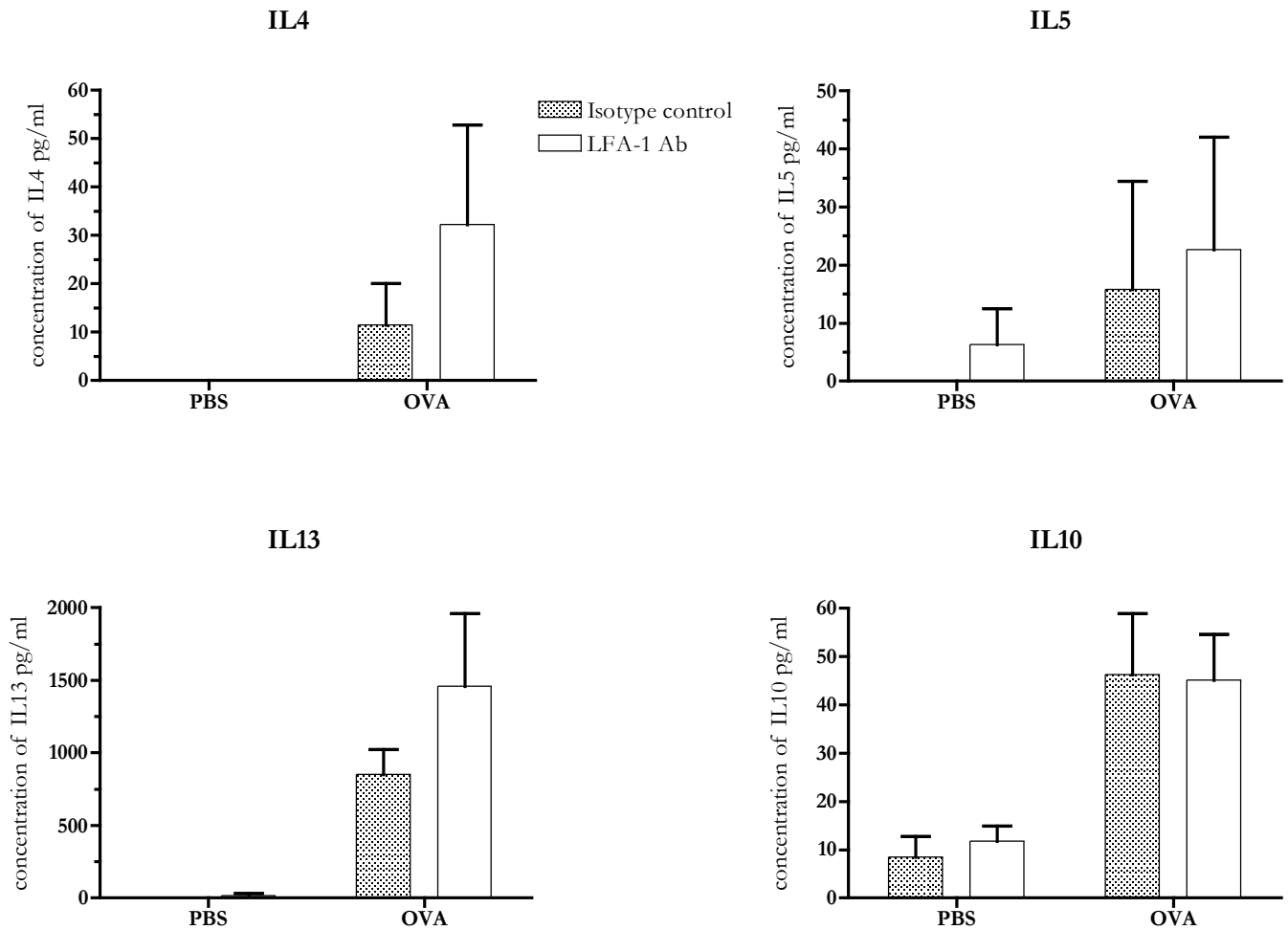


Figure 3.22 The effect of an LFA-1 blocking Ab on the antigen specific production of Th2 cytokines

BALB/c mice were injected with DO11.10 T cells, immunised in the footpad with OVA/CFA and treated with either an isotype control Ab or an LFA-1 blocking Ab. After 72 hrs DLNs were removed and re-stimulated with antigen *in vitro* for a further 72 hours. Supernatants were analysed for the presence of the pro-inflammatory cytokines. Treatment with an LFA-1 blocking ab did not result in a significant reduction of IL4, IL5, IL13 or IL10

Results show the mean of triplicate samples \pm s.d.

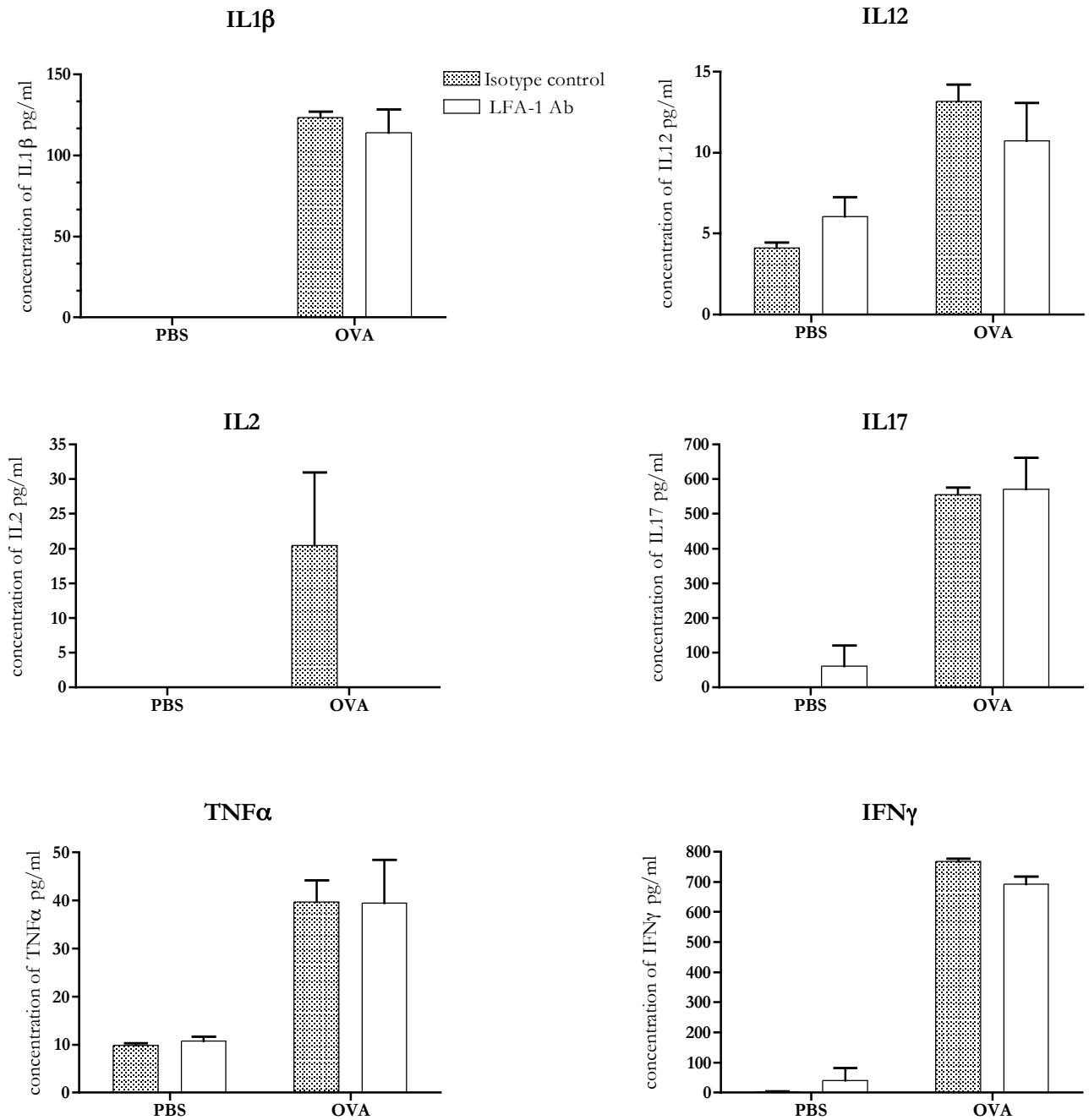


Figure 3.21 The effect of an LFA-1 blocking Ab on the antigen specific production of Th1 cytokines

BALB/c mice were injected with DO11.10 T cells, immunised in the footpad with OVA/CFA and treated with either an isotype control Ab or an LFA-1 blocking Ab. After 72 hrs DLNs were removed and re-stimulated with antigen in vitro for a further 72 hours. Supernatants were analysed for the presence of the pro-inflammatory cytokines. Treatment with an LFA-1 blocking Ab did not result in a significant reduction of IL1 β , IL12, IL2, IL17, TNF α , IFN γ . Results show the mean of triplicate samples \pm s.d.

Chapter 4

Developing and characterising a LN transplant model

4.1 Introduction

The overall aim of this PhD was to investigate the relationship between DC-T cell interactions taking place within a tissue site of inflammation and its DLN. In the previous chapter, the interactions between DCs and CD4⁺ T cells were investigated *in vitro* and *in vivo* by MPLSM. However, to fully address the relationship between the cellular interactions taking place at a tissue site of inflammation and its DLN, there was a requirement for the investigation to progress to an *in vivo* context in which both locations could be examined in parallel. This chapter shows the first stage in this progression and describes the development of a novel LN transplant model, in which a LN is transplanted into the ear pinna of a mouse. As outlined in chapter 1, the next step in this study would be to develop a model of tissue inflammation upstream of the transplanted LN in the ear pinna. Having both sites in the convenient location of the ~200µm thick ear pinna, would permit the cellular interactions taking place at, and between, each site to be easily accessible to MPLSM, without the need for invasive surgical procedures to expose either site.

In this chapter, a novel model was developed in which a LN was transplanted into the ear pinna of a syngeneic recipient. While the concept of transplanting a LN in the ear pinna of the mouse was novel, the transplantation of lymphoid tissue has long been established as a suitable method to study the development of lymphoid tissue *in vivo* (94, 293, 294). In particular, the use of the kidney capsule as the site of engraftment has been shown to provide an optimum environment for the rapid vascularisation and function of transplanted embryonic and adult lymphoid tissue (94). This experimental system has allowed the cellular and molecular requirements for the development and organisation of lymphoid tissue to be investigated (94, 295). Moreover, ‘custom-built’ lymphoid tissue consisting of, or excluding, particular cell types have been transplanted under the kidney capsule to assess the relative requirement of individual cellular features or molecules in the development and function of lymphoid tissue (94, 295). However, while the technique of LN transplantation has yielded much information on LN development, the technique has also been proposed as a novel therapeutic to relieve recovering cancer patients of fluid retention and tissue swelling (lymphedema), which can occur following the surgical removal of LNs and associated tissue draining lymphatics as part of cancer therapy (296). Tammela *et al.* developed a novel mouse

model in which LNs could be replaced and collecting lymphatic vessels could be regenerated by treating mice with adenovirally delivered vascular endothelial growth factors in combination with LN transplants (293). Thus, LN transplantation has been used as a method to study LN development and has been proposed as a potential therapy for lymphedema in humans. However, it has never been employed to create a model system in a convenient anatomical location in which the cellular interactions in a tissue site of inflammation and its DLN could be imaged *in vivo* using MPLSM.

The ear pinna has never been previously employed as a site of transplantation for LNs, however, it has been a popular location for the engraftment of other tissues. In 1963 Fulmer *et al.* were the first to pioneer the engraftment of murine neonatal cardiac tissue into the ear pinnae of rats (297). Due to the thin nature of the ear pinna, they could demonstrate graft viability, without the need for surgical exposure, by directly observing the presence of autonomous beating of the cardiac tissue (297). This approach was subsequently modified to demonstrate that neonatal spleens could be successfully grafted into the ear pinna of the mouse, to facilitate improved efficacy of intrasplenic immunisation for the induction of antibody production (294). Histological and functional studies showed that the spleen grafts contained normal percentages of functional T and B cells and that repeated injection of small quantities of soluble antigen directly into the grafts resulted in the production of specific antibodies (294). Moreover, the engraftment of human synovium into the ear pinnae of SCID mice was successfully demonstrated and proposed as a useful model in the study of rheumatoid arthritis (298).

Thus, the transplantation of lymphoid organs and the use of the ear pinna as a site of engraftment have been previously explored, with the feasibility of each technique clearly established (94, 294, 298-300). However, in this chapter these techniques were combined to develop a novel model in which a LN was transplanted in the ear pinna. Moreover, this chapter details the structural and functional consequences of the engraftment procedure on the LN and shows preliminary multi-photon imaging data of lymphocytes migrating in the transplanted LN within the ear pinna. The objective of developing this model was to ultimately combine it with a tissue site of inflammation in the ear pinna, which would allow

the relationship between the cellular interactions taking place at and between each site to be assessed and analysed.

4.2 Results

A series of complex cellular interactions and signalling events guide the development of LNs in the embryo (301-304). Developing LNs actively secrete factors necessary for their growth and development and it was postulated that this may aid their engraftment (301-304). Thus, the LN transplant model aimed to employ the use of the youngest possible source of LN available. In accordance with home office licence restrictions, the youngest source of donor LNs permitted was from newly weaned 3 week old mice. However, in later experiments Home Office restrictions were altered to allow the engraftment of LNs from neonatal mice. Thus, other than where indicated, all LN engraftments were carried out using LNs from 3 week old mice.

4.3 A LN transplanted into the ear pinna can survive and is histologically normal

Initially, it was important to establish whether the LN transplant technique was successful with respect to LN survival and viability. Thus, the first experiment carried out involved the engraftment of a C57BL/6J LN into the ear pinna of a syngeneic C57BL/6J mouse. In the first week following the procedure the ear pinna became red and inflamed at the site of the engraftment. After 3 weeks, the outward appearance of the ear pinna returned to normal, with no visible signs of the engrafted LN, as shown in figure 4.1 A. However, once dissected the tLN was revealed within the ear tissue and appeared to have maintained its shape and size, with evidence of associated blood vessels clearly visible (highlighted by arrows in figure 4.1 A). To further assess the survival of the tLN, sections of the ear pinna containing the tLN were cut and stained with hematoxylin and eosin (H&E). This staining method highlights the nuclei and cytoplasm of the cell and therefore allows live cells to be clearly differentiated from dead or dying cells. Figure 4.1 B shows a bright-field image of an H&E stained control LN, while figure 4.1 C shows a bright-field image of an H&E stained section of the ear pinna containing the tLN. The results show that in comparison with a control LN, the tLN appeared to be histologically normal and to contain live viable cells with compact and non-fragmented nuclei.

4.4 Age and type of LN transplanted can influence success rate of grafting procedure

As noted above, initial transplants employed 3 week old donors. However, to establish whether the age of the recipient mouse or the anatomical source of LN to be grafted had any effect on the success rate of the engraftment procedure, a variety of transplants were setup using LNs from diverse anatomical locations and recipient mice aged either 6, 8 or 10 weeks. In this experiment the engraftments were carried out in triplicate for each LN type, either cervical, brachial, axillary, inguinal or popliteal for each recipient of either 6, 8 or 10 weeks of age. Summarised in figure 4.2 A, the results show that out of a possible 18, only 3 successful transplants were recorded when using a recipient of 6 weeks of age. A successful engraftment procedure was observed following the transplant of 1 of the cervical LNs and 2 of the brachial LNs. When using a recipient of 8 weeks of age, a slightly higher number of transplants were recorded with 5 out of a possible 18 proving successful. In this case 1 axillary, 1 inguinal and 3 brachial LNs provided successful engraftments. However, when using a recipient of 10 weeks of age the success rate decreased to below that observed when using a recipient of 6 weeks of age. Out of a possible 18, only 2 transplants were successful, which were of brachial and inguinal origin. Overall, the popliteal was the only source of LN that provided no successful transplants, while in contrast the most successful source of LN was the brachial with 6 out of 9 providing successful transplants. In conclusion, the most successful age of recipient was 8 weeks and the most successful source of LN was the brachial. In addition, the total cell count from each transplanted LN was determined and revealed comparable numbers of cells within the LN after the transplant process as before, figure 4.2 B. Next, in a further attempt to optimise the engraftment procedure and increase success rates, neonatal mice were employed as a source of donor LNs.

Transplanting a neonatal LN under the ear pinna was not successful

Neonatal LNs are in a continuous phase of development and are therefore considered more plastic and adaptable than adult LNs (76, 103, 303, 305). As discussed previously, in the

preliminary stages of LN development, LN inducer cells and stromal organiser cells interact to stimulate the release of chemokines and growth factors, which may aid the engraftment of the LN into the ear pinna (76, 303). Initially Home Office licence restrictions prevented the use of neonatal mice, however, once the licence was amended, LNs from 3 day old neonatal mice were employed for transplantation with the aim of increasing the success rate of the engraftment procedure. Surprisingly, no successful transplants were recorded using neonatal LNs. Sections of the ear pinna containing the neonatal LN were stained with H&E to establish cell viability. Figure 4.3 A shows an image of an H&E stained tLN within the ear pinna. Figure 4.3 B shows an image of an H&E stained neonatal tLN within the ear pinna. The results show that in comparison with a successful tLN carried out using a 3 week old donor LN, the neonatal tLN (ntLN) did not appear histologically normal and appeared necrotic with few viable cells. The reduced size of a neonatal LN made it difficult to recover the LN from the ear pinna 3 weeks post transplant. Thus, flow cytometric analysis of the cellular populations within the neonatal tLN was not feasible. However, sections of the ntLN were stained to detect the presence of CD4⁺ T cells, B220⁺ B cells and lyve-1⁺ lymphatic vessels. Figure 4.3 C, shows a confocal image of the ntLN and while the lymphatic vessels of the ear pinna could be clearly visualised the lymphocyte compartment was absent and appeared necrotic, figure 4.3 C.

4.5 The tLN maintains the cellular populations and organisation of a conventional LN

LNs are highly evolved, structurally complex organs consisting of a variety of cell types, which together function as a surveillance system to collect and present antigens from local tissues in an appropriate manner to lymphocytes of the immune system. The complex micro-architecture and cellular populations of the LN are described in chapter 1. In the LN transplant experiments, it was presumed that the engraftment procedure would result in a temporary interruption to the blood and lymphatic supply. It was therefore important to establish whether this had any impact on the basic structural features of the LN. Thus, to ensure the LN transplant model provided a system comparable with a conventional LN, the

cellular compartments and architectural organisation of the tLN were assessed and measured using fluorescence immunohistochemistry and flow cytometry.

Sections of the ear pinna containing the tLN were cut and stained for a series of cellular, stromal and chemokine markers. As discussed previously, the principal haematopoietic cell types of the LN are T and B cells and under the guidance of specific chemokines, each cell type can be found to reside in distinct anatomical locations (60, 92). Thus, sections were stained to detect the presence of CD4 and CD3 co-expressing CD4⁺ T cells and B220 expressing B cells and to confirm the organisation of each cell type into their respective area of the LN. The results shown in figure 4.4, detail confocal images of a control non-transplanted LN at x10 and x40 magnification and the tLN within the ear pinna at x10 and x40 magnification. Consistent with expected results, CD3⁺CD4⁺ T cells and B220⁺ B cells could be clearly identified within the control LN, figure 4.4 A+B. Moreover, each cell type was segregated into distinct areas of the LN, with CD3⁺CD4⁺ T cells mainly concentrated in the central paracortical region of the LN, while B220⁺ B cells formed defined follicles around the outer edge of the LN, figure 4.4 A+B. Similarly, within the tLN, CD3⁺CD4⁺ T cells and B220⁺ B cells could be clearly identified and appeared segregated into distinct regions, figure 4.4 C+D.

DCs are a phenotypically diverse group of cells that represent about 1% of the total population of cells within the LN (23, 306-308). They can be either blood derived, LN resident DCs or be tissue specific DCs which migrate to the LN via the afferent lymphatics carrying a sample of antigens from the local tissue (23, 285, 306-308). DCs are a key cell type within the LN and through their antigen specific interaction with CD4⁺ T cells, they are responsible for the initiation of the adaptive immune response (5, 9, 285). There are a variety of DC populations within the LN that express a range of distinct cell surface markers (23, 309). CD11c is one of the many markers used to identify murine DCs and was the marker selected here to detect the presence of DCs within the tLN (119, 310). Figure 4.5 A + B, shows confocal images of the control non-transplanted LN stained for CD11c⁺ DCs, CD4⁺ T cells and B220⁺ B cells at x10 magnification and x40 magnification. Figure 4.5 C + D, shows confocal images of the tLN within the ear pinna stained for CD11c⁺ DCs, CD4⁺ T

cells and B220⁺ B cells at x10 magnification and x40 magnification. In comparison with the control, non-transplanted LN, the distribution of CD11c⁺ DCs throughout the LN appeared to be similar with no obvious differences. Once again, the T cell compartment of the tLN appeared to be consistent with the control LN, while the B cell compartment appeared slightly less compact in comparison with the control LN.

Lymphocytes and CD11c⁺ DCs were identified within the tLN 3 weeks following the transplant procedure. However, whether the stromal backbone of the LN that supports these cellular populations remained intact following the engraftment procedure was next investigated since defects in the stromal cell compartment can lead to reduced size and cellularity of the LN (94). BP-3 is a glycosylated cell surface protein primarily expressed by stromal cells of the B220⁺ B cell area but can be found throughout the LN (311). Sections of the ear pinna containing the tLN were analysed for the expression of BP-3 and to assess whether the stromal network had been disrupted following the engraftment procedure. Figure 4.6 A + B show confocal images of the control non-transplanted LN stained to detect the presence of BP-3⁺ stromal cells, CD4⁺ T cells and B220⁺ B cells, at x10 magnification and x40 magnification. Figure 4.6 C + D, show confocal images of the tLN stained to detect the presence of BP-3⁺ stromal cells, CD4⁺ T cells and B220⁺ B cells, at x10 magnification and x40 magnification. The distribution of BP-3⁺ stromal cells throughout the LN suggested no marked differences in comparison with the control, non-transplanted LN.

LNs have the capacity to selectively localise and trap antigen and antigen presenting cells trafficked there via tissue draining afferent lymphatics (44). This continual flow of communication between the tissues and their draining LNs, ensures the rapid generation of an antigen specific immune response in the case of a pathogenic insult. Thus, the afferent lymphatic vessels that exist between a tissue and its draining LN are critical to ensuring successful immune function. To visualise the presence of a lymphatic vascular supply to the tLN, sections were examined for gp-38, a cell surface glycoprotein preferentially expressed by stromal cells in T cell dependent areas of secondary lymphoid organs and lymphatic endothelial cells (89, 312). Figure 4.7 A + B show confocal images of the control non-

transplanted LN, examined for the presence of gp-38⁺ lymphatic vessels and CD4⁺ T cells, at x10 magnification and x40 magnification. Figure 4.7 C + D, show confocal images of the tLN, stained for the presence of gp-38⁺ lymphatic vessels and CD4⁺ T cells, at x10 magnification and x40 magnification. In comparison with the control non-transplanted LN, the distribution of gp-38⁺ lymphatic vessels throughout the tLN appeared to be similar. The gp-38⁺ staining was evenly distributed throughout the LN and was seen to be associated with CD4⁺ T cells, which is consistent with published reports of the glycoprotein being predominantly expressed in T cell areas of the LN (89, 312).

CCL21 is a chemokine produced by the high endothelial cells (HEVs) of the vasculature supply to the LN and by stromal FRCs within the LN (313, 314). It is responsible for actively recruiting and directing re-circulating T cells to the paracortical area of the LN. Moreover, the importance of CCL21 was first demonstrated by mice homozygous for the spontaneous mutation, *paucity of LN T cells (plt)*, in which expression of CCL21 is defective and T cell migration into LNs is ablated (315). Previously, staining with CD4 and CD3, demonstrated the presence of T cells within the tLN, suggesting the expression of CCL21. However, to confirm this, sections of the ear pinna containing the tLN were examined for CCL21. Figure 4.8 A + B, shows confocal images of the control non-transplanted LN, stained for the presence of CCL21, CD4⁺ T cells and B220⁺ B cells, at x10 magnification and x40 magnification. Figure 4.8 C + D shows confocal images of the tLN, stained for the presence of CCL21, CD4⁺ T cells and B220⁺ B cells, at x10 magnification and x40 magnification. In both the control and tLN, CCL21 positive staining appeared to be associated with larger cell types, presumably FRCs or HEVs (313, 314). Moreover, the distribution of CCL21 staining throughout the T cell area appeared to be similar in the tLN, with no marked differences, in comparison with the control LN.

The blood vessels that supply the LN are referred to as HEVs and differ from conventional endothelial cells by their specific expression of several genes, which increase their adhesive properties for recirculating lymphocytes (316). Vascular cell adhesion molecule (VCAM-1), has been shown to be involved in the adhesion of lymphocytes to the vascular wall of the HEV and has been implicated in the migration of lymphocytes from the blood into the LN (317). To test for the presence of a vasculature supply to the tLN, sections were stained for

the expression of VCAM-1. Figure 4.9 A + B, show confocal images of the control non-transplanted LN, stained for the presence of VCAM⁺ endothelial cells, CD4⁺ T cells and B220⁺ B cells, at x10 magnification and x40 magnification. Figure 4.9 A + B, show confocal images of the tLN, stained for the presence of VCAM⁺ endothelial cells, CD4⁺ T cells and B220⁺ B cells, at x10 magnification and x40 magnification. The expression of VCAM-1 appeared slightly more pronounced in the tLN in comparison with the control non-transplanted LN, and since expression of VCAM-1 has been reported to increase during inflammation, it is possible that the tLN was somewhat inflamed following the transplant procedure (318).

Using fluorescence immunohistochemistry and confocal microscopy, the cellular populations of the tLN were detected and visualised. However, to quantify the proportion of B220⁺ B cells, CD8⁺ T cells and CD4⁺ T cells in the tLN in comparison with a control non-transplanted LN, flow cytometry was necessary. A representative flow cytometric plot in figure 4.10 A shows that lymphocytes from control LNs were first identified on the basis of size and granularity. Lymphocytes were next analysed for their expression of B220 or the T cell markers CD4 and CD8, (figure 4.10 C). Similarly, lymphocytes from the tLN were identified on the basis of size and granularity, figure 4.10 D and their expression of B220 or the T cell markers CD4 and CD8, figure 4.10 E + F. The proportions of each cell type in the tLN were compared to the proportions of each cell type in a control non-transplanted LN and were summarised in figure 4.10 G. Overall, the proportion of CD4⁺ T cells and B220⁺ B cells were similar to those in the control LNs. However, in comparison with the control LNs, the proportion of CD8⁺ T cells in the tLN was significantly lower ($p=0.0252$). In conclusion, the images shown of the tLN in this section revealed that the LN had maintained the structural and cellular organisation typical of a normal LN, with some minor exceptions including the organisation of the B cell follicle and the expression of VCAM-1. However, while the proportions of CD4⁺ T cells and B cells were unchanged, flow cytometry revealed a significantly lower than expected proportion of CD8⁺ T cells in the LN following the transplant procedure.

4.6 LN inducer cells of host mouse origin can be detected within the tLN

Among the early events that give rise to LNs during embryonic development is the colonisation of the developing LN with $CD45^+CD4^+CD3^-$ inducer cells. Inducer cells express high levels of lymphotoxin- β , which upon binding to lymphotoxin receptors on stromal organiser cells, stimulates the expression of the B cell homing chemokine CXCL13 and the T cell chemo-attractant, CCL21 (59, 319). Thus, clustering of inducer cells with stromal cells is a vital step in LN development and organisation. Moreover, studies using lymphotoxin deficient mice have suggested that in adult LNs, inducer cells continue to maintain the segregation of B and T cells into their respective areas of the LN (97, 320). Inducer cells have also been implicated in supporting CD4-dependent class-switched memory antibody responses by stimulating and promoting the survival of B helper $CD4^+$ T cells (320). Thus, inducer cells play an important role in LN development, maintenance and function. Fluorescence immunohistochemistry was carried out to test whether LN inducer cells were present within the tLN or whether the engraftment procedure had resulted in an increase or decrease in the presence of this cell type. An inguinal LN from a 3 week old C57BL/6J/CD45.1 mouse was transplanted into the ear pinna of a congenic C57BL/6J/CD45.2 recipient mouse and 3 weeks later, the ear pinna was removed and prepared for fluorescence immunohistochemistry. Cells that were considered to be inducer cells were those which stained positively for the expression of $CD4^+$ and $CD45.2^+$ and stained negatively for $CD3^-$, $CD11c^-$ and $B220^-$ to exclude T cells, DCs and B cells. The results in figure 4.11 A + B, outline confocal images of a control C57BL/6J/CD45.2 LN stained for the presence of LN inducer cells. Possible inducer cells were highlighted by a yellow box and stained positively for the expression of CD4 and CD45.2 while they stained negatively for all other markers examined. Figure 4.11 C–E, shows confocal images of the tLN stained for the presence of LN inducer cells. Cells surrounded by a white box were positive for the expression of CD4 and negative for the expression of all other markers. Thus, these were possible $CD45.1^+$ inducer cells of donor LN origin, while cells surrounded by a yellow box were double positive for CD4 and CD45.2 expression and were considered to be possible inducer cells of host mouse origin.

4.7 The tLN can participate in lymphocyte re-circulation with its new host

in its new anatomical location

As outlined in chapter 1, the LN continually receives an input of circulating naive T and B cells from the blood. This process is known as lymphocyte recirculation and was first described in detail in 1964 by Gowans and Knight (65). Lymphocytes enter the LN through the HEVs and migrate to their respective areas under the guidance of specific chemokines, before exiting via the efferent lymphatic vessels (67, 92, 93, 233, 277, 279, 315). As outlined in chapter 1, the process of lymphocyte recirculation ensures the even distribution of rare lymphocyte specificities, which allows them to survey the secondary lymphoid organs for the presence of their specific antigen ensuring a rapid response to an invading pathogen (279). Thus far, analysis of the cellular populations and structural organisation of the tLN by fluorescence immunohistochemistry and flow cytometry had shown the presence of viable lymphocytes and a vascular and lymphatic supply to the tLN. These results strongly indicated that the tLN had developed a functional vasculature and lymphatic supply in its new anatomical location, capable of supporting lymphocyte re-circulation. However, to demonstrate this function conclusively, congenic strains of mice were employed. An inguinal LN from a 3 week old C57BL/6J/CD45.1 mouse was transplanted into the ear pinna of a congenic C57BL/6J/CD45.2 mouse. The use of these mice, which were genetically identical with the exception of the expression of the CD45.1 molecule, instead of CD45.2, on the cell surface, allowed the analysis of whether host CD45.2⁺ T cells could migrate into, and be detected within, the tLN and vice versa using flow cytometry (321). Figure 4.12 shows a series of representative flow cytometric plots. Figure 4.12 A shows that lymphocytes from the tLN were first identified on the basis of size and granularity. Figure 4.12 B shows that 82.5% of lymphocytes within tLN expressed the cell surface molecule CD45.2, while only 0.77% expressed CD45.1. The LNs and spleen from the recipient mouse were next pooled and analysed for the presence of CD45.1⁺ lymphocytes originating from the tLN. Lymphocytes were first identified on the basis of their size and granularity, figure 4.12 C. Figure 4.12 D shows that 66.2% of lymphocytes expressed CD45.2, while only 0.065% of lymphocytes expressed CD45.1. Thus, the results revealed that 3 weeks post transplant, the tLN lymphocyte population consisted entirely of CD45.2⁺ lymphocytes, which had re-circulated into the donor tLN. However, surprisingly the original CD45.1 population of the tLN was not detected in either the tLN or the LNs of the recipient mouse.

4.8 Adoptively transferred CFSE labelled lymphocytes can migrate into and be detected within the tLN

Developed by Jenkins *et al.*, the adoptive transfer system involves the transfer of a population of antigen specific T cells into syngeneic normal recipient mice (176). This allows a population of cells to be tracked and analysed. Lymphocytes adoptively transferred from one mouse to another should mirror the behaviour of host lymphocytes by recirculating to and from the secondary lymphoid organs via the blood and lymphatic supply. To determine whether the tLN could support the recirculation of adoptively transferred lymphocytes to the same degree as host LNs, fluorescently CFSE labelled lymphocytes were delivered intravenously into the tail vein of the mouse. Following 24 hours, host LNs and the tLN were examined by flow cytometry. Figure 4.13 A + B, displays representative flow cytometric plots with lymphocytes from the control LN being identified on the basis of size and granularity, followed by CFSE expression. As can also be seen in, figure 4.13 C + D, representative flow cytometric plots with lymphocytes from the tLN were identified on the basis of size and granularity, followed by CFSE expression. The results, representing triplicate samples, were summarised in figure 4.13 E, to reveal that 0.97% (+/-0.13) of adoptively transferred CFSE labelled lymphocytes re-circulated into the control LN, while a significantly lower 0.45% (+/-0.2) of CFSE lymphocytes re-circulated into the tLN.

4.9 Antigen injected into the tip of the ear pinna can drain into and be detected within the tLN

Described by Von Andrian and colleagues as a "...strategically positioned collecting station", a key feature of all LNs is their ability to drain antigen from the local tissues (44). Previously, analysis of the tLN by fluorescence immunohistochemistry revealed the presence of gp38⁺ lymphatic vessels. However, the functional capability of those lymphatic vessels to drain antigen from the tissue was not demonstrated by this approach. Thus, to test whether the tLN had gained the capacity to drain antigen from its new anatomical location in the ear,

0.04 μ m alexa-fluor-660 beads were injected into the tip of the ear pinna upstream of the tLN. 24 hours later the ear pinna was removed for analysis by fluorescence immunohistochemistry to detect whether the beads had drained from the ear tissue and could be detected within the tLN. As a positive and negative control, either beads or PBS were injected into the footpad and the draining popliteal LN was removed after 24 hours and prepared for fluorescence immunohistochemistry. Sections of the ear pinna containing the tLN were stained with DAPI to highlight the nuclei and anti-CD4 to highlight CD4⁺ T cells. Figure 4.14 A, shows a confocal image of the negative control LN, in which no fluorescent micro-beads and only PBS was injected subcutaneously into the footpad. Consistent with the expected result, when no fluorescent micro-beads were injected, only CD4⁺ T cells could be detected within the LN. Figure 4.14 B, shows a confocal image of the positive control LN, in which fluorescent micro-beads were injected subcutaneously into the footpad and could be clearly identified 24 hours later within the CD4⁺ T cell area of the LN. Similarly, figure 4.14 C + D show confocal images of the tLN within the ear pinna following the injection of fluorescent micro-beads subcutaneously into the tip of the ear pinna. Micro-beads could be clearly identified within the tLN in combination with CD4⁺ T cells, demonstrating the ability of the transplant to form functional afferent lymphatics in its new tissue location within the ear pinna.

4.10 The tLN can respond to immunisation at level comparable to a conventional LN

To facilitate the generation of a highly specific immune response, the LN brings antigen presenting DCs and antigen specific T and B cells into close physical contact and provides the ideal microenvironment for the many complex interactions required to take place between these cell types (44). Thus far, the novel model of transplanting a LN into the ear pinna has been shown to provide an LN that possesses the cellular populations, organisation and structural features of a conventional LN. Moreover, the tLN has been shown to re-vascularise to permit the ingress of adoptively transferred lymphocytes and to develop functional tissue draining afferent lymphatics. Thus, to test whether all the necessary elements can congregate and collaborate within the tLN to facilitate the generation of a

highly specific immune response, its ability to respond to antigenic challenge in a conventional manner was next examined (176). Three weeks post transplant of a BALB/c LN into the ear pinna of a BALB/c recipient, DO11.10 T cells were adoptively transferred as described in chapter 2. The mice were then immunised in the tip of the ear pinna with heat aggregated OVA (HAO) and 72 hours later the draining cervical and tLN were removed for analysis of antigen specific proliferation by flow cytometry. In control, PBS challenged mice, the proportion of CD4⁺KJ⁺ cells in both the control LN and tLN was small, 0.58% and 0.16% respectively. Moreover, there was no substantial loss in the intensity of CFSE, reflecting the lack of antigen specific cell division. However, of note, the cellularity of the tLN appeared less than that of the control LN, perhaps due to its reduced size. Consistent with the expected results, the proportion of CD4⁺KJ⁺ cells in both the control LN and tLN substantially increased in response to immunisation with HAO, to 5.84% and 4.1% respectively figure 4.15 C + G (176). Moreover, this expansion of the transgenic T cell population was reflected in the incremental loss of CFSE, a fluorescent label that becomes diluted by every round of cell division, from both CD4⁺KJ⁺ cells in the control LN and tLN, Figure 4.15 D + H (322). Summarised in figure 4.15 I, the graph shows that the tLN appeared to have retained its ability to respond to antigen challenge as CD4⁺KJ⁺ cells in the tLN underwent equivalent rounds of cell division to the CD4⁺KJ⁺ cells in the control LN.

4.11 Lymphocytes migrate at a comparable speed in the transplanted and control LN

Detailed analysis carried out to establish whether the tLN maintained the features of a conventional LN following the engraftment procedure revealed few differences in the tLN, with the exception of the proportion of CD8⁺ T cells, which were significantly less. The objective of developing this model in the ear pinna was to allow a tissue site of inflammation to be established within close proximity of the LN and the relationship between the cellular interactions taking place at and between each site to be investigated dynamically using MPLSM. It was therefore important before using the model to analyse cellular interactions, to first confirm whether lymphocytes could migrate through the tLN in a comparable manner to a control non-transplanted LN. Following the engraftment of a C57BL/6J LN into the ear pinna of a C57BL/6J mouse, a population of lymphocytes labelled with a red

fluorescent dye, CMTPX, were adoptively transferred iv. A skin flap in the ear pinna was created and, using MPLSM, CMTPX labelled lymphocytes from a C57BL/6J mouse were imaged within the tLN. Analysis of the migration of the lymphocytes was carried out using Volocity software (Improvision). Figure 4.16 A + B, presents still images from the multi-photon movies acquired of the CMTPX labelled lymphocytes migrating in a control LN and the tLN, respectively. Detailed analysis of the speed at which lymphocytes migrated through the LN was carried out using Volocity software (Improvision). Summarised in figure 4.16 C, the mean velocity of CMTPX labelled lymphocytes within the control LN was $3.3\mu\text{m}/\text{min}$ (± 0.86) and $4.31\mu\text{m}/\text{min}$ (± 0.2) in the tLN. These values were not significantly different and therefore the ability of lymphocytes to migrate within the tLN was comparable to a control non transplanted LN.

4.12 Discussion

This chapter establishes a novel model of LN transplantation in the ear pinna of the mouse. The results show that this technique provides a fully functional LN in an anatomical location accessible to *in vivo* multi-photon imaging without the need for invasive surgical procedures required to expose a native LN.

Initially all transplants were carried out using LNs from newly weaned mice aged 3 weeks. However, transplanting 3 week old LNs into the ear pinnae of adult mice had a varied success rate and age of recipient and type of LN transplanted appeared to influence the overall outcome. The highest success rates were achieved using brachial LNs while lowest success rates were observed using popliteal LNs. Overall, using recipient mice aged 8 weeks provided greater success rates than using recipients of either 6 or 10 weeks of age. In mice, the development of peripheral LNs is dependent on signalling via the lymphotoxin- α receptor and the IL7 receptor (302, 323-325). *In vivo* blocking experiments in which this signalling was modulated at a variety of time points revealed that peripheral LNs develop sequentially (76, 305, 326-328). The cervical LN develops at approximately 11.5 days of embryonic development, while the brachial and axillary follow at 12.5 days. The inguinal and popliteal LNs are among the last of the peripheral LNs to develop, at 15.5 days and 16.5 days respectively. However, with the exception of their sequential development there are no other documented variations between the peripheral LNs. Thus, there was no clear explanation for the varied success rates observed when transplanting different LNs. However, it is important to note that greater sample sizes would be required for a definitive determination of the importance of age of recipient.

Further experiments employed neonatal mice as a source of LNs for transplantation in an attempt to increase overall success rates of the technique. Previously, experiments involving the transplantation of lymphoid tissue demonstrated the use of either neonatal LNs transplanted under the kidney capsule or neonatal spleens in the ear pinna (94, 294). Neonatal lymphoid tissue is substantially smaller than adult tissue and is therefore considered to place less demand on the development of a blood supply during the engraftment procedure. Moreover, neonatal lymphoid tissue is considered to be in a continued phase of development, actively secreting factors important in growth and differentiation and it was assumed that this age related quality could aid their engraftment

(295, 303). In contrast to the expected outcome, the smaller size of the neonatal LNs made them more difficult to recover from the ear pinna. Furthermore, while it was expected that neonatal LNs would graft into the ear pinna with a high success rate, no successful neonatal transplants were recorded with the ntLN appearing necrotic or disappearing completely. Thus, the technique was resumed using 3 week old mice as the source of donor LN.

Analysis of the structural organisation and cellular populations of the tLN by flow cytometry and fluorescence immunohistochemistry revealed that the engraftment procedure was not associated with any major defects or changes. Structural features of the tLN appeared intact with the BP-3⁺ stromal cell network appearing to mirror that of a conventional LN. Evidence of a blood and lymphatic supply to the node, was also observed. Moreover, the T cell attracting chemokine, CCL21, was also detected within the tLN, co-localised with CD4⁺ T cells. Moreover, the key cellular types required in a LN for the initiation of an adaptive immune response were all detected, including T cells, B cells and CD11c⁺ DCs in the usual proportions. Finally, CD45⁺CD4⁺CD3⁻ LN inducer cells were detected within the tLN and were shown to be of both host and donor origin. These cells are known to play a critical role in LN development through their interactions with stromal organiser cells, which induces the release of chemokines and growth factors (97, 302, 304). Moreover, their continued presence in adult LNs is considered to be important in maintaining the organisation of the LN. Of the differences noted, only the proportion of CD8⁺ T cells was significantly reduced following the engraftment procedure. However, the cellular populations in the tLN were consistently analysed 3 weeks post transplant and perhaps a longer period of time was required for some populations to fully equilibrate and return to normal following the engraftment procedure.

It was noted that when the cells of the LNs were analysed on the basis of size and granularity by flow cytometry, the tLN displayed increased numbers of large granular cell types that were not present in the control LN. These cell types resemble macrophages, which are known to play a pivotal role in modulating the repair process following tissue damage, which may have been caused as a result of the engraftment procedure. The functional importance of the macrophage in tissue repair and remodeling was first demonstrated in 1975, when Leibovich and Ross showed that monocyte and macrophage

depleted guinea pigs exhibited significantly delayed wound repair (329). At sites of tissue injury, macrophages secrete growth factors and proteins that promote tissue repair and influence the proliferation and differentiation of endothelial cells, fibroblasts and keratinocytes (330, 331). Thus, it is plausible that the increased number of large granular cell types observed in the tLN and not in the control non-transplanted LN may be the result of an influx of macrophages involved in the tissue repair process. Using flow cytometry and staining for the cell surface marker F4/80, could be a way to confirm in future experiments whether these cells are macrophages (332).

In the first of a series of functional studies of the tLN, congenic strains of mice were used to test the ability of the tLN to graft into the ear pinna and participate in the process of lymphocyte re-circulation with the secondary lymphoid organs of the recipient mouse. Three weeks following the engraftment procedure, the tLN was shown to contain CD45.2⁺ cells from the recipient mouse. However, surprisingly the original CD45.1⁺ cell population of the tLN could not be detected in either the tLN or the LNs of the recipient mouse. This may have been the result of the small donor population being diluted out by the larger host population, or the result of cell death due to a temporary interruption to the vascular and lymphatic supplies during the transplantation process.

The capacity of the tLN to form a functional vascular supply to support lymphocyte recirculation in its new anatomical location was evidenced when lymphocytes from the host mouse were shown to migrate into the tLN. This was confirmed when an exogenous population of CFSE labelled cells were adoptively transferred and shown to re-circulate into the tLN by flow cytometry. However, a significantly lower proportion of CFSE labelled lymphocytes were detected in the tLN, in comparison with the proportion detected in the native LNs. This could possibly indicate an impaired vascular supply to the tLN following the engraftment procedure. The engraftment of lymphoid tissue is generally carried out under the subcapsular region of the kidney capsule, which due to its high levels of vascularisation provides an ideal site for tissue transplant. Moreover, engraftment of neonatal spleens into the ear pinna was carried out at the base of the ear close to the auricular artery and problems of impaired vascularisation were not reported (294). However, to ensure the tLN was accessible to multi-photon imaging studies it was not feasible to insert

the LN too close to the base of the ear pinna, thus it is possible that the blood supply in the outer regions of the ear pinna is less in comparison.

The next functional study investigated the capacity of the tLN to form functional afferent lymphatic vessels capable of draining antigen from the ear pinna. Fluorescent beads injected into the ear pinna upstream of the tLN could drain into and be detected within the tLN. The capacity of a tLN to develop afferent lymphatic vessels capable of draining antigen from its new anatomical location has never been previously explored. Neonatal spleens transplanted into the ear pinna, were shown to be capable of responding to antigen challenge (294). However, unlike LNs, spleens do not possess afferent and efferent lymphatic vessels and the transplanted spleen was immunised directly with a targeted injection of antigen, thus, circumventing the requirement for tissue draining lymphatic vessels (294). Growth factors capable of directly inducing the growth of lymphatic vessels have been characterised (333, 334). These factors, VEGF-C and VEGF-D can be up-regulated in response to environmental stress, including hypoxia and tissue damage (333-335). Tammela *et al.* employed adenovirally delivered VEGF-C/D to regenerate tissue draining lymphatic vessels in mice (293). However, in 2006 Ikomi *et al.* demonstrated that mature tissue draining afferent lymphatics are able to regenerate spontaneously in adult lymphoid tissues. Using rabbits, they showed that 4 weeks after making incisions in lymphatic vasculature, recanalisation was observed between cut ends of the lymphatic vessels (336). Thus, the tLN appears to develop ear draining afferent lymphatic vessels and while it has never been shown previously that engrafted LNs can develop tissue draining afferent lymphatics, the ability of lymphatic vessels to regenerate has been explored.

The adoptive transfer model was used to test the ability of the tLN to respond to antigen challenge. Developed by Jenkins *et al.*, the adoptive transfer system involves the transfer of DO11.10 TCR-transgenic T cells into syngeneic normal recipient mice (176, 177, 337). In their germline DNA, these mice contain rearranged TCR-V α and -V β genes that encode a TCR specific for chicken ovalbumin peptide 323-339, bound to I-A^d class II MHC molecules (337). This produces a peptide/MHC-specific T-cell population within the recipient, which is large enough (0.2–1%) to be easily tracked *in vivo* using the KJL.26 monoclonal antibody or CFSE labeling prior to transfer, yet the population is small enough

to behave in a relatively physiological manner when confronted with antigen (338). Flow cytometric analysis revealed that in response to immunisation with HAO in the ear pinna, the OVA specific DO11.10 T cells in the tLN proliferated to a comparable level as control LN. This final functional study, conclusively demonstrated that not only can the tLN re-vascularise to receive adoptively transferred cells but it can also drain antigen from the ear pinna and respond in a conventional manner by facilitating the clonal expansion of antigen specific T cells.

When imaged dynamically using MPLSM, lymphocytes migrated around the control LN and the tLN at a comparable rate. A variety of publications have reported that average T cell velocity in the LN, in the absence of priming conditions can range between 10 $\mu\text{m}/\text{min}$ and 40 $\mu\text{m}/\text{min}$ (7-9, 339). However, the average of velocity observed here was substantially lower at $\sim 4\mu\text{m}/\text{min}$. A recent paper by Huang *et al.* revealed that the speed at which naïve lymphocytes migrate through the LN can vary considerably depending on the temperature, oxygenation, and perfusion rate conditions at which the LN is maintained throughout the imaging period (192, 339). Thus, it is possible that the imaging conditions may have affected the overall rate at which CMTX labeled lymphocytes migrated on the day of imaging. Moreover, the migration of cells within the control LN and tLN were not significantly different from one another, indicating that the ability of lymphocytes to migrate dynamically through the tLN was not impaired.

The data presented in this chapter establishes a novel model of LN transplantation in the ear pinna and demonstrates that this system provides a fully function LN in a more convenient anatomical location, than a native LN, for immunological assay and MPLSM. However, the objective of this PhD thesis was to investigate the relationship between the DC-T cell interactions taking place at a tissue site of inflammation and its draining LN. Thus, the next step in these studies was to develop a model of tissue inflammation in the ear pinna that could be combined with the LN transplant system and this is discussed in the next chapter.

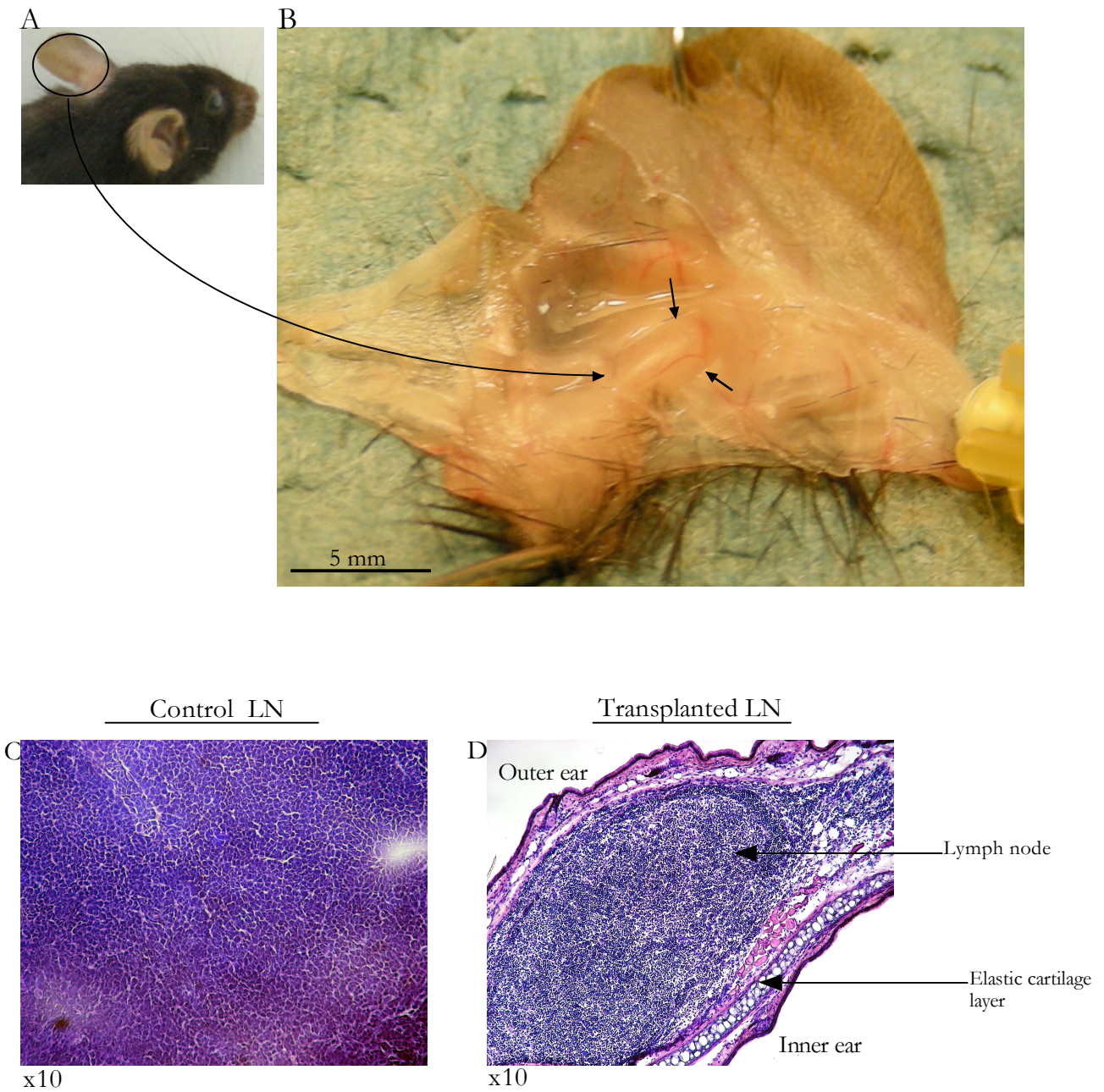


Figure 4.1 The tLN appeared histologically normal

3 weeks following the transplant of a C57BL/6J/CD45.1 LN into the ear pinna of a C57BL/6J/CD45.2 mouse, the ear pinna was dissected to examine the LN (A) Photograph of ear pinna prior to dissection (B) Photograph of tLN within the ear pinna following dissection of the epidermis. Black arrows indicate the tLN surrounded by blood vessels. (C) Bright-field image of a section of a control LN stained with H&E (D) Bright-field image of a section of an ear pinna containing a tLN.

A.

	6 week old recipient			8 week old recipient			10 week old recipient			Total
	Mouse 1	Mouse 2	Mouse 3	Mouse 1	Mouse 2	Mouse 3	Mouse 1	Mouse 2	Mouse 3	
Source of donor LN										
Popliteal	--	-	-	-	-	-	-	-	-	0
Cervical	+	-	-	-	-	-	-	-	-	1
Axillary	-	-	-	+	-	-	-	-	-	1
Brachial	+	+	-	+	+	+	-	-	+	6
Inguinal	-	-	-	-	+	-	-	+	-	2
	Total number of successful transplants using 6 week recipients: 3 out of a possible 15			Total number of successful transplants using 8 week recipients: 5 out of a possible 15			Total number of successful transplants using 10 week recipients: 2 out of a possible 15			

Key: transplant unsuccessful: - transplant successful: +

B.

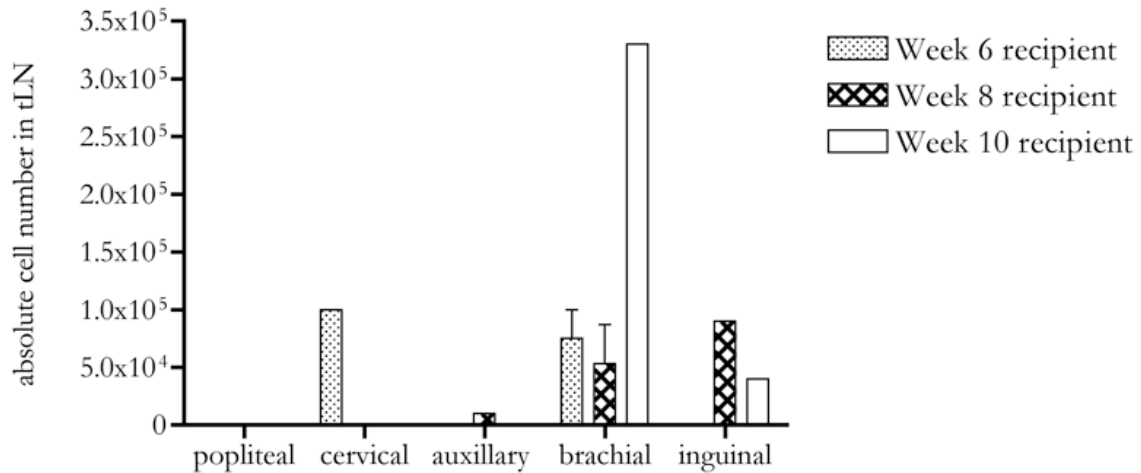


Figure 4.2 Age of recipient and type of LN transplanted, alters success rate of LN transplantation procedure

To establish whether the age of the recipient mouse or the source of the LN had any impact on the overall success rate of the transplant procedure, a variety of 3 ages and 5 types of LN were trialled in triplicate. The age of the donor mouse remained constant throughout at 3 weeks of age. (A) Table summarises the success rate of varying the source of LN and the age of the recipient mouse (B) The graph displays the absolute cell numbers counted in the successful transplants.

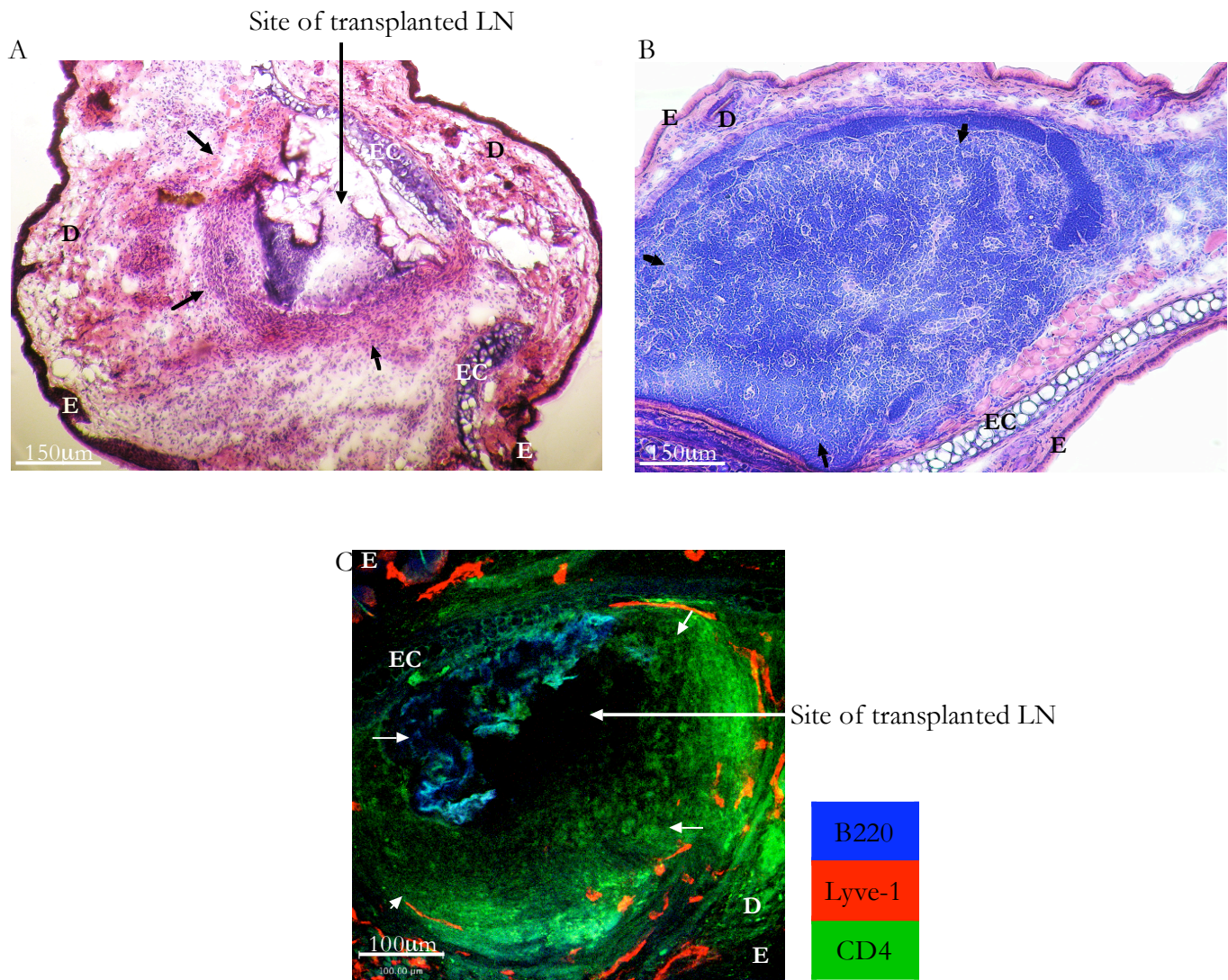


Figure 4.3 Using neonatal LNs for the transplant procedure proved unsuccessful.

3 weeks following the transplant of a 3 day old neonatal BALB/c LN into the ear pinna of a BALB/c recipient mouse, fluorescence immunohistochemistry was performed to detect the presence of CD4⁺ T cells (green), B220⁺ B cells (blue) and Lyve-1⁺ lymphatic vessels (red). EC=elastic cartilage layer E=epidermis D=dermis (A) Image of ntLN stained with H&E at x20 magnification. Arrows indicate the area of necrotic tissue where the LN was transplanted. (B) Image of histologically normal tLN stained with H&E at x20 magnification. Arrows indicate the LN from 3 week old donor within the ear pinna. (C) Confocal image of ear pinna containing the tLN at x40 magnification. Section was stained to detect CD4⁺ T cells (green), B220⁺ B cells (blue) and Lyve-1⁺ lymphatic vessels (red). White arrows indicate the necrotic auto-fluorescent tissue of the failed transplant. No CD4 or BB20 positive staining was observed, however, lymphatic vessels of the ear pinna could be clearly visualised.

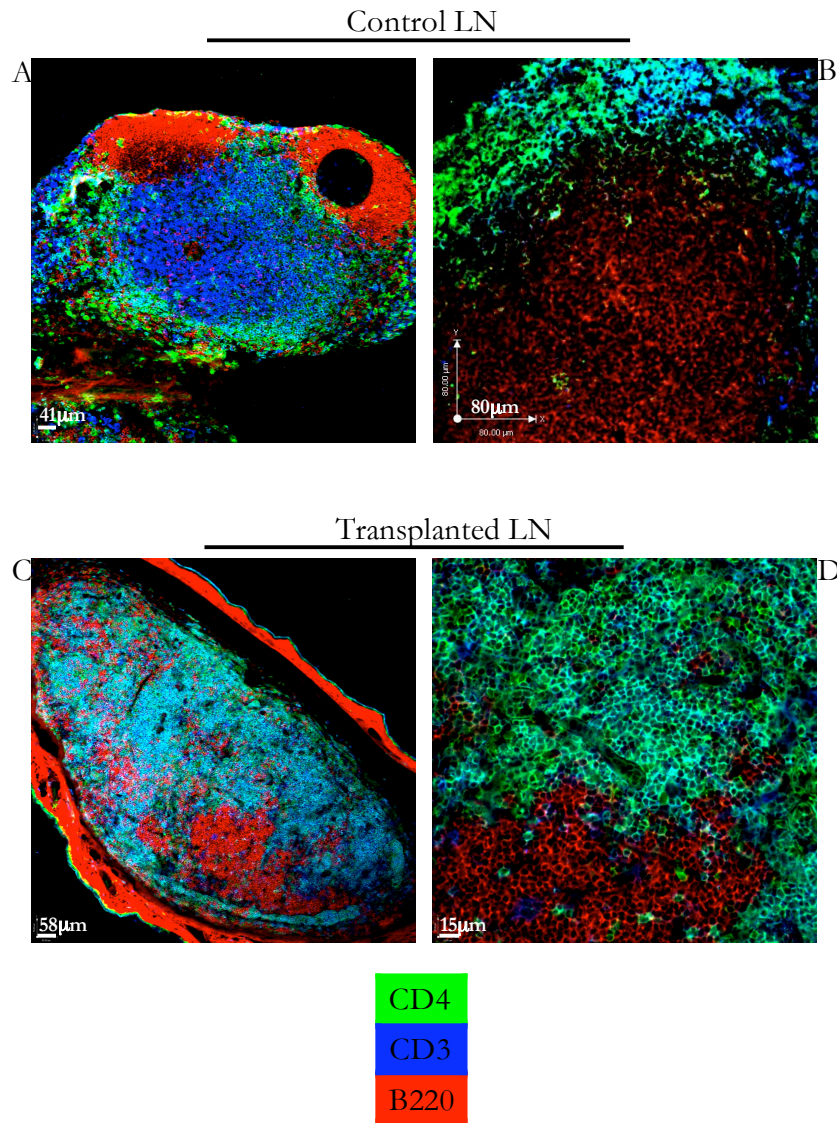


Figure 4.4 T and B lymphocyte areas can be visualised within the tLN

3 weeks following the transplant of a C57BL/6J/CD45.1 LN into the ear pinna of a C57BL/6J/CD45.2 mouse, fluorescence immunohistochemistry was performed to detect the presence of the CD3⁺ (blue) CD4⁺ (green) T cells and B220⁺ B cells (red) within the tLN. As a control, a C57BL/6J/CD45.2 LN was also prepared for immunofluorescence. (A) Confocal image of a control LN at x10 magnification (B) Confocal image of a control LN at x40 magnification (C) Confocal image of ear pinna containing the tLN at x10 magnification (D) Confocal image of ear pinna containing the tLN at x40 magnification. The images shown here are representative of 3 replicate mice

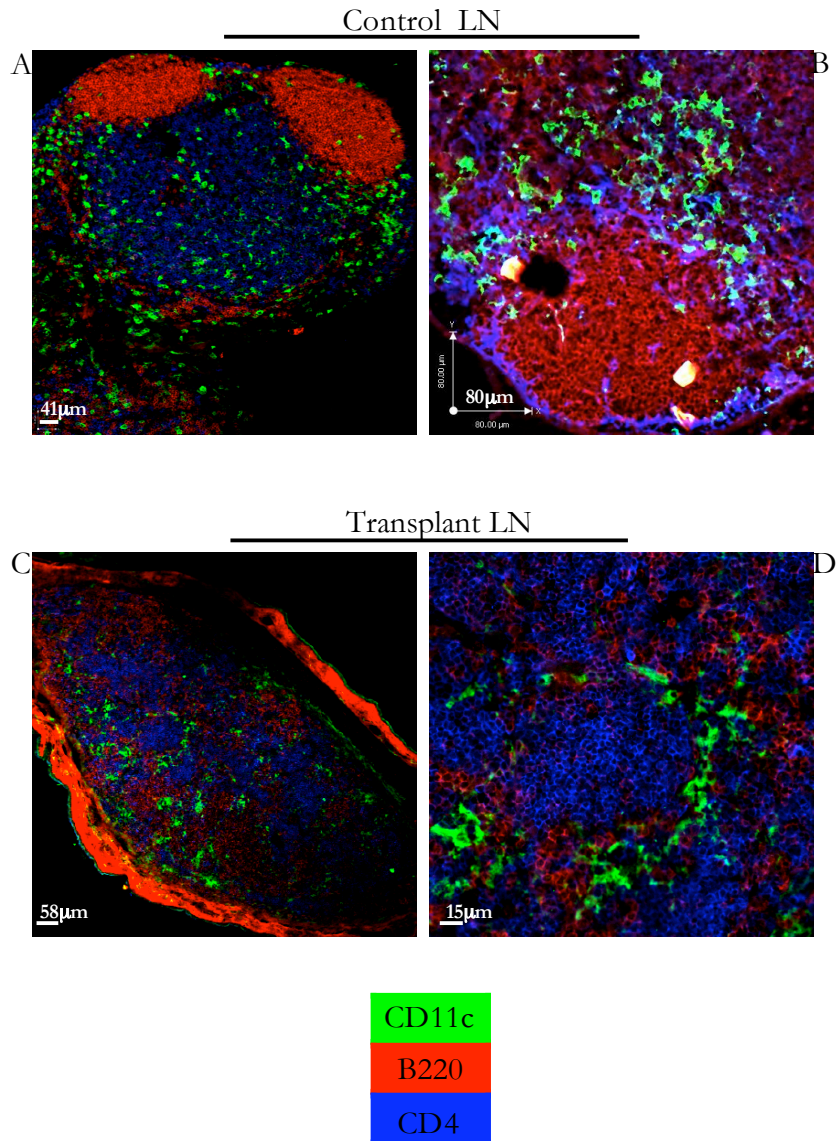


Figure 4.5 CD11c expressing dendritic cells can be detected in the tLN

3 weeks following the transplant of a C57BL/6J/CD45.1 LN into the ear pinna of a C57BL/6J/CD45.2 mouse, fluorescence immunohistochemistry was performed to detect the presence of the CD4⁺ T cells (blue), B220⁺ B cells (red) and CD11c⁺ DCs (green). As a control, a C57BL/6J/CD45.2 LN was also prepared for immunofluorescence. (A) Confocal image of a control LN at x10 magnification (B) Confocal image of a control LN at x40 magnification (C) Confocal image of ear pinna containing the tLN at x10 magnification (D) Confocal image of ear pinna containing the tLN at x40 magnification. Images shown here are representative of 2 replicate mice.

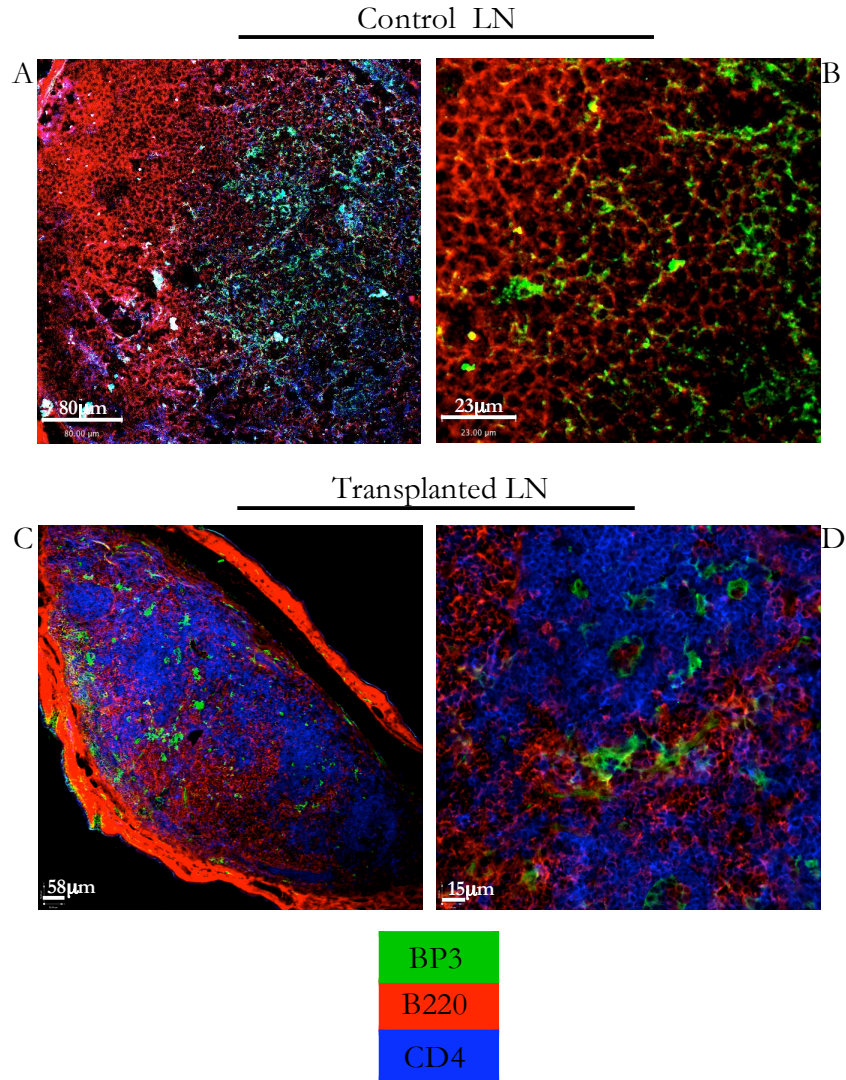


Figure 4.6 BP3⁺ stromal cells can be detected in the tLN

3 weeks following the transplant of a CD45.1 LN into the ear pinna of a C57BL/6J/CD45.2 mouse, fluorescence immunohistochemistry was performed to detect the presence of CD4⁺ T cells (blue), B220⁺ B cells (red) and BP3⁺ stromal cells (green). As a control, a C57BL/6J/CD45.2 LN was also prepared for immunofluorescence. (A) Confocal image of a control LN at x10 magnification (B) Confocal image of a control LN at x40 magnification (C) Confocal image of an ear pinna containing the tLN at x10 magnification (D) Confocal image of an ear pinna containing the tLN at x40 magnification. Images shown here are representative of 2 replicate mice.

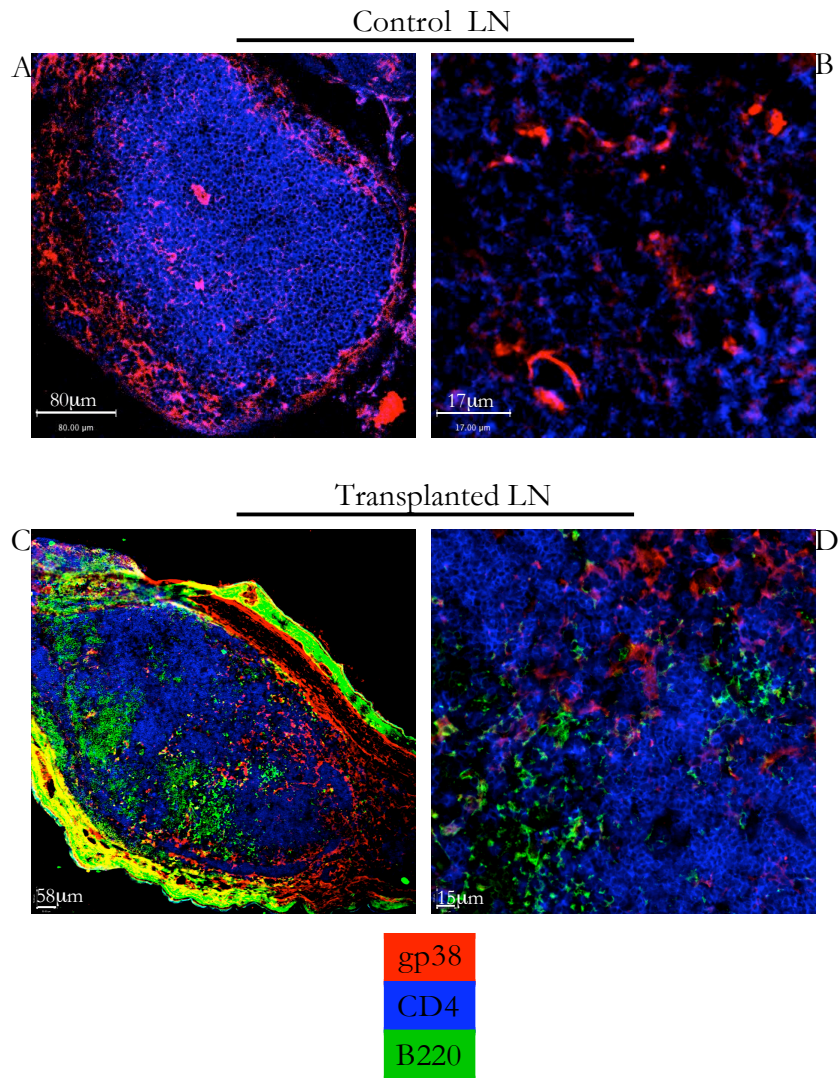


Figure 4.7 Gp38⁺ lymphatic endothelial cells can be detected in the tLN

3 weeks following the transplant of a C57BL/6J/CD45.1 LN into the ear pinna of a C57BL/6J/CD45.2 mouse, fluorescence immunohistochemistry was performed to detect the presence of CD4⁺ T cells (blue), B220⁺ B cells and gp38⁺ (red) lymphatic endothelial cells (red). As a control, a C57BL/6J/CD45.2 LN was also prepared for IHC. (A) Confocal image of a control LN at x10 magnification (B) Confocal image of a control LN at x40 magnification (C) Confocal image of ear pinna containing the tLN at x10 magnification (D) Confocal image of ear pinna containing the tLN at x40 magnification.

The images shown here are representative of 2 replicate mice.

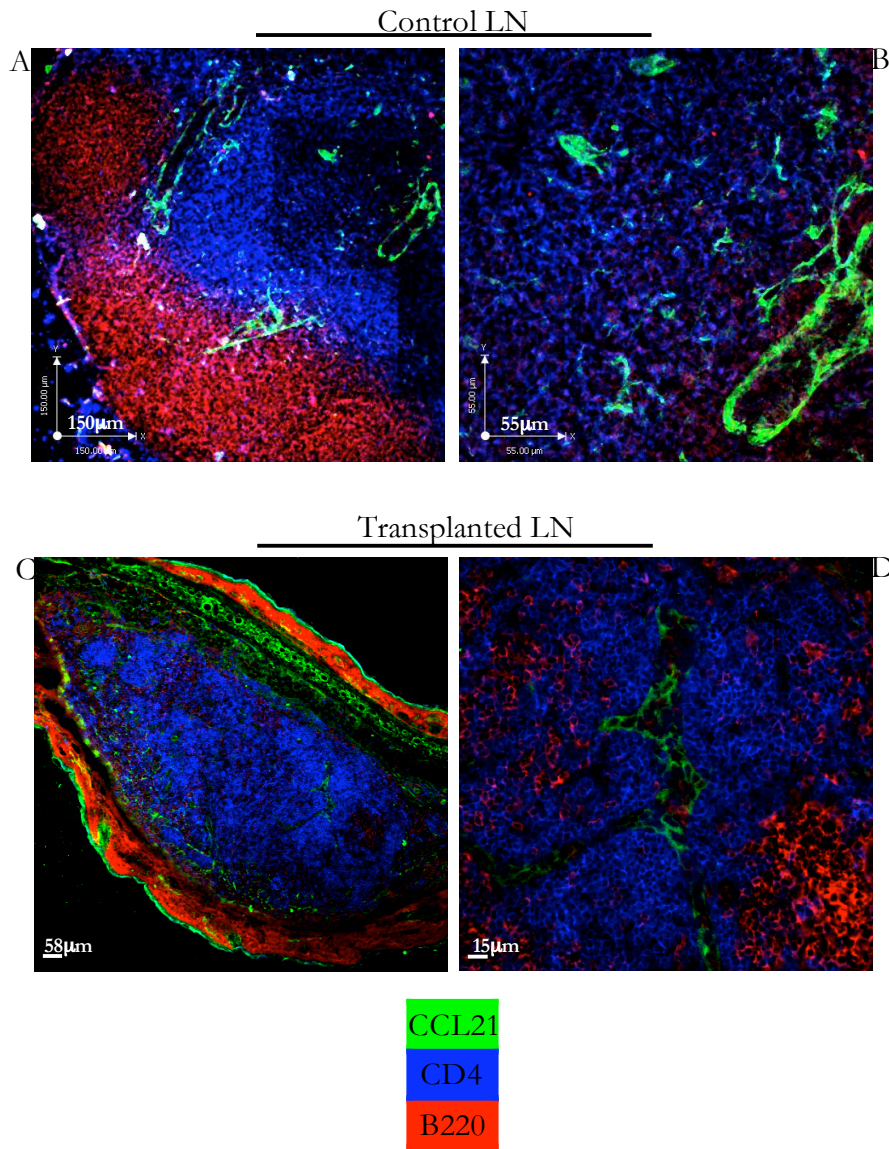


Figure 4.8 The T cell attracting chemokine CCL21 can be detected within the tLN

3 weeks following the transplant of a C57BL/6J/CD45.1 LN into the ear pinna of a C57BL/6J/CD45.2 mouse, fluorescence immunohistochemistry was performed to detect the presence of the chemokine CCL21. As a control, a C57BL/6J/CD45.2 LN was also prepared for immunofluorescence. Sections were stained to detect CD4⁺ T cells (blue), B220⁺ B cells (red) and the chemokine CCL21 (green). (A) Confocal image of a control LN at x10 magnification (B) Confocal image of control LN at x40 magnification (C) Confocal image of ear pinna containing the tLN at x10 magnification (D) Confocal image of ear pinna containing the tLN at x40 magnification. Images shown here are representative of 2 replicate mice.

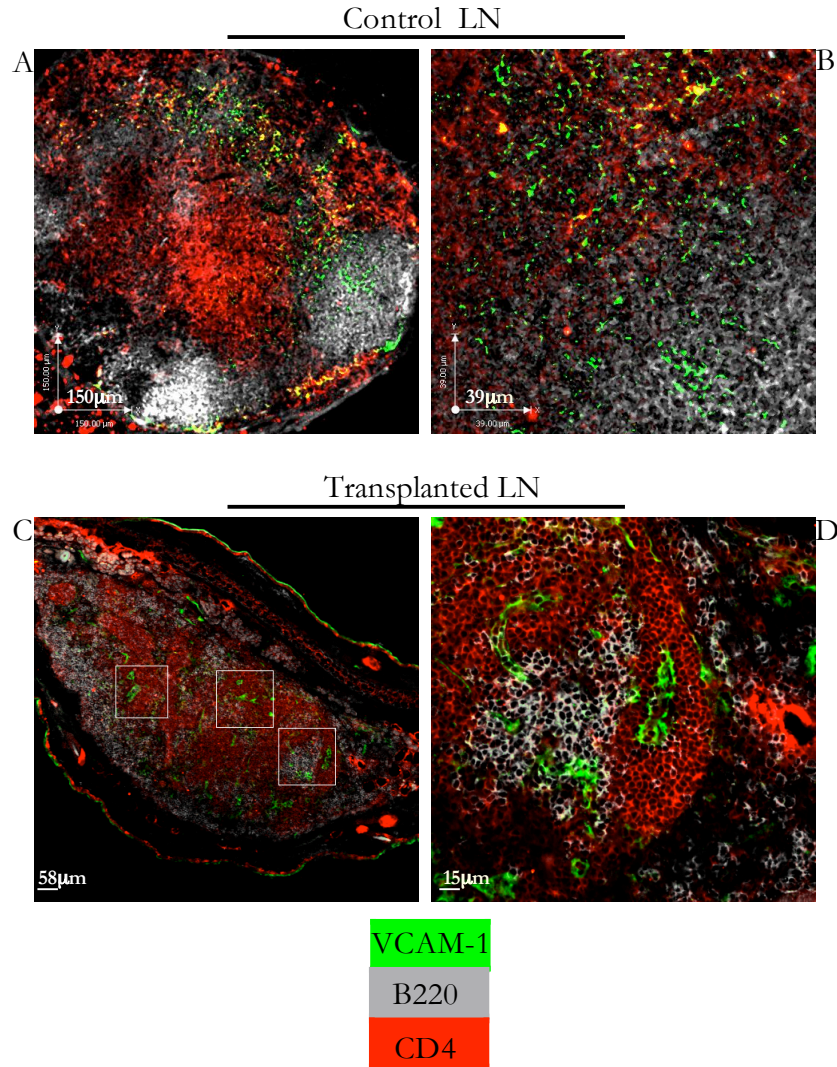


Figure 4.9 Vascular cell adhesion molecule 1 (VCAM-1) can be detected in the tLN

3 weeks following the transplant of a CD45.1 LN into the ear pinna of a C57BL/6J/CD45.2 mouse, fluorescence immunohistochemistry was performed to detect the presence of the CD4⁺ T cells (red) and B220⁺ B cells (grey) and the vascular endothelial cell marker, VCAM-1 (green). As a control, a C57BL/6J/CD45.2 LN was also prepared for immunofluorescence. (A) Confocal image of a control LN at x10 magnification (B) Confocal image of a control LN at x40 magnification (C) Confocal image of an ear pinna containing the tLN at x10 magnification (D) Confocal image of ear pinna containing the tLN at x40 magnification. Images shown here are representative of 2 replicate mice.

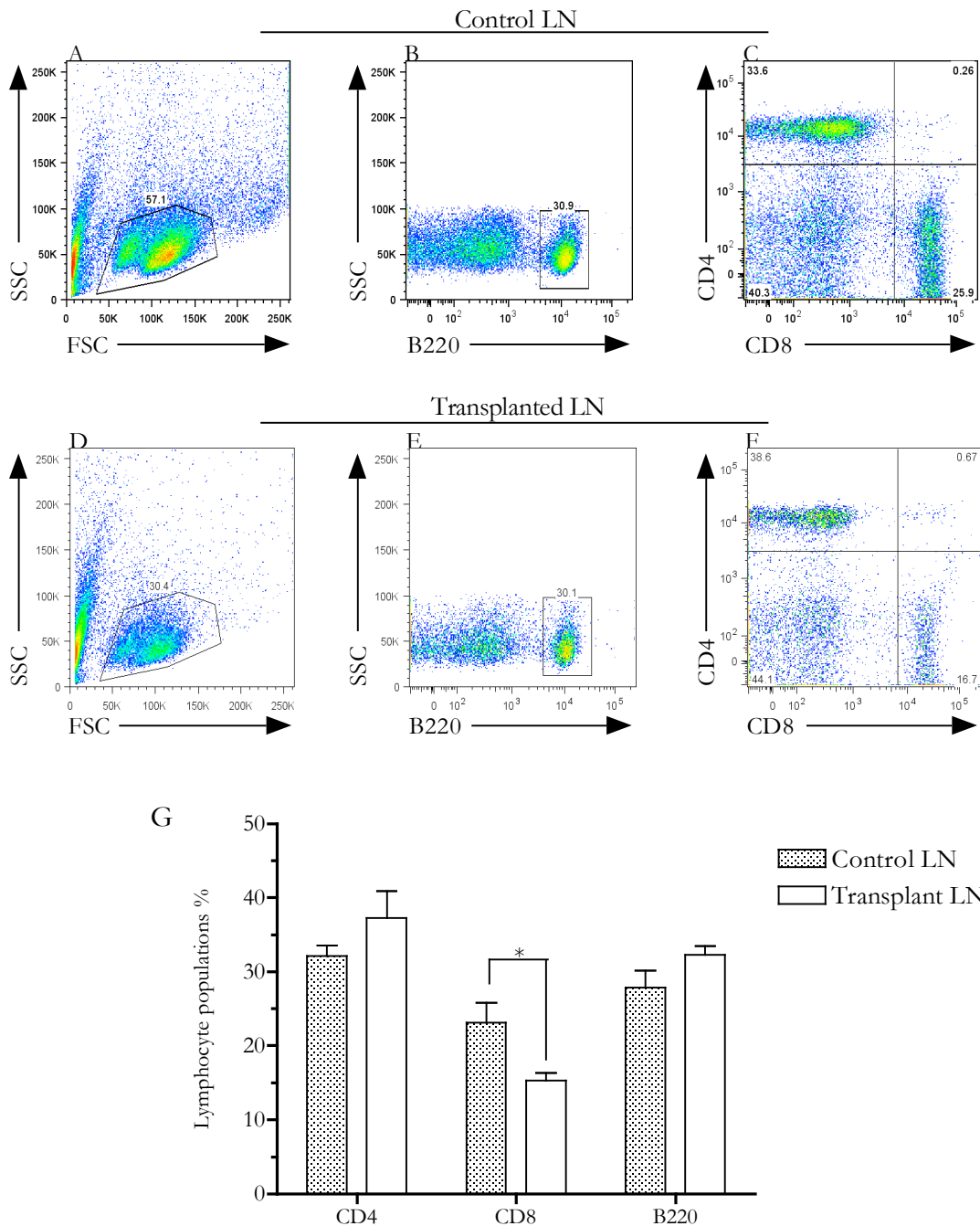
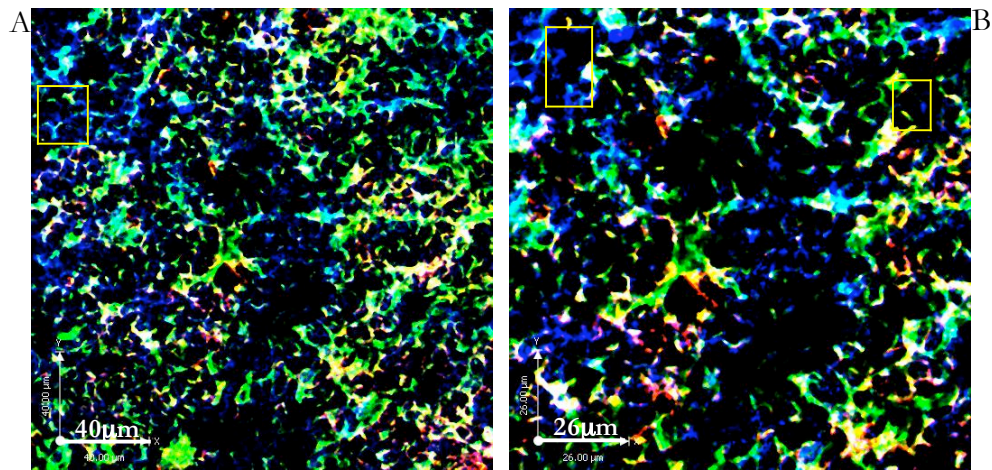


Figure 4.10 A comparison of the populations of lymphocytes within the tLN to the populations in a control LN

Flow cytometry was used to establish the proportion of B220⁺ B cells, CD4⁺ T cells and CD8⁺ T cells in both a control LN and the tLN, 3 weeks following the engraftment procedure.

Representative flow cytometric plots show (A) lymphocytes from control LN identified on basis of size and granularity (B) A population of B220⁺ lymphocytes (C) and CD4 expressing and CD8 expressing T lymphocytes within the control LN (D) lymphocytes from tLN identified on basis of size and granularity (E) Gate identifies a population of B220⁺ lymphocytes within the tLN (F) Gates identify CD4 expressing and CD8 expressing T lymphocytes within the tLN (G) Graph summarises the proportions of each cell type detected in the control LN and tLN. The proportions of CD4⁺ T cells and B220⁺ B cells were comparable between the control and tLN, however, the proportion of CD8⁺ T cells was significantly lower in the tLN (*p=0.0252). Data show mean of 5 replicate mice +/- SD

Control LN



Transplanted LN

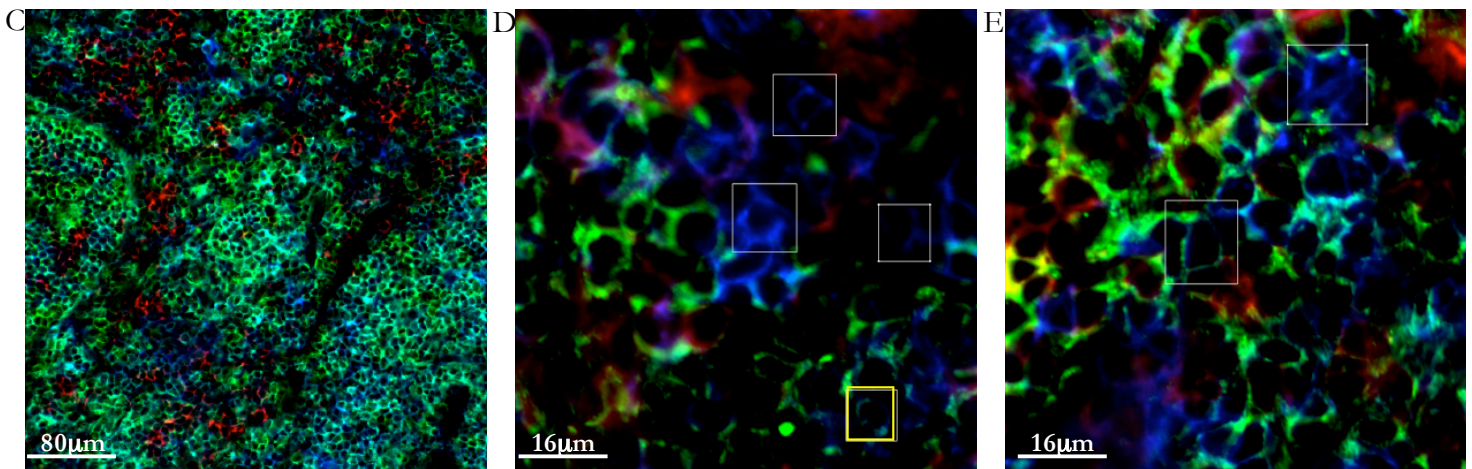


Figure 4.11 LN inducer cells of host mouse origin can be detected within the tLN

3 weeks following the transplant of a CD45.1 LN into the ear pinna of a C57BL/6J/CD45.2 mouse, IHC was performed to detect the presence of Lymph node inducer cells within the tLN. As a control, a C57BL/6J/CD45.2 LN was also prepared for fluorescence immunohistochemistry. Sections were stained with CD4 (blue), CD45.2 (green), CD3, CD11c and B220 (red). Cells were considered possible LN inducer cells on the basis of being CD4⁺CD45.2⁺CD3⁻CD11c⁻B220⁻ (A) Confocal image of a control LN at x40 magnification. Possible inducer cells are highlighted by a yellow box (B) Confocal image of control LN at x40 magnification with digital zoom 2. Possible inducer cells are highlighted by a yellow box. Confocal images (D) and (E) show the tLN at x40 magnification with digital zoom 4. Cells surrounded by a white box are single positive CD4 cells and are suspected CD45.1⁺ inducer cells of donor LN origin, while cells surrounded by a yellow box are double positive for CD4 and CD45.2 and are possible inducer cells of host origin. Images shown here are representative of 2 replicate experiments.

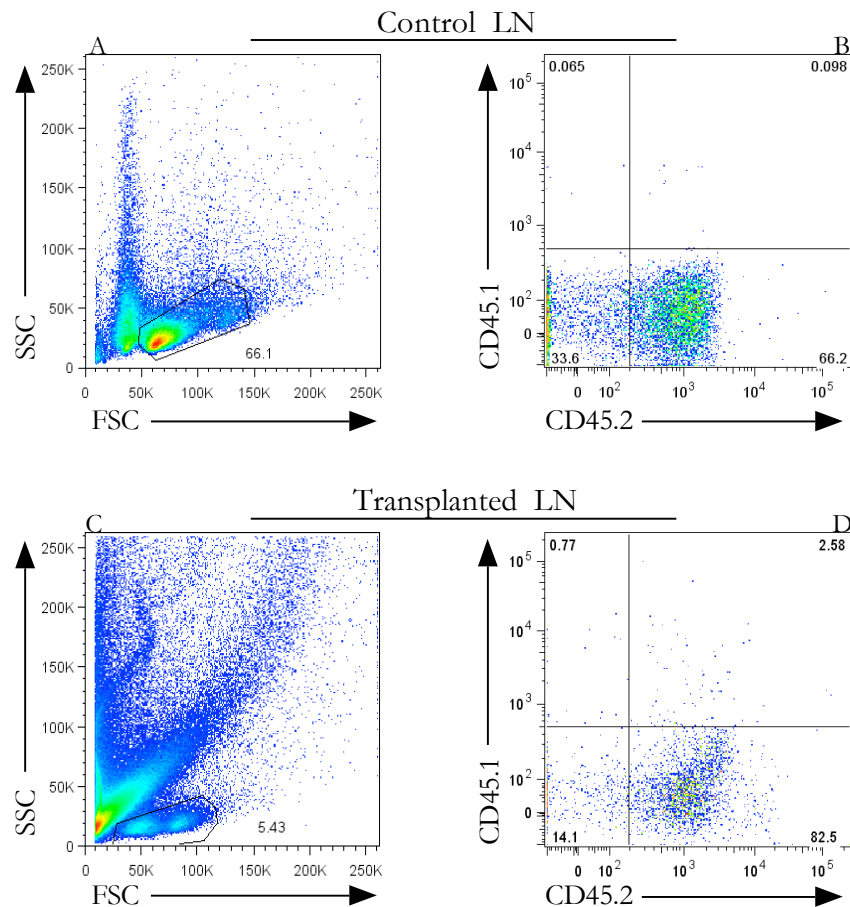


Figure 4.12 Lymphocytes from the recipient mouse re-circulate into the transplanted LN

A LN was transplanted from a CD45.1⁺ C57BL/6J mouse into the ear pinna of a CD45.2⁺ C57BL/6J mouse. After 3 weeks, all LNs were removed for flow cytometric analysis to test for the presence of CD45.1⁺ and CD45.2⁺ cells in both the host LNs and the transplanted LN. Representative flow cytometric plots of (A) Host LNs were pooled and lymphocytes were identified on the basis of their size and granularity (B) Lymphocytes from host LNs were then examined for their expression of CD45.1⁺ and CD45.2⁺. Gate identifies a population of CD45.2⁺ lymphocytes cells while no CD45.1⁺ cells of donor mouse origin were detected. (C) Lymphocytes from the transplanted LN were identified on the basis of their size and granularity (D) Lymphocytes from the transplanted LN were then examined for their expression of CD45.1⁺ and CD45.2⁺. Gate identifies a population of CD45.2⁺ lymphocytes of host mouse origin within the transplanted LN. The original CD45.1⁺ cell population was not detected. Representative plots taken from a group of 3 replicate mice from 2 experiments.

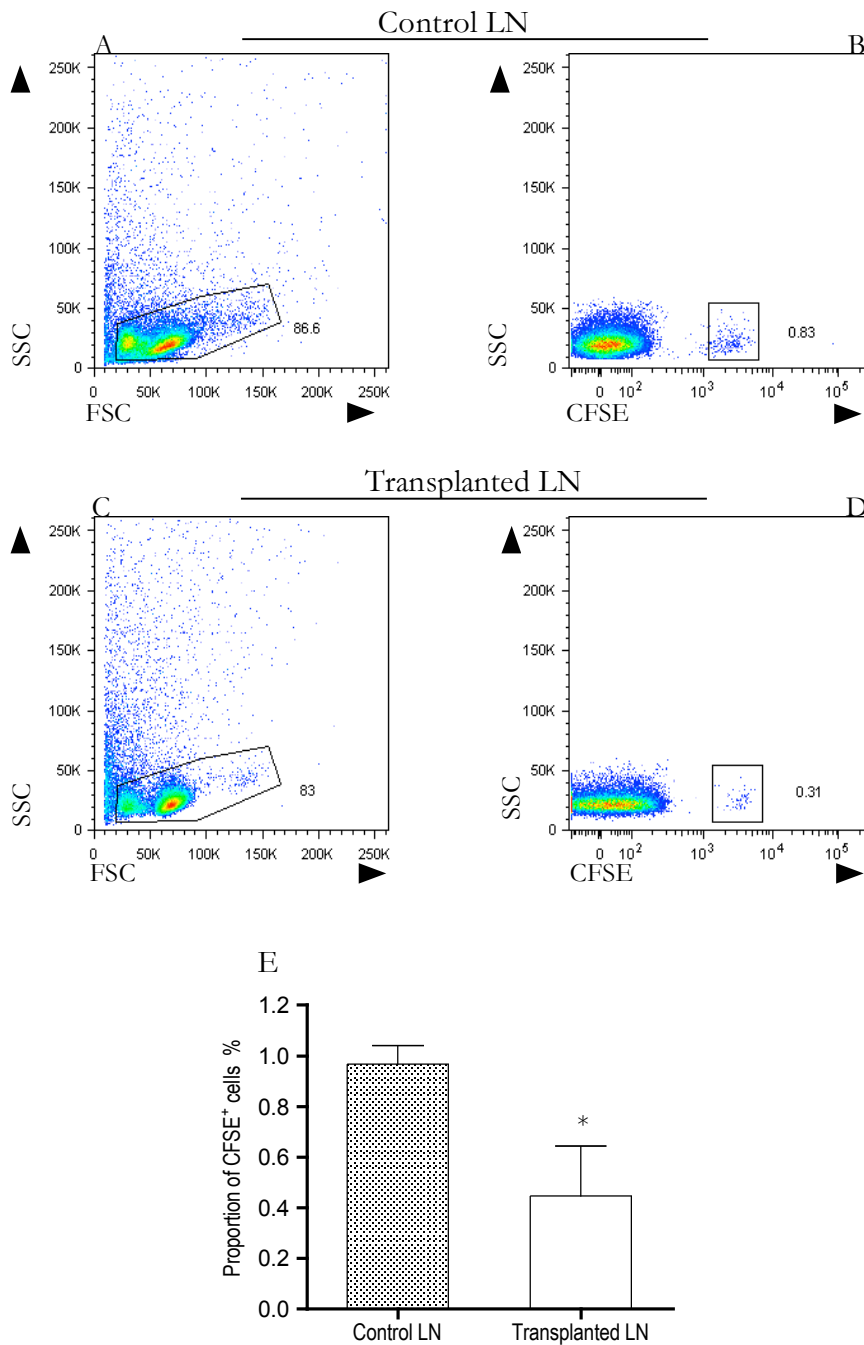


Figure 4.13 Adoptively transferred CFSE labelled lymphocytes re-circulate into host LNs and the tLN

LN were transplanted into the ear pinna of BALB/c mice. After 3 weeks, CFSE labelled lymphocytes were adoptively transferred intravenously via the tail vein. Cells were detected within the LNs using flow cytometry 24 hours later. Representative flow cytometric plots showed. (A) Lymphocytes from the brachial LN being identified on basis of size and granularity. (B) A population of transferred CFSE labelled lymphocytes were detected within the brachial LN (C) Lymphocytes from the tLN were identified on basis of size and granularity. (D) A population of transferred CFSE labelled lymphocytes were detected within the tLN. (E) Summary of the proportion of CFSE transferred cells detected in host LNs and tLN. Significantly fewer CFSE cells were detected in the tLN in comparison with the host LNs (* $p=0.0178$). Data shows mean of 3 replicate mice +/- SD

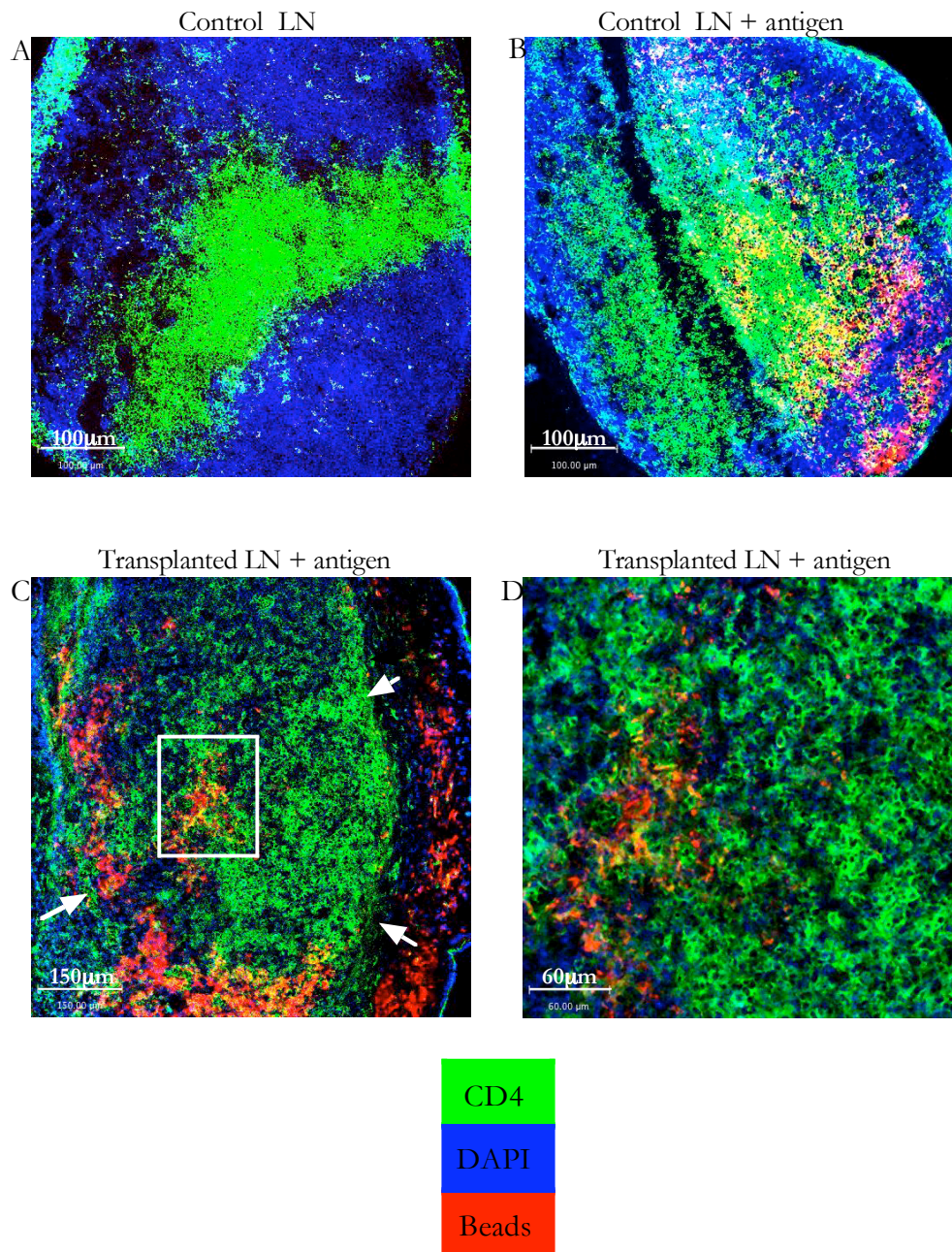
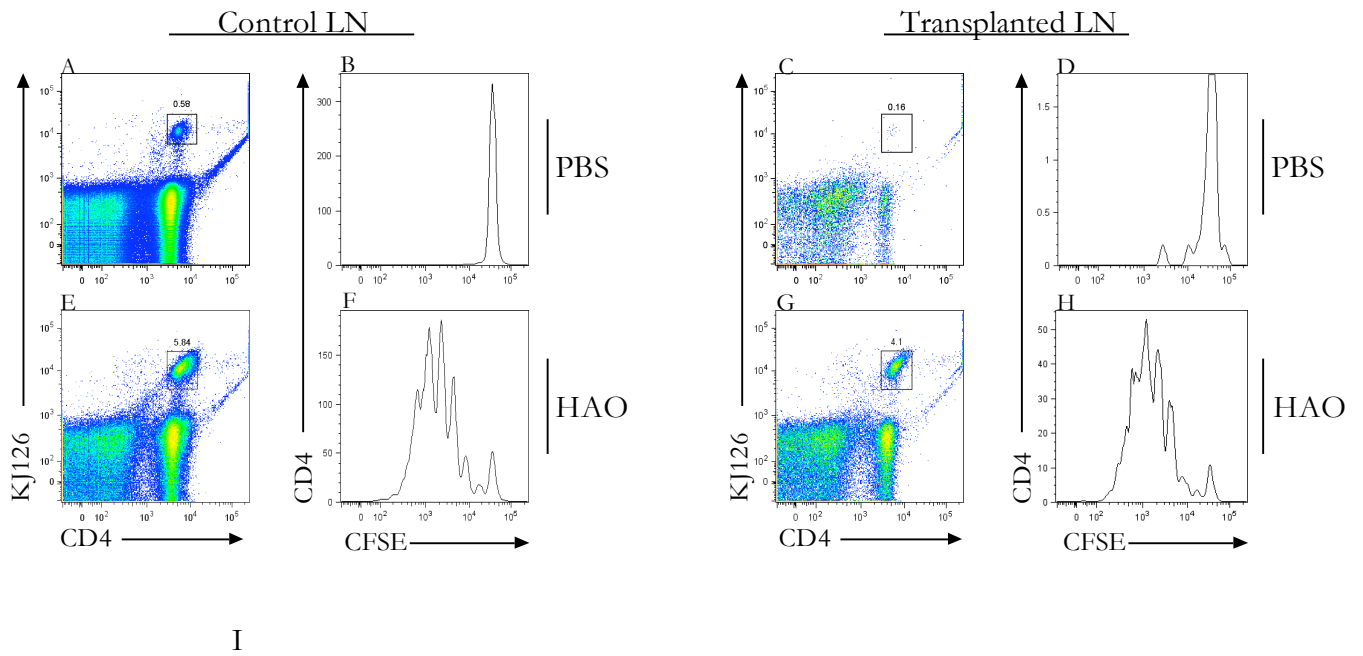


Figure 4.14 The tLN can drain antigen from its new anatomical location within the ear pinna

Alexa-fluor-660 microbeads of diameter 0.04µm (red) were injected into the footpad or the ear pinna. Following 24 hours, the draining popliteal LN or the tLN and small portion of the surrounding ear pinna were removed, sectioned and analysed for CD4⁺ T cells (green) and DAPI (blue) to highlight the nuclei. (A) Section of popliteal LN from negative control mouse injected subcutaneously with PBS. (B) Section of popliteal LN from positive control mouse injected subcutaneously with red beads. (C) Section of ear pinna containing tLN following subcutaneous injection with red beads at the tip of the ear pinna, white arrows indicate the edges of the tLN within the ear pinna. Red beads can be seen draining into and the tLN. The white box highlights the area presented at higher magnification in image E (E) Section of tLN at x40 magnification to highlight CD4⁺ cells and clear presence of red beads within the tLN



I

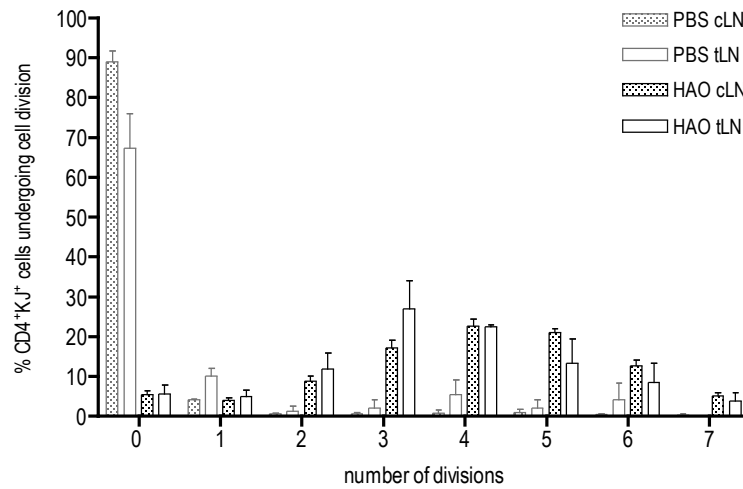


Figure 4.15 The tLN can respond to antigen challenge in a conventional manner

3 weeks following the transplant of a BALB/c LN into the ear pinna of a BALB/c mouse, CFSE labelled DO11.10 T cells were adoptively transferred *iv*. Mice were either challenged with PBS as a control, or immunised with HAO in the tip of the ear pinna. 3 days later, the tLN and the draining cervical LN were removed for flow cytometric analysis. Lymphocytes were gated on the basis of size and granularity and DO11.10 T cells were classified as CD4⁺KJ1.26⁺ and their incremental loss of CFSE intensity was used as a marker of cell division. Representative flow cytometric plots following PBS challenge in the ear pinna show DO11.10 T cells in the (A) cervical LN and (C) tLN identified on the basis of co-expression of CD4 and KJ1.26. (B) CD4⁺KJ1.26⁺ cells in the cervical LN and (D) tLN showed no incremental loss of CFSE. Representative flow cytometric plots following immunisation in the ear pinna with HAO show DO11.10 T cells in the (E) cervical LN and (G) tLN identified on the basis of co-expression of CD4 and KJ1.26. Incremental loss of CFSE intensity in the (F) cervical LN and (H) tLN, reflecting antigen specific proliferation. (I) Graph summaries the number of rounds of cell division undertaken by CD4⁺KJ1.26⁺ cells in the cervical LN in comparison to the tLN in response to HAO challenge. Data represents the mean of triplicate samples +/- SD. (n=2)

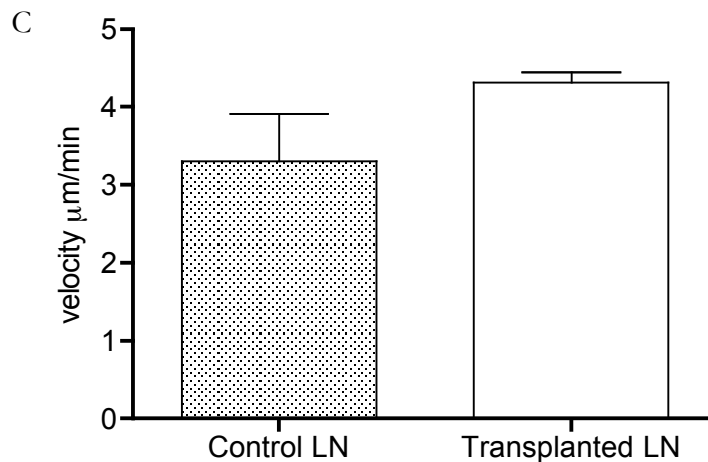
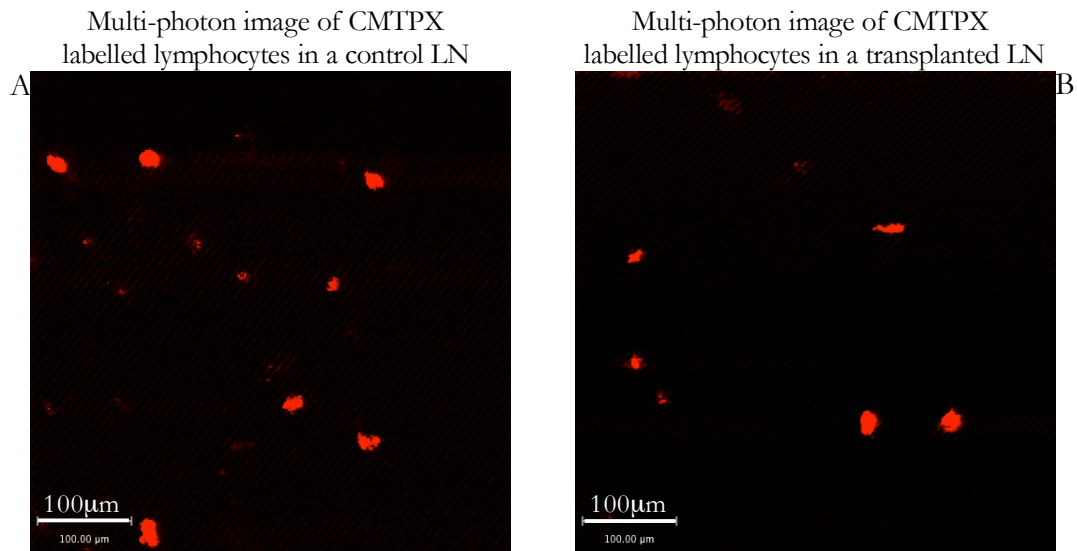


Figure 4.16 Multi-photon imaging of the tLN in situ reveals that lymphocytes migrate within the tLN at comparable velocities to lymphocytes within a control LN

3 weeks following the transplant of a C57BL/6J LN into the ear pinna of a C57BL/6J mouse, CMTPX labelled lymphocytes were adoptively transferred iv. Following 24hrs, the tissue was perfused with warmed oxygenated medium and CMTPX labelled cells in the tLN and control LN were imaged by multi-photon microscopy. Images represent a z-compressed 30- μm stack from a single time point (full sequences available as movies on attached CD). (A) Image of CMTPX labelled lymphocytes migrating in the control LN (B) Image of CMTPX labelled lymphocytes migrating in the tLN (C) Graph summarises lymphocyte migration, calculated using Volocity software and shows the mean velocity of cells \pm SD, $\mu\text{m}/\text{min}$. Data shown are representative of triplicate samples from 2 similar experiments.

Chapter 5

Developing an imageable tissue site of inflammation in the ear pinna

5.1 Introduction

The overall aim of this PhD was to develop systems to investigate DC-T cell interactions taking place within a tissue site of inflammation and its DLN. A novel model of LN transplantation in the ear pinna was outlined in the previous chapter. This system was shown to provide a fully functional LN in a more convenient anatomical location for *in vivo* MPLSM, than a native LN. However, to facilitate the study of DC-T cell interactions in and between both the tLN and the tissue site of inflammation, it was necessary to further develop the LN transplant model to include a site of inflammation within close proximity. This chapter therefore outlines the development of a model of tissue inflammation in the ear pinna of the mouse and explores the potential for analysing the site using MPLSM and immunological assay. In addition, to enable DCs and T cells to be visualised and tracked at and between each anatomical location *in vivo* by MPLSM, fluorescent probes are required to label each cell type. This chapter outlines the technical difficulties associated with tracking cells between distinct anatomical locations and discusses the development of a novel photo-switchable fluorescent probe which should allow cells to be tracked between the tissue site of inflammation and DLN in future imaging studies of the *in vivo* model systems established in this chapter and in chapter 4.

Infections are generally initiated in non-lymphoid peripheral tissues and protective immunity at these sites is therefore crucial. However, the initial activation of T cells, which mediate this protection during localised infection, takes place within draining secondary lymphoid organs (9, 269, 285). Antigen and antigen presenting cells from a tissue site of infection drain to the LN, where they specifically interact with, and activate, antigen specific T cells to initiate their proliferation and differentiation. The resulting effector T cells migrate from the LN to the site of inflammation where they can mediate protective immunity (47). As outlined in chapter 1, the kinetics and dynamics of DC-T cell interactions in the DLN during the initiation of an adaptive immune response are well characterised (4, 7, 9, 236, 237, 280, 339). However, while it is well established that both DCs and T cells are present at the tissue site of inflammation, the kinetics and dynamics of their interactions in non lymphoid tissues are poorly defined (18, 51-53). However, what is known is that effector memory T cells can be re-activated to produce inflammatory cytokines at the tissue site of infection, through direct

interaction with antigen presenting dermal DCs (18, 120, 216, 219). In contrast, the behaviour of newly activated effector T cells at the tissue site of inflammation in a primary response is less clear. In particular, whether effector T cells proliferate in non-lymphoid tissues in response to re-encounter with antigen loaded DCs or simply carry out effector functions such as cytokine production is contentious. Furthermore, whether activated effector T cells are maintained at the tissue site of inflammation or are required to migrate back to the DLN is unknown. Consequently, understanding whether DCs and T cells interact in non-lymphoid tissue sites and whether this is important in the maintenance and regulation of an immune response could provide novel targets in the therapeutic enhancement or inhibition of T cell activation at these sites.

A more detailed knowledge of the dynamic migration and cellular interactions of effector T cells will have important consequences for the development of immuno-therapeutics, which generally aim to manipulate secondary immune responses, such as vaccines or treatments of chronic inflammatory diseases. Using MPLSM the motility of naïve, primed and tolerised CD4⁺ T cells and their interactions with DCs, were imaged and characterised within the LN to show that naïve, primed and tolerised T cells migrate at distinct velocities and interact with DCs differently before and after secondary antigen-encounter (205). However, since effector T cells carry out their functions in inflamed non-lymphoid tissues, it is critical that imaging studies of secondary immune responses progress to characterising the dynamics of effector T cells at the tissue site of inflammation, as well as in the LN. Thus far, few attempts have been made to visualise effector T cells and their interactions within non-lymphoid tissue sites of inflammation due to the technical difficulties associated with such experiments. However, CD8⁺ cytotoxic T cells have been imaged using MPLSM infiltrating solid tumours and brain tissue in mouse models of cancer and experimental autoimmune encephalomyelitis, respectively. These studies have focused on tracking CD8⁺ cytotoxic T cell interacting with and killing target cells in the inflamed tissue site (210-214). In addition, CD4⁺ effector memory T cells have been imaged migrating within the ear pinna during a DTH response and their behaviour characterised in the presence and absence of a calcium channel blocking molecule (211, 212). CD4⁺ effector memory T cells stably attached to and interacted with antigen presenting cells during the DTH reaction and blocking calcium signalling could inhibit the migration of these cells through the tissue, suggesting a

requirement for continued stimulation of activated effector T cells during an inflammatory response in non-lymphoid tissues and a potential therapeutic target for the treatment of chronic inflammatory disease (211, 212). These studies have provided key insights into effector T cell dynamics at the tissue site of inflammation, however, in comparison with imaging studies of naïve T cell migration and DC-T cell interactions in the LN, progress to characterise effector T cells and their interactions with DCs in non-lymphoid tissues has been slow. Imaging by MPLSM has a limited depth of tissue penetration of approximately 200µm (340). Thus, to image an inflamed tissue, the site would need to be relatively superficial or exposed. Moreover, the field of view is limited to a small region and it is therefore necessary to maximise the number of cells within the site to ensure that enough cells can be imaged in a single area. As a result, the memory response is often deemed easier to image than the primary response, due to the higher number of clonally expanded T cells (19, 341-343). Lastly, labeling cells with conventional fluorescent dyes for imaging is technically challenging since often T cells lose fluorescence with each round of cell division (344). Thus, while imaging T cells during the early stages of activation in the LN can be done, imaging the same T cells at the tissue site of inflammation following their clonal expansion is not feasible due to the loss of fluorescence (345). Thus, by combining the novel systems developed in this chapter with the LN transplant system of chapter 4, a unique model for exploring unanswered questions regarding T cell behaviour at the tissue site of inflammation should be provided. Moreover, by employing the use of endogenously labelled T cells and the thin ear pinna as the tissue site of inflammation, some of the technical caveats associated with conventional fluorescent probes and MPLSM may be overcome.

In this chapter, two models of tissue inflammation are explored, the air pouch model and delayed type hypersensitivity reaction (DTH). First described in 1987 by Sedgwick *et al.*, the air pouch model is achieved by the repeated injection of sterile air into the subcutaneous tissue of the dorsal flank of the mouse or rat (346). The injected air mechanically disrupts the subcutaneous connective tissue and gives rise to the formation of a structurally defined *in vivo* culture chamber in which to study inflammation (346-350). Examination of the air pouch cavity by electron microscopy revealed a distinct cell lining consisting of two main cell types (351). Firstly, a fibroblast like cell with prominent rough endoplasmic reticulum and secondly, a macrophage like cell with many vacuoles and vesicles (346). Morphologically the

air pouch lining has been shown to closely resemble the synovial layer of the large joints, such as the knee (228). Thus, the air pouch model has been proposed for use in the study of rheumatoid arthritis, a painful and debilitating auto-immune disease, characterised by chronic inflammation of the synovial membrane (351-353). However, the location of the synovial tissue, deep within the joint, renders it a technically challenging structure to study. Thus, by creating a synovium-like structure in the more convenient location of the rump, the air pouch model has proved useful in studies of the behaviour and reactivity of synovial lining tissue towards irritants known to cause inflammation (346, 347). However, while the rump has proved a suitable anatomical location for the injection of substances and collection of cells and inflammatory mediators, more complex assays of the air pouch and DLN using MPLSM could not be achieved without surgical exposure of either site. Thus, this chapter attempted to create a synovium-like structure in the more anatomically accessible location of the ear pinna, with the potential of combining it with the LN transplant model. Moreover, the use of this model would permit the dissection of the components involved in the inflammatory reactivity of synovial tissue and may help explain the sensitivity of synovium to chronic inflammation.

As outlined in the results section, the air pouch model proved difficult to achieve in the ear pinna. It was therefore necessary to develop an alternative model of tissue inflammation and the DTH reaction was selected. First described in 1882 by Robert Koch, a DTH reaction is an antigen specific cell mediated immune response characterised by induration, swelling and monocyte infiltration into the site of antigen exposure within a period of 24 to 72 hours (354). The reaction was further characterised by Landsteiner and Chase in a series of articles in which they detailed the cellular nature of the response (355, 356). Their key finding was to observe that the DTH reaction could be transferred to a naïve recipient using cells from an immunised animal, indicating the dependence of the response on pre-exposed antigen specific memory cells (355, 356). Thus, following re-exposure to an antigen, local APCs process and present the antigen to effector memory CD4⁺ T cells, a subset of T cells situated in peripheral non lymphoid tissues that display immediate effector function upon re-exposure to antigen (212, 357). These cells initiate a localised inflammatory immune response through the release of inflammatory mediators such as IFN γ , which recruit and activate effector cells to the site of antigen exposure, such as macrophages, which in turn

secrete inflammatory mediators such as, $\text{TNF}\alpha$ and IL1 (212, 358-360). In addition to CD4^+ T cells, macrophages are thought to be the major effector cells in the DTH reaction, however, CD8^+ T cells, and NK cells are also thought to serve as effector cells in DTH reactions (361). Together, these events inaugurate the self-propagating localised inflammatory immune response that is typical of the DTH reaction and a variety of autoimmune diseases. Thus, the DTH reaction is known to provide a site of tissue inflammation within a window of 24 to 72 hours in which effector memory CD4^+ T cells are essential mediators. Moreover, these cells are also known to be the essential mediators of numerous chronic inflammatory autoimmune diseases, including rheumatoid arthritis (10, 362). Thus, the DTH should provide a convenient model for MPLSM of activated effector T cells during an inflammatory response and in this chapter, the model was adapted to the ear pinna to provide a site of inflammation in which methods to image CD4^+ T cells and DCs could be explored.

In addition to the development and characterisation of an imageable site of tissue inflammation in the ear, this chapter outlines the preliminary studies carried to develop the use of the photo-switchable fluorescent probe, Kaede. Conventional monochromatic (single coloured) fluorescent probes, such as CFSE and CMTPX, are routinely employed to label cells for a variety of studies, including imaging and assays of proliferation (322, 345, 363). However, while monochromatic fluorescent probes have proved useful in the studies carried out in previous chapters, their use in future imaging studies of DC-T cell interaction at and between the tissue site of inflammation and DLN, may present limitations. In particular, there would be no way of discriminating one cell from another on the basis of colour when attempting to track and distinguish individual cells or groups of cells participating in a particular interaction of interest or migrating between the tissue site of inflammation and the DLN. However, in recent years the complexity of imaging studies has increased and has driven the discovery of novel fluorescent optical highlighters, which overcome the limitations associated with monochromatic fluorescent probes, by allowing cells and organelles of interest to be differentially labelled for tracking purposes. Optical highlighting involves a rapid, light-induced change in the excitation/emission spectrum of the fluorescent probe and can be achieved by either stimulating fluorescence emission from a poorly fluorescent precursor (photo-activation), or by evoking a clearly distinguishable color change

in the fluorescent protein emission spectrum (photo-conversion) (364, 365). Both strategies represent essential tools for tracking applications, since they can be used to directly track objects of interest after their photo-activation or photo-conversion. The key properties of an optical highlighter for live cell imaging are maximum duration and degree of colour change, combined with minimum toxicity of the probe to the cell. Currently, there are a variety of optical highlighters available, however, none of which fulfill all of the key requirements and are currently undergoing refinement (364, 366).

Photo-activatable fluorescent probes, which are switched on during imaging, would not be suitable for labeling DCs and T cells in the *in vivo* model systems developed in this thesis, since they do not permit cells to be imaged and identified as potential candidates for tracking prior to their photo-activation. In contrast, photo-convertible fluorescent probes, which are switched from one colour to another during imaging would be ideal for tracking DC-T cell interactions between the tissue site of inflammation and DLN (364, 365). The anthozoan red fluorescent protein, DsRed, was one of the first photo-convertible optical highlighters to be developed for use in live mammalian cell imaging (364, 366). Multi-photon excitation of DsRed at short wavelengths evokes a rapid change in fluorescence emission from a red to a green species, when viewed by epi-fluorescence microscopy. The multiphoton-evoked “greening” method can be used to label cells and defined subcellular regions within target cells expressing soluble DsRed protein (364). The color change occurs as a consequence of the tetrameric structure of DsRed, which takes several days to mature from a green to a red species via fluorescence-resonance energy transfer (FRET) (364, 366, 367). However, multi-photon excitation with appropriate wavelength can selectively bleach the mature, red-emitting species and enhance green fluorescence emission through de-quenching of the intrinsic FRET process. The resultant color change can persist for approximately 30 hours without affecting cell viability. This technique allows individual cells, organelles, and fusion proteins to be optically marked and has potential for studying protein trafficking and selective retrieval of cells from a population (364). However, the red fluorescence of DsRed takes several days to mature, passing through an obligatory green fluorescent intermediate phase (368). This time delayed fluorescence does not make DsRed an ideal candidate for labeling and tracking DCs and T cells in the *in vivo* model systems developed in this thesis and a photo-convertible probe, such as Kaede, which instantly labels cells would be more

suitable as cells would be available for immediate use.

Kaede is a naturally occurring green fluorescent protein extracted from the stony coral, *Trachyphyllia geoffroyi* and can be irreversibly photo-converted from a green to a red fluorescence emitting protein following exposure to UV or violet light (350-410nm) (365, 369-371). Prior to its photo-conversion with UV light, Kaede protein emits green fluorescence with a peak of 518nm, when excited with 480nm light (365). However, following its photo-conversion, Kaede protein emits red fluorescence with a peak of 582nm, when excited with 480nm light (365). Thus, exposure to UV light gives rise to a fundamental change in fluorescence properties of the Kaede protein. This can be attributed to a UV mediated peptide cleavage event within the Kaede protein and can be observed by SDS-PAGE analysis, in which proteins are separated and analysed on the basis of size (369). Unconverted green Kaede appears as a single band of 28 kDa in size, while converted Kaede appears as two bands of 18 kDa and 10 kDa (369). Kaede is therefore a green fluorescent protein, which has the potential to be irreversibly photo-converted to a red fluorescent protein using UV light, providing a simple and powerful tool for regional labeling and tracking of cells of interest *in vivo* during MPLSM studies. Thus, the use of Kaede would overcome the limitations associated with monochromatic CFSE and CMTPIX in future imaging studies of the tissue site of inflammation and DLN. When applied to the systems developed in this chapter and in chapter 4, Kaede should provide a powerful tool for studying the relationship between DC-T cell interactions taking place at the tissue site of inflammation and DLN, by allowing cells of interest to be identified, photo-switched and subsequently tracked between sites on the basis of their new fluorescent colour (372, 373).

The number of studies which have reported the use of Kaede as a fluorescent label for imaging techniques are few, yet extremely diverse, ranging from the use of Kaede to visualise the recycling of G-protein coupled receptors, to the use of Kaede to assess neural development in zebrafish (374, 375). However, the most relevant study to date has involved the development of a transgenic mouse model in which the Kaede protein was ubiquitously expressed in all cell types to monitor the migration of lymphocytes to and from lymphoid organs *in vivo* (371). The study involved the use of UV light to photo-convert the cellular contents of the inguinal LN. To monitor rates of lymphocyte migration, the proportion of

non-photo-switched Kaede expressing T and B cells that had re-populated the LN, was analysed at various time points by flow cytometry (371). This allowed the analysis of the kinetics of cellular movement and revealed that each subset of lymphocytes within the LN, displayed distinct migration patterns *in vivo* (371). Thus, the Kaede transgenic mouse system is an ideal tool for the generation of endogenously labeled cells and circumvents the technical difficulties associated with Kaede not yet being developed into a freely diffusible form for cell labeling. Moreover, targeted expression of the Kaede protein to specific cell types, such as CD4⁺ T cells and DCs would allow cellular migration and their interactions to be tracked *in vivo* at and between the tissue site of inflammation and DLN (371). However, the Kaede transgenic mouse is not commercially available and in this chapter, a mammalian expression vector containing the Kaede gene was acquired and employed in expression and photo-conversion studies. In addition, the Kaede protein was cloned, expressed, purified and employed in a number of preliminary studies to develop the future use of Kaede in the novel *in vivo* model systems developed in this chapter and in chapter 4.

In conclusion, this chapter outlines the development of a model of tissue inflammation in the ear pinna, in which the dynamic behaviour of effector T cells and their interactions with DCs can be imaged and assessed. The first technique explored was the air pouch model, however, while successful in the rump, it was not technically feasible in the ear pinna. The second technique outlined was the DTH reaction and from the preliminary studies carried out, the model appeared successful with respect to establishing imaging methods for visualising DCs and T cells *in situ*. Finally, this chapter outlines the preliminary studies carried out to develop the use of the photo-switchable probe kaede. This fluorescent probe will be employed in combination with MPLSM in future imaging studies, to track cellular migration and cellular interactions at and between the LN and tissue site of inflammation in the ear pinna.

5.2 Results

5.3 Histological analysis shows successful induction of the air pouch model in the rump but not the ear pinna

According to the method outlined by Sedgewick, the air pouch is classically induced in the rump of the mouse or rat (346). In this investigation, for the purpose of MPLSM, the model was adapted to the ear pinna. Air was injected into the ear pinna and to determine the success of inducing an air pouch in this novel site, an air pouch was also induced in the rump to provide a positive control for comparison. Air pouches were generated in the rump and ear pinna according to the method outlined in chapter 2. After seven days, air pouches were dissected from surrounding tissue and fixed in formalin for histological evaluation by H&E staining. The histological appearance of the air pouches created in the rump and ear pinna, are illustrated in figure 5.1. Figure 5.1 A, shows a section of control rump, in which the various layers of the cutaneous tissue are highlighted. However, without the injection of air, the various tissue layers appear undisturbed. Figure 5.2 B, shows a bright-field image of a section of air pouch created in the rump. 7 days after the formation of the air pouch, light microscopy revealed multiple layers of flattened cells surrounding the air pouch cavity, indicated by black arrows (346, 347). Figure 5.2 C shows a bright-field image of a section of control ear pinna, in which the various layers of the ear tissue are highlighted. However, without the injection of air, the various tissue layers appear undisturbed. Figure 5.2 D shows a bright-field image of a section of ear pinna 7 days following the repeated injection of sterile air. However, unlike the air pouch lining of the rump, light microscopy revealed an absence of the flattened cells and when compared with a section of control ear pinna, there was no clear evidence of an air pouch cavity. Although in both figure 5.2 C + D, the epidermis appears detached from the remaining layers of the cutaneous tissue. This was representative of all sections of the ear pinna and appeared to occur during tissue processing of the thinner, more delicate tissue of the ear pinna. Thus, compared with the flattened cell lining surrounding the air pouch cavity of the rump, sections of the ear pinna following repeated

injection of air failed to show clear evidence that an air pouch had been successfully induced at that site.

5.4 Granulocytes can be identified in the air pouch of the rump but not the ear pinna

Initial attempts to create an air pouch in the ear pinna appeared unsuccessful. Histological analysis failed to show the presence of a defined air space within the ear pinna or the flattened structure typical of the air pouch cavity. To further test whether an air pouch had been successfully created in the ear pinna, the infiltrating cell types were analysed and compared. Air was injected in the rump and ear pinna according to the method outlined in chapter 2. The unstimulated air pouch contained insufficient liquid exudate to aspirate. Thus, the air pouch was perfused using saline to recover any cells that had infiltrated the air filled cavity. Cells were characterised phenotypically using flow cytometry. Consistent with the expected results, granulocytes were the predominant cell type within the air pouch of the rump, while lymphocytes were absent (346, 351). Figure 5.2 shows representative flow cytometric plots of the results obtained from the phenotypic analysis of cells recovered from the air pouch in the rump. Cells were first analysed on the basis of size and granularity and the majority appeared to be large granular cell types, figure 5.2 A. Cells were next analysed for their expression of the cell surface integrin, CD11b and the GPI-anchored protein Gr1 (376-378). 68.8% were CD11b⁺ while 5.168% were double positive for the expression of CD11b⁺ and Gr1⁺. These cells most likely represented macrophages/dendritic cells and neutrophils, respectively. In addition, 65.15% of the cells expressed the macrophage marker F4/80⁺. In contrast to the high proportion of granulocytes, no B220/CD19 expressing B cells or CD4/CD8 expressing T cells were detected within the air pouch in the rump, which was consistent with previously published reports (346, 347). Figure 5.3 shows representative flow cytometric plots of the results obtained from the phenotypic analysis of cells recovered from the ear pinna. Figure 5.3 A, cells were first analysed on the basis of size and granularity and it was immediately apparent that cells recovered from the ear pinna were not as large or

as granular as those recovered from the rump. Cells were next analysed for their expression of the DC, macrophage and neutrophil markers CD11b, F4/80 and Gr1, figure 5.3 B + C. In contrast to the results obtained from the air pouch in the rump, no cells were recovered that stained positively for the granulocytic and monocytic markers. Moreover, no B220/CD19 expressing B cells or CD4/CD8 expressing T cells were detected, figure 5.3 D + E. Thus, flow cytometric analysis of the cells infiltrating the air pouch and histological analysis of cellular lining surrounding the air pouch cavity, revealed a failure of the subcutaneous injection of air in the ear pinna to induce an air pouch.

5.5 Ear pinna thickness increases during a DTH reaction

From histological and flow cytometric analysis it became clear that the adaptation of the air pouch model from the rump to the ear pinna was not feasible. While the skin of the rump is loose and can accommodate the introduction of air to the site, the skin of the ear pinna is extremely taut and as a result, failed to maintain the injected air at the desired site. It was therefore necessary to devise a new model of tissue inflammation in which DCs and T cells could be imaged by MPLSM and assessed by immunological assay. The DTH reaction was selected. Following the adoptive transfer of OVA-specific T cells, mice were primed in the nape of the neck with OVA/CFA and challenged 10 days later in the ear pinna with either HAO or PBS. As a measure of the induction of inflammation at the site of injection, ear thickness was measured at 24, 48 and 72 hours post HAO or PBS control challenge. The resulting changes in ear thickness are summarised in figure 5.4, which shows that the injection of PBS failed to significantly alter ear thickness. However, the injection of HAO gave rise to a red and inflamed site with a significantly increased ear thickness in comparison with control PBS challenged ears at 24 hours ($p < 0.001$), 48 and 72 hours ($p < 0.01$) post challenge. Thus, initial results suggested a DTH reaction had been successfully induced in the ear pinna.

5.6 Antigen specific T cells can be detected within the ear pinna

The aim of developing a model of tissue inflammation in the ear pinna was to provide a non-lymphoid site of inflammation in close proximity to a secondary lymphoid organ, in which the interactions between DCs and T cells taking place at each site can be assessed and analysed and compared. The induction of a DTH reaction in the ear pinna resulted in a red, swollen inflammatory site 24-72 hours following challenge with HAO in the ear tissue. To determine which cells, cytokines and chemokines were mediating the inflammatory response observed in this model, the cell types present were characterised phenotypically by flow cytometry and the cytokine profile was assessed using the luminex system. A population of OVA-specific T cells from OTII⁺ C57BL/6J were selected for adoptive transfer into C57BL/6J mice. These transgenic mice express a TCR specific for an MHC class II-restricted epitope of OVA, enabling the use of flow cytometry to track adoptively transferred cells in the recipient mouse. With a view to imaging the site of inflammation using MPLSM, it was first necessary to establish whether adoptively transferred T cells were present at the site of inflammation. Mice were then immunised with OVA/CFA in the nape of the neck and challenged in the ear pinna with HAO or PBS control 10 days later. At 24, 48 and 72 hours post challenge, ears were removed and dermal layers were carefully teased apart. The split ear tissue was cultured overnight to encourage cells from the inflammatory site to transfer into the culture medium. Cells recovered from the inflamed ear tissue were analysed for the presence of OVA-specific, transgenic T cells using flow cytometry. The results shown in figure 5.5 outline representative flow cytometric plots, in which lymphocytes recovered from the overnight split ear cultures were first identified on the basis of size and granularity, figure 5.5 A. Lymphocytes were next assessed for their expression of the T cell marker CD4 (not shown), followed by their co-expression of the OVA TCR markers, Va2 and Vb5, figure 5.5 B. The graph in figure 5.5 C summarises the absolute number of OVA-specific transgenic T cells recovered from the split ear cultures over a period of 24-72 hours post HAO or PBS control challenge. In comparison with PBS control challenged mice, mice challenged with HAO contained a larger proportion of OVA-specific transgenic T cells within the ear pinna. Moreover, following HAO challenge the number of OVA-specific transgenic T cells in the ear pinna increased significantly from 24 to 72 hours ($p=0.0048$).

Thus, antigen specific T cells can be recovered from the ear pinna, using the split ear technique, during a DTH reaction in response to HAO challenge.

5.7 Macrophages and Neutrophils are present in the DTH reaction in the ear pinna

The split ear technique, which was developed to recover cells and cytokines from the site of inflammation, revealed antigen specific T cells within the ear pinna following HAO challenge. However, it was clear (from the forward side scatter plot, in which cells were analysed on the basis of size and granularity) that a variety of larger more granular cells that did not fall into the lymphocyte gate, were also recovered from the ear pinna. Flow cytometry was employed to characterise those cell types phenotypically. Figure 5.6 shows representative flow cytometric plots detailing the analysis of the various cell types recovered from the split ear culture following the induction of a DTH reaction. Cells were first analysed on the basis of size and granularity, figure 5.6 A. Cells were next analysed for their expression of the neutrophil marker Ly6G, that is also known as the myeloid differentiation antigen Gr1, figure 5.6 B (378). Furthermore, cells were analysed for their expression of the pan macrophage marker F4/80, figure 5.6 C (332). The proportion of Ly6G⁺ neutrophils detected in the split ear culture were summarised in figure 5.6 D, and show that in comparison with PBS control challenged ears, the proportion of Ly6G⁺ neutrophils detected in the ear pinna in response to HAO challenge was substantially higher. The influx of neutrophils to the site of HAO injection peaked at 24 hours with 61.67% (+/-5.86) and decreased significantly over the following 48 to 72 hours from 48.93% (+/-10.37) to 37.93% (+/-1.99) ($p=0.0027$). The proportion of F4/80⁺ macrophages detected in the split ear culture at various times are summarised in figure 5.6 E, and show that in comparison with PBS control challenged ears, the proportion of F4/80⁺ macrophages detected in the ear pinna in response to HAO challenge was substantially higher. The influx of macrophages to the site of HAO challenge appeared to remain relatively constant over the 24, 48 and 72 hour time points post injection, ranging from 38.3% (+/-3.84) to 41.83% (+/-6.33) to 39% (+/-5.65). Thus, following the induction of a DTH reaction in the ear pinna, neutrophils and

macrophages migrate into the site in response to HAO challenge and can be recovered from the ear tissue using the split ear technique.

5.8 Cytokine profile of the DTH reaction in the ear pinna

Antigen specific T cells, macrophages and neutrophils were identified within the inflammatory site created following the induction of a DTH reaction in the ear pinna. Next the production of pro-inflammatory cytokines, chemokines and growth factors in response to the induction of a DTH reaction in the ear pinna, was tested according to methods outlined in chapter 2, and compared with results obtained from PBS control ears, summarised in table 5.1. Of note, the production of a variety of cytokines, chemokines and growth factors was elevated following PBS control, thus background levels were high. In comparison with the results obtained from PBS control ears, the production of IL6 was substantially higher 24 hours following HAO challenge and was significantly higher after 48 hours ($p=0.0281$), figure 5.7. Moreover, in comparison with the PBS control, the production of IL1 α was substantially higher 24 hours following HAO challenge and was significantly higher after 72 hours ($p=0.0089$), figure 5.7. However, the levels of the pro-inflammatory cytokine TNF α and the anti-inflammatory cytokine IL10 were not significantly altered by HAO challenge in comparison with PBS control challenge, figure 5.7. No IFN γ was detected in the split ear cultures following HAO or PBS control challenge.

The production of chemokines in response to the induction of a DTH reaction in the ear pinna was tested and compared with results obtained from PBS control challenged ears, figure 5.8. In comparison with the PBS control, the production of macrophage inflammatory protein, MIP-1 α , was increased following HAO challenge, though not significantly. However, the production of monocyte chemotactic protein 1 (MCP-1), monokine induced by gamma interferon (MIG) and neutrophil chemotactic protein, KC, in response to HAO challenge was unchanged in comparison with PBS control challenge.

The production of growth and repair factors in response to the induction of a DTH reaction in the ear pinna was tested and compared with results obtained from PBS control challenged

ears, figure 5.9. Production of the granulocyte macrophage colony stimulating factor, GM-CSF, was significantly higher 48 hours following HAO challenge ($p=0.0116$) in comparison with PBS challenge. Furthermore, in comparison with the results obtained from PBS control challenged ears, the production of vascular endothelial growth factor, VEGF, was substantially higher at 24 and 48 hours and the production of fibroblast growth factor, FGF, was also substantially higher 24 hours post HAO challenge, however, neither increase was significant. In conclusion, cytokines, chemokines and growth factors were detected in both PBS and HAO challenged ears, however, despite high background levels the production of IL1 α , IL6 and GM-CSF was significantly increased following HAO challenge in comparison with PBS control.

Cytokine/Chemokine tested	24 hours HAO compared with PBS	48 hours HAO compared with PBS	72 hours HAO compared with PBS
IL1 α	not significantly altered	not significantly altered	Sig increased $p=0.0089$
IL6	not significantly altered	Sig increased $p=0.0281$	not significantly altered
TNF α	not significantly altered	not significantly altered	not significantly altered
IL10	not significantly altered	not significantly altered	not significantly altered
MCP-1	not significantly altered	not significantly altered	not significantly altered
MIG	not significantly altered	not significantly altered	not significantly altered
MIP-1 α	not significantly altered	not significantly altered	not significantly altered
KC	not significantly altered	not significantly altered	not significantly altered
GM-CSF	not significantly altered	Sig increased $p=0.0116$	not significantly altered
VEGF	not significantly altered	not significantly altered	not significantly altered
FGF	not significantly altered	not significantly altered	not significantly altered

Table 5.1 Summary of cytokines, chemokines and growth factors detected in split ear culture of DTH reaction

5.9 Antigen specific T cells can be imaged within the ear pinna during the DTH response

DTH is an inflammatory immune response initiated upon re-exposure to antigen by effector memory CD4⁺ T cells that is followed by the recruitment of inflammatory cells, including macrophages, to the tissue site of antigen re-exposure. In this chapter, a DTH reaction was successfully established in the ear pinna with cells and inflammatory mediators being recovered from the site using the split ear technique. These were subsequently characterised using flow cytometry and the luminex system. However, the aim of creating a tissue site of inflammation in the ear was to develop a model in which the behaviour of T cells and their interactions with DCs could be visualised and characterised using MPLSM. Thus, to establish whether the migration of antigen specific T cells could be imaged dynamically in the ear pinna following the induction of a DTH response using MPLSM, it was necessary to develop a method of in situ imaging of ear tissue. The DTH response was created in C57BL/6J mice following the adoptive transfer of OVA-specific, GFP expressing, transgenic T cells. These double transgenic mice express a TCR specific for an MHC class II-restricted epitope of OVA and their T cells constitutively express the green fluorescent protein (GFP), enabling the use of flow cytometry and MPLSM to track and image, adoptively transferred cells in the recipient mouse. Mice were primed in the nape of the neck with OVA/CFA and challenged 10 days later in the ear pinna with HAO. Twenty four hours post HAO challenge, the ear pinna was removed and prepared for imaging. Imaging through the ear pinna of the mouse proved technically difficult initially, due to the highly auto-fluorescent properties of the dermal layer of the ear tissue. Thus, it became necessary to expose the subcutaneous tissue of the site of inflammation by teasing back a small area of dermal tissue prior to imaging the site. Moreover, while the ultimate goal of the system is to image the site of inflammation in the live mouse, initially the ear pinna was removed and maintained in warmed oxygenated medium for the duration of the imaging period to allow imaging methods to be established. Figure 5.10 A, shows a bright-field image of a cross-section of H&E stained ear pinna detailing the various tissue layers and the site removed for imaging. Figure 5.10 shows images of the multi-photon movies acquired of OVA-specific, GFP expressing, transgenic T cells migrating within the DTH site in the ear pinna (indicated by white arrows), figure 5.10 B + C and migrating within the DLN, figure D (for full movies see attached CD). Control PBS challenged ears were also imaged, however, in the absence of antigen no OVA-specific GFP expressing T cells were detected within the ear pinna (data not shown). Using Volocity software (Improvision), the velocity of the transgenic T cells

migrating in the inflamed ear tissue was calculated and compared with the velocity of transgenic T cells migrating in the DLN, figure 5.11 A. The average speed of T cells migrating in the DTH site was $4.19\mu\text{m}/\text{min}$ (± 2.89) and $5.15\mu\text{m}/\text{min}$ (± 2.56) in the DLN. Thus, T cells migrated at a significantly slower speed in the tissue site of inflammation than in the DLN ($p=0.0291$). To quantify the directional component of T cell migration at both sites, the meandering index (a ratio of displacement from origin to track length) on individual T cells was calculated. These analyses revealed an average meandering index of 0.61 (± 0.33) in the DTH site and 0.72 (± 0.3) in the DLN, indicating that T cell paths in the DTH site and DLN were relatively straight and not significantly different from one another, figure 5.11 B. Moreover, tracks of individual T cells were plotted showing distance travelled from a single point of origin. T cells in the DTH site and the DLN appeared to migrate over similar distances, figure 5.11 C + D. Thus, while the speed at which T cells migrated in the DTH site was significantly slower than in the DLN, their pattern of migration at each site was similar.

5.10 Antigen specific T cells can be imaged within the ear pinna in combination with fluorescent beads during the DTH response

Antigen specific GFP expressing T cells were successfully imaged within the ear pinna, however, as a result of procedure required to prepare the ear pinna for MPLSM, the site of inflammation proved difficult to pinpoint due to the loss of the red and inflamed characteristics associated with the site. Thus, in an attempt to simplify this procedure, red fluorescent beads were injected in combination with HAO at the point of challenge. The beads were clearly visible to the naked eye, allowing the site of inflammation to be clearly identified. The DTH response was created in C57BL/6J mice following the adoptive transfer of OVA-specific, GFP expressing transgenic T cells. Mice were primed in the nape of the neck with OVA/CFA and challenged 10 days later in the ear pinna with HAO in combination with red fluorescent beads. 24 hours post HAO challenge, the ear pinna was removed and prepared for imaging. Figure 5.12 shows images of the multi-photon movies acquired of the site. The red fluorescent beads appeared to have been taken up by local APCs and displayed cellular like properties. However, on this occasion no OVA-specific,

GFP expressing transgenic T cells were observed at the site of inflammation and analysis of their migration was not possible.

5.11 Antigen specific T cells and DCs can be imaged within the ear pinna during the DTH response

Transgenic T cells were successfully imaged in the ear pinna using MPLSM following the induction of a DTH response. However, the ultimate aim of this system was to image DC-T cell interactions in the tissue site of inflammation. Thus, HAO challenge was substituted for the injection of fluorescently labelled bone marrow derived OVA pulsed DCs to provide a population of antigen presenting cells that can be visualised by MPLSM. The DTH response was created in C57BL/6J mice following the adoptive transfer of OVA-specific, GFP⁺ transgenic T cells. Mice were primed in the nape of the neck with OVA/CFA and challenged 10 days later in the ear pinna with either OVA pulsed DCs or un pulsed control DCs labelled with the red fluorescent dye, CMTPX. Twenty four hours post challenge with antigen loaded DCs, the ear pinna was removed and prepared for imaging by exposing the subcutaneous tissue of the site of inflammation, as previously described. Figure 5.13 A, shows an image of OVA-specific, GFP expressing, transgenic T cells in the multi-photon movie acquired of the ear pinna following challenge with OVA pulsed DCs. Both cell types could be observed migrating and interacting within the inflammatory site. In figure 5.13 B, tracks of individual T cells were plotted showing distance travelled from a single point of origin. In comparison with T cells in the HAO challenged DTH site (figure 5.11 C), T cells in the DTH site, challenged with OVA DCs, appeared to migrate over a similar distance, figure 5.13 B. Consistent with the expected results, in the control ear pinna, un-pulsed CMTPX labelled DCs injected into the site could be visualised there by MPLSM. However, no OVA-specific, GFP expressing, transgenic T cells were present and they could therefore not be imaged (results not shown). To quantify the interactions between OVA pulsed DCs and OVA-specific T cells in the DTH site, the degree of colocalisation between green T cells and red DCs was analysed to calculate a colocalisation coefficient representing the proportion of green voxels that were also red. The results in figure 5.13 C, show that the DCs and T cells colocalised and in the multi-photon movie (see attached CD), DCs and T

cells appeared to interact throughout the imaging period. Thus, DCs and T cells interacted in the DTH site 24 hours following antigen challenge with OVA pulsed DCs and the results of this preliminary study therefore appeared to be consistent with previously published reports that during a DTH reaction, DCs and CD4⁺ T cells interact (211, 212).

5.12 HEK cells transfected with the Kaede expression vector express Kaede protein and can be photo-switched

The Kaede gene is commercially available in the form of a mammalian expression vector, (MBL International). Due to the technical difficulty associated with the transfection of primary cells, such as DCs and T cells, a human embryonic kidney cell line, HEK 293, was employed in preliminary studies using Kaede. HEK 293 cells have been widely used in cell biology research for a number of years due to their robust cell culture qualities and high transfection rates (379). In figure 5.14, HEK 293 cells were transfected with the Kaede expression vector using lipofectamine, as described in chapter 2, and examined for their expression of the Kaede protein by epi-fluorescent microscopy 24 hours later. Figure 5.14 A shows an image of HEK 293 cells excited with 488nm light expressing green fluorescent protein. Figure 5.14 B, shows an image of HEK 293 cells excited with 550nm light following a 1 second pulse with UV light. Thus, HEK 293 cells transfected with the Kaede expression vector successfully expressed the green fluorescent Kaede protein, which could be photo-converted to the red fluorescent form following a 1 second UV pulse.

5.13 Primers were designed to amplify the Kaede gene

HEK 293 cells were transfected with the Kaede expression vector and successfully expressed the Kaede protein. However, if Kaede was to be employed in studies of DC-T cell interactions, it was necessary to label DCs or T cells with the fluorescent protein. However, transfecting primary cells is technically challenging and it was therefore necessary to obtain the Kaede protein for future studies. Thus, it was necessary to clone the Kaede protein from

the mammalian expression vector into a protein expression system and the champion™ pET100 directional TOPO® expression kit with BL21 Star™ (DE3) One Shot® Chemically Competent E. coli (Invitrogen) was selected to clone and express the Kaede gene. The first step in this process involved the design of primers to amplify and obtain large copies of the Kaede gene from the mammalian expression vector, to allow it to be incorporated into the pET-TOPO expression vector. These vectors are provided linearized with topoisomerase I covalently bound to each 3' phosphate, which enables them to readily ligate DNA sequences with compatible ends. The key to pET-TOPO cloning is the enzyme DNA topoisomerase I, which functions both as a restriction enzyme and as a ligase, to cleave and rejoin DNA during replication. Topoisomerase I specifically recognises and binds to the sequence 5'-CCCTT-3'. The enzyme then cleaves the DNA strand, creating an overhang compatible with the TOPO sequence incorporated onto the end of the PCR product, which ligated into the vector by the same enzyme. Thus, it was necessary to incorporate the TOPO sequence into the 5' end of the forward primer to ensure successful cloning of the Kaede gene into the pET-TOPO vector. Using Invitrogen primer design package, suitable forward and reverse primers were designed to amplify Kaede based on the Kaede gene sequence. The pET-TOPO sequence 'CACC' was incorporated into the 5' end of the forward primer to give rise to copies of the Kaede gene that would be successfully cloned into the pET-TOPO expression vector. Figure 5.15 A shows the primer sequences employed to amplify the Kaede gene. Figure 5.15 B shows an image of a gel showing the products of the Kaede gene amplification using the aforementioned primers. By comparing the size of the bands with the molecular markers revealed that the Kaede gene had been successfully amplified using the designed primers since each band corresponded to the 677 base pair sized Kaede.

5.14 Kaede gene was successfully cloned into pET-TOPO vector

The Kaede gene that was amplified from the previous experiment was quantified and next employed in the cloning reaction to allow its incorporation into the pET-TOPO expression vector (according to the protocol outlined in Materials and Methods). To confirm whether the Kaede gene had been successfully cloned into the pET-TOPO expression vector, PCR using Kaede primers was carried out using the pET-TOPO vector as template DNA. If the

Kaede gene had been successfully cloned into the pET-TOPO vector, the primers would be able to amplify the gene segment and a band of 677bp would be detected on a gel as in figure 5.15 B. As seen in figure 5.16 A, PCR products were separated on an agarose gel and a band of equal size to the Kaede gene, indicated by arrow, was detected from each cloning reaction. In addition, faint bands representing the larger pET-TOPO vector, which was used as the template could also be observed. However, while the presence of the Kaede gene within the pET-TOPO vectors was confirmed by PCR, it was necessary to sequence each Kaede containing pET-TOPO vector to ensure the gene had been incorporated in the correct orientation and without any base pair errors. The results obtained following the sequencing of each plasmid revealed that only a single plasmid generated from the cloning reaction contained the Kaede gene in the correct orientation and free of base pair errors. This plasmid was therefore selected and used throughout the following stages of the expression procedure.

5.15 BL21 StarTM were transformed with Kaede-pET-TOPO vector and expression of Kaede was induced using IPTG

Kaede-pET-TOPO vector was transformed into BL21 StarTM *E.coli* following the method outlined in chapter 2. pET-TOPO expression vectors encode the T7 RNA polymerase, which is expressed by host *E. coli* under the control of the IPTG-inducible lacUV5 promoter. This allowed transcription of the Kaede protein to be directly regulated with IPTG. Thus, following overnight culture of BL21 StarTM *E.coli* containing the Kaede-pET-TOPO vector to allow for their exponential replication, the *E.coli* were induced to express the Kaede protein using IPTG. To calculate the time point which yielded the optimum expression of the Kaede protein, a sample of *E.coli* was taken for SDS-PAGE analysis at 2, 4 and 6 hours following the addition of IPTG to the culture. Throughout this process the culture was sheltered from light to prevent premature photo-switching of the Kaede protein, due to the natural occurrence of UV light. As a quick check to ensure the Kaede protein was being expressed by the BL21 StarTM *E.coli*, a small aliquot of bacteria were examined under the epi-fluorescent microscope for green fluorescence and their ability to be photo-converted. Figure 5.17 outlines images obtained of BL21 StarTM *E.coli* expressing Kaede

protein at 100x magnification. Figure 5.17 A shows an image of BL21 StarTM *E.coli* excited with 488nm light expressing green fluorescent protein prior to a UV pulse. Figure 5.17 C, shows an image of BL21 StarTM *E.coli* excited with 550nm light prior to a UV pulse. Consistent with the expected result, the cells failed to express the red fluorescent form of the Kaede protein in the absence of UV treatment. Figure 5.17 B, shows an image of BL21 StarTM *E.coli* excited with 550nm light following a 1 second pulse with UV light. The bacteria clearly expressed the red fluorescent form of the Kaede protein and had therefore been photo-converted. In contrast to the results obtained prior to the UV treatment, BL21 StarTM *E.coli* excited with 488nm light following a 1 second UV pulse, lost their expression of the green fluorescent protein. Next, the products of the pilot expression were analysed by SDS-PAGE and western blot to establish the optimum time point with respect to expression levels of the protein.

5.16 Kaede protein was purified and quantified

The expression of Kaede protein was carried out in accordance to the protocol outlined in Materials and Methods. An SDS-PAGE and Western blot were carried out to detect the protein and assess which time point from the pilot expression produced the highest yield. Western blot is an analytical technique used to detect specific proteins. Proteins are denatured and separated in accordance to their molecular weight and detected using antibodies specific to the protein in question. The presence of Kaede protein was detected using an antibody specific for histidine, a protein tag, which was encoded onto the end of the Kaede protein to facilitate its purification from *E.coli* and other proteins present in the expression mixture. Figure 5.18 shows an image of the nitrocellulose membrane from the Western Blot analysis. A pre-stained protein ladder containing protein bands of known molecular weights was run alongside the samples from the pilot expression to provide an indication of the molecular weights of the purified products. As a negative control, BL21 StarTM *E.coli* were transformed with the empty non Kaede containing pET-TOPO vector. Consistent with the expected result, figure 5.18 shows these samples did not stain with the anti-histidine antibody due to the absence of the Kaede gene and therefore the inability of the BL21 StarTM *E.coli* to express it. In contrast, when the Kaede containing pET-TOPO

vector expressing BL21 StarTM *E.coli* were analysed for the presence of the Kaede protein using the anti-histidine antibody, several bands could be observed. Indicated by the arrows, a band of molecular weight corresponding to the monomeric, dimeric and trimeric forms of the protein was observed. However, the monomeric form of the protein was present at higher levels than the others and the band was heaviest at the 6 hour time point, which indicated that protein expression was optimum at this time point. Thus, the induction of protein expression was confirmed and the level of Kaede expression appeared highest at 6 hours. Thus, the Kaede-pET-TOPO vector containing BL21 StarTM *E.coli* were induced using IPTG and following 6 hours the Kaede protein was purified from the *E.coli* over a nickel column in accordance with the protocol outlined in chapter 2.

5.17 Kaede protein was conjugated to beads and taken up by DCs *in vitro*

The photoconversion of intracellular Kaede using UV light has previously been shown to have no adverse effects on cellular function (371). Thus, once the Kaede protein had been expressed and purified for use, the next step was to attempt to label primary cells with the fluorescent protein. T cells do not readily take up soluble proteins, however, DCs constantly sample their environment, capturing soluble and particulate proteins via phagocytosis and pinocytosis, which they can then process and present to antigen specific T cells (110). Initially, DCs were incubated with the purified soluble Kaede protein, however, they failed to consume adequate quantities to ensure effective labelling of the cell with the fluorescent protein (results not shown). Thus, in an attempt to improve the uptake of Kaede by DCs, Kaede was converted from a soluble to a particulate format by conjugating it to 2 μ m polystyrene beads, following the protocol outlined in Materials and Methods. Bone marrow derived DCs were incubated with Kaede conjugated beads *in vitro* for 1 hour. DCs were then washed with complete RPMI to remove excess beads and imaged using an epi-fluorescent microscope. Figure 5.19 A + B, show images of *in vitro* movies acquired of Kaede conjugated beads within DCs. Figure 5.19 A shows DCs excited with 488nm light prior to a UV pulse and green fluorescence can be clearly observed. Figure 5.19 B shows DCs, excited with 550nm light post UV pulse, expressing the red form of the Kaede protein (see attached CD for full QuickTime movies of DCs *in vitro* and their photo-conversion).

5.18 Kaede conjugated beads were taken up by DCs and visualised in the LN *in vivo*

The ultimate aim of developing the photo-switchable fluorescent protein, Kaede, was to employ it in the *in vivo* model systems developed in this chapter and in chapter 4. Thus, it was next important to establish whether Kaede could be photo-switched and both green and red fluorescence emitting forms of the protein could be distinguished using MPLSM. Bone marrow derived DCs from a CD45.1⁺ C57BL/6J mouse were incubated with Kaede conjugated beads *in vitro* for 1 hour. DCs were then washed in complete RPMI, to remove excess beads, and injected subcutaneously into the footpad of a congenic CD45.2⁺ C57BL/6J mouse. 20 hours later, the draining popliteal LN was removed and prepared for MPLSM as described in Materials and Methods. In Figure 5.20 A + B, images of multi-photon movies acquired of DCs containing Kaede conjugated beads migrating within the LN. Although previously published, it was not technically possible to photo-convert Kaede using the available MPLSM, as the energy of the Ti-sapphire wasn't high enough to induce photo-switching of the Kaede (370, 371). Thus, to ensure both green and red fluorescence emitting forms of the protein could be excited using MPLSM, the LN was pulsed with UV light from an epi-fluorescence microscope, and re-imaged using the MPLSM.

Figure 5.20 A + B, shows images of DCs migrating within the LN prior to, and following a UV pulse, respectively. A colour change from green to red can be clearly observed between both images. Following MPLSM, the imaged LN and a control, non imaged LN, were homogenised and DCs were assessed for their expression of Kaede associated fluorescence using flow cytometry. In figure 5.20 B, DCs were identified on the basis of their size and granularity. In figure 5.20 C, DCs were next identified and distinguished from endogenous cells on the basis of their expression of the congenic marker CD45.1. In figure 5.20 D, DCs pulsed with beads only or Kaede beads, were examined for their expression of green fluorescence. Control DCs that were pulsed with beads only failed to express green fluorescence. DCs pulsed with Kaede beads expressed green fluorescence, which was

substantially reduced following exposure to UV light. In figure 5.20 E, DCs were examined for their expression of red fluorescence. Control DCs pulsed with beads only, did not express red fluorescence. DCs pulsed with Kaede beads expressed low levels of red fluorescence, which increased following exposure to UV light. Thus, prior to a UV pulse, DCs expressed high levels of green fluorescence and low levels of red fluorescence, however, in contrast following a UV pulse, DCs expressed high levels of red and low levels of green fluorescence. Therefore, when examined *in vivo* by MPLSM, DCs appeared photo-converted, which was confirmed by flow cytometric analysis.

5.19 Discussion

The dynamic interactions that take place between DCs and T cells during the activation phase of an immune response in the LN have been well characterised (4, 5, 7, 8, 235, 236, 269). However, while both DCs and T cells are known to be present at the tissue site of inflammation following the induction of an antigen specific immune response, little is known regarding how these cells interact and migrate dynamically during the effector phase of a protective immune response at the tissue site (18, 53). Moreover, the relationship between the DC-T cell interactions taking place at and between the tissue site of inflammation and the DLN is relatively unexplored. Understanding how T cells are maintained and regulated at the tissue site of inflammation and deciphering whether and what role the DLN plays in this process should be critical in understanding the pathogenesis of chronic inflammatory conditions and in identifying novel therapeutic targets in such diseases. In this chapter, the air pouch model and DTH reaction were both explored as suitable models of tissue inflammation in the ear pinna. Moreover, the models were examined for their potential for *in situ* imaging of T cell dynamics at the site using MPLSM and immunological assay. However, the overall aim would be to combine the tissue site of inflammation developed here with the tLN model of chapter 4 in the ear pinna, for comparisons of T cell migration, behaviour and interaction with DCs at and between both sites.

The air pouch model, in which sterile air is repeatedly injected into the subcutaneous tissue of the dorsal flank of the mouse or rat, was the first system explored to create a tissue site of

inflammation in the ear pinna (346). The model was adapted from the rump to the ear pinna in an attempt to create a synovium-like structure in which inflammation could be induced and DCs and activated effector T cells could be imaged and assessed. Histological and flow cytometric analysis of the positive control air pouch in the rump revealed a flattened cell lining surrounding the air cavity with myeloid and granulocytic cell types predominating. However, these results were not mirrored in the ear pinna. In the rump, the skin was loose and could accommodate and maintain injected air at the site. However, the skin of the ear pinna was taut and presumably the injected air escaped. Thus, the formation of a synovium-like layer of macrophages and fibroblasts was not possible due to the absence of the air induced mechanical disruption to the connective tissue. It was therefore clear that while adapting the air pouch model to the ear pinna was a good idea in theory, it was impractical. This finding was an unfortunate set back, since the air pouch model would have allowed the study of a synovium-like structure and previously the air pouch model has been employed to study the reactivity of the synovium-like layer to inflammatory and anti-inflammatory agents (346, 350-353). Thus, if successful, the air pouch in the ear pinna could have provided a model in which to study the chronic inflammatory condition, rheumatoid arthritis and to explore the sensitivity of synovium to chronic inflammation. Moreover, studying the relationship between the DC-T cell interactions taking place at the tissue site of inflammation and the DLN, in the context of a disease model of rheumatoid arthritis, would have provided a clinical relevance to the system and potentially identified novel therapeutic targets for the treatment of the disease.

The air pouch was not technically achievable in the ear pinna and consequently an alternative model of tissue inflammation was investigated. The DTH is an antigen specific cell mediated immune response characterised by induration, swelling and monocytic infiltration into the site of antigen exposure within a period of 24 to 72 hours (354). The effector memory CD4⁺ T cells, which mediate this self-propagating localised inflammatory response, are also essential mediators of numerous chronic inflammatory autoimmune diseases, such as rheumatoid arthritis (10, 362). Thus, the DTH reaction is a convenient model for studying activated effector T cells during an inflammatory response and in this chapter, the model was adapted to the ear pinna to provide a site of inflammation in a tissue site accessible for MPLSM. The magnitude of tissue swelling induced by HAO challenge in the ear pinna, was

taken as a measure of the DTH response. Consistent with the expected results, the ear became red and swollen following HAO challenge and in comparison with PBS control, ear thickness increased significantly (354). Thus, the appearance of the ear following HAO challenge suggested successful induction of a DTH reaction, however, if the site was to be used for imaging T cells it was important to determine whether antigen specific T cells were present at the inflammatory site. The split ear technique, in which dermal layers were separated and incubated in warmed medium, allowed cells and soluble mediators to be released from the tissue site of inflammation without the need for traditional tissue digestion techniques, which often cleave cell surface molecules and affect cell viability. Cells from the tissue site of inflammation were characterised using flow cytometry and cytokines were measured using the luminex system. The DTH reaction is known to be directly dependent on the presence of antigen specific, effector memory CD4⁺ T cells (211, 212, 354, 356). Flow cytometric analysis of the cell suspension released from the dermal layers of the ear pinna revealed that OVA-specific GFP expressing transgenic T cells could be recovered from the site and that they were most numerous at 72 hours post HAO challenge. Moreover, macrophages and neutrophils were also recovered from the site of HAO challenge. Thus, initial results strongly suggested that a DTH reaction had been successfully induced in the ear pinna, with a red swollen site containing an influx of inflammatory cells and antigen specific T cells. Surprisingly the cytokine profile of the HAO challenged site did not appear to vary considerably from the PBS control challenged site, moreover the background level of some cytokines was high. This may have been the result of the split ear technique itself causing tissue damage, which may have resulted in the release of pre-formed inflammatory cytokines. The inflammatory cytokines, TNF α and IFN γ are known to be key mediators of the DTH response, however, levels were not detectable following HAO challenge in comparison with PBS challenge (380, 381). However levels of IL6, IL1 α and GM-CSF were all significantly increased in response to HAO challenge. IL6 is a pro-inflammatory cytokine released by activated macrophages, which was consistent with the flow cytometric results, which revealed a large population of F4/80⁺ macrophages within the site of inflammation (382-384). Moreover, IL1 α is produced by monocytes and macrophages as a pro-protein and is proteolytically processed and released in response to cell injury (382-385). The DTH response is reduced in mice lacking expression of the IL-1 receptor and IL-1 has been shown to contribute to the development of the reaction by promoting the maturation of

antigen-specific T cells and by augmenting IL-12 dependent IFN- γ production by Th1 cells (386-388). Moreover, IL-1 derived from activated memory T cells had been shown to induce DC mediated production of TNF α , resulting in local inflammation upon secondary stimulation (389). Finally, the growth factor GM-CSF, which stimulates the production and survival of granulocytic cell types such as dendritic cells and macrophages, was also detected at significantly higher levels following HAO challenge (390). The presence of increased levels of this growth factor was consistent with the number of granulocytic cell types at the tissue site and was most likely released to maintain those cell types.

The DTH reaction is mediated by previously activated CD4⁺ T cells and in this chapter the T cells being characterised by flow cytometry and imaged by MPLSM were therefore memory T cells participating in a secondary immune response. Previously, T cells were imaged dynamically in rat ear pinnae during a DTH response by Matheu et al. (211, 212). By injecting fluorescently labelled antigen, they also demonstrated DC-T cell contacts in the ear pinna during the inflammatory reaction. Moreover, work by McLachlan et al. showed that during the memory response, dermal DCs interacted with and stimulated effector memory T cells to produce inflammatory cytokines (216). In the preliminary imaging studies carried out in this chapter, antigen specific T cells were observed migrating within the ear pinna with reduced velocity in comparison with the DLN. During the activation of an immune response in the LN, prolonged interactions between DCs and antigen specific T cells are seen after 6-12 hours (6, 8, 14, 199). After approximately 24 hours, T cells dissociate from stable clusters and migrate with increased velocity, adopting a 'swarming' behavior (200). During this time T cells begin to proliferate and differentiate into activated effector cells, which migrate from the LN to the tissue site of inflammation (200). During the activation of a secondary immune response, memory T cells migrate with increased velocity and do not form the stable prolonged interactions typical of the initiation of a primary immune response (205, 391). Analysis of the DTH site in the ear pinna by MPLSM revealed that DCs and T cells interacted throughout the duration of the imaging period, which could account for the reduced velocity of the T cells observed in the previous experiment, as they may have slowed down to make stable contacts with endogenous DCs. Moreover, the increased velocity of the T cells in the DLN at 24 hours was consistent with published reports that T cells make fewer

contacts with DCs at this time point, particularly in the activation of secondary immune responses (205, 391). Thus, from these preliminary studies, antigen specific T cells and DCs can be imaged within a tissue site of inflammation in the ear pinna by MPLSM and the cells appear to migrate with reduced velocity and form stable interactions.

However, less is known with respect to the dynamic behaviour of newly activated effector T cells participating in primary responses. Thus, it would be interesting to employ novel models developed here in the ear pinna to analyse the relationship between DC-T cell interactions taking place in the tissue site of inflammation and DLN during a primary immune response. However, such experiments would come with an extra level of complexity and technical difficulty. Firstly, the use of conventional fluorescent probes for cell labelling, such as CFSE and CMTPX, would not be feasible to image effector T cells in the tissue during a primary response. While these fluorescent dyes are extremely bright, their level of fluorescence is diluted out every time a cell undergoes division. This is a useful property for the study of cellular proliferation and allows naïve T cells to be imaged during the early stages of T cell activation prior to their clonal expansion (322). However, following their clonal expansion and differentiation, T cells migrate from the LN to the tissue site of inflammation, by which time the level of CFSE or CMTPX within the cell would be negligible. Thus, labelling naïve T cells with a view to imaging them as effector cells at the site of inflammation is technically, extremely difficult. The use of reporter mice, which express fluorescent proteins endogenously, such as the GFP expressing T cell mice employed in this chapter, would overcome this difficulty. In addition, the field of view when imaging using MPLSM is focused on a small area of tissue and ensuring a high frequency of cells at the site is therefore critical. Thus, imaging the primary response over a memory response will inevitably prove more technically challenging since T cells are at a lower frequency. In these studies, GFP transgenic mice were acquired late in the project and since the secondary memory response is known to rapidly provide a large number of effector cells at the tissue site of inflammation, the DTH reaction was chosen as a good model for some preliminary studies of imaging T cells at the site of inflammation. However, the ultimate aim would be to create a tissue site of inflammation in which newly activated, effector T cells could be imaged during a primary immune response.

In conclusion, the studies carried out in this chapter to develop and characterise a tissue site of inflammation in the ear pinna were preliminary however they revealed the potential for imaging DCs and T cells within a tissue site of inflammation in the ear. The next step would be to characterise the dynamic behaviour of those cell types and by combining the site with the tLN model from chapter 4, comparisons of DC-T cell dynamics could be made between lymphoid and non-lymphoid sites. Furthermore, gaining a clearer understanding of these parameters in protective immune responses and comparing them to aberrant immune responses, such as the chronic inflammatory condition rheumatoid arthritis, may provide novel therapeutic targets for the intervention in disease.

The number of studies employing MPLSM to characterise the kinetics and dynamics of the generation of an immune response *in vivo*, have risen sharply in recent years and as result have contributed much knowledge to the field (7, 12, 207, 210, 211, 236, 237). However, as imaging studies continue to progress in complexity with improved technology, the demand for more sophisticated fluorescent probes for cell labelling has increased. Recently, a novel group of photo-switchable fluorescent proteins have been developed, which allow selective conversion of fluorescence signals after optical illumination, which in comparison to conventional monochromatic fluorescent probes, provide a powerful tool for studying the dynamic processes of fluorescently labeled individual cells or groups of cells by allowing them to be distinguished from other cells via a colour change (364, 365, 392). In this chapter, the photo-switchable probe Kaede, was cloned, expressed, purified and conjugated to beads to label DCs. Kaede can be photo-converted irreversibly from a green to a red fluorescent protein using UV light, without inflicting UV mediated cellular damage (371). The ultimate aim of employing Kaede in this PhD thesis was to combine it with the *in vivo* model systems of a tissue site of inflammation and DLN, developed in this chapter and in chapter 4. By labeling DCs or T cells with the fluorescent protein, these cells and their interactions could be tracked between the tissue site of inflammation and the DLN in the ear pinna by MPLSM. More specifically, Kaede could be employed to monitor the cellular interactions taking place between DCs and T cells at the tissue site of inflammation and DLN, by photo-switching and subsequently tracking T cells, to determine whether they migrate back to the DLN to interact with DCs or whether they are maintained in the tissue of inflammation. This would provide an *in vivo* model system that would allow some of the unanswered

questions regarding DC-T cell interactions at the tissue site of inflammation to be explored. Moreover, understanding how T cells are maintained at the tissue site of inflammation during the effector phase of the immune response and whether they are required to interact with DCs on site or back in the DLN, could facilitate the generation of novel therapeutic targets or allow better targeting of existing therapies.

The Kaede gene was purchased as part of a mammalian expression vector. This is the only commercially available form of the Kaede gene and was suitable for the induction of Kaede expression in stable cell lines. However, it was not suitable for inducing the expression of Kaede in primary cells such as DCs and T cells, which were the principal cells of interest in this project, since transfection rates of these cells are extremely low. Thus, the Kaede gene was cloned into an expression vector to produce large volumes of the protein, which could be isolated and purified to label primary cells and enable some preliminary imaging experiments to be carried out. The cloning and expression process was carried out according to manufacturer's guidelines and did not prove problematic. However, during the first round of protein purification, the process was not protected from the light and when the protein was examined by epi-fluorescent microscopy, it was evident that naturally occurring UV light had induced photo-conversion of the protein from green to red. This demonstrated the sensitivity of the protein to photo-conversion and served to confirm previously published reports that cell damaging levels of UV light are not required to induce photo-switching from green to red fluorescence (371).

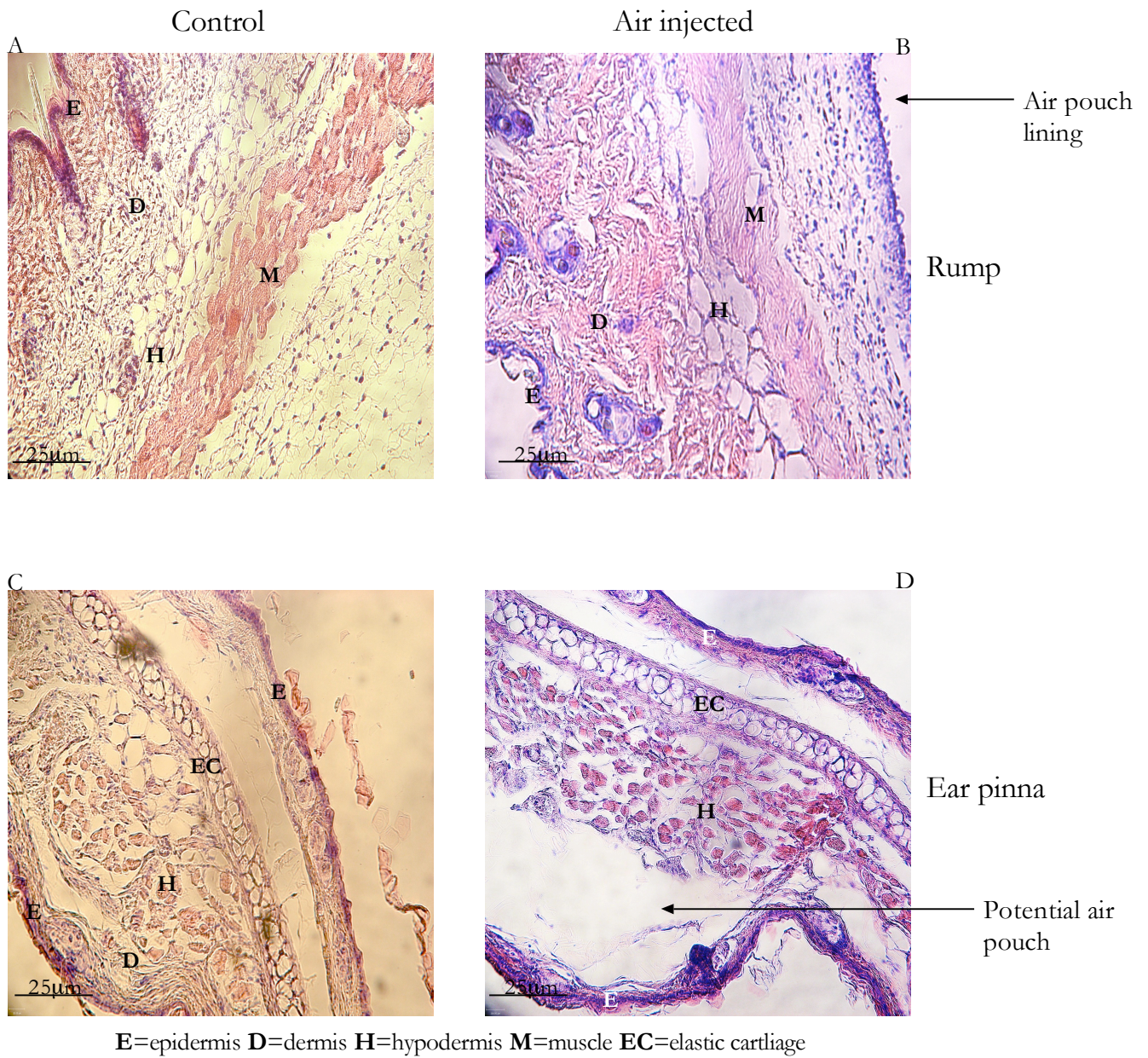
Previously, Kaede has been employed to label cells and organelles *in vivo* and has been visualised and photo-switched by MPLSM (370, 371). However, thus far, there have been no studies reporting the combination of Kaede with MPLSM to track cellular migration between anatomical locations. A study carried out using the Kaede transgenic mouse has demonstrated that lymphocytes expressing Kaede can be photo-switched *in vivo* and subsequently tracked by flow cytometry *ex vivo* (371). In addition, Kaede has been employed to track the movement of mitochondrion using MPLSM, by monitoring the photo-converted fluorescence of Kaede in isolated tobacco BY-2 cells (370). However, in the experiments carried out here, photo-switching of the Kaede using MPLSM was not successful, due to the insufficient energy of the Ti-sapphire laser to penetrate the LN and

induce photo-conversion (370). Thus, when DCs labeled with Kaede beads were imaged *in vivo*, the fluorescent protein was photo-converted from the green to the red fluorescent form using UV light from an epi-fluorescent microscope. This successfully converted the Kaede protein as seen by MPLSM and flow cytometric analysis, however, if Kaede is to be employed in future imaging studies of cellular interactions at the tissue site of inflammation and DLN, a system in which Kaede can be photo-converted during imaging would be favourable. Moreover, a dual scan head, which would allow different wavelengths of laser light to be applied simultaneously during imaging would also be a useful tool for future MPLSM studies. This would allow Kaede labeled cells and other fluorescently labeled cells to be imaged while UV light is applied to the target cells to induce their photo-conversion. Although the studies carried out here were preliminary and met with technical limitations, the results have demonstrated that DCs can be labeled with Kaede and imaged *in vitro* and *in vivo*, highlighting the potential use of this fluorescent probe in the *in vivo* model systems of the tissue site of inflammation and DLN.

DCs were labelled with the Kaede protein and imaged *in vitro* by epi-fluorescent microscopy and *in vivo* by MPLSM. DCs are a highly specialised cell type designed to sample their environment and will readily engulf protein antigen. This characteristic of DCs was harnessed to label this cell type with the purified Kaede protein (393). However, initially DCs were incubated with the soluble form of the Kaede protein and the level of protein engulfed by the DCs was not substantial enough to ensure effective labelling of the cell. Thus, to convert the Kaede protein from a soluble to a particulate antigen, the fluorescent protein was coated onto 2 μ m polystyrene beads. Once in a particulate format, DCs readily engulfed sufficient amounts of the fluorescent protein to enable *in vitro* and *in vivo* imaging. Developing a system in which antigen specific T cells could also be labelled with Kaede would be the next logical progression for these studies. However, in contrast to DCs, T cells do not sample proteins from their environment and do not readily engulf particulate antigen. Thus, while this method of labelling DCs with Kaede proved successful, it could not be employed to label T cells. Generating a population of transgenic T cells that endogenously express the Kaede gene would be the most effective way of acquiring a population of Kaede labelled T cells. However, the Kaede transgenic mouse is not commercially available therefore an alternative method of acquiring Kaede labelled T cells would be required to be

employ Kaede in the systems developed in this chapter and in chapter 4. A potential alternative to the Kaede transgenic mouse would be the human coxsackie adenovirus receptor (HCAR) system, in which a transgenic mouse has been generated to express a truncated HCAR on the cell surface. This system allows the delivery of target genes to specific cells in the mouse, *in vivo* or *ex vivo*, using an adenoviral vector, in which genes of interest are inserted (394, 395). In particular, employing HCAR mice, which have been crossed with DO11.10 mice, would allow the expression of the HCAR receptor and the delivery of the gene of interest within the adenoviral vector to be restricted to OVA specific DO11.10 T cells. In future studies this system could therefore be employed here to overcome the technical difficulties associated with labelling T cells with a soluble fluorescent protein by cloning the Kaede gene into an adenoviral vector and then subsequently infecting the HCAR/DO11.10 mouse with the adenovirus (394, 395). In future studies, this would be the best option available to label T cells and to allow both the migration and interactions between T cells and DCs to be tracked at and between the tissue site of inflammation and DLN.

In conclusion, this chapter explored the use of the photo-switchable fluorescent probe, Kaede. The Kaede gene was cloned, expressed, purified and conjugated to polystyrene beads to label DCs with the green fluorescent protein. Kaede labelled DCs were imaged *in vitro* and *in vivo* and photo-switched from the green fluorescent form to the red fluorescent form, following a single second UV pulse. Developing a method to label T cells with the protein would be the next logical step. However, the potential for employing Kaede in future experiments involving the *in vivo* model systems developed in this chapter and in chapter 4, has been outlined by the results obtained in this here. Moreover, while photo-switchable probes are still in the preliminary stages of development, a number of studies employing them in a variety of diverse experiments have already been reported and their continued development will undoubtedly facilitate a host of more complex *in vitro* and *in vivo* imaging studies (371, 375, 396, 397).



E=epidermis D=dermis H=hypodermis M=muscle EC=elastic cartilage

Figure 5.1 An air pouch lining can be created in the rump but not the ear pinna

To attempt to create an air pouch, sterile air was injected subcutaneously into either the rump (A+B) or ear pinna (C+D) over a period of 6 days. Control mice were not injected. On day 7 the rump and ear pinna were removed, fixed in formalin and 10µm sections were prepared for histological analysis. (A) Bright-field image at x10 magnification of a section of control rump stained with H&E (B) Bright-field image at x10 magnification of a section of rump stained with H&E. Black arrow indicates air pouch cavity with the compact cellular lining clearly visible. (C) Bright-field image at x10 magnification of a section of control ear pinna stained with H&E. (D) Bright-field image at x10 magnification of a section of ear pinna stained with H&E. Potential air pouch indicated by black arrow, however, it lacks the compact structure of the air pouch observed in the rump and a similar cavity can be observed in control image C. Thus it is unlikely to be a true air pouch cavity.

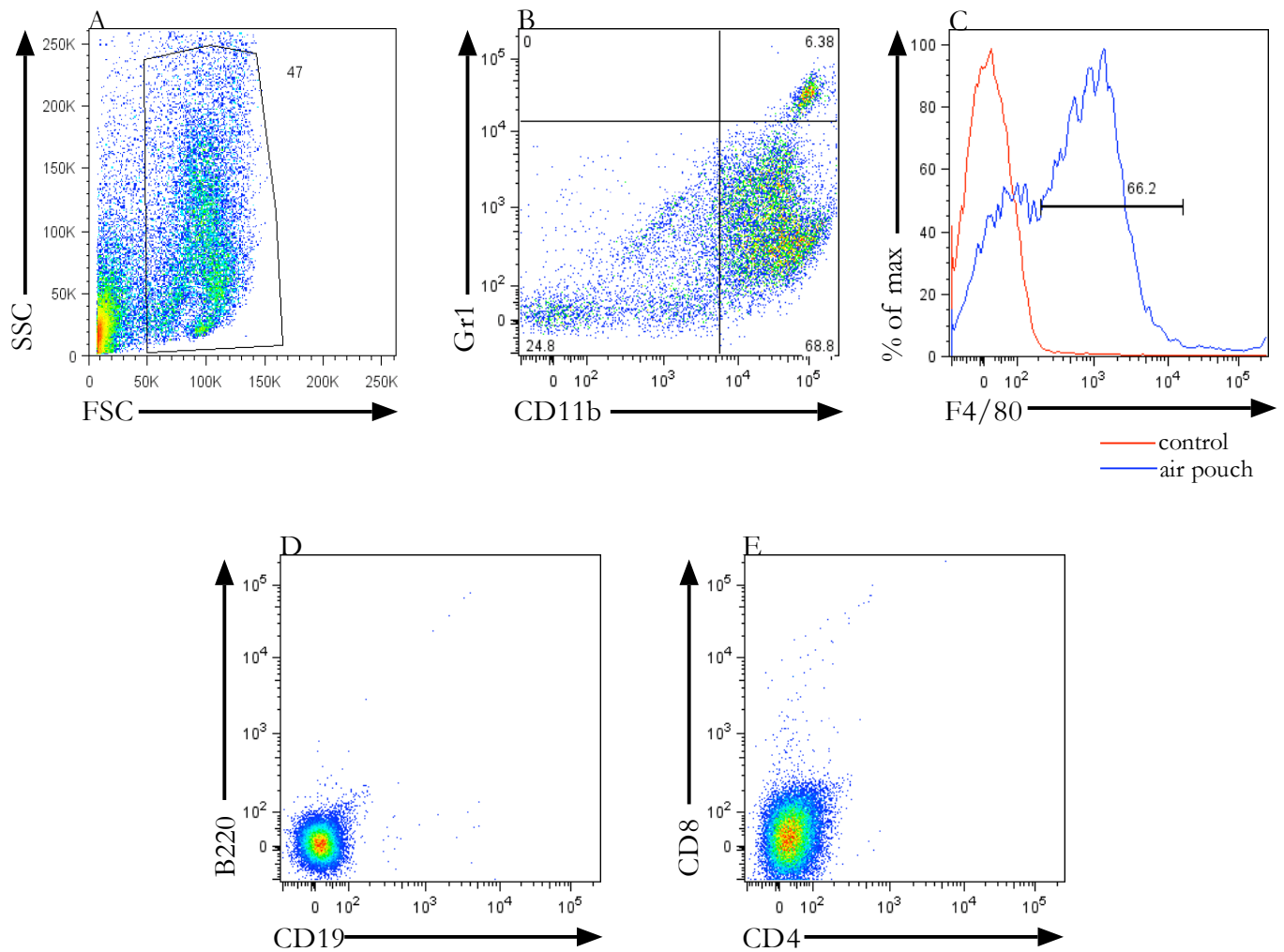


Figure 5.2 Identification of cells infiltrating the air pouch of the rump

To create an air pouch in the rump, sterile air was injected subcutaneously over a period of 6 days. Control mice were not injected. On day 7, the air pouch was washed using saline and cells recovered were analysed by flow cytometry. (A) Cells were identified on the basis of size and granularity. Large and granular cell types predominated. (B) A population of cells expressing either CD11b or both CD11b and Gr1 cells were identified in the air pouch (C) Cells expressing the pan macrophage marker F4/80 could be detected in the air pouch (D) Cells within the air pouch failed to express the B cell markers CD19 and B220. (E) Cells within the air pouch failed to express the T cell markers CD4 and CD8

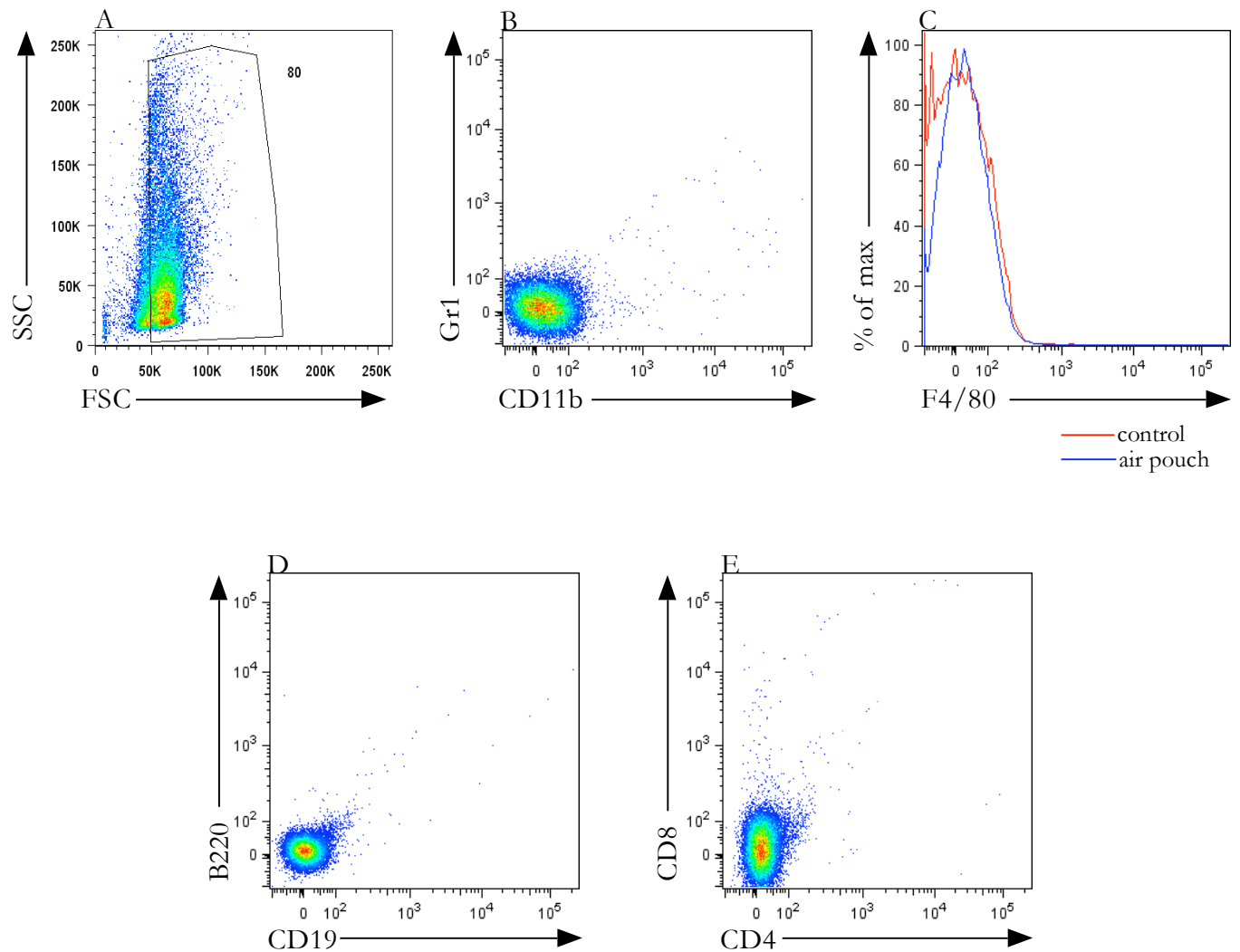


Figure 5.3 Identification of cells infiltrating the air pouch in the ear pinna

To create an air pouch in the ear pinna, sterile air was injected subcutaneously over a period of 6 days. Control mice were not injected. On day 7, the air pouch was washed using saline and recovered cells were analysed by flow cytometry. (A) Cells were identified on the basis of size and granularity. Fewer large granular cell types were detected in comparison to the air pouch of the rump (B) Cells failed to express the myeloid markers CD11b and the neutrophil marker Gr1. (C) Cells also failed to express the macrophage marker F4/80. Cells recovered from the air pouch of the ear pinna failed to express the (D) B cell markers CD19 and B220 and (E) T cell markers CD4 and CD8.

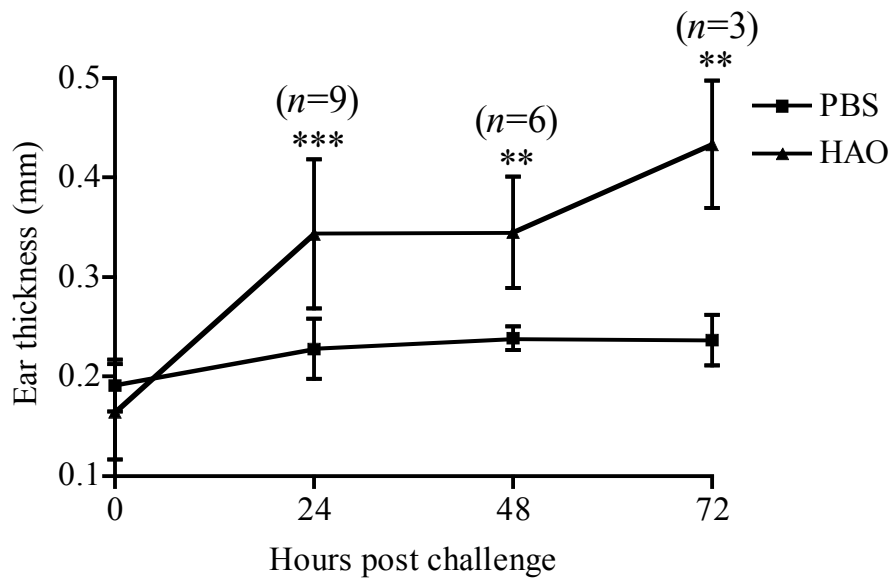
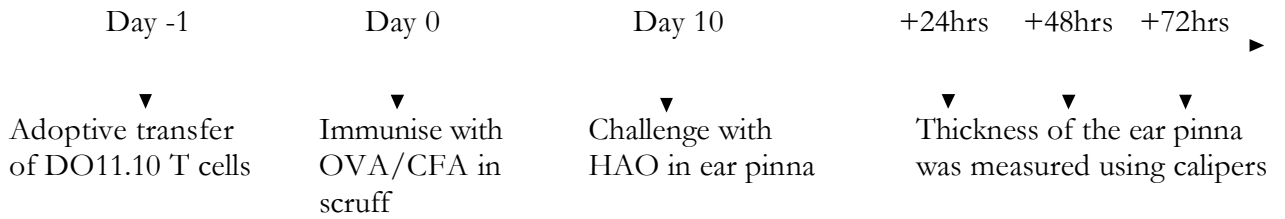


Figure 5.4 Measure of changes in ear thickness in response to the induction of a DTH reaction

To initiate a DTH reaction in the ear pinna, OVA specific DO11.10 T cells were adoptively transferred into BALB/c recipients. Mice were primed with OVA/CFA in the scruff and challenged 10 days later with either HAO or PBS control in the ear pinna. Ear thickness was measured using calipers prior to and 24, 48 and 72 hours following HAO or PBS challenge. (A) Graph summarises ear thickness following HAO challenge. (B) Bar chart summarises ear thickness at 0h. ** p < 0.01, *** p < 0.001

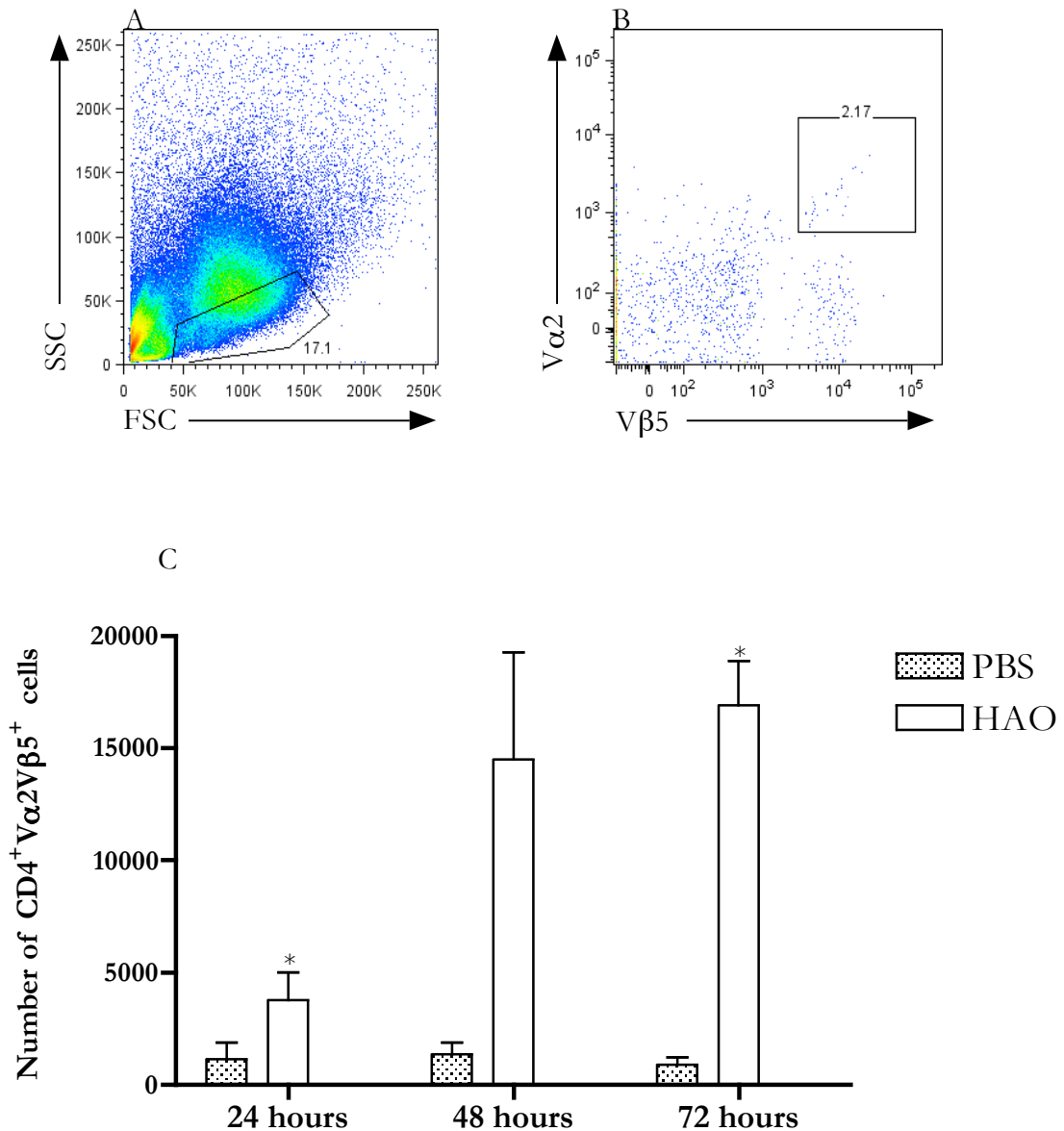


Figure 5.5 Antigen specific T cells can be recovered from the ear pinna following the induction of a DTH reaction

To initiate a DTH reaction in the ear pinna, OVA specific TCR transgenic (OTII) T cells were adoptively transferred into C57BL/6J recipients. Mice were primed with OVA/CFA in the nape of the neck and challenged 10 days later with either HAO or PBS control in the ear pinna. Ears were removed at 24, 48 and 72 hours and dermal layers were separated to release cells for flow cytometric analysis. Representative flow cytometric plots show results obtained following HAO challenge (A) Lymphocytes released from the dermal layers of the ear pinna were identified on the basis of size and granularity (B) Lymphocytes were next analysed for their expression of the transgenic CD4⁺ OVA specific T CR (C) Graph summarises the absolute number of antigen specific T cells infiltrating the ear pinna in response to HAO challenge or PBS control over a time course of 24 to 72 hours. The number of OVA specific, TCR transgenic T cells in the ear pinna at 72 hours was significantly higher than the number in the ear pinna at 24 hours following HAO challenge (*p=0.0048)

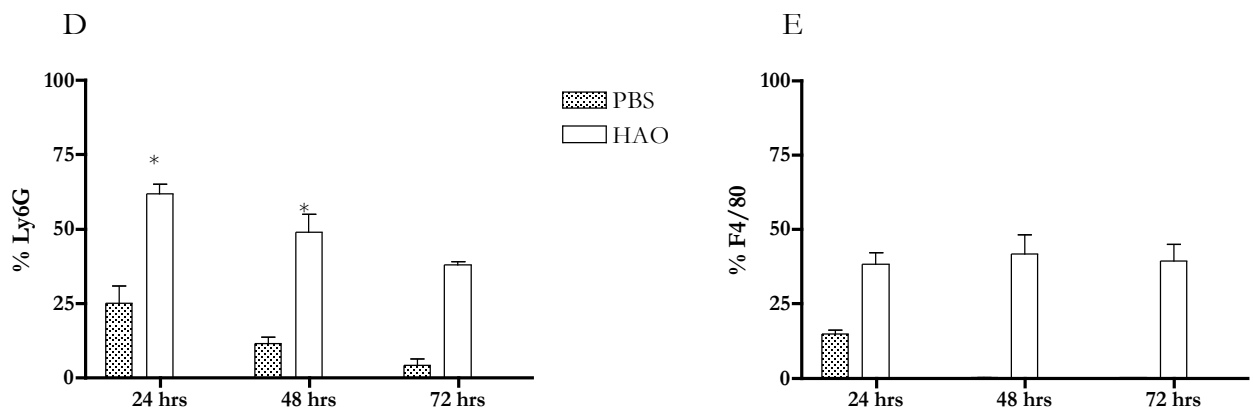
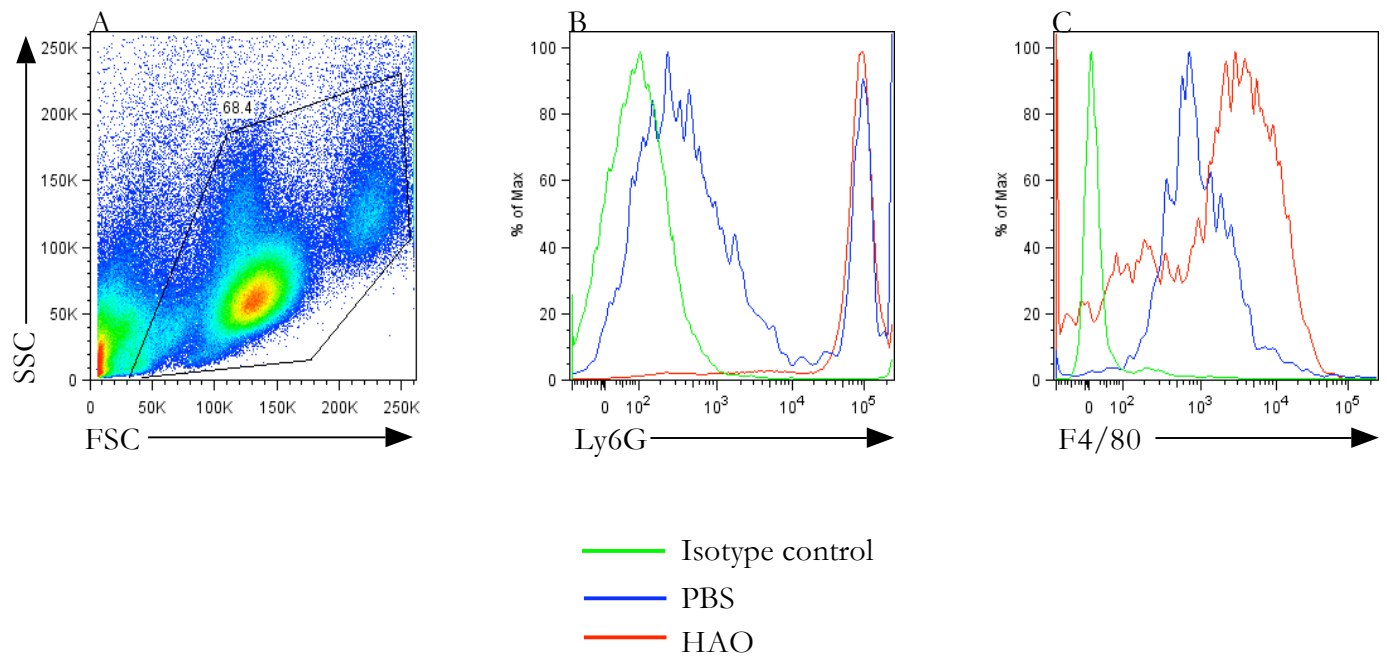


Figure 5.6 Macrophages and neutrophils can be recovered from the ear pinna following the induction of a DTH reaction

To initiate a DTH reaction in the ear pinna, OVA specific DO11.10 T cells were adoptively transferred into BALB/c recipients. Mice were primed with OVA/CFA in the nape of the neck and 10 days later were challenged with either HAO or PBS control in the ear pinna. Ears were removed at 24, 48 and 72 hours and dermal layers were separated to release cells for flow cytometric analysis. Representative flow cytometric plots show results obtained following HAO challenge and PBS control (A) Granulocytic and mononuclear cells released from the dermal layers of the ear pinna were identified on the basis of size and granularity (B) Cells were next analysed for their expression of the neutrophil marker Ly6G (C) Cells were analysed for their expression of the macrophage marker F4/80 (D) Graph summarises the proportion of Ly6G⁺ cells infiltrating the ear pinna in response to HAO challenge or PBS control over a time course of 24 to 72 hours. The number of Ly6G⁺ cells in the ear pinna significantly decreased from 24 to 48 hours following HAO challenge (*p=0.0027) (E) Graph summarises the proportion of F4/80⁺ cells infiltrating the ear pinna in response to HAO challenge or PBS control over a time course of 24 to 72 hours.

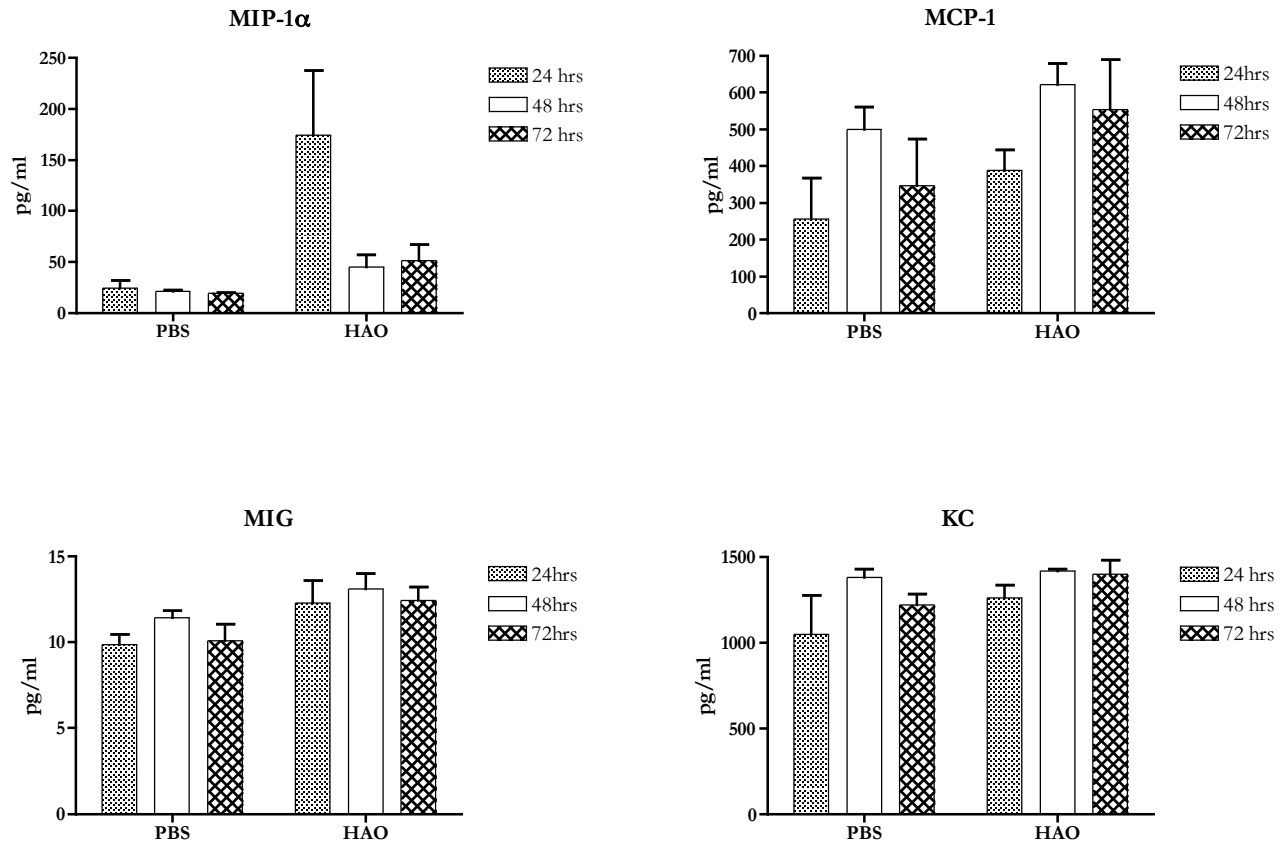


Figure 5.8 The production of chemokines in the ear pinna following the induction of a DTH reaction

To initiate a DTH reaction in the ear pinna, OVA specific TCR transgenic (OTII) T cells were adoptively transferred into C57BL/6J recipients. Mice were primed with OVA/CFA in the nape of the neck and challenged 10 days later with either HAO or PBS control in the ear pinna. After 24, 48 and 72 hours, ear pinnae were removed and epidermal layers were split and placed into overnight culture. Culture media was analysed for the presence of the pro-inflammatory chemokines, KC, MCP-1, MIG, MIP-1 α and HAO challenge did not significantly alter their production. Results show the mean of triplicate samples \pm s.d.

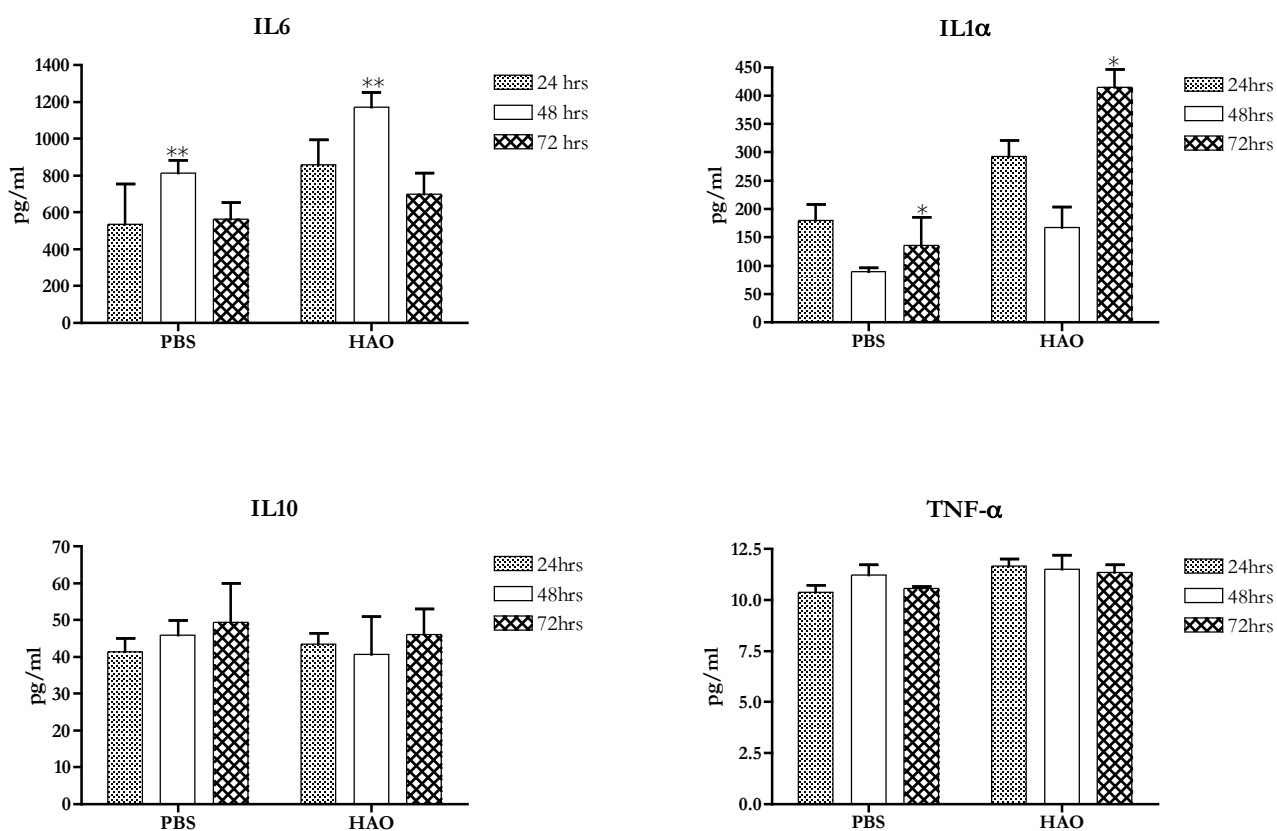


Figure 5.7 The production of proinflammatory cytokines in the ear pinna following the induction of a DTH reaction

To initiate a DTH reaction in the ear pinna, OVA specific TCR transgenic (OTII) T cells were adoptively transferred into C57BL/6J recipients. Mice were primed with OVA/CFA in the nape of the neck and challenged 10 days later with either HAO or PBS control in the ear pinna. After 24, 48 and 72 hours, ear pinnae were removed and epidermal layers were split and placed into overnight culture. Culture media was analysed for the presence of the pro-inflammatory cytokines, TNF- α , IL1- α , IL6 and the anti-inflammatory cytokine IL10. In comparison with PBS control, HAO challenge in the ear pinna gave rise to a significantly higher level of IL1- α production at 72 hours post challenge (* $p=0.0089$) and IL6 production at 48 hours post challenge (** $p=0.0281$) Results show the mean of triplicate samples \pm s.d.

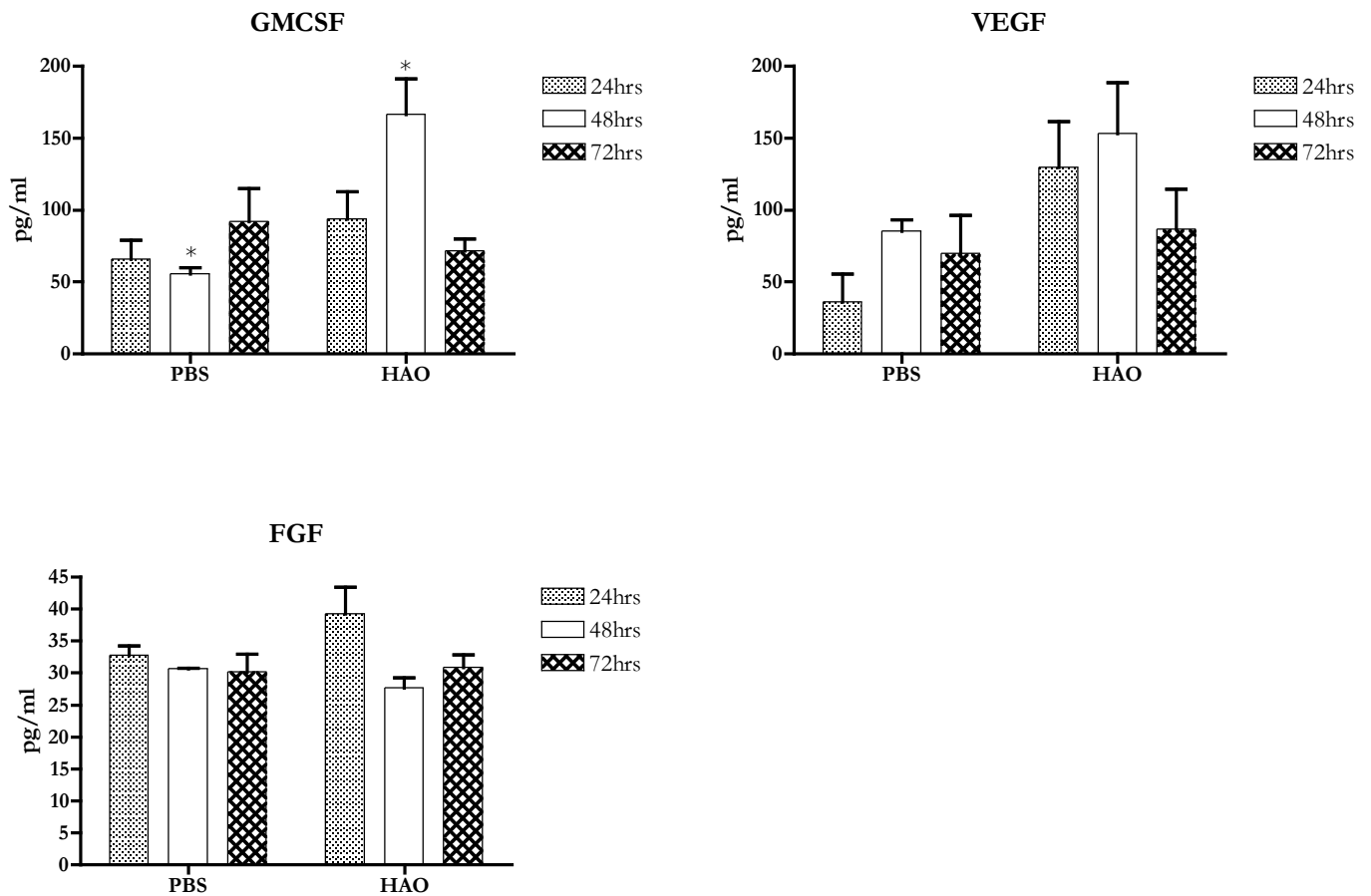


Figure 5.9 The production of growth and repair factors in the ear pinna following the induction of a DTH reaction

To initiate a DTH reaction in the ear pinna, OVA specific TCR transgenic (OTII) T cells were adoptively transferred into C57BL/6J recipients. Mice were primed with OVA/CFA in the nape of the neck and challenged 10 days later with either HAO or PBS control in the ear pinna. After 24, 48 and 72 hours, ear pinnae were removed and epidermal layers were split and placed into overnight culture. Culture medium was analysed for the presence of the growth and repair factors VEGF, FGF and GM-CSF. In comparison with PBS control, HAO challenge did not significantly alter the production of VEGF or FGF, however HAO injection gave rise to a significantly higher level of GM-CSF production at 48 hours post challenge (* $p=0.0116$)

Results show the mean of triplicate samples \pm s.d.

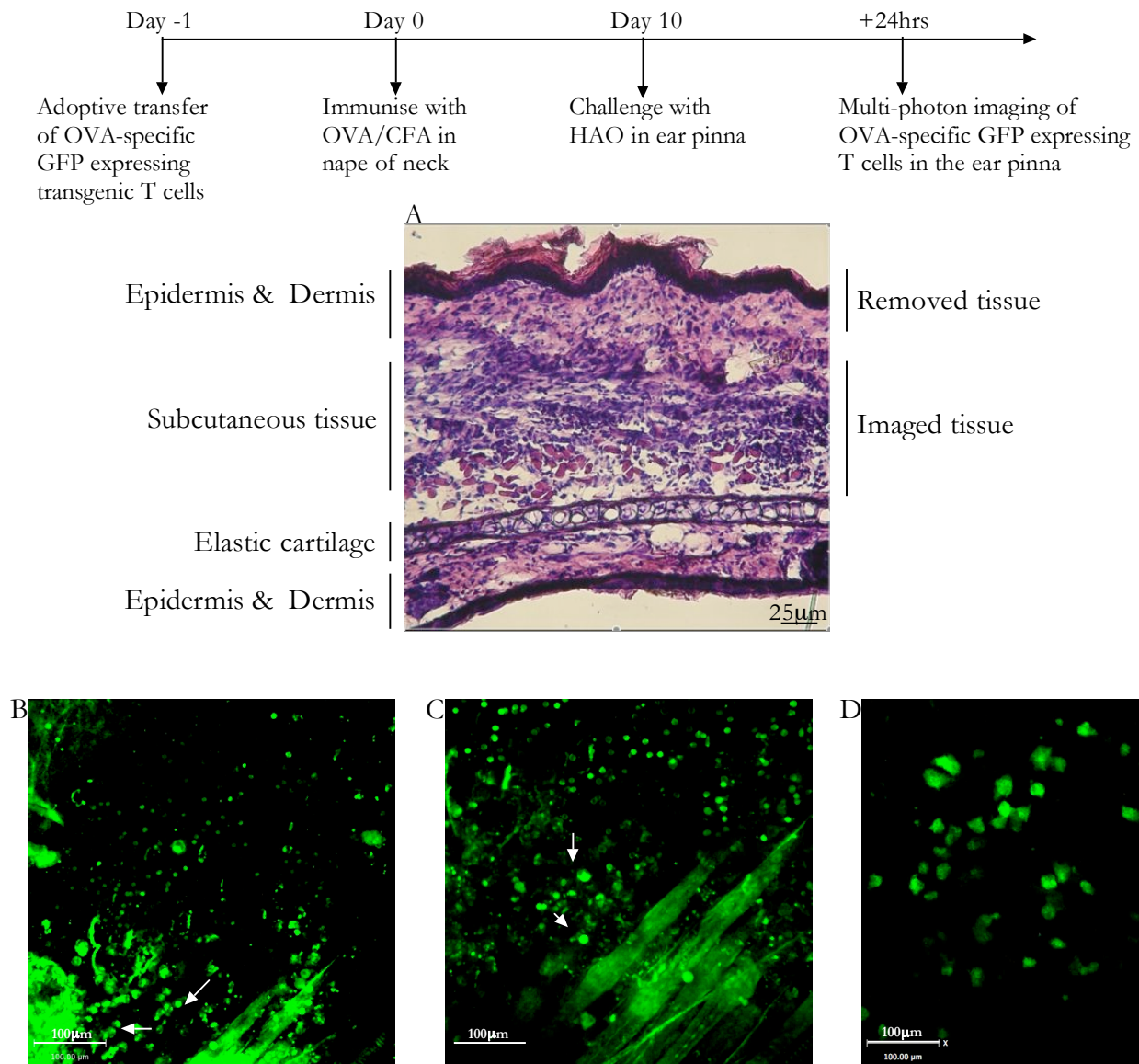


Figure 5.10 Antigen specific T cells can be imaged in the ear pinna during the DTH reaction

To initiate a DTH reaction in the ear pinna, OVA-specific, GFP expressing, TCR transgenic (OTII) T cells were adoptively transferred into C57BL/6J recipients. Mice were primed with OVA/CFA in the nape of the neck and challenged 10 days later with either HAO or PBS control in the ear pinna. Ears were prepared for imaging 24 hours post challenge and a small section of the dermal layer was removed for MPLSM. (A) Bright-field image of a cross-section of ear pinna stained with H&E. The various tissue layers are indicated, showing the dermal layers that were removed for imaging (B) Image taken at x40 magnification of multi-photon movie of OVA-specific, GFP expressing transgenic T cells migrating in the subcutaneous region of the HAO challenged ear pinna. OVA-specific, GFP expressing T cells are indicated by white arrows. (C) Image at x40 magnification of multi-photon movie of OVA-specific, GFP expressing transgenic T cells migrating in the subcutaneous region of the HAO challenged ear pinna. OVA-specific, GFP expressing T cells are indicated by white arrows. (D) Image of multi-photon movie of OVA-specific, GFP expressing transgenic T cells migrating in the DLN. n= 2 mice per group

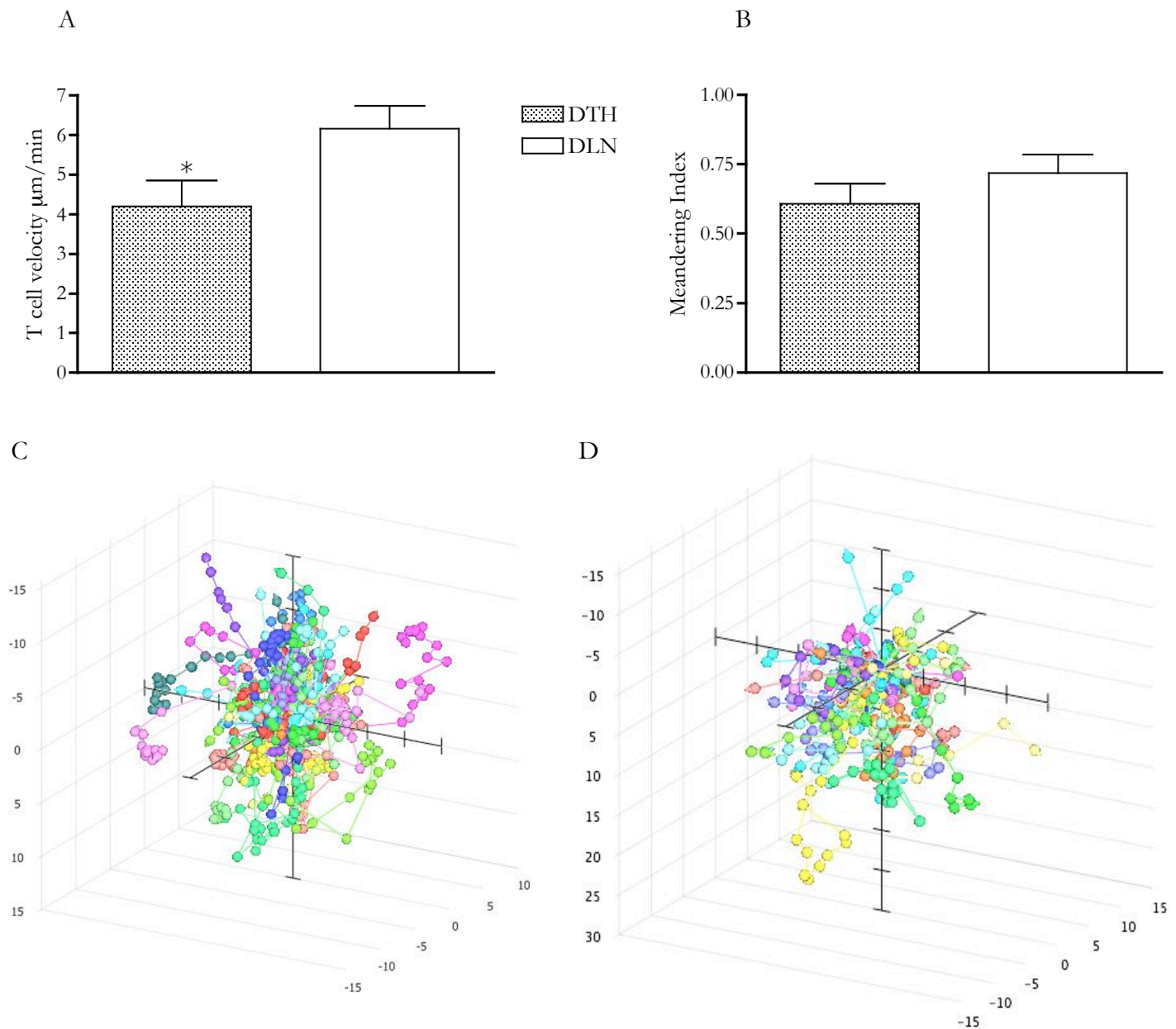


Figure 5.11 Comparison of mean velocity, meandering index and displacement of T cells in a site of inflammation in the ear pinna and the DLN

To initiate a DTH reaction in the ear pinna, OVA-specific, GFP expressing, TCR transgenic (OTII) T cells were adoptively transferred into C57BL/6J recipients. Mice were primed with OVA/CFA in the nape of the neck and challenged 10 days later with either HAO or PBS control in the ear pinna. Ears were prepared for imaging 24 hours post challenge and a small section of the dermal layer was removed for MPLSM. T cells were imaged in HAO challenged ears and DLN by MPLSM (No T cells were observed within the ears of PBS control challenged mice). T cell behaviour was analysed using Velocity software. (A) The mean velocity of transgenic T cells from 2 samples from 2 mice was calculated. T cells within the DLN migrated at a significantly faster speed than those in the tissue site of inflammation (* $p=0.0291$) (B) The mean meandering index of transgenic T cells from 2 samples from 2 mice were calculated (C) The tracks of several individual T cells migrating within the DTH site, were plotted to demonstrate distance travelled from point of origin (D) The tracks of several individual T cells migrating within the DLN, were plotted to demonstrate distance travelled from point of origin

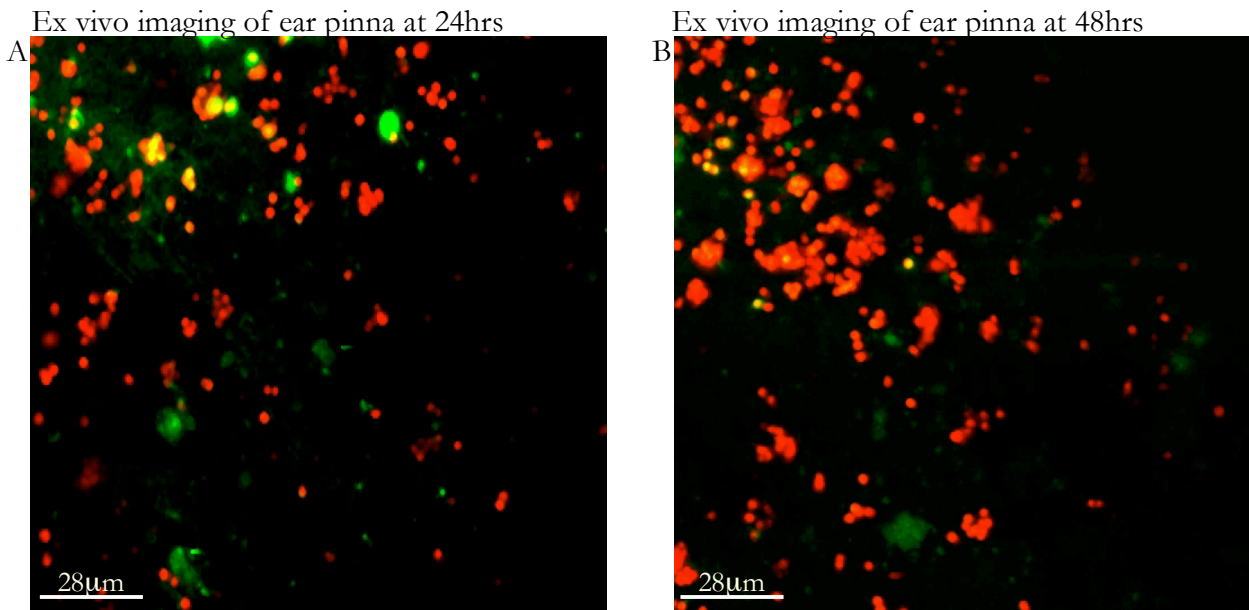
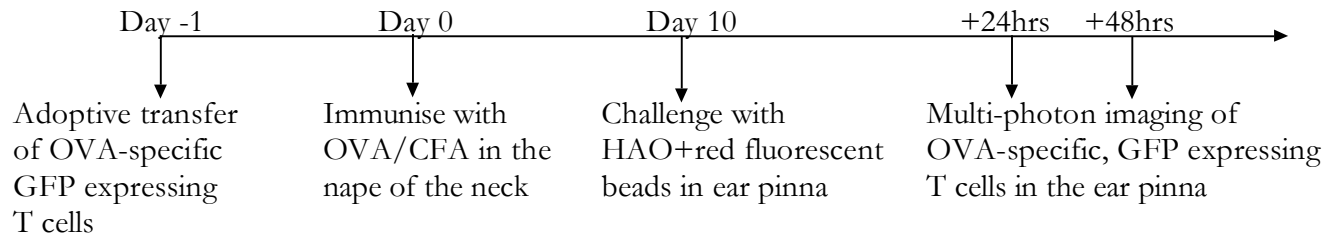


Figure 5.12 Fluorescent beads injected with HAO are taken up by local APCs and can be imaged in the ear pinna

To initiate a DTH reaction in the ear pinna, OVA-specific, GFP expressing, TCR transgenic (OTII) T cells were adoptively transferred into C57BL/6J recipients. Mice were primed with OVA/CFA in the nape of the neck and challenged 10 days later with either HAO or PBS control in the ear pinna. Ears were prepared for imaging 24 hours post challenge and a small section of the dermal layer was removed for MPLSM. (A) Image of multi-photon movie taken at x40 magnification, 24 hours post challenge. Few OVA-specific, GFP expressing, TCR transgenic T cells can be seen migrating in the subcutaneous region of the HAO challenged ear pinna. Red fluorescent beads injected in combination with HAO can be clearly seen and appear to be motile suggesting they had been internalised by migrating cells (B) Image of multi-photon movie taken at x40 magnification, 24 hours post challenge. Few OVA-specific, GFP expressing, TCR transgenic T cells can be seen migrating in the subcutaneous region of the HAO challenged ear pinna. Red fluorescent beads injected in combination with HAO can be clearly seen and appear to be motile. n= 2 mice per group

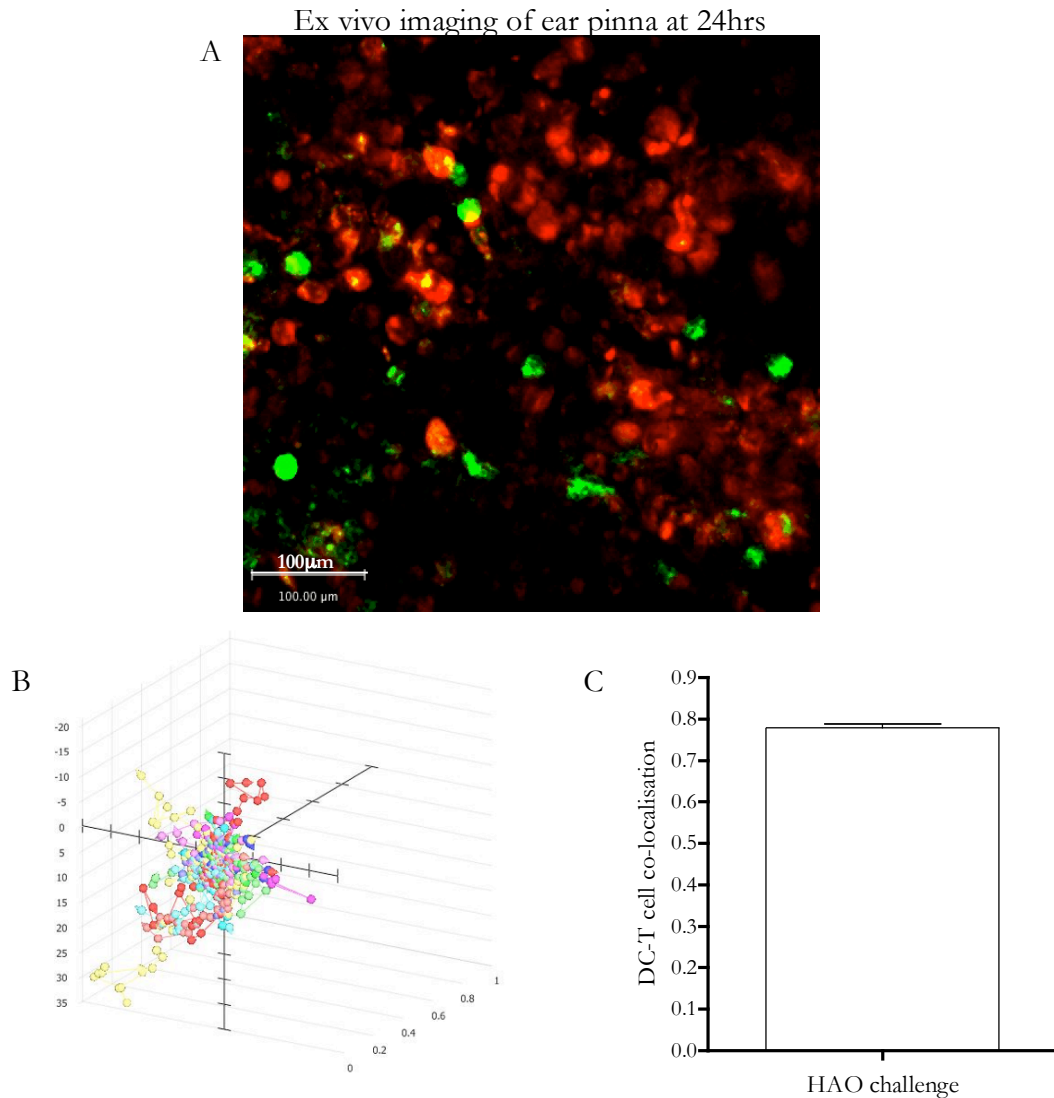
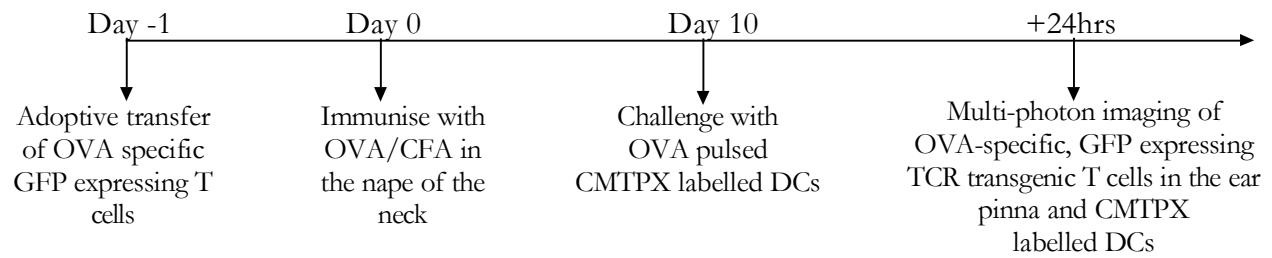


Figure 5.13 Antigen presenting DCs and antigen specific T cells interact in the ear pinna during the DTH reaction

To initiate a DTH reaction in the ear pinna, OVA-specific, GFP expressing, TCR transgenic (OTII) T cells were adoptively transferred into C57BL/6J recipients. Mice were primed with OVA/CFA in the nape of the neck and challenged 10 days later with either OVA or PBS pulsed DCs in the ear pinna. Ears were prepared for imaging 24 hours post challenge and a small section of the dermal layer was removed for MPLSM. (A) Image of multi-photon movie taken at x40 magnification, 24 hours post challenge. CMTPX labelled, OVA presenting DCs and OVA-specific, GFP expressing, transgenic T cells can be seen migrating and interacting in the subcutaneous region of the ear pinna. T cell behaviour was analysed using Volocity software (B) The tracks of several individual T cells migrating within the DTH site, were plotted to demonstrate distance travelled from point of origin (C) DC-T cell interactions were measured by quantifying the colocalisation of green voxels with red to determine the proportion of DC volume in contact with T cells.

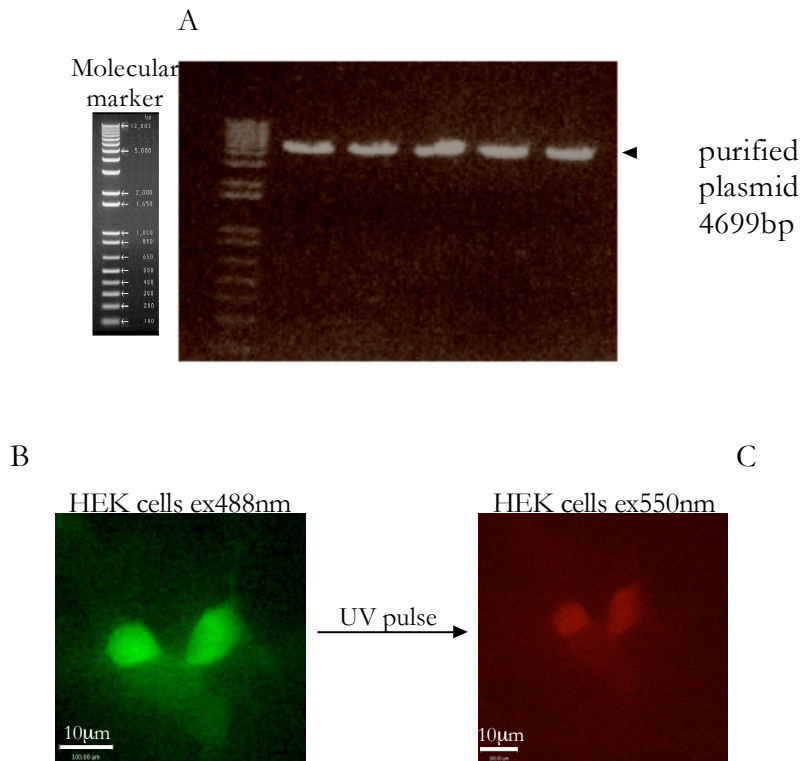


Figure 5.14 HEK 293 cells were transfected with the Kaede expression vector

A mammalian expression vector containing the Kaede gene was transformed into DH5 α *E.coli* and cultured overnight to amplify and obtain high copy numbers of the Kaede expression vector. The Kaede expression vector was eluted and purified from the DH5 α *E.coli*. (A) Samples were resolved on an agarose gel by electrophoresis. A band of approximately 4699 base pairs was detected and corresponded to the size of the Kaede expression vector (indicated by arrow). To test the expression vector and the ability of Kaede to be photo-converted, HEK 293 cells were transfected with the vector using lipofectamine and analysed by epi-fluorescent microscopy. (B) HEK293 cells expressing the green form of the Kaede protein following excitation with 488nm light prior to a UV pulse with 405nm light for 1 second (C) HEK293 cells expressing the red form of the Kaede protein following excitation with 550nm light following a 1 second UV pulse with 405nm light.

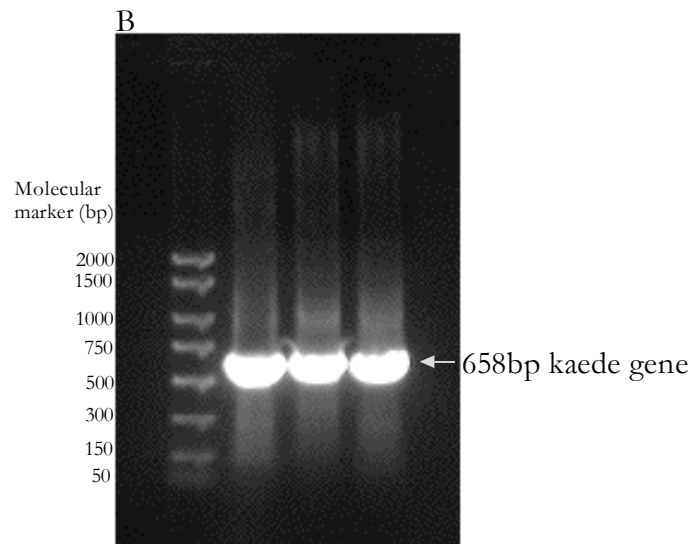
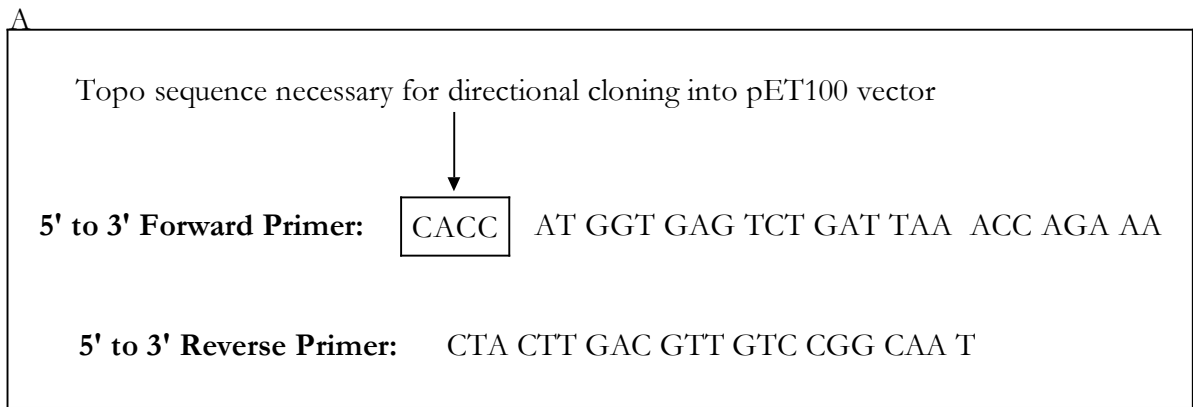


Figure 5.15 Primers were designed to amplify the Kaede gene from the mammalian expression vector into the pET-TOPO vector

(A) Sequence of primers designed to amplify Kaede gene (B) PCR was carried out on the Kaede mammalian expression vector using the designed Kaede primers. The products of the PCR reaction were resolved on a 1% agarose gel by electrophoresis. The primers successfully amplified the Kaede gene as confirmed by the presence of a band corresponding to approximately 658bp.

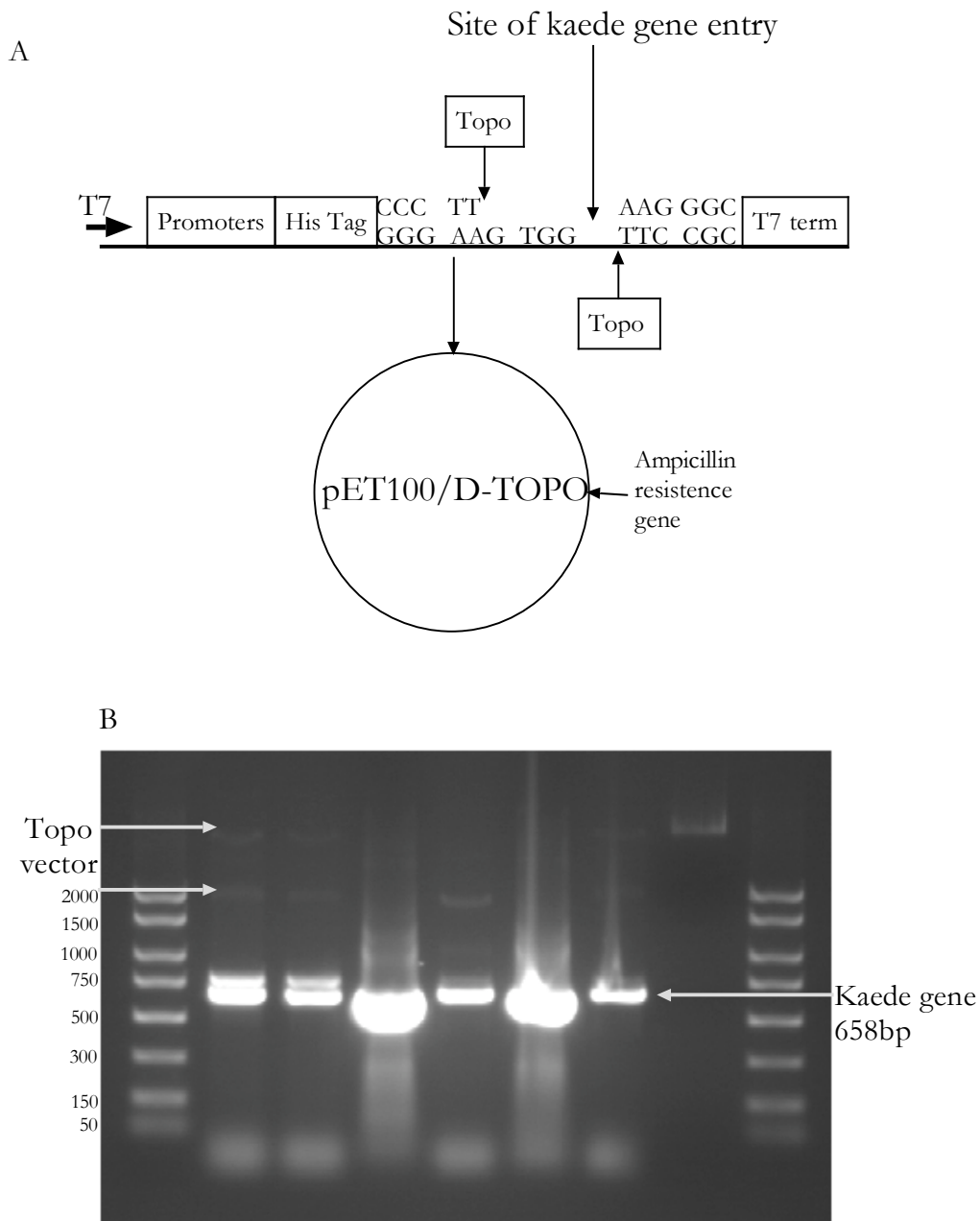


Figure 5.16 Kaede gene was cloned into the pET-TOPO expression vector

(A) Illustration of the pET-TOPO expression vector, highlighting the region into which the Kaede gene was inserted (B) PCR was carried out on the Kaede-pET-TOPO vector acquired from the cloning reaction, using Kaede primers described in figure 6.2. The products of the PCR reaction were resolved on a 1% agarose gel by electrophoresis. The Kaede gene was confirmed as being present within the pET-TOPO vector as a band corresponding to approximately 658bp was detected in each well. The Kaede-pET-TOPO vector was subsequently sent for sequencing to ensure the gene was incorporated in the correct orientation and without any base pair errors.

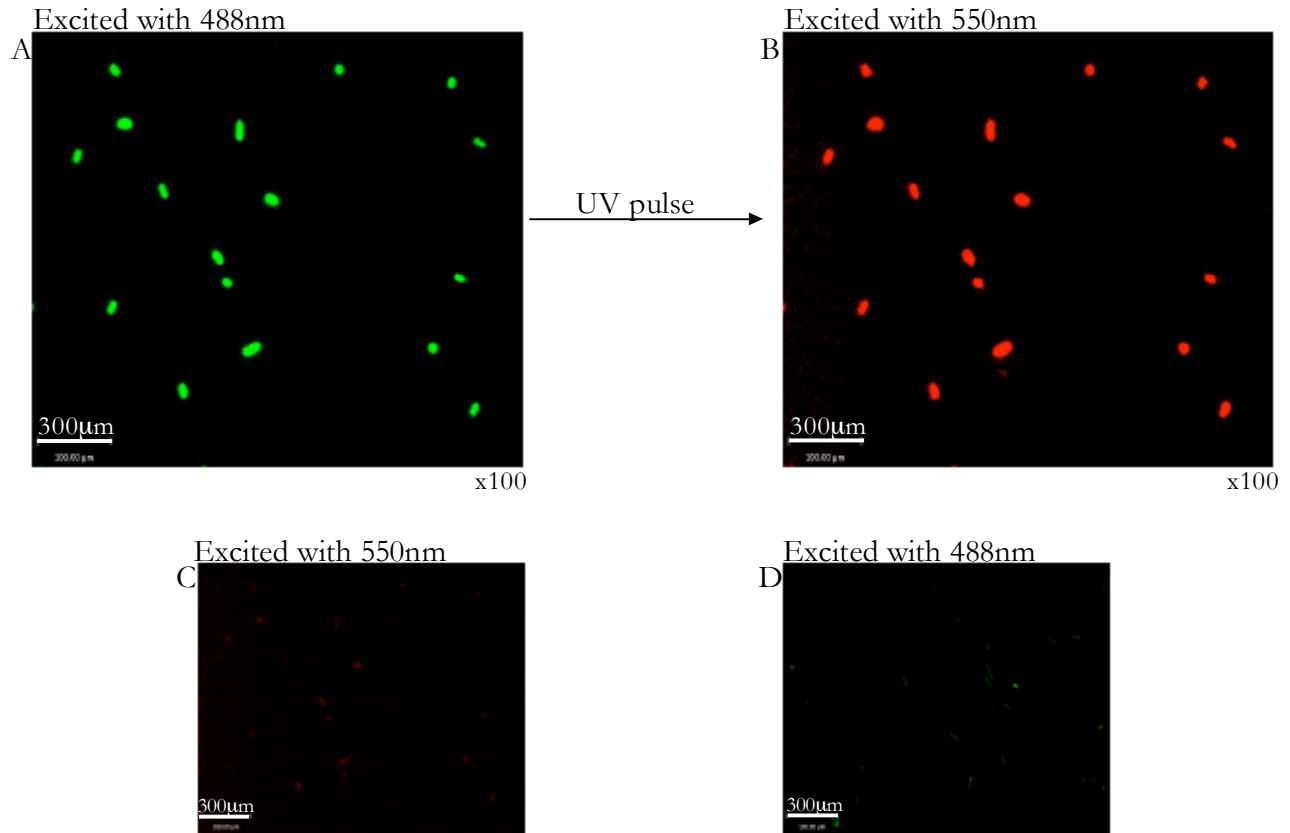


Figure 5.17 BL21 Star *E.coli* were transfected with the Kaede-pET-TOPO expression vector

BL21 Star *E.coli* were transfected with Kaede-pET-TOPO expression vector and were induced to express Kaede protein using IPTG. A small aliquot of bacteria were examined under the epi-fluorescent microscope for green fluorescence and their ability to be photo-converted. (A) Shows an image of BL21 Star *E.coli* excited with 488nm light expressing green fluorescent protein prior to a UV pulse (C) shows an image of BL21 Star *E.coli* excited with 550nm light prior to a UV pulse. The bacteria failed to express the red fluorescent form of the Kaede protein in the absence of UV treatment. (B) shows an image of BL21 Star *E.coli* excited with 550nm light following a 1 second pulse with UV light. The bacteria clearly expressed the red fluorescent form of the Kaede protein and had therefore been photo-converted. (D) BL21 Star *E.coli* excited with 488nm light following a 1 second UV pulse, failed to express the green form of the fluorescent protein.

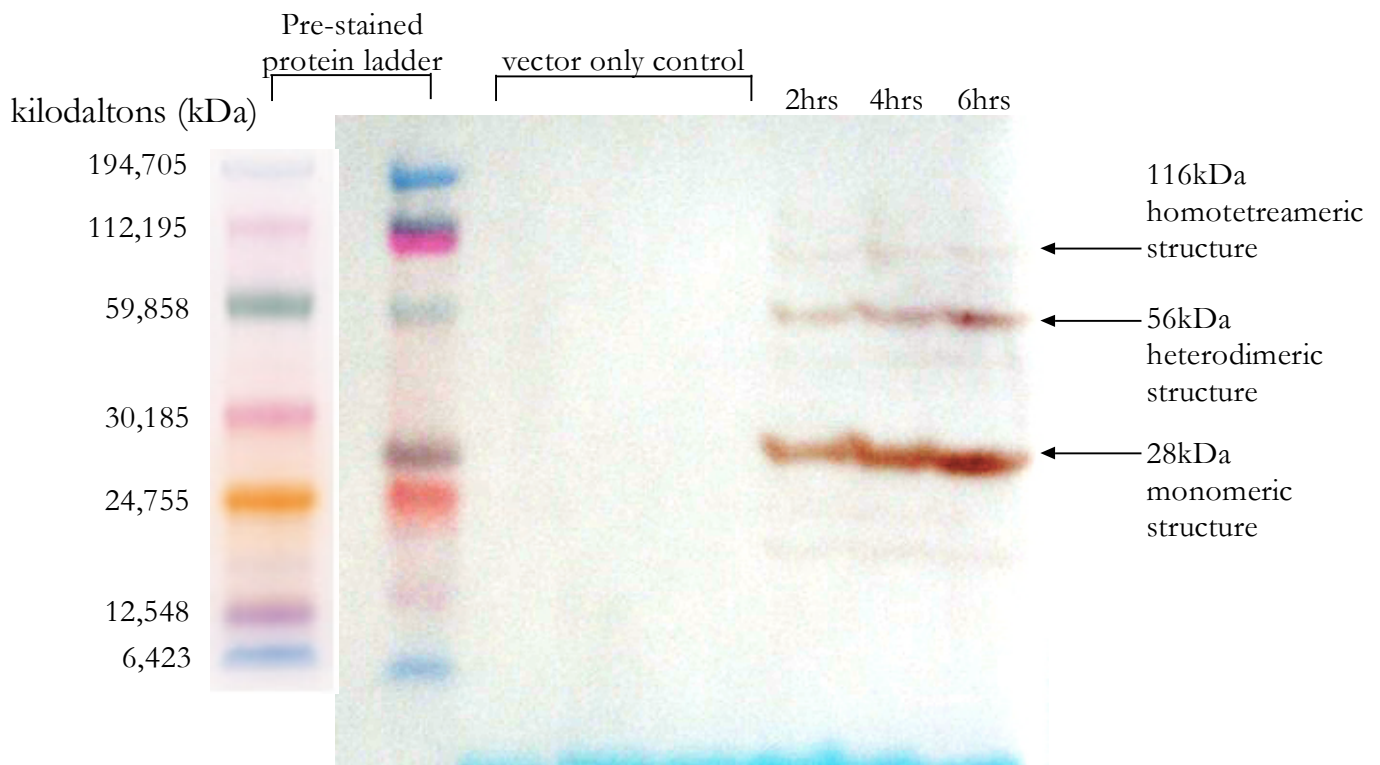


Figure 5.18 SDS-PAGE and Western Blot analysis of pilot expression of Kaede protein

The expression of Kaede protein was carried out in accordance to the protocol outlined in Materials and Methods. An SDS-PAGE and Western blot were carried out to detect the protein, using an anti-histidine antibody, and to assess which time point from the pilot expression produced the highest yield. The results show that in the control expression experiments, which were set up using empty pET-TOPO vectors, no Kaede protein was detected. When Kaede containing pET-TOPO vectors were transformed into BL21 Star E.coli the Kaede protein was expressed. Indicated by arrows, bands of molecular weight corresponding to the monomeric, dimeric and trimeric forms of Kaede was observed. However, the monomeric form of the protein was present at higher level than the dimeric and trimer forms and the band was heaviest at the 6 hour time point, which indicated that protein expression was optimum at this time point.

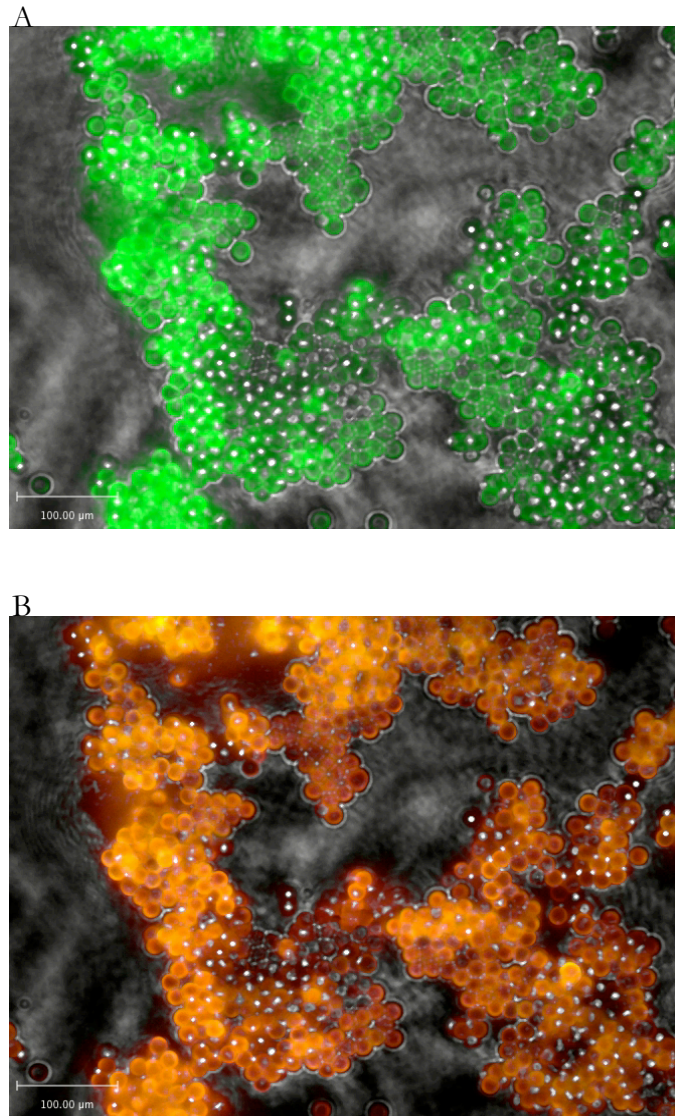


Figure 5.19 DCs pulsed with Kaede beads were imaged *in vitro* and photo-converted using UV light

Bone marrow derived DCs were pulsed with Kaede beads and imaged *in vitro* using epi-fluorescence microscopy. (A) Image of *in vitro* movie of Kaede pulsed DCs prior to UV pulse. Excited with 488nm light the DCs emitted green fluorescence (B) Image of *in vitro* movie of Kaede pulsed DCs following a 1 second UV pulse. Excited with 550nm light the DCs emitted red fluorescence. For QuickTime movies see attached CD

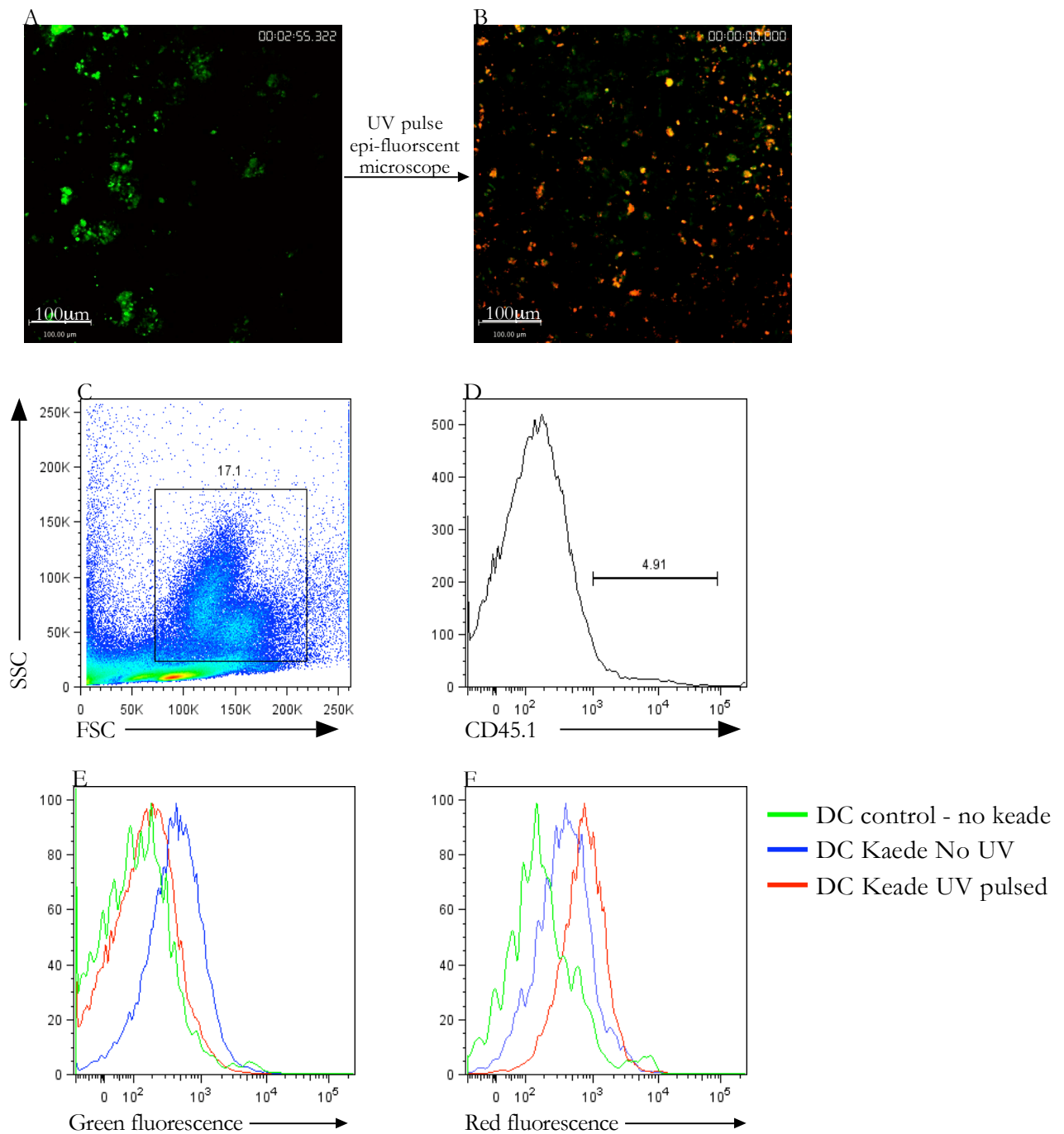


Figure 5.20 DCs pulsed with Kaede conjugated to beads were visualised *in vivo* using MPLSM

Bone marrow derived DCs from C57BL/6J CD45.1⁺ mouse were pulsed with Kaede beads and transferred into the footpad of a C57BL/6J mouse. 20 hours later the draining popliteal LN was removed and prepared for MPLSM. Imaged LNs and a control, non-imaged LN were also analysed for photo-conversion of Kaede by flow cytometry. (A) Image of *in vivo* movie obtained of Kaede pulsed DCs in the DLN prior to UV pulse (B) Image of *in vivo* movie obtained of Kaede pulsed red fluorescence expressing DCs in the DLN post UV pulse using an epi-fluorescent microscope. (C) Representative flow cytometric plot of DCs identified on the basis of size and granularity (D) Transferred DCs were next identified on the basis of CD45.1 expression (E) DCs alone or DCs pulsed with Kaede or DCs pulsed with Kaede and UV treated were analysed for their expression of green non photo-converted form of Kaede fluorescence (F) DCs alone or DCs pulsed with Kaede or DCs pulsed with Kaede and UV treated were analysed for their expression of the red photo-converted form of Kaede fluorescence

Chapter 6

Summary, Conclusions and Future Work

As highlighted in chapter 1, the kinetics and dynamics of DC-T cell interactions in the LN are thought to be critical in initiating and regulating immune responses in both health and disease (7, 9). DCs are localised in lymphoid and non-lymphoid tissues and effector and memory T cells continually migrate between both sites (19-24). However, the relationship and degree of interaction between the non-lymphoid site of tissue inflammation and the DLN remains relatively uncharacterised. Whether T cells require to see antigen presented by DCs at the tissue site of inflammation to initiate or maintain a response is not clear. This thesis aimed to develop novel *in vivo* model systems that would allow identifiable antigen specific T cells and DCs and their interactions in the tissue site of inflammation and DLN to be imaged and characterised using MPLSM. A better understanding of the relationship between DC-T cell interactions at the tissue site of inflammation and the DLN, will hopefully provide novel therapeutic targets in circumstances of autoimmunity and inflammatory disease and facilitate improved targeting of current therapies.

The first objective of this thesis was to create an *in vitro* model system in which DC-T cell interactions and the effects of modulating these interactions could be assessed and characterised. In these *in vitro* systems, the immunosuppressive drug FTY720, which blocks T cell egress from the LN, and the integrin blocking, LFA-1 binding antibody, were employed to target distinct aspects of T cell function, namely adhesion and migration, in an attempt to modulate DC-T cell interactions. Chapter 3 describes the design of novel *in vitro* systems for analysis of DC-T cell interactions and outlines the ability of FTY720 and an LFA-1 blocking Ab to reduce stable DC-T cell interactions and to modulate T cell proliferation and differentiation. Next, the impact of FTY720 and the LFA-1 blocking Ab on DC-T cells interactions in the physiological environment of the LN *in vivo*, was assessed by MPLSM. However, the results did not mirror those obtained from the *in vitro* systems and revealed an inability of these molecules to modulate DC-T cell interactions *in vivo* or to alter T cell proliferation and differentiation. Moreover, this contrasting set of results served to emphasise the importance of *in vivo* experimentation. While *in vitro* work offers a cheaper, faster and easier alternative to *in vivo* work, it does not accurately represent the physiological environment of the intact immune system and results are therefore often misleading. In conclusion, chapter 3 did not provide the expected results with respect to the potential use of FTY720 and an LFA-1 blocking Ab as tools to assess and analyse the relative requirement

of DC-T cell interactions at both the tissue site of inflammation and the DLN, in future *in vivo* studies. However, the results presented in chapter 3 provided novel data with respect to the effects of FTY720 on DC-T cell dynamics *in vivo*.

To fully address the relationship between the cellular interactions taking place at a tissue site of inflammation and its DLN, there was a requirement for the investigation to progress to an *in vivo* context in which both locations could be examined in parallel. Chapter 4 shows the first stage in this progression and describes the development of a novel model, in which a LN is transplanted into the murine ear pinna. Analysis of the structural organisation and cellular populations of the tLN by flow cytometry and fluorescence immunohistochemistry revealed that the engraftment procedure was not associated with any major defects or changes to the LN. The capacity of the tLN to form a functional vascular supply to support lymphocyte recirculation in its new anatomical location was evident when lymphocytes from the host mouse were shown to migrate into the tLN. Moreover, the capacity of the tLN to form functional afferent lymphatic vessels capable of draining antigen from its new anatomical location in the ear pinna was clearly shown. Finally, the tLN responded to antigen challenge in a comparable manner to a native LN and preliminary multi-photon imaging studies, revealed similar migration behaviour of lymphocytes in both the control LN and the tLN. It was therefore concluded that the engraftment procedure provided a fully functional LN in an anatomical location that would be accessible to future *in vivo* multi-photon imaging studies, without the need for invasive surgical procedures to expose a native LN.

As outlined in chapter 1, the objective of this thesis was to investigate the relationship between the DC-T cell interactions taking place at a tissue site of inflammation and its DLN. Thus, the next step in these studies was to establish and characterise an imageable site of tissue inflammation in the ear pinna that could be introduced upstream of the LN transplant model. Having both sites in the convenient location of the $\sim 200\mu\text{m}$ thick ear pinna, would permit the cellular interactions taking place at and between each site to be easily accessible to MPLSM, without the need for invasive surgical procedures to expose either site. Chapter 5 therefore outlines the development of a model of tissue inflammation in the ear pinna of the mouse and explores the potential for analysing the site using MPLSM and immunological

assay. The air pouch model was the first technique to be explored. However, while successful in the rump, it was not technically feasible in the ear pinna. The second technique outlined was the DTH reaction and from the preliminary studies carried out, the model appeared successful with respect to establishing an inflammatory site in which DCs and T cells could be visualised *in situ*. Finally, chapter 5 also shows the preliminary studies carried out to develop the use of the fluorescent photo-switchable probe, Kaede, for tracking DC-T cell interactions between the tissue site of inflammation and DLN (364, 365). The Kaede gene was cloned, expressed, purified and conjugated to polystyrene beads to enable DCs to be labelled with the green fluorescent protein. Kaede labelled DCs were imaged *in vitro* and *in vivo* and photo-switched from the green fluorescent form to the red fluorescent form, following a single second UV pulse. Developing a method to label T cells with the Kaede protein would be the next logical step, while the potential for employing Kaede to track DCs in future experiments involving the *in vivo* model systems developed in chapters 4 and 5, has been outlined by the results obtained in chapter 5. However, the goal of employing Kaede in the *in vivo* model systems developed in this thesis was to enable the study of DC and T cell migration and interactions at and between the tissue site of inflammation and DLN. This photoswitchable probe will allow cells of interest to be distinguished from other cells and isolated for analysis. Employing Kaede to label cells in the *in vivo* model systems developed in chapters 4 and 5 in combination with MPLSM of two distinct anatomical locations is a technically challenging goal. To enable both sites to be imaged simultaneously, the microscope would be required to be equipped with two objective lenses. Moreover, if cells are to be tracked and identified as candidates for photo-switching, the microscope would require a dual scan head to allow cells to be imaged and photo-switched at the same time. This technology would allow the fluorescently labelled cells in the focal point to be excited and visualised while an additional wavelength of light is applied, in this case UV, to allow cells of interest to be accurately identified and photo-switched. Thus, applying the use of Kaede to track DCs and/or T cells in the *in vivo* model systems outlined in this thesis would require further development of both the probe for improved labelling of DCs and T cells and the microscope, to facilitate simultaneous imaging of two distinct sites using two distinct wavelengths.

In this thesis, the LN transplant system was developed to facilitate a suitable model in which

the relationship between the tissue site of inflammation and DLN could be investigated. However, this novel model has the potential to be employed in a variety of studies, including lymphatic vessel development (lymphangiogenesis) and T cell imprinting. In the LN transplant model developed in chapter 4, the tLN appeared to develop afferent lymphatic vessels capable of draining the local tissue site in the ear pinna. As outlined in chapter 1, LNs and associated lymphatic vessels develop early in neonatal life and as outlined in chapter 4, several important molecular regulators have been implicated in lymphangiogenesis, including VEGF-C and VEGF-D (398, 399). Understanding how lymphatic vessels grow and respond to biochemical and biophysical cues, is necessary to facilitate the development of therapies for the treatment of lymphoedema, a pathology of insufficient lymphatic transport (400). However, the difficulty in observing this processes during embryonic development and the lack of a suitable model in which to study lymphangiogenesis, has resulted in a poor understanding of the morphological, spatial, and temporal aspects of lymphangiogenesis. The LN transplant model in the ear pinna could potentially provide a site of lymphangiogenesis in the adult mouse in which the development of lymphatic vessels could be manipulated, analysed and directly observed *in vivo* by MPLSM.

Naïve lymphocytes continually re-circulate between the blood and the lymph via the secondary lymphoid organs (20). However, antigen dependent stimulation appears to reprogram the trafficking properties of naive T cells in the periphery, producing memory and effector cells that can specifically traffic to anatomically distinct non-lymphoid sites of tissue inflammation, such as the gastrointestinal tract or the skin (20, 401, 402). This process is known as ‘T cell imprinting’ and lymphocytes activated in the mesenteric LNs (draining lymph from the gut) or peripheral LNs (draining lymph from cutaneous tissues), differentiate and up-regulate adhesion molecules and chemokine receptors that guide their migration back to either the mucosal tissues, such as the small intestine or to the skin, where they can mediate their effects (21, 403, 404). This process is thought to allow tissue specific immune responses to be compartmentalised, such as T cells activated in the gut to acquire a regulatory phenotype to maintain peripheral tolerance and gut homeostasis (20, 405). However, it is not clear how plastic this phenotype is and whether lymphocytes primed to acquire the gut homing phenotype can re-differentiate and migrate to inflamed sites in the skin if required. DCs have been implicated in instructing T cells to acquire a gut homing

phenotype during priming, while the skin homing phenotype has been suggested to be the default (403). However, whether DCs are conditioned in the LN or are a specialised subset is unclear. The LN transplant model could enable some of these unanswered questions to be addressed. The system would provide a method of determining whether gut imprinting is induced by the local environment by allowing a mesenteric LN from the gut to be transplanted into the ear pinna of a congenic mouse strain. Moreover, it would be possible to assess whether the tLN loses its capacity to instruct T cells to acquire a gut homing phenotype and whether T cells primed in the mesenteric LN located within the ear pinna would re-circulate to the gut or to the skin. Thus, the novel LN transplant model developed here will facilitate future multi-photon imaging studies of the relationship between the DC-T cell interactions taking place at the tissue site of inflammation and the DLN, however, the system has the potential to be applied in a variety of other studies, including lymphoid organ development and function.

In conclusion, in this thesis, *in vitro* and *in vivo* model systems were developed to investigate DC-T cell interactions. Moreover, a novel model of LN transplantation was established in the ear pinna, which provides a lymphoid organ, vascular and lymphatic supply in a convenient location for *in vivo* MPLSM. When combined with the imageable site of tissue inflammation developed in chapter 5, the model systems developed in this thesis should allow DC-T cell interactions to be assessed and characterised in both a non-lymphoid tissue site of inflammation and its DLN, by MPLSM. Moreover applying the photo-switchable probe, Kaede, in future imaging studies, should allow cellular migration and cellular interactions to be tracked at, and between, the tissue site of inflammation and the DLN in the ear pinna. Altogether, with some further development, the systems developed in this thesis should allow some of the unanswered questions regarding the relationship between the tissue site of inflammation and DLN to be addressed, including how immune responses are initiated, maintained and regulated at the tissue site of inflammation and what role DC-T cell interactions play in this, both at the tissue site of inflammation or back in the DLN.

References

1. Du Pasquier, L. 1992. Origin and evolution of the vertebrate immune system. *Apmis* 100:383-392.
2. Lanzavecchia, A., and F. Sallusto. 2001. Antigen decoding by T lymphocytes: from synapses to fate determination. *Nat Immunol* 2:487-492.
3. Smith-Garvin, J. E., G. A. Koretzky, and M. S. Jordan. 2009. T cell activation. *Annu Rev Immunol* 27:591-619.
4. Celli, S., F. Lemaitre, and P. Bousso. 2007. Real-time manipulation of T cell-dendritic cell interactions in vivo reveals the importance of prolonged contacts for CD4+ T cell activation. *Immunity* 27:625-634.
5. Germain, R. N., and M. K. Jenkins. 2004. In vivo antigen presentation. *Curr Opin Immunol* 16:120-125.
6. Mempel, T. R., S. E. Henrickson, and U. H. Von Andrian. 2004. T-cell priming by dendritic cells in lymph nodes occurs in three distinct phases. *Nature* 427:154-159.
7. Hugues, S., A. Boissonnas, S. Amigorena, and L. Fetler. 2006. The dynamics of dendritic cell-T cell interactions in priming and tolerance. *Curr Opin Immunol* 18:491-495.
8. Hugues, S., L. Fetler, L. Bonifaz, J. Helft, F. Amblard, and S. Amigorena. 2004. Distinct T cell dynamics in lymph nodes during the induction of tolerance and immunity. *Nat Immunol* 5:1235-1242.
9. Jenkins, M. K., A. Khoruts, E. Ingulli, D. L. Mueller, S. J. McSorley, R. L. Reinhardt, A. Itano, and K. A. Pape. 2001. In vivo activation of antigen-specific CD4 T cells. *Annu Rev Immunol* 19:23-45.
10. Zhang, X., T. Nakajima, J. J. Goronzy, and C. M. Weyand. 2005. Tissue trafficking patterns of effector memory CD4+ T cells in rheumatoid arthritis. *Arthritis Rheum* 52:3839-3849.
11. Henrickson, S. E., and U. H. von Andrian. 2007. Single-cell dynamics of T-cell priming. *Curr Opin Immunol* 19:249-258.
12. Schneider, H., J. Downey, A. Smith, B. H. Zinselmeyer, C. Rush, J. M. Brewer, B. Wei, N. Hogg, P. Garside, and C. E. Rudd. 2006. Reversal of the TCR stop signal by CTLA-4. *Science* 313:1972-1975.
13. Tadokoro, C. E., G. Shakhar, S. Shen, Y. Ding, A. C. Lino, A. Maraver, J. J. Lafaille, and M. L. Dustin. 2006. Regulatory T cells inhibit stable contacts between CD4+ T cells and dendritic cells in vivo. *J Exp Med* 203:505-511.
14. Miller, M. J., O. Safrina, I. Parker, and M. D. Cahalan. 2004. Imaging the single cell dynamics of CD4+ T cell activation by dendritic cells in lymph nodes. *J Exp Med* 200:847-856.
15. Zou, Y., P. Stastny, C. Susal, B. Dohler, and G. Opelz. 2007. Antibodies against MICA antigens and kidney-transplant rejection. *N Engl J Med* 357:1293-1300.
16. Strid, J., R. E. Tigelaar, and A. C. Hayday. 2009. Skin immune surveillance by T cells--a new order? *Semin Immunol* 21:110-120.
17. Strid, J., S. J. Roberts, R. B. Filler, J. M. Lewis, B. Y. Kwong, W. Schpero, D. H. Kaplan, A. C. Hayday, and M. Girardi. 2008. Acute upregulation of an NKG2D ligand promotes rapid reorganization of a local immune compartment with pleiotropic effects on carcinogenesis. *Nat Immunol* 9:146-154.

18. Wakim, L. M., J. Waithman, N. van Rooijen, W. R. Heath, and F. R. Carbone. 2008. Dendritic cell-induced memory T cell activation in nonlymphoid tissues. *Science* 319:198-202.
19. Sallusto, F., J. Geginat, and A. Lanzavecchia. 2004. Central memory and effector memory T cell subsets: function, generation, and maintenance. *Annu Rev Immunol* 22:745-763.
20. Kunkel, E. J., and E. C. Butcher. 2002. Chemokines and the tissue-specific migration of lymphocytes. *Immunity* 16:1-4.
21. Campbell, D. J., and E. C. Butcher. 2002. Rapid acquisition of tissue-specific homing phenotypes by CD4(+) T cells activated in cutaneous or mucosal lymphoid tissues. *J Exp Med* 195:135-141.
22. Romani, N., S. Holzmann, C. H. Tripp, F. Koch, and P. Stoitzner. 2003. Langerhans cells - dendritic cells of the epidermis. *Apmsis* 111:725-740.
23. Merad, M., and M. G. Manz. 2009. Dendritic cell homeostasis. *Blood* 113:3418-3427.
24. Banchereau, J., and R. M. Steinman. 1998. Dendritic cells and the control of immunity. *Nature* 392:245-252.
25. Janeway, C. A., Jr., and R. Medzhitov. 2002. Innate immune recognition. *Annu Rev Immunol* 20:197-216.
26. Pancer, Z., and M. D. Cooper. 2006. The evolution of adaptive immunity. *Annu Rev Immunol* 24:497-518.
27. Zinkernagel, R. M., M. F. Bachmann, T. M. Kundig, S. Oehen, H. Pirchet, and H. Hengartner. 1996. On immunological memory. *Annu Rev Immunol* 14:333-367.
28. Sakaguchi, S., M. Ono, R. Setoguchi, H. Yagi, S. Hori, Z. Fehervari, J. Shimizu, T. Takahashi, and T. Nomura. 2006. Foxp3⁺ CD25⁺ CD4⁺ natural regulatory T cells in dominant self-tolerance and autoimmune disease. *Immunol Rev* 212:8-27.
29. Zhu, J., and W. E. Paul. 2008. CD4 T cells: fates, functions, and faults. *Blood* 112:1557-1569.
30. Bevan, M. J. 1977. In a radiation chimaera, host H-2 antigens determine immune responsiveness of donor cytotoxic cells. *Nature* 269:417-418.
31. Rudolph, M. G., R. L. Stanfield, and I. A. Wilson. 2006. How TCRs bind MHCs, peptides, and coreceptors. *Annu Rev Immunol* 24:419-466.
32. Saito, T., and R. N. Germain. 1988. The generation and selection of the T cell repertoire: insights from studies of the molecular basis of T cell recognition. *Immunol Rev* 101:81-113.
33. Davis, M. M., Y. H. Chien, N. R. Gascoigne, and S. M. Hedrick. 1984. A murine T cell receptor gene complex: isolation, structure and rearrangement. *Immunol Rev* 81:235-258.
34. Zuniga-Pflucker, J. C. 2004. T-cell development made simple. *Nat Rev Immunol* 4:67-72.
35. Jameson, S. C., K. A. Hogquist, and M. J. Bevan. 1995. Positive selection of thymocytes. *Annu Rev Immunol* 13:93-126.
36. Sebзда, E., V. A. Wallace, J. Mayer, R. S. Yeung, T. W. Mak, and P. S. Ohashi. 1994. Positive and negative thymocyte selection induced by different concentrations of a single peptide. *Science* 263:1615-1618.
37. Carding, S. R., and P. J. Egan. 2002. Gammadelta T cells: functional plasticity and heterogeneity. *Nat Rev Immunol* 2:336-345.

38. Konig, R., L. Y. Huang, and R. N. Germain. 1992. MHC class II interaction with CD4 mediated by a region analogous to the MHC class I binding site for CD8. *Nature* 356:796-798.
39. Andersen, M. H., D. Schrama, P. Thor Straten, and J. C. Becker. 2006. Cytotoxic T cells. *J Invest Dermatol* 126:32-41.
40. Suzuki, Y., M. A. Orellana, R. D. Schreiber, and J. S. Remington. 1988. Interferon-gamma: the major mediator of resistance against *Toxoplasma gondii*. *Science* 240:516-518.
41. Fazilleau, N., L. Mark, L. J. McHeyzer-Williams, and M. G. McHeyzer-Williams. 2009. Follicular helper T cells: lineage and location. *Immunity* 30:324-335.
42. Shedlock, D. J., and H. Shen. 2003. Requirement for CD4 T cell help in generating functional CD8 T cell memory. *Science* 300:337-339.
43. Ahmed, R., L. D. Butler, and L. Bhatti. 1988. T4+ T helper cell function in vivo: differential requirement for induction of antiviral cytotoxic T-cell and antibody responses. *J Virol* 62:2102-2106.
44. von Andrian, U. H., and T. R. Mempel. 2003. Homing and cellular traffic in lymph nodes. *Nat Rev Immunol* 3:867-878.
45. Davis, M. M., and P. J. Bjorkman. 1988. T-cell antigen receptor genes and T-cell recognition. *Nature* 334:395-402.
46. Petrie, H. T., F. Livak, D. G. Schatz, A. Strasser, I. N. Crispe, and K. Shortman. 1993. Multiple rearrangements in T cell receptor alpha chain genes maximize the production of useful thymocytes. *J Exp Med* 178:615-622.
47. Lefrancois, L., and D. Masopust. 2002. T cell immunity in lymphoid and non-lymphoid tissues. *Curr Opin Immunol* 14:503-508.
48. Butcher, E. C., M. Williams, K. Youngman, L. Rott, and M. Briskin. 1999. Lymphocyte trafficking and regional immunity. *Adv Immunol* 72:209-253.
49. Saady, J. J., and A. Poklis. 1989. Determination of atropine in blood by gas chromatography/mass spectrometry. *J Anal Toxicol* 13:296-299.
50. Leon, B., M. Lopez-Bravo, and C. Ardavin. 2007. Monocyte-derived dendritic cells formed at the infection site control the induction of protective T helper 1 responses against *Leishmania*. *Immunity* 26:519-531.
51. Woodland, D. L., and J. E. Kohlmeier. 2009. Migration, maintenance and recall of memory T cells in peripheral tissues. *Nat Rev Immunol* 9:153-161.
52. Masopust, D., V. Vezys, E. J. Usherwood, L. S. Cauley, S. Olson, A. L. Marzo, R. L. Ward, D. L. Woodland, and L. Lefrancois. 2004. Activated primary and memory CD8 T cells migrate to nonlymphoid tissues regardless of site of activation or tissue of origin. *J Immunol* 172:4875-4882.
53. Wakim, L. M., T. Gebhardt, W. R. Heath, and F. R. Carbone. 2008. Cutting edge: local recall responses by memory T cells newly recruited to peripheral nonlymphoid tissues. *J Immunol* 181:5837-5841.
54. Wang, D., J. A. Hill, A. M. Jevnikar, E. Cairns, and D. A. Bell. 2002. Induction of transient arthritis by the adoptive transfer of a collagen II specific Th1 clone to HLA-DR4 (B1*0401) transgenic mice. *J Autoimmun* 19:37-43.
55. Brinkmann, V. 2004. FTY720: mechanism of action and potential benefit in organ transplantation. *Yonsei Med J* 45:991-997.
56. Dragun, D., L. Fritsche, T. Boehler, H. Peters, K. Budde, and H. H. Neumayer. 2004. FTY720: early clinical experience. *Transplant Proc* 36:544S-548S.

57. Wang, F., W. Tan, D. Guo, and S. He. 2007. Reduction of CD4 positive T cells and improvement of pathological changes of collagen-induced arthritis by FTY720. *Eur J Pharmacol* 573:230-240.
58. Futterer, A., K. Mink, A. Luz, M. H. Kosco-Vilbois, and K. Pfeffer. 1998. The lymphotoxin beta receptor controls organogenesis and affinity maturation in peripheral lymphoid tissues. *Immunity* 9:59-70.
59. Luther, S. A., K. M. Ansel, and J. G. Cyster. 2003. Overlapping roles of CXCL13, interleukin 7 receptor alpha, and CCR7 ligands in lymph node development. *J Exp Med* 197:1191-1198.
60. Luther, S. A., H. L. Tang, P. L. Hyman, A. G. Farr, and J. G. Cyster. 2000. Coexpression of the chemokines ELC and SLC by T zone stromal cells and deletion of the ELC gene in the plt/plt mouse. *Proc Natl Acad Sci U S A* 97:12694-12699.
61. Lehmann, J. C., D. Jablonski-Westrich, U. Haubold, J. C. Gutierrez-Ramos, T. Springer, and A. Hamann. 2003. Overlapping and selective roles of endothelial intercellular adhesion molecule-1 (ICAM-1) and ICAM-2 in lymphocyte trafficking. *J Immunol* 171:2588-2593.
62. Brinkmann, V., J. G. Cyster, and T. Hla. 2004. FTY720: sphingosine 1-phosphate receptor-1 in the control of lymphocyte egress and endothelial barrier function. *Am J Transplant* 4:1019-1025.
63. Mann, J. D., and G. M. Higgins. 1950. Lymphocytes in thoracic duct intestinal and hepatic lymph. *Blood* 5:177-190.
64. Gesner, B. M., and J. L. Gowans. 1962. The output of lymphocytes from the thoracic duct of unanaesthetized mice. *Br J Exp Pathol* 43:424-430.
65. Gowans, J. L., and E. J. Knight. 1964. The Route of Re-Circulation of Lymphocytes in the Rat. *Proc R Soc Lond B Biol Sci* 159:257-282.
66. Kaldjian, E. P., J. E. Gretz, A. O. Anderson, Y. Shi, and S. Shaw. 2001. Spatial and molecular organization of lymph node T cell cortex: a labyrinthine cavity bounded by an epithelium-like monolayer of fibroblastic reticular cells anchored to basement membrane-like extracellular matrix. *Int Immunol* 13:1243-1253.
67. Gretz, J. E., C. C. Norbury, A. O. Anderson, A. E. Proudfoot, and S. Shaw. 2000. Lymph-borne chemokines and other low molecular weight molecules reach high endothelial venules via specialized conduits while a functional barrier limits access to the lymphocyte microenvironments in lymph node cortex. *J Exp Med* 192:1425-1440.
68. Gretz, J. E., A. O. Anderson, and S. Shaw. 1997. Cords, channels, corridors and conduits: critical architectural elements facilitating cell interactions in the lymph node cortex. *Immunol Rev* 156:11-24.
69. Gretz, J. E., E. P. Kaldjian, A. O. Anderson, and S. Shaw. 1996. Sophisticated strategies for information encounter in the lymph node: the reticular network as a conduit of soluble information and a highway for cell traffic. *J Immunol* 157:495-499.
70. Phan, T. G., J. A. Green, E. E. Gray, Y. Xu, and J. G. Cyster. 2009. Immune complex relay by subcapsular sinus macrophages and noncognate B cells drives antibody affinity maturation. *Nat Immunol* 10:786-793.
71. Phan, T. G., I. Grigorova, T. Okada, and J. G. Cyster. 2007. Subcapsular encounter and complement-dependent transport of immune complexes by lymph node B cells. *Nat Immunol* 8:992-1000.
72. Junt, T., E. A. Moseman, M. Iannaccone, S. Massberg, P. A. Lang, M. Boes, K. Fink, S. E. Henrickson, D. M. Shayakhmetov, N. C. Di Paolo, N. van Rooijen, T. R. Mempel, S. P. Whelan, and U. H. von Andrian. 2007. Subcapsular sinus

- macrophages in lymph nodes clear lymph-borne viruses and present them to antiviral B cells. *Nature* 450:110-114.
73. Tew, J. G., J. Wu, D. Qin, S. Helm, G. F. Burton, and A. K. Szakal. 1997. Follicular dendritic cells and presentation of antigen and costimulatory signals to B cells. *Immunol Rev* 156:39-52.
 74. Klaus, G. G., J. H. Humphrey, A. Kunkl, and D. W. Dongworth. 1980. The follicular dendritic cell: its role in antigen presentation in the generation of immunological memory. *Immunol Rev* 53:3-28.
 75. Cyster, J. G., K. M. Ansel, K. Reif, E. H. Ekland, P. L. Hyman, H. L. Tang, S. A. Luther, and V. N. Ngo. 2000. Follicular stromal cells and lymphocyte homing to follicles. *Immunol Rev* 176:181-193.
 76. Rennert, P. D., J. L. Browning, R. Mebius, F. Mackay, and P. S. Hochman. 1996. Surface lymphotoxin alpha/beta complex is required for the development of peripheral lymphoid organs. *J Exp Med* 184:1999-2006.
 77. Mackay, F., G. R. Majeau, P. Lawton, P. S. Hochman, and J. L. Browning. 1997. Lymphotoxin but not tumor necrosis factor functions to maintain splenic architecture and humoral responsiveness in adult mice. *Eur J Immunol* 27:2033-2042.
 78. Fu, Y. X., G. Huang, M. Matsumoto, H. Molina, and D. D. Chaplin. 1997. Independent signals regulate development of primary and secondary follicle structure in spleen and mesenteric lymph node. *Proc Natl Acad Sci U S A* 94:5739-5743.
 79. Link, A., T. K. Vogt, S. Favre, M. R. Britschgi, H. Acha-Orbea, B. Hinz, J. G. Cyster, and S. A. Luther. 2007. Fibroblastic reticular cells in lymph nodes regulate the homeostasis of naive T cells. *Nat Immunol* 8:1255-1265.
 80. Ngo, V. N., H. Korner, M. D. Gunn, K. N. Schmidt, D. S. Riminton, M. D. Cooper, J. L. Browning, J. D. Sedgwick, and J. G. Cyster. 1999. Lymphotoxin alpha/beta and tumor necrosis factor are required for stromal cell expression of homing chemokines in B and T cell areas of the spleen. *J Exp Med* 189:403-412.
 81. Tykocinski, M., R. A. Schinella, and M. A. Greco. 1983. Fibroblastic reticulum cells in human lymph nodes. An ultrastructural study. *Arch Pathol Lab Med* 107:418-422.
 82. Clark, S. L., Jr. 1962. The reticulum of lymph nodes in mice studied with the electron microscope. *Am J Anat* 110:217-257.
 83. Anderson, A. O., and N. D. Anderson. 1975. Studies on the structure and permeability of the microvasculature in normal rat lymph nodes. *Am J Pathol* 80:387-418.
 84. Bairati, A., L. Amante, S. Depetris, and B. Pernis. 1964. Studies on the Ultrastructure of the Lymph Nodes. I. the Reticular Network. *Z Zellforsch Mikrosk Anat* 63:644-672.
 85. Bajenoff, M., J. G. Egen, L. Y. Koo, J. P. Laugier, F. Brau, N. Glaichenhaus, and R. N. Germain. 2006. Stromal cell networks regulate lymphocyte entry, migration, and territoriality in lymph nodes. *Immunity* 25:989-1001.
 86. Anderson, A. O., and S. Shaw. 1993. T cell adhesion to endothelium: the FRC conduit system and other anatomic and molecular features which facilitate the adhesion cascade in lymph node. *Semin Immunol* 5:271-282.
 87. Sixt, M., N. Kanazawa, M. Selg, T. Samson, G. Roos, D. P. Reinhardt, R. Pabst, M. B. Lutz, and L. Sorokin. 2005. The conduit system transports soluble antigens from the afferent lymph to resident dendritic cells in the T cell area of the lymph node. *Immunity* 22:19-29.
 88. Anderson, A. O., and S. Shaw. 2005. Conduit for privileged communications in the lymph node. *Immunity* 22:3-5.

89. Farr, A. G., M. L. Berry, A. Kim, A. J. Nelson, M. P. Welch, and A. Aruffo. 1992. Characterization and cloning of a novel glycoprotein expressed by stromal cells in T-dependent areas of peripheral lymphoid tissues. *J Exp Med* 176:1477-1482.
90. Suzuki, K., I. Grigorova, T. G. Phan, L. M. Kelly, and J. G. Cyster. 2009. Visualizing B cell capture of cognate antigen from follicular dendritic cells. *J Exp Med* 206:1485-1493.
91. Liu, Y. J., G. Grouard, O. de Bouteiller, and J. Banchereau. 1996. Follicular dendritic cells and germinal centers. *Int Rev Cytol* 166:139-179.
92. Legler, D. F., M. Loetscher, R. S. Roos, I. Clark-Lewis, M. Baggiolini, and B. Moser. 1998. B cell-attracting chemokine 1, a human CXC chemokine expressed in lymphoid tissues, selectively attracts B lymphocytes via BLR1/CXCR5. *J Exp Med* 187:655-660.
93. Anderson, A. O., and N. D. Anderson. 1976. Lymphocyte emigration from high endothelial venules in rat lymph nodes. *Immunology* 31:731-748.
94. Carragher, D., R. Johal, A. Button, A. White, A. Eliopoulos, E. Jenkinson, G. Anderson, and J. Caamano. 2004. A stroma-derived defect in NF-kappaB2-/- mice causes impaired lymph node development and lymphocyte recruitment. *J Immunol* 173:2271-2279.
95. Katakai, T., T. Hara, J. H. Lee, H. Gonda, M. Sugai, and A. Shimizu. 2004. A novel reticular stromal structure in lymph node cortex: an immuno-platform for interactions among dendritic cells, T cells and B cells. *Int Immunol* 16:1133-1142.
96. Cueni, L. N., and M. Detmar. 2008. The lymphatic system in health and disease. *Lymphat Res Biol* 6:109-122.
97. Lane, P. J., F. M. Gaspal, and M. Y. Kim. 2005. Two sides of a cellular coin: CD4(+)/CD3- cells regulate memory responses and lymph-node organization. *Nat Rev Immunol* 5:655-660.
98. Mueller, S. N., and R. N. Germain. 2009. Stromal cell contributions to the homeostasis and functionality of the immune system. *Nat Rev Immunol* 9:618-629.
99. Wigle, J. T., N. Harvey, M. Detmar, I. Lagutina, G. Grosveld, M. D. Gunn, D. G. Jackson, and G. Oliver. 2002. An essential role for Prox1 in the induction of the lymphatic endothelial cell phenotype. *Embo J* 21:1505-1513.
100. Wigle, J. T., and G. Oliver. 1999. Prox1 function is required for the development of the murine lymphatic system. *Cell* 98:769-778.
101. Oliver, G. 2004. Lymphatic vasculature development. *Nat Rev Immunol* 4:35-45.
102. Hong, Y. K., N. Harvey, Y. H. Noh, V. Schacht, S. Hirakawa, M. Detmar, and G. Oliver. 2002. Prox1 is a master control gene in the program specifying lymphatic endothelial cell fate. *Dev Dyn* 225:351-357.
103. Mebius, R. E., P. Rennert, and I. L. Weissman. 1997. Developing lymph nodes collect CD4+CD3- LTbeta+ cells that can differentiate to APC, NK cells, and follicular cells but not T or B cells. *Immunity* 7:493-504.
104. Ansel, K. M., V. N. Ngo, P. L. Hyman, S. A. Luther, R. Forster, J. D. Sedgwick, J. L. Browning, M. Lipp, and J. G. Cyster. 2000. A chemokine-driven positive feedback loop organizes lymphoid follicles. *Nature* 406:309-314.
105. Dejardin, E., N. M. Droin, M. Delhase, E. Haas, Y. Cao, C. Makris, Z. W. Li, M. Karin, C. F. Ware, and D. R. Green. 2002. The lymphotoxin-beta receptor induces different patterns of gene expression via two NF-kappaB pathways. *Immunity* 17:525-535.

106. Degli-Esposti, M. A., and M. J. Smyth. 2005. Close encounters of different kinds: dendritic cells and NK cells take centre stage. *Nat Rev Immunol* 5:112-124.
107. Sozzani, S., P. Allavena, G. D'Amico, W. Luini, G. Bianchi, M. Kataura, T. Imai, O. Yoshie, R. Bonecchi, and A. Mantovani. 1998. Differential regulation of chemokine receptors during dendritic cell maturation: a model for their trafficking properties. *J Immunol* 161:1083-1086.
108. Sallusto, F., P. Schaerli, P. Loetscher, C. Schaniel, D. Lenig, C. R. Mackay, S. Qin, and A. Lanzavecchia. 1998. Rapid and coordinated switch in chemokine receptor expression during dendritic cell maturation. *Eur J Immunol* 28:2760-2769.
109. Mellman, I., and R. M. Steinman. 2001. Dendritic cells: specialized and regulated antigen processing machines. *Cell* 106:255-258.
110. C, R. e. S. 2001. Dendritic cells as sensors of infection. *Immunity* 14:495-498.
111. Takeuchi, O., and S. Akira. 2002. Genetic approaches to the study of Toll-like receptor function. *Microbes Infect* 4:887-895.
112. Qureshi, S. T., L. Lariviere, G. Leveque, S. Clermont, K. J. Moore, P. Gros, and D. Malo. 1999. Endotoxin-tolerant mice have mutations in Toll-like receptor 4 (Tlr4). *J Exp Med* 189:615-625.
113. Doyle, S. E., R. O'Connell, S. A. Vaidya, E. K. Chow, K. Yee, and G. Cheng. 2003. Toll-like receptor 3 mediates a more potent antiviral response than Toll-like receptor 4. *J Immunol* 170:3565-3571.
114. Steinman, R. M. 2001. Dendritic cells and the control of immunity: enhancing the efficiency of antigen presentation. *Mt Sinai J Med* 68:160-166.
115. Lanzavecchia, A., and F. Sallusto. 2001. Regulation of T cell immunity by dendritic cells. *Cell* 106:263-266.
116. Steinman, R. M., and Z. A. Cohn. 1973. Identification of a novel cell type in peripheral lymphoid organs of mice. I. Morphology, quantitation, tissue distribution. *J Exp Med* 137:1142-1162.
117. Steinman, R. M., B. Gutchinov, M. D. Witmer, and M. C. Nussenzweig. 1983. Dendritic cells are the principal stimulators of the primary mixed leukocyte reaction in mice. *J Exp Med* 157:613-627.
118. Saito, M., T. Iwawaki, C. Taya, H. Yonekawa, M. Noda, Y. Inui, E. Mekada, Y. Kimata, A. Tsuru, and K. Kohno. 2001. Diphtheria toxin receptor-mediated conditional and targeted cell ablation in transgenic mice. *Nat Biotechnol* 19:746-750.
119. Jung, S., D. Unutmaz, P. Wong, G. Sano, K. De los Santos, T. Sparwasser, S. Wu, S. Vuthoori, K. Ko, F. Zavala, E. G. Pamer, D. R. Littman, and R. A. Lang. 2002. In vivo depletion of CD11c(+) dendritic cells abrogates priming of CD8(+) T cells by exogenous cell-associated antigens. *Immunity* 17:211-220.
120. Zammit, D. J., L. S. Cauley, Q. M. Pham, and L. Lefrancois. 2005. Dendritic cells maximize the memory CD8 T cell response to infection. *Immunity* 22:561-570.
121. van Rijt, L. S., S. Jung, A. Kleinjan, N. Vos, M. Willart, C. Duez, H. C. Hoogsteden, and B. N. Lambrecht. 2005. In vivo depletion of lung CD11c+ dendritic cells during allergen challenge abrogates the characteristic features of asthma. *J Exp Med* 201:981-991.
122. Tian, T., J. Woodworth, M. Skold, and S. M. Behar. 2005. In vivo depletion of CD11c+ cells delays the CD4+ T cell response to Mycobacterium tuberculosis and exacerbates the outcome of infection. *J Immunol* 175:3268-3272.
123. Scumpia, P. O., P. F. McAuliffe, K. A. O'Malley, R. Ungaro, T. Uchida, T. Matsumoto, D. G. Remick, M. J. Clare-Salzler, L. L. Moldawer, and P. A. Efron.

2005. CD11c+ dendritic cells are required for survival in murine polymicrobial sepsis. *J Immunol* 175:3282-3286.
124. Probst, H. C., K. McCoy, T. Okazaki, T. Honjo, and M. van den Broek. 2005. Resting dendritic cells induce peripheral CD8+ T cell tolerance through PD-1 and CTLA-4. *Nat Immunol* 6:280-286.
125. Lahoud, M. H., A. I. Proietto, F. Ahmet, S. Kitsoulis, L. Eidsmo, L. Wu, P. Sathe, S. Pietersz, H. W. Chang, I. D. Walker, E. Maraskovsky, H. Braley, A. M. Lew, M. D. Wright, W. R. Heath, K. Shortman, and I. Caminschi. 2009. The C-type lectin Clec12A present on mouse and human dendritic cells can serve as a target for antigen delivery and enhancement of antibody responses. *J Immunol* 182:7587-7594.
126. Kassim, S. H., N. K. Rajasagi, X. Zhao, R. Chervenak, and S. R. Jennings. 2006. In vivo ablation of CD11c-positive dendritic cells increases susceptibility to herpes simplex virus type 1 infection and diminishes NK and T-cell responses. *J Virol* 80:3985-3993.
127. deWalick, S., F. H. Amante, K. A. McSweeney, L. M. Randall, A. C. Stanley, A. Haque, R. D. Kuns, K. P. MacDonald, G. R. Hill, and C. R. Engwerda. 2007. Cutting edge: conventional dendritic cells are the critical APC required for the induction of experimental cerebral malaria. *J Immunol* 178:6033-6037.
128. Heath, W. R., and F. R. Carbone. 2009. Dendritic cell subsets in primary and secondary T cell responses at body surfaces. *Nat Immunol* 10:1237-1244.
129. Jongbloed, S. L., R. A. Benson, M. B. Nickdel, P. Garside, I. B. McInnes, and J. M. Brewer. 2009. Plasmacytoid dendritic cells regulate breach of self-tolerance in autoimmune arthritis. *J Immunol* 182:963-968.
130. Cella, M., D. Jarrossay, F. Facchetti, O. Alebardi, H. Nakajima, A. Lanzavecchia, and M. Colonna. 1999. Plasmacytoid monocytes migrate to inflamed lymph nodes and produce large amounts of type I interferon. *Nat Med* 5:919-923.
131. Asselin-Paturel, C., A. Boonstra, M. Dalod, I. Durand, N. Yessaad, C. Dezutter-Dambuyant, A. Vicari, A. O'Garra, C. Biron, F. Briere, and G. Trinchieri. 2001. Mouse type I IFN-producing cells are immature APCs with plasmacytoid morphology. *Nat Immunol* 2:1144-1150.
132. den Haan, J. M., and M. J. Bevan. 2001. Antigen presentation to CD8+ T cells: cross-priming in infectious diseases. *Curr Opin Immunol* 13:437-441.
133. Belz, G. T., F. R. Carbone, and W. R. Heath. 2002. Cross-presentation of antigens by dendritic cells. *Crit Rev Immunol* 22:439-448.
134. Iwasaki, A. 2003. The importance of CD11b+ dendritic cells in CD4+ T cell activation in vivo: with help from interleukin 1. *J Exp Med* 198:185-190.
135. Malissen, B. 2008. CD3 ITAMs count! *Nat Immunol* 9:583-584.
136. Rojo, J. M., R. Bello, and P. Portoles. 2008. T-cell receptor. *Adv Exp Med Biol* 640:1-11.
137. Jenkins, M. K., and R. H. Schwartz. 1987. Antigen presentation by chemically modified splenocytes induces antigen-specific T cell unresponsiveness in vitro and in vivo. *J Exp Med* 165:302-319.
138. Jenkins, M. K., D. M. Pardoll, J. Mizuguchi, H. Quill, and R. H. Schwartz. 1987. T-cell unresponsiveness in vivo and in vitro: fine specificity of induction and molecular characterization of the unresponsive state. *Immunol Rev* 95:113-135.
139. Grewal, I. S., and R. A. Flavell. 1996. A central role of CD40 ligand in the regulation of CD4+ T-cell responses. *Immunol Today* 17:410-414.

140. Linsley, P. S., and J. A. Ledbetter. 1993. The role of the CD28 receptor during T cell responses to antigen. *Annu Rev Immunol* 11:191-212.
141. Shahinian, A., K. Pfeffer, K. P. Lee, T. M. Kundig, K. Kishihara, A. Wakeham, K. Kawai, P. S. Ohashi, C. B. Thompson, and T. W. Mak. 1993. Differential T cell costimulatory requirements in CD28-deficient mice. *Science* 261:609-612.
142. Watts, T. H. 2005. TNF/TNFR family members in costimulation of T cell responses. *Annu Rev Immunol* 23:23-68.
143. Cella, M., D. Scheidegger, K. Palmer-Lehmann, P. Lane, A. Lanzavecchia, and G. Alber. 1996. Ligation of CD40 on dendritic cells triggers production of high levels of interleukin-12 and enhances T cell stimulatory capacity: T-T help via APC activation. *J Exp Med* 184:747-752.
144. Abbas, A. K., K. M. Murphy, and A. Sher. 1996. Functional diversity of helper T lymphocytes. *Nature* 383:787-793.
145. Mosmann, T. R., H. Cherwinski, M. W. Bond, M. A. Giedlin, and R. L. Coffman. 2005. Two types of murine helper T cell clone. I. Definition according to profiles of lymphokine activities and secreted proteins. 1986. *J Immunol* 175:5-14.
146. Mosmann, T. R., H. Cherwinski, M. W. Bond, M. A. Giedlin, and R. L. Coffman. 1986. Two types of murine helper T cell clone. I. Definition according to profiles of lymphokine activities and secreted proteins. *J Immunol* 136:2348-2357.
147. Romagnani, S. 1994. Lymphokine production by human T cells in disease states. *Annu Rev Immunol* 12:227-257.
148. O'Garra, A., and D. Robinson. 2004. Development and function of T helper 1 cells. *Adv Immunol* 83:133-162.
149. Murphy, K. M., and S. L. Reiner. 2002. The lineage decisions of helper T cells. *Nat Rev Immunol* 2:933-944.
150. Szabo, S. J., S. T. Kim, G. L. Costa, X. Zhang, C. G. Fathman, and L. H. Glimcher. 2000. A novel transcription factor, T-bet, directs Th1 lineage commitment. *Cell* 100:655-669.
151. Lighvani, A. A., D. M. Frucht, D. Jankovic, H. Yamane, J. Aliberti, B. D. Hissong, B. V. Nguyen, M. Gadina, A. Sher, W. E. Paul, and J. J. O'Shea. 2001. T-bet is rapidly induced by interferon-gamma in lymphoid and myeloid cells. *Proc Natl Acad Sci U S A* 98:15137-15142.
152. Kaplan, M. H., Y. L. Sun, T. Hoey, and M. J. Grusby. 1996. Impaired IL-12 responses and enhanced development of Th2 cells in Stat4-deficient mice. *Nature* 382:174-177.
153. Zhu, J., L. Guo, C. J. Watson, J. Hu-Li, and W. E. Paul. 2001. Stat6 is necessary and sufficient for IL-4's role in Th2 differentiation and cell expansion. *J Immunol* 166:7276-7281.
154. Shimoda, K., J. van Deursen, M. Y. Sangster, S. R. Sarawar, R. T. Carson, R. A. Tripp, C. Chu, F. W. Quelle, T. Nosaka, D. A. Vignali, P. C. Doherty, G. Grosveld, W. E. Paul, and J. N. Ihle. 1996. Lack of IL-4-induced Th2 response and IgE class switching in mice with disrupted Stat6 gene. *Nature* 380:630-633.
155. Park, H., Z. Li, X. O. Yang, S. H. Chang, R. Nurieva, Y. H. Wang, Y. Wang, L. Hood, Z. Zhu, Q. Tian, and C. Dong. 2005. A distinct lineage of CD4 T cells regulates tissue inflammation by producing interleukin 17. *Nat Immunol* 6:1133-1141.
156. Harrington, L. E., R. D. Hatton, P. R. Mangan, H. Turner, T. L. Murphy, K. M. Murphy, and C. T. Weaver. 2005. Interleukin 17-producing CD4+ effector T cells

- develop via a lineage distinct from the T helper type 1 and 2 lineages. *Nat Immunol* 6:1123-1132.
157. Weaver, C. T., L. E. Harrington, P. R. Mangan, M. Gavrieli, and K. M. Murphy. 2006. Th17: an effector CD4 T cell lineage with regulatory T cell ties. *Immunity* 24:677-688.
 158. Dong, C. 2009. Differentiation and function of pro-inflammatory Th17 cells. *Microbes Infect* 11:584-588.
 159. Stockinger, B., and M. Veldhoen. 2007. Differentiation and function of Th17 T cells. *Curr Opin Immunol* 19:281-286.
 160. Garside, P., E. Ingulli, R. R. Merica, J. G. Johnson, R. J. Noelle, and M. K. Jenkins. 1998. Visualization of specific B and T lymphocyte interactions in the lymph node. *Science* 281:96-99.
 161. Banchereau, J., F. Bazan, D. Blanchard, F. Briere, J. P. Galizzi, C. van Kooten, Y. J. Liu, F. Rousset, and S. Saeland. 1994. The CD40 antigen and its ligand. *Annu Rev Immunol* 12:881-922.
 162. Kelsoe, G. 1995. The germinal center reaction. *Immunol Today* 16:324-326.
 163. Liu, Y. J., F. Malisan, O. de Bouteiller, C. Guret, S. Lebecque, J. Banchereau, F. C. Mills, E. E. Max, and H. Martinez-Valdez. 1996. Within germinal centers, isotype switching of immunoglobulin genes occurs after the onset of somatic mutation. *Immunity* 4:241-250.
 164. Smith, K. M., L. Pottage, E. R. Thomas, A. J. Leishman, T. N. Doig, D. Xu, F. Y. Liew, and P. Garside. 2000. Th1 and Th2 CD4+ T cells provide help for B cell clonal expansion and antibody synthesis in a similar manner in vivo. *J Immunol* 165:3136-3144.
 165. Nurieva, R. I., Y. Chung, D. Hwang, X. O. Yang, H. S. Kang, L. Ma, Y. H. Wang, S. S. Watowich, A. M. Jetten, Q. Tian, and C. Dong. 2008. Generation of T follicular helper cells is mediated by interleukin-21 but independent of T helper 1, 2, or 17 cell lineages. *Immunity* 29:138-149.
 166. Spolski, R., and W. J. Leonard. 2008. Interleukin-21: basic biology and implications for cancer and autoimmunity. *Annu Rev Immunol* 26:57-79.
 167. Vinuesa, C. G., S. G. Tangye, B. Moser, and C. R. Mackay. 2005. Follicular B helper T cells in antibody responses and autoimmunity. *Nat Rev Immunol* 5:853-865.
 168. Benacerraf, B., and R. N. Germain. 1981. A single major pathway of T-lymphocyte interactions in antigen-specific immune suppression. *Scand J Immunol* 13:1-10.
 169. Miyara, M., and S. Sakaguchi. 2007. Natural regulatory T cells: mechanisms of suppression. *Trends Mol Med* 13:108-116.
 170. Sakaguchi, S. 2004. Naturally arising CD4+ regulatory t cells for immunologic self-tolerance and negative control of immune responses. *Annu Rev Immunol* 22:531-562.
 171. Sakaguchi, S. 2005. Naturally arising Foxp3-expressing CD25+CD4+ regulatory T cells in immunological tolerance to self and non-self. *Nat Immunol* 6:345-352.
 172. Groux, H., A. O'Garra, M. Bigler, M. Rouleau, S. Antonenko, J. E. de Vries, and M. G. Roncarolo. 1997. A CD4+ T-cell subset inhibits antigen-specific T-cell responses and prevents colitis. *Nature* 389:737-742.
 173. Bacchetta, R., S. Gregori, and M. G. Roncarolo. 2005. CD4+ regulatory T cells: mechanisms of induction and effector function. *Autoimmun Rev* 4:491-496.
 174. Levings, M. K., S. Gregori, E. Tresoldi, S. Cazzaniga, C. Bonini, and M. G. Roncarolo. 2005. Differentiation of Tr1 cells by immature dendritic cells requires IL-10 but not CD25+CD4+ Tr cells. *Blood* 105:1162-1169.

175. Tse, H. Y., R. H. Schwartz, and W. E. Paul. 1980. Cell-cell interactions in the T cell proliferative response. I. Analysis of the cell types involved and evidence for nonspecific T cell recruitment. *J Immunol* 125:491-500.
176. Kearney, E. R., K. A. Pape, D. Y. Loh, and M. K. Jenkins. 1994. Visualization of peptide-specific T cell immunity and peripheral tolerance induction in vivo. *Immunity* 1:327-339.
177. Kyburz, D., P. Aichele, D. E. Speiser, H. Hengartner, R. M. Zinkernagel, and H. Pircher. 1993. T cell immunity after a viral infection versus T cell tolerance induced by soluble viral peptides. *Eur J Immunol* 23:1956-1962.
178. Cahalan, M. D., I. Parker, S. H. Wei, and M. J. Miller. 2003. Real-time imaging of lymphocytes in vivo. *Curr Opin Immunol* 15:372-377.
179. Bromley, S. K., W. R. Burack, K. G. Johnson, K. Somersalo, T. N. Sims, C. Sumen, M. M. Davis, A. S. Shaw, P. M. Allen, and M. L. Dustin. 2001. The immunological synapse. *Annu Rev Immunol* 19:375-396.
180. Tseng, S. Y., and M. L. Dustin. 2002. T-cell activation: a multidimensional signaling network. *Curr Opin Cell Biol* 14:575-580.
181. Krummel, M. F., and M. M. Davis. 2002. Dynamics of the immunological synapse: finding, establishing and solidifying a connection. *Curr Opin Immunol* 14:66-74.
182. Dustin, M. L., and J. A. Cooper. 2000. The immunological synapse and the actin cytoskeleton: molecular hardware for T cell signaling. *Nat Immunol* 1:23-29.
183. Grakoui, A., S. K. Bromley, C. Sumen, M. M. Davis, A. S. Shaw, P. M. Allen, and M. L. Dustin. 1999. The immunological synapse: a molecular machine controlling T cell activation. *Science* 285:221-227.
184. Monks, C. R., B. A. Freiberg, H. Kupfer, N. Sciaky, and A. Kupfer. 1998. Three-dimensional segregation of supramolecular activation clusters in T cells. *Nature* 395:82-86.
185. Hommel, M., and B. Kyewski. 2003. Dynamic changes during the immune response in T cell-antigen-presenting cell clusters isolated from lymph nodes. *J Exp Med* 197:269-280.
186. McGavern, D. B., U. Christen, and M. B. Oldstone. 2002. Molecular anatomy of antigen-specific CD8(+) T cell engagement and synapse formation in vivo. *Nat Immunol* 3:918-925.
187. Reichert, P., R. L. Reinhardt, E. Ingulli, and M. K. Jenkins. 2001. Cutting edge: in vivo identification of TCR redistribution and polarized IL-2 production by naive CD4 T cells. *J Immunol* 166:4278-4281.
188. Ingulli, E., A. Mondino, A. Khoruts, and M. K. Jenkins. 1997. In vivo detection of dendritic cell antigen presentation to CD4(+) T cells. *J Exp Med* 185:2133-2141.
189. Gunzer, M., A. Schafer, S. Borgmann, S. Grabbe, K. S. Zanker, E. B. Brocker, E. Kampgen, and P. Friedl. 2000. Antigen presentation in extracellular matrix: interactions of T cells with dendritic cells are dynamic, short lived, and sequential. *Immunity* 13:323-332.
190. Holdorf, A. D., K. H. Lee, W. R. Burack, P. M. Allen, and A. S. Shaw. 2002. Regulation of Lck activity by CD4 and CD28 in the immunological synapse. *Nat Immunol* 3:259-264.
191. Trautmann, A., and S. Valitutti. 2003. The diversity of immunological synapses. *Curr Opin Immunol* 15:249-254.
192. Huang, J. H., L. I. Cardenas-Navia, C. C. Caldwell, T. J. Plumb, C. G. Radu, P. N. Rocha, T. Wilder, J. S. Bromberg, B. N. Cronstein, M. Sitkovsky, M. W. Dewhirst,

- and M. L. Dustin. 2007. Requirements for T lymphocyte migration in explanted lymph nodes. *J Immunol* 178:7747-7755.
193. Miller, M. J., S. H. Wei, M. D. Cahalan, and I. Parker. 2003. Autonomous T cell trafficking examined in vivo with intravital two-photon microscopy. *Proc Natl Acad Sci U S A* 100:2604-2609.
 194. Denk, W., J. H. Strickler, and W. W. Webb. 1990. Two-photon laser scanning fluorescence microscopy. *Science* 248:73-76.
 195. Helmchen, F., and W. Denk. 2005. Deep tissue two-photon microscopy. *Nat Methods* 2:932-940.
 196. Lindquist, R. L., G. Shakhar, D. Dudziak, H. Wardemann, T. Eisenreich, M. L. Dustin, and M. C. Nussenzweig. 2004. Visualizing dendritic cell networks in vivo. *Nat Immunol* 5:1243-1250.
 197. Miller, M. J., A. S. Hejazi, S. H. Wei, M. D. Cahalan, and I. Parker. 2004. T cell repertoire scanning is promoted by dynamic dendritic cell behavior and random T cell motility in the lymph node. *Proc Natl Acad Sci U S A* 101:998-1003.
 198. Wei, S. H., I. Parker, M. J. Miller, and M. D. Cahalan. 2003. A stochastic view of lymphocyte motility and trafficking within the lymph node. *Immunol Rev* 195:136-159.
 199. Bousso, P., and E. Robey. 2003. Dynamics of CD8+ T cell priming by dendritic cells in intact lymph nodes. *Nat Immunol* 4:579-585.
 200. Miller, M. J., S. H. Wei, I. Parker, and M. D. Cahalan. 2002. Two-photon imaging of lymphocyte motility and antigen response in intact lymph node. *Science* 296:1869-1873.
 201. Borowski, A. B., A. C. Boesteanu, Y. M. Mueller, C. Carafides, D. J. Topham, J. D. Altman, S. R. Jennings, and P. D. Katsikis. 2007. Memory CD8+ T cells require CD28 costimulation. *J Immunol* 179:6494-6503.
 202. Fuse, S., W. Zhang, and E. J. Usherwood. 2008. Control of memory CD8+ T cell differentiation by CD80/CD86-CD28 costimulation and restoration by IL-2 during the recall response. *J Immunol* 180:1148-1157.
 203. Ndejemi, M. P., J. R. Teijaro, D. S. Patke, A. W. Bingaman, M. R. Chandok, A. Azimzadeh, S. G. Nadler, and D. L. Farber. 2006. Control of memory CD4 T cell recall by the CD28/B7 costimulatory pathway. *J Immunol* 177:7698-7706.
 204. Boesteanu, A. C., and P. D. Katsikis. 2009. Memory T cells need CD28 costimulation to remember. *Semin Immunol* 21:69-77.
 205. Rush, C. M., O. R. Millington, S. Hutchison, K. Bryson, J. M. Brewer, and P. Garside. 2009. Characterization of CD4+ T-cell-dendritic cell interactions during secondary antigen exposure in tolerance and priming. *Immunology* 128:463-471.
 206. Sumen, C., T. R. Mempel, I. B. Mazo, and U. H. von Andrian. 2004. Intravital microscopy: visualizing immunity in context. *Immunity* 21:315-329.
 207. Zinselmeyer, B. H., J. Dempster, A. M. Gurney, D. Wokosin, M. Miller, H. Ho, O. R. Millington, K. M. Smith, C. M. Rush, I. Parker, M. Cahalan, J. M. Brewer, and P. Garside. 2005. In situ characterization of CD4+ T cell behavior in mucosal and systemic lymphoid tissues during the induction of oral priming and tolerance. *J Exp Med* 201:1815-1823.
 208. Tang, Q., J. Y. Adams, A. J. Tooley, M. Bi, B. T. Fife, P. Serra, P. Santamaria, R. M. Locksley, M. F. Krummel, and J. A. Bluestone. 2006. Visualizing regulatory T cell control of autoimmune responses in nonobese diabetic mice. *Nat Immunol* 7:83-92.
 209. Friedl, P., A. T. den Boer, and M. Gunzer. 2005. Tuning immune responses: diversity and adaptation of the immunological synapse. *Nat Rev Immunol* 5:532-545.

210. Kawakami, N., U. V. Nagerl, F. Odoardi, T. Bonhoeffer, H. Wekerle, and A. Flugel. 2005. Live imaging of effector cell trafficking and autoantigen recognition within the unfolding autoimmune encephalomyelitis lesion. *J Exp Med* 201:1805-1814.
211. Matheu, M. P., C. Beeton, I. Parker, K. G. Chandy, and D. C. M. 2008. Imaging effector memory T cells in the ear after induction of adoptive DTH. *J Vis Exp*.
212. Matheu, M. P., C. Beeton, A. Garcia, V. Chi, S. Rangaraju, O. Safrina, K. Monaghan, M. I. Uemura, D. Li, S. Pal, L. M. de la Maza, E. Monuki, A. Flugel, M. W. Pennington, I. Parker, K. G. Chandy, and M. D. Cahalan. 2008. Imaging of effector memory T cells during a delayed-type hypersensitivity reaction and suppression by Kv1.3 channel block. *Immunity* 29:602-614.
213. Mrass, P., H. Takano, L. G. Ng, S. Daxini, M. O. Lasaro, A. Iparraguirre, L. L. Cavanagh, U. H. von Andrian, H. C. Ertl, P. G. Haydon, and W. Weninger. 2006. Random migration precedes stable target cell interactions of tumor-infiltrating T cells. *J Exp Med* 203:2749-2761.
214. Boissonnas, A., L. Fetler, I. S. Zeelenberg, S. Hugues, and S. Amigorena. 2007. In vivo imaging of cytotoxic T cell infiltration and elimination of a solid tumor. *J Exp Med* 204:345-356.
215. Schaeffer, M., S. J. Han, T. Chtanova, G. G. van Dooren, P. Herzmark, Y. Chen, B. Roysam, B. Striepen, and E. A. Robey. 2009. Dynamic imaging of T cell-parasite interactions in the brains of mice chronically infected with *Toxoplasma gondii*. *J Immunol* 182:6379-6393.
216. McLachlan, J. B., D. M. Catron, J. J. Moon, and M. K. Jenkins. 2009. Dendritic cell antigen presentation drives simultaneous cytokine production by effector and regulatory T cells in inflamed skin. *Immunity* 30:277-288.
217. McGill, J., N. Van Rooijen, and K. L. Legge. 2008. Protective influenza-specific CD8 T cell responses require interactions with dendritic cells in the lungs. *J Exp Med* 205:1635-1646.
218. Aldridge, J. R., Jr., C. E. Moseley, D. A. Boltz, N. J. Negovetich, C. Reynolds, J. Franks, S. A. Brown, P. C. Doherty, R. G. Webster, and P. G. Thomas. 2009. TNF/iNOS-producing dendritic cells are the necessary evil of lethal influenza virus infection. *Proc Natl Acad Sci U S A* 106:5306-5311.
219. Lemos, M. P., F. Esquivel, P. Scott, and T. M. Laufer. 2004. MHC class II expression restricted to CD8alpha+ and CD11b+ dendritic cells is sufficient for control of *Leishmania major*. *J Exp Med* 199:725-730.
220. Seder, R. A., and R. Ahmed. 2003. Similarities and differences in CD4+ and CD8+ effector and memory T cell generation. *Nat Immunol* 4:835-842.
221. Lira, S. A. 2005. A passport into the lymph node. *Nat Immunol* 6:866-868.
222. Walunas, T. L., C. Y. Bakker, and J. A. Bluestone. 1996. CTLA-4 ligation blocks CD28-dependent T cell activation. *J Exp Med* 183:2541-2550.
223. Krummel, M. F., and J. P. Allison. 1996. CTLA-4 engagement inhibits IL-2 accumulation and cell cycle progression upon activation of resting T cells. *J Exp Med* 183:2533-2540.
224. Murphy, K. M., A. B. Heimberger, and D. Y. Loh. 1990. Induction by antigen of intrathymic apoptosis of CD4+CD8+TCRlo thymocytes in vivo. *Science* 250:1720-1723.
225. Barnden, M. J., J. Allison, W. R. Heath, and F. R. Carbone. 1998. Defective TCR expression in transgenic mice constructed using cDNA-based alpha- and beta-chain

- genes under the control of heterologous regulatory elements. *Immunol Cell Biol* 76:34-40.
226. de Boer, J., A. Williams, G. Skavdis, N. Harker, M. Coles, M. Tolaini, T. Norton, K. Williams, K. Roderick, A. J. Potocnik, and D. Kioussis. 2003. Transgenic mice with hematopoietic and lymphoid specific expression of Cre. *Eur J Immunol* 33:314-325.
 227. Lutz, M. B., N. Kukutsch, A. L. Ogilvie, S. Rossner, F. Koch, N. Romani, and G. Schuler. 1999. An advanced culture method for generating large quantities of highly pure dendritic cells from mouse bone marrow. *J Immunol Methods* 223:77-92.
 228. Edwards, J. C., A. D. Sedgwick, and D. A. Willoughby. 1981. The formation of a structure with the features of synovial lining by subcutaneous injection of air: an in vivo tissue culture system. *J Pathol* 134:147-156.
 229. Idzko, M., H. Hammad, M. van Nimwegen, M. Kool, T. Muller, T. Soullie, M. A. Willart, D. Hijdra, H. C. Hoogsteden, and B. N. Lambrecht. 2006. Local application of FTY720 to the lung abrogates experimental asthma by altering dendritic cell function. *J Clin Invest* 116:2935-2944.
 230. Pinschewer, D. D., A. F. Ochsenbein, B. Odermatt, V. Brinkmann, H. Hengartner, and R. M. Zinkernagel. 2000. FTY720 immunosuppression impairs effector T cell peripheral homing without affecting induction, expansion, and memory. *J Immunol* 164:5761-5770.
 231. Dittrich, P. S., S. P. Schafer, and P. Schwille. 2005. Characterization of the photoconversion on reaction of the fluorescent protein Kaede on the single-molecule level. *Biophys J* 89:3446-3455.
 232. Abraham, C., J. Griffith, and J. Miller. 1999. The dependence for leukocyte function-associated antigen-1/ICAM-1 interactions in T cell activation cannot be overcome by expression of high density TCR ligand. *J Immunol* 162:4399-4405.
 233. Matloubian, M., C. G. Lo, G. Cinamon, M. J. Lesneski, Y. Xu, V. Brinkmann, M. L. Allende, R. L. Proia, and J. G. Cyster. 2004. Lymphocyte egress from thymus and peripheral lymphoid organs is dependent on S1P receptor 1. *Nature* 427:355-360.
 234. Flechner, E. R., P. S. Freudenthal, G. Kaplan, and R. M. Steinman. 1988. Antigen-specific T lymphocytes efficiently cluster with dendritic cells in the human primary mixed-leukocyte reaction. *Cell Immunol* 111:183-195.
 235. Mempel, T. R. H. S. E. V. A. U. H. 2004. T-cell priming by dendritic cells in lymph nodes occurs in three distinct phases. *nature* 437:154-159.
 236. Celli, S., Z. Garcia, H. Beuneu, and P. Bousso. 2008. Decoding the dynamics of T cell-dendritic cell interactions in vivo. *Immunol Rev* 221:182-187.
 237. Shakhar, G., R. L. Lindquist, D. Skokos, D. Dudziak, J. H. Huang, M. C. Nussenzweig, and M. L. Dustin. 2005. Stable T cell-dendritic cell interactions precede the development of both tolerance and immunity in vivo. *Nat Immunol* 6:707-714.
 238. Grierson, A. M., P. Mitchell, C. L. Adams, A. M. Mowat, J. M. Brewer, M. M. Harnett, and P. Garside. 2005. Direct quantitation of T cell signaling by laser scanning cytometry. *J Immunol Methods* 301:140-153.
 239. Davignon, D., E. Martz, T. Reynolds, K. Kurzinger, and T. A. Springer. 1981. Lymphocyte function-associated antigen 1 (LFA-1): a surface antigen distinct from Lyt-2,3 that participates in T lymphocyte-mediated killing. *Proc Natl Acad Sci U S A* 78:4535-4539.

240. Nueda, A., M. Lopez-Cabrera, A. Vara, and A. L. Corbi. 1993. Characterization of the CD11a (alpha L, LFA-1 alpha) integrin gene promoter. *J Biol Chem* 268:19305-19311.
241. Stanley, P., A. Smith, A. McDowall, A. Nicol, D. Zicha, and N. Hogg. 2008. Intermediate-affinity LFA-1 binds alpha-actinin-1 to control migration at the leading edge of the T cell. *Embo J* 27:62-75.
242. Smith, A., P. Stanley, K. Jones, L. Svensson, A. McDowall, and N. Hogg. 2007. The role of the integrin LFA-1 in T-lymphocyte migration. *Immunol Rev* 218:135-146.
243. Semmrich, M., A. Smith, C. Feterowski, S. Beer, B. Engelhardt, D. H. Busch, B. Bartsch, M. Laschinger, N. Hogg, K. Pfeffer, and B. Holzmann. 2005. Importance of integrin LFA-1 deactivation for the generation of immune responses. *J Exp Med* 201:1987-1998.
244. Hogg, N., A. Smith, A. McDowall, K. Giles, P. Stanley, M. Laschinger, and R. Henderson. 2004. How T cells use LFA-1 to attach and migrate. *Immunol Lett* 92:51-54.
245. Perez, O. D., D. Mitchell, G. C. Jager, S. South, C. Murriel, J. McBride, L. A. Herzenberg, S. Kinoshita, and G. P. Nolan. 2003. Leukocyte functional antigen 1 lowers T cell activation thresholds and signaling through cytohesin-1 and Jun-activating binding protein 1. *Nat Immunol* 4:1083-1092.
246. Saraceno, R., G. Scotto, A. Chiricozzi, and S. Chimenti. 2009. Urticaria associated with hyper-IgE in a patient with psoriasis undergoing treatment with efalizumab. *Acta Derm Venereol* 89:412-413.
247. Gisondi, P., F. Prignano, P. Grossi, T. Lotti, and G. Girolomoni. 2009. Treatment of Psoriasis with Efalizumab in Patients with Hepatitis C Viral Infection: Report of Five Cases. *Dermatology*.
248. Molloy, E. S., and L. H. Calabrese. 2009. Therapy: Targeted but not trouble-free: efalizumab and PML. *Nat Rev Rheumatol* 5:418-419.
249. Munoz-Santos, C., M. Yebenes, J. Romani, and J. Luelmo. 2009. Response of keratosis lichenoides chronica to efalizumab therapy. *Arch Dermatol* 145:867-869.
250. Korman, B. D., K. L. Tyler, and N. J. Korman. 2009. Progressive multifocal leukoencephalopathy, efalizumab, and immunosuppression: a cautionary tale for dermatologists. *Arch Dermatol* 145:937-942.
251. Miquel, F. J., J. Colomina, J. I. Marii, and C. Ortega. 2009. Cytomegalovirus infection in a patient treated with efalizumab for psoriasis. *Arch Dermatol* 145:961-962.
252. Smith, J. R., R. S. Akin, and M. J. Wells. 2009. Alopecia areata treated with efalizumab: a case with significant hair re-growth after long-term therapy. *J Drugs Dermatol* 8:758-760.
253. Li, S., H. Wang, B. Peng, M. Zhang, D. Zhang, S. Hou, Y. Guo, and J. Ding. 2009. Efalizumab binding to the LFA-1 alphaL I domain blocks ICAM-1 binding via steric hindrance. *Proc Natl Acad Sci U S A* 106:4349-4354.
254. Graler, M. H., and E. J. Goetzl. 2004. The immunosuppressant FTY720 down-regulates sphingosine 1-phosphate G-protein-coupled receptors. *Faseb J* 18:551-553.
255. Maeda, Y., H. Matsuyuki, K. Shimano, H. Kataoka, K. Sugahara, and K. Chiba. 2007. Migration of CD4 T cells and dendritic cells toward sphingosine 1-phosphate (S1P) is mediated by different receptor subtypes: S1P regulates the functions of murine mature dendritic cells via S1P receptor type 3. *J Immunol* 178:3437-3446.

256. Wang, W., M. H. Graeler, and E. J. Goetzl. 2005. Type 4 sphingosine 1-phosphate G protein-coupled receptor (S1P4) transduces S1P effects on T cell proliferation and cytokine secretion without signaling migration. *Faseb J* 19:1731-1733.
257. Schwab, S. R., J. P. Pereira, M. Matloubian, Y. Xu, Y. Huang, and J. G. Cyster. 2005. Lymphocyte sequestration through S1P lyase inhibition and disruption of S1P gradients. *Science* 309:1735-1739.
258. Jin, Y., E. Knudsen, L. Wang, Y. Bryceson, B. Damaj, S. Gessani, and A. A. Maghazachi. 2003. Sphingosine 1-phosphate is a novel inhibitor of T-cell proliferation. *Blood* 101:4909-4915.
259. Sanchez, T., T. Estrada-Hernandez, J. H. Paik, M. T. Wu, K. Venkataraman, V. Brinkmann, K. Claffey, and T. Hla. 2003. Phosphorylation and action of the immunomodulator FTY720 inhibits vascular endothelial cell growth factor-induced vascular permeability. *J Biol Chem* 278:47281-47290.
260. Benvenuti, F., S. Hugues, M. Walmsley, S. Ruf, L. Fetler, M. Popoff, V. L. Tybulewicz, and S. Amigorena. 2004. Requirement of Rac1 and Rac2 expression by mature dendritic cells for T cell priming. *Science* 305:1150-1153.
261. Petranyi, G. G., E. Pocsik, B. Kotlan, G. Gorog, and M. Benczur. 1986. Regulatory function of cell surface molecules CD2-, LFA- and beta 2-microglobulin in natural killer cell activity. *Mol Immunol* 23:1275-1279.
262. van Agthoven, A. J., and A. Truneh. 1985. Lymphocyte function-associated antigens one (LFA-1) on B and on T lymphocytes bind a monoclonal antibody with different affinities. *Cell Immunol* 91:255-262.
263. Cella, M., A. Engering, V. Pinet, J. Pieters, and A. Lanzavecchia. 1997. Inflammatory stimuli induce accumulation of MHC class II complexes on dendritic cells. *Nature* 388:782-787.
264. Guermonprez, P., J. Valladeau, L. Zitvogel, C. Thery, and S. Amigorena. 2002. Antigen presentation and T cell stimulation by dendritic cells. *Annu Rev Immunol* 20:621-667.
265. Hertz, C. J., S. M. Kiertcher, P. J. Godowski, D. A. Bouis, M. V. Norgard, M. D. Roth, and R. L. Modlin. 2001. Microbial lipopeptides stimulate dendritic cell maturation via Toll-like receptor 2. *J Immunol* 166:2444-2450.
266. Rescigno, M., F. Granucci, S. Citterio, M. Foti, and P. Ricciardi-Castagnoli. 1999. Coordinated events during bacteria-induced DC maturation. *Immunol Today* 20:200-203.
267. Hemmi, H., and S. Akira. 2005. TLR signalling and the function of dendritic cells. *Chem Immunol Allergy* 86:120-135.
268. Kaisho, T., O. Takeuchi, T. Kawai, K. Hoshino, and S. Akira. 2001. Endotoxin-induced maturation of MyD88-deficient dendritic cells. *J Immunol* 166:5688-5694.
269. Itano, A. A., S. J. McSorley, R. L. Reinhardt, B. D. Ehst, E. Ingulli, A. Y. Rudensky, and M. K. Jenkins. 2003. Distinct dendritic cell populations sequentially present antigen to CD4 T cells and stimulate different aspects of cell-mediated immunity. *Immunity* 19:47-57.
270. Singer, A., S. Adoro, and J. H. Park. 2008. Lineage fate and intense debate: myths, models and mechanisms of CD4- versus CD8-lineage choice. *Nat Rev Immunol* 8:788-801.
271. Reiner, S. L. 2001. Helper T cell differentiation, inside and out. *Curr Opin Immunol* 13:351-355.

272. Cyster, J. G. 2005. Chemokines, sphingosine-1-phosphate, and cell migration in secondary lymphoid organs. *Annu Rev Immunol* 23:127-159.
273. Brinkmann, V., S. Chen, L. Feng, D. Pinschewer, Z. Nikolova, and R. Hof. 2001. FTY720 alters lymphocyte homing and protects allografts without inducing general immunosuppression. *Transplant Proc* 33:530-531.
274. Verwilghen, J., P. Vandenberghe, G. Wallays, M. de Boer, N. Anthony, G. S. Panayi, and J. L. Ceuppens. 1993. Simultaneous ligation of CD5 and CD28 on resting T lymphocytes induces T cell activation in the absence of T cell receptor/CD3 occupancy. *J Immunol* 150:835-846.
275. Cebrian, M., E. Yague, M. Rincon, M. Lopez-Botet, M. O. de Landazuri, and F. Sanchez-Madrid. 1988. Triggering of T cell proliferation through AIM, an activation inducer molecule expressed on activated human lymphocytes. *J Exp Med* 168:1621-1637.
276. Shioh, L. R., D. B. Rosen, N. Brdickova, Y. Xu, J. An, L. L. Lanier, J. G. Cyster, and M. Matloubian. 2006. CD69 acts downstream of interferon-alpha/beta to inhibit S1P1 and lymphocyte egress from lymphoid organs. *Nature* 440:540-544.
277. Gallatin, W. M., I. L. Weissman, and E. C. Butcher. 1983. A cell-surface molecule involved in organ-specific homing of lymphocytes. *Nature* 304:30-34.
278. Siegelman, M. H., M. van de Rijn, and I. L. Weissman. 1989. Mouse lymph node homing receptor cDNA clone encodes a glycoprotein revealing tandem interaction domains. *Science* 243:1165-1172.
279. Butcher, E. C., and L. J. Picker. 1996. Lymphocyte homing and homeostasis. *Science* 272:60-66.
280. Adler, A. J., C. T. Huang, G. S. Yochum, D. W. Marsh, and D. M. Pardoll. 2000. In vivo CD4+ T cell tolerance induction versus priming is independent of the rate and number of cell divisions. *J Immunol* 164:649-655.
281. Coffman, R. L., and T. R. Mosmann. 1991. CD4+ T-cell subsets: regulation of differentiation and function. *Res Immunol* 142:7-9.
282. Allen, C. D., T. Okada, and J. G. Cyster. 2007. Germinal-center organization and cellular dynamics. *Immunity* 27:190-202.
283. MacLennan, I. C. 1994. Germinal centers. *Annu Rev Immunol* 12:117-139.
284. Bhardwaj, N., S. M. Friedman, B. C. Cole, and A. J. Nisanian. 1992. Dendritic cells are potent antigen-presenting cells for microbial superantigens. *J Exp Med* 175:267-273.
285. Catron, D. M., A. A. Itano, K. A. Pape, D. L. Mueller, and M. K. Jenkins. 2004. Visualizing the first 50 hr of the primary immune response to a soluble antigen. *Immunity* 21:341-347.
286. Scharffetter-Kochanek, K., H. Lu, K. Norman, N. van Nood, F. Munoz, S. Grabbe, M. McArthur, I. Lorenzo, S. Kaplan, K. Ley, C. W. Smith, C. A. Montgomery, S. Rich, and A. L. Beaudet. 1998. Spontaneous skin ulceration and defective T cell function in CD18 null mice. *J Exp Med* 188:119-131.
287. van Seventer, G. A., W. Newman, Y. Shimizu, T. B. Nutman, Y. Tanaka, K. J. Horgan, T. V. Gopal, E. Ennis, D. O'Sullivan, H. Grey, and et al. 1991. Analysis of T cell stimulation by superantigen plus major histocompatibility complex class II molecules or by CD3 monoclonal antibody: costimulation by purified adhesion ligands VCAM-1, ICAM-1, but not ELAM-1. *J Exp Med* 174:901-913.
288. Salomon, B., and J. A. Bluestone. 1998. LFA-1 interaction with ICAM-1 and ICAM-2 regulates Th2 cytokine production. *J Immunol* 161:5138-5142.

289. Yanagawa, Y., Y. Hoshino, H. Kataoka, T. Kawaguchi, M. Ohtsuki, K. Sugahara, and K. Chiba. 1999. FTY720, a novel immunosuppressant, prolongs rat skin allograft survival by decreasing T-cell infiltration into grafts. *Transplant Proc* 31:1227-1229.
290. Han, S., X. Zhang, G. Wang, H. Guan, G. Garcia, P. Li, L. Feng, and B. Zheng. 2004. FTY720 suppresses humoral immunity by inhibiting germinal center reaction. *Blood* 104:4129-4133.
291. Kandula, S., and C. Abraham. 2004. LFA-1 on CD4+ T cells is required for optimal antigen-dependent activation in vivo. *J Immunol* 173:4443-4451.
292. Henderson, R. B., L. H. Lim, P. A. Tessier, F. N. Gavins, M. Mathies, M. Perretti, and N. Hogg. 2001. The use of lymphocyte function-associated antigen (LFA)-1-deficient mice to determine the role of LFA-1, Mac-1, and alpha4 integrin in the inflammatory response of neutrophils. *J Exp Med* 194:219-226.
293. Tammela, T., A. Saaristo, T. Holopainen, J. Lyytikka, A. Kotronen, M. Pitkonen, U. Abo-Ramadan, S. Yla-Herttuala, T. V. Petrova, and K. Alitalo. 2007. Therapeutic differentiation and maturation of lymphatic vessels after lymph node dissection and transplantation. *Nat Med* 13:1458-1466.
294. Cardillo, F., J. Mengel, S. B. Garcia, and F. Q. Cunha. 1995. Mouse ear spleen grafts: a model for intrasplenic immunization with minute amounts of antigen. *J Immunol Methods* 188:43-49.
295. White, A., D. Carragher, S. Parnell, A. Msaki, N. Perkins, P. Lane, E. Jenkinson, G. Anderson, and J. H. Caamano. 2007. Lymphotoxin α -dependent and -independent signals regulate stromal organizer cell homeostasis during lymph node organogenesis. *Blood* 110:1950-1959.
296. Becker, C., J. Assouad, M. Riquet, and G. Hidden. 2006. Postmastectomy lymphedema: long-term results following microsurgical lymph node transplantation. *Ann Surg* 243:313-315.
297. Fulmer RI, C. A., Liebelt RA, Liebelt AG. 1963. Transplantation of cardiac tissue into the mouse ear. *Am. J. Anat* 113:273-285.
298. Proudman, S. M., L. G. Cleland, M. Fusco, and G. Mayrhofer. 1999. Accessible xenografts of human synovium in the subcutaneous tissues of the ears of SCID mice. *Immunol Cell Biol* 77:109-120.
299. Hillebrands, J. L., F. A. Klatter, H. P. Raue, R. A. Koops, M. N. Hylkema, and J. Rozing. 1999. An alternative model to study intrathymic tolerance induction: the neonatal heart-in-ear transplantation model in the rat. *Transplant Proc* 31:1563-1566.
300. Judd, K. P., C. J. Bryant, R. J. Ruckman, and J. J. Trentin. 1971. Cardiac transplantation in mice. IV. Relationship between antithymocyte-globulin (ATG) dose, allograft survival and anti-ATG immunity. *Rev Eur Etud Clin Biol* 16:1002-1006.
301. Vondenhoff, M. F., G. Kraal, and R. E. Mebius. 2007. Lymphoid organogenesis in brief. *Eur J Immunol* 37 Suppl 1:S46-52.
302. Cupedo, T., and R. E. Mebius. 2005. Cellular interactions in lymph node development. *J Immunol* 174:21-25.
303. Mebius, R. E. 2003. Organogenesis of lymphoid tissues. *Nat Rev Immunol* 3:292-303.
304. Cupedo, T., G. Kraal, and R. E. Mebius. 2002. The role of CD45+CD4+CD3- cells in lymphoid organ development. *Immunol Rev* 189:41-50.
305. Rennert, P. D., D. James, F. Mackay, J. L. Browning, and P. S. Hochman. 1998. Lymph node genesis is induced by signaling through the lymphotoxin beta receptor. *Immunity* 9:71-79.

306. Merad, M., F. Ginhoux, and M. Collin. 2008. Origin, homeostasis and function of Langerhans cells and other langerin-expressing dendritic cells. *Nat Rev Immunol* 8:935-947.
307. Jakubzick, C., M. Bogunovic, A. J. Bonito, E. L. Kuan, M. Merad, and G. J. Randolph. 2008. Lymph-migrating, tissue-derived dendritic cells are minor constituents within steady-state lymph nodes. *J Exp Med* 205:2839-2850.
308. Merad, M., and F. Ginhoux. 2007. Dendritic cell genealogy: a new stem or just another branch? *Nat Immunol* 8:1199-1201.
309. Henri, S., D. Vremec, A. Kamath, J. Waithman, S. Williams, C. Benoist, K. Burnham, S. Saeland, E. Handman, and K. Shortman. 2001. The dendritic cell populations of mouse lymph nodes. *J Immunol* 167:741-748.
310. Oshugi, Y., S. Vuckovic, and D. N. Hart. 2002. Myeloid blood CD11c(+) dendritic cells and monocyte-derived dendritic cells differ in their ability to stimulate T lymphocytes. *Blood* 100:2858-2866.
311. McNagny, K. M., R. P. Bucy, and M. D. Cooper. 1991. Reticular cells in peripheral lymphoid tissues express the phosphatidylinositol-linked BP-3 antigen. *Eur J Immunol* 21:509-515.
312. Farr, A., A. Nelson, and S. Hosier. 1992. Characterization of an antigenic determinant preferentially expressed by type I epithelial cells in the murine thymus. *J Histochem Cytochem* 40:651-664.
313. Worbs, T., T. R. Mempel, J. Bolter, U. H. von Andrian, and R. Forster. 2007. CCR7 ligands stimulate the intranodal motility of T lymphocytes in vivo. *J Exp Med* 204:489-495.
314. Gunn, M. D., K. Tangemann, C. Tam, J. G. Cyster, S. D. Rosen, and L. T. Williams. 1998. A chemokine expressed in lymphoid high endothelial venules promotes the adhesion and chemotaxis of naive T lymphocytes. *Proc Natl Acad Sci U S A* 95:258-263.
315. Nakano, H., S. Mori, H. Yonekawa, H. Nariuchi, A. Matsuzawa, and T. Kakiuchi. 1998. A novel mutant gene involved in T-lymphocyte-specific homing into peripheral lymphoid organs on mouse chromosome 4. *Blood* 91:2886-2895.
316. Girard, J. P., and T. A. Springer. 1995. High endothelial venules (HEVs): specialized endothelium for lymphocyte migration. *Immunol Today* 16:449-457.
317. Faveeuw, C., M. E. Di Mauro, A. A. Price, and A. Ager. 2000. Roles of alpha(4) integrins/VCAM-1 and LFA-1/ICAM-1 in the binding and transendothelial migration of T lymphocytes and T lymphoblasts across high endothelial venules. *Int Immunol* 12:241-251.
318. Burne, M. J., A. Elghandour, M. Haq, S. R. Saba, J. Norman, T. Condon, F. Bennett, and H. Rabb. 2001. IL-1 and TNF independent pathways mediate ICAM-1/VCAM-1 up-regulation in ischemia reperfusion injury. *J Leukoc Biol* 70:192-198.
319. Yoshida, H., A. Naito, J. Inoue, M. Satoh, S. M. Santee-Cooper, C. F. Ware, A. Togawa, S. Nishikawa, and S. Nishikawa. 2002. Different cytokines induce surface lymphotoxin-alpha-beta on IL-7 receptor-alpha cells that differentially engender lymph nodes and Peyer's patches. *Immunity* 17:823-833.
320. Lane, P. J., F. M. McConnell, D. Withers, F. Gaspal, M. Saini, and G. Anderson. 2009. Lymphoid tissue inducer cells: bridges between the ancient innate and the modern adaptive immune systems. *Mucosal Immunol* 2:472-477.
321. Ordemann, R., R. Hutchinson, J. Friedman, S. J. Burakoff, P. Reddy, U. Duffner, T. M. Braun, C. Liu, T. Teshima, and J. L. Ferrara. 2002. Enhanced allostimulatory

- activity of host antigen-presenting cells in old mice intensifies acute graft-versus-host disease. *J Clin Invest* 109:1249-1256.
322. Fulcher, D., and S. Wong. 1999. Carboxyfluorescein succinimidyl ester-based proliferative assays for assessment of T cell function in the diagnostic laboratory. *Immunol Cell Biol* 77:559-564.
 323. von Freeden-Jeffry, U., P. Vieira, L. A. Lucian, T. McNeil, S. E. Burdach, and R. Murray. 1995. Lymphopenia in interleukin (IL)-7 gene-deleted mice identifies IL-7 as a nonredundant cytokine. *J Exp Med* 181:1519-1526.
 324. Peschon, J. J., P. J. Morrissey, K. H. Grabstein, F. J. Ramsdell, E. Maraskovsky, B. C. Gliniak, L. S. Park, S. F. Ziegler, D. E. Williams, C. B. Ware, J. D. Meyer, and B. L. Davison. 1994. Early lymphocyte expansion is severely impaired in interleukin 7 receptor-deficient mice. *J Exp Med* 180:1955-1960.
 325. Maki, K., S. Sunaga, Y. Komagata, Y. Kodaira, A. Mabuchi, H. Karasuyama, K. Yokomuro, J. I. Miyazaki, and K. Ikuta. 1996. Interleukin 7 receptor-deficient mice lack gammadelta T cells. *Proc Natl Acad Sci U S A* 93:7172-7177.
 326. Yoshida, H., K. Honda, R. Shinkura, S. Adachi, S. Nishikawa, K. Maki, K. Ikuta, and S. I. Nishikawa. 1999. IL-7 receptor alpha+ CD3(-) cells in the embryonic intestine induces the organizing center of Peyer's patches. *Int Immunol* 11:643-655.
 327. Fukuyama, S., T. Hiroi, Y. Yokota, P. D. Rennert, M. Yanagita, N. Kinoshita, S. Terawaki, T. Shikina, M. Yamamoto, Y. Kurono, and H. Kiyono. 2002. Initiation of NALT organogenesis is independent of the IL-7R, LTbetaR, and NIK signaling pathways but requires the Id2 gene and CD3(-)CD4(+)CD45(+) cells. *Immunity* 17:31-40.
 328. Finke, D., H. Acha-Orbea, A. Mattis, M. Lipp, and J. Kraehenbuhl. 2002. CD4+CD3- cells induce Peyer's patch development: role of alpha4beta1 integrin activation by CXCR5. *Immunity* 17:363-373.
 329. Leibovich, S. J., and R. Ross. 1975. The role of the macrophage in wound repair. A study with hydrocortisone and antimacrophage serum. *Am J Pathol* 78:71-100.
 330. Wilson, K. 1997. Wound healing: the role of macrophages. *Nurs Crit Care* 2:291-296.
 331. Polverini, P. J., P. S. Cotran, M. A. Gimbrone, Jr., and E. R. Unanue. 1977. Activated macrophages induce vascular proliferation. *Nature* 269:804-806.
 332. Zwadlo, G., E. B. Brocker, D. B. von Bassewitz, U. Feige, and C. Sorg. 1985. A monoclonal antibody to a differentiation antigen present on mature human macrophages and absent from monocytes. *J Immunol* 134:1487-1492.
 333. Pytowski, B., J. Goldman, K. Persaud, Y. Wu, L. Witte, D. J. Hicklin, M. Skobe, K. C. Boardman, and M. A. Swartz. 2005. Complete and specific inhibition of adult lymphatic regeneration by a novel VEGFR-3 neutralizing antibody. *J Natl Cancer Inst* 97:14-21.
 334. Goldman, J., J. M. Rutkowski, J. D. Shields, M. C. Pasquier, Y. Cui, H. G. Schmokel, S. Willey, D. J. Hicklin, B. Pytowski, and M. A. Swartz. 2007. Cooperative and redundant roles of VEGFR-2 and VEGFR-3 signaling in adult lymphangiogenesis. *Faseb J* 21:1003-1012.
 335. Schoppmann, S. F., A. Fenzl, M. Schindl, T. Bachleitner-Hofmann, K. Nagy, M. Gnant, R. Horvat, R. Jakesz, and P. Birner. 2006. Hypoxia inducible factor-1alpha correlates with VEGF-C expression and lymphangiogenesis in breast cancer. *Breast Cancer Res Treat* 99:135-141.

336. Ikomi, F., Y. Yokoyama, N. Ogiwara, K. Sasaki, R. Mizuno, and T. Ohhashi. 2006. Recanalization of the collecting lymphatics in rabbit hind leg. *Microcirculation* 13:365-376.
337. JW, K. 1987. A T cell receptor V_p segment that imparts reactivity to a class II major histocompatibility complex product. *cell* 49:263-271.
338. Pape, K. A., E. R. Kearney, A. Khoruts, A. Mondino, R. Merica, Z. M. Chen, E. Ingulli, J. White, J. G. Johnson, and M. K. Jenkins. 1997. Use of adoptive transfer of T-cell-antigen-receptor-transgenic T cell for the study of T-cell activation in vivo. *Immunol Rev* 156:67-78.
339. Bousso, P., and E. A. Robey. 2004. Dynamic behavior of T cells and thymocytes in lymphoid organs as revealed by two-photon microscopy. *Immunity* 21:349-355.
340. Stutzmann, G. E., and I. Parker. 2005. Dynamic multiphoton imaging: a live view from cells to systems. *Physiology (Bethesda)* 20:15-21.
341. Sprent, J., and C. D. Surh. 2002. T cell memory. *Annu Rev Immunol* 20:551-579.
342. Dutton, R. W., L. M. Bradley, and S. L. Swain. 1998. T cell memory. *Annu Rev Immunol* 16:201-223.
343. Cerottini, J. C., and H. R. MacDonald. 1989. The cellular basis of T-cell memory. *Annu Rev Immunol* 7:77-89.
344. Parish, C. R. 1999. Fluorescent dyes for lymphocyte migration and proliferation studies. *Immunol Cell Biol* 77:499-508.
345. Thompson, B. S., and T. C. Mitchell. 2004. Measurement of daughter cell accumulation during lymphocyte proliferation in vivo. *J Immunol Methods* 295:79-87.
346. Sedgwick, A. D., R. Hooke, J. Dawson, and P. Lees. 1987. The activation of carrageenan air pouch inflammation by silica and its effects on cartilage degradation. *Int J Tissue React* 9:477-484.
347. Sin, Y. M., A. D. Sedgwick, E. P. Chea, and D. A. Willoughby. 1986. Mast cells in newly formed lining tissue during acute inflammation: a six day air pouch model in the mouse. *Ann Rheum Dis* 45:873-877.
348. Sedgwick, A. D., and P. Lees. 1986. A comparison of air pouch, sponge and pleurisy models of acute carrageenan inflammation in the rat. *Agents Actions* 18:439-446.
349. Sin, Y. M., A. D. Sedgwick, A. Moore, and D. A. Willoughby. 1984. Studies on the clearance of calcium pyrophosphate crystals from facsimile synovium. *Ann Rheum Dis* 43:487-492.
350. Shin, S., J. H. Jeon, D. Park, J. Y. Jang, S. S. Joo, B. Y. Hwang, S. Y. Choe, and Y. B. Kim. 2009. Anti-inflammatory effects of an ethanol extract of *Angelica gigas* in a Carrageenan-air pouch inflammation model. *Exp Anim* 58:431-436.
351. Kowanko, I. C., T. P. Gordon, M. A. Rozenbils, P. M. Brooks, and P. J. Roberts-Thomson. 1986. The subcutaneous air pouch model of synovium and the inflammatory response to heat aggregated gammaglobulin. *Agents Actions* 18:421-428.
352. Bottomley, K. M., R. J. Griffiths, T. J. Rising, and A. Steward. 1988. A modified mouse air pouch model for evaluating the effects of compounds on granuloma induced cartilage degradation. *Br J Pharmacol* 93:627-635.
353. Romano, M., R. Faggioni, M. Sironi, S. Sacco, B. Echtenacher, E. Di Santo, M. Salmons, and P. Ghezzi. 1997. Carrageenan-induced acute inflammation in the mouse air pouch synovial model. Role of tumour necrosis factor. *Mediators Inflamm* 6:32-38.
354. Black, C. A. 1999. Delayed type hypersensitivity: current theories with an historic perspective. *Dermatol Online J* 5:7.

355. Landsteiner, K., and M. W. Chase. 1942. Experiments on transfer of cutaneous sensitivity to simple compounds. *Proc. Soc. Exp. Biol. Med.* 49:688.
356. W, C. M. 1945. The cellular transfer of cutaneous hypersensitivity to tuberculin. . *Proc. Soc. Exp. Biol. Med.* 59:134.
357. Rodriguez-Pena, R., S. Lopez, C. Mayorga, C. Antunez, T. D. Fernandez, M. J. Torres, and M. Blanca. 2006. Potential involvement of dendritic cells in delayed-type hypersensitivity reactions to beta-lactams. *J Allergy Clin Immunol* 118:949-956.
358. Hancock, W. W., S. J. Khoury, C. B. Carpenter, and M. H. Sayegh. 1994. Differential effects of oral versus intrathymic administration of polymorphic major histocompatibility complex class II peptides on mononuclear and endothelial cell activation and cytokine expression during a delayed-type hypersensitivity response. *Am J Pathol* 144:1149-1158.
359. Gaga, M., A. J. Frew, V. A. Varney, and A. B. Kay. 1991. Eosinophil activation and T lymphocyte infiltration in allergen-induced late phase skin reactions and classical delayed-type hypersensitivity. *J Immunol* 147:816-822.
360. Szabo, S. J., B. M. Sullivan, S. L. Peng, and L. H. Glimcher. 2003. Molecular mechanisms regulating Th1 immune responses. *Annu Rev Immunol* 21:713-758.
361. Mody, C. H., R. Paine, 3rd, C. Jackson, G. H. Chen, and G. B. Toews. 1994. CD8 cells play a critical role in delayed type hypersensitivity to intact *Cryptococcus neoformans*. *J Immunol* 152:3970-3979.
362. Brennan, F. M., N. M. Smith, S. Owen, C. Li, P. Amjadi, P. Green, A. Andersson, A. C. Palfreeman, P. Hillyer, A. Foey, J. T. Beech, and M. Feldmann. 2008. Resting CD4+ effector memory T cells are precursors of bystander-activated effectors: a surrogate model of rheumatoid arthritis synovial T-cell function. *Arthritis Res Ther* 10:R36.
363. Millington, O. R., V. B. Gibson, C. M. Rush, B. H. Zinselmeyer, R. S. Phillips, P. Garside, and J. M. Brewer. 2007. Malaria impairs T cell clustering and immune priming despite normal signal 1 from dendritic cells. *PLoS Pathog* 3:1380-1387.
364. Marchant, J. S., G. E. Stutzmann, M. A. Leissring, F. M. LaFerla, and I. Parker. 2001. Multiphoton-evoked color change of DsRed as an optical highlighter for cellular and subcellular labeling. *Nat Biotechnol* 19:645-649.
365. Ando, R., H. Hama, M. Yamamoto-Hino, H. Mizuno, and A. Miyawaki. 2002. An optical marker based on the UV-induced green-to-red photoconversion of a fluorescent protein. *Proc Natl Acad Sci U S A* 99:12651-12656.
366. Mizuno, H., A. Sawano, P. Eli, H. Hama, and A. Miyawaki. 2001. Red fluorescent protein from *Discosoma* as a fusion tag and a partner for fluorescence resonance energy transfer. *Biochemistry* 40:2502-2510.
367. Karasawa, S., T. Araki, T. Nagai, H. Mizuno, and A. Miyawaki. 2004. Cyan-emitting and orange-emitting fluorescent proteins as a donor/acceptor pair for fluorescence resonance energy transfer. *Biochem J* 381:307-312.
368. Terskikh, A., A. Fradkov, G. Ermakova, A. Zaraisky, P. Tan, A. V. Kajava, X. Zhao, S. Lukyanov, M. Matz, S. Kim, I. Weissman, and P. Siebert. 2000. "Fluorescent timer": protein that changes color with time. *Science* 290:1585-1588.
369. Mizuno, H., T. K. Mal, K. I. Tong, R. Ando, T. Furuta, M. Ikura, and A. Miyawaki. 2003. Photo-induced peptide cleavage in the green-to-red conversion of a fluorescent protein. *Mol Cell* 12:1051-1058.

370. Watanabe, W., T. Shimada, S. Matsunaga, D. Kurihara, K. Fukui, S. Shin-Ichi Arimura, N. Tsutsumi, K. Isobe, and K. Itoh. 2007. Single-organelle tracking by two-photon conversion. *Opt Express* 15:2490-2498.
371. Tomura, M., N. Yoshida, J. Tanaka, S. Karasawa, Y. Miwa, A. Miyawaki, and O. Kanagawa. 2008. Monitoring cellular movement in vivo with photoconvertible fluorescence protein "Kaede" transgenic mice. *Proc Natl Acad Sci U S A* 105:10871-10876.
372. Lippincott-Schwartz, J., and G. H. Patterson. 2003. Development and use of fluorescent protein markers in living cells. *Science* 300:87-91.
373. Patterson, G. H., and J. Lippincott-Schwartz. 2002. A photoactivatable GFP for selective photolabeling of proteins and cells. *Science* 297:1873-1877.
374. McLean, D. L., and J. R. Fetcho. 2009. Spinal interneurons differentiate sequentially from those driving the fastest swimming movements in larval zebrafish to those driving the slowest ones. *J Neurosci* 29:13566-13577.
375. Schmidt, A., B. Wiesner, K. Weisshart, K. Schulz, J. Furkert, B. Lamprecht, W. Rosenthal, and R. Schulein. 2009. Use of Kaede fusions to visualize recycling of G protein-coupled receptors. *Traffic* 10:2-15.
376. Kurzinger, K., and T. A. Springer. 1982. Purification and structural characterization of LFA-1, a lymphocyte function-associated antigen, and Mac-1, a related macrophage differentiation antigen associated with the type three complement receptor. *J Biol Chem* 257:12412-12418.
377. Ho, M. K., and T. A. Springer. 1982. Mac-1 antigen: quantitative expression in macrophage populations and tissues, and immunofluorescent localization in spleen. *J Immunol* 128:2281-2286.
378. Fleming, T. J., M. L. Fleming, and T. R. Malek. 1993. Selective expression of Ly-6G on myeloid lineage cells in mouse bone marrow. RB6-8C5 mAb to granulocyte-differentiation antigen (Gr-1) detects members of the Ly-6 family. *J Immunol* 151:2399-2408.
379. Huang, Z., G. Li, W. Pei, L. A. Sosa, and L. Niu. 2005. Enhancing protein expression in single HEK 293 cells. *J Neurosci Methods* 142:159-166.
380. Higashi, N., N. Yoshizuka, A. Ohuchi, T. Osawa, and Y. Kobayashi. 1995. Involvement of inflammatory cytokines in a delayed-type hypersensitivity reaction. *Cell Immunol* 161:288-294.
381. Ferreri, N. R., I. Millet, V. Paliwal, W. Herzog, D. Solomon, R. Ramabhadran, and P. W. Askenase. 1991. Induction of macrophage TNF alpha, IL-1, IL-6, and PGE2 production by DTH-initiating factors. *Cell Immunol* 137:389-405.
382. Mosser, D. M., and J. P. Edwards. 2008. Exploring the full spectrum of macrophage activation. *Nat Rev Immunol* 8:958-969.
383. Gordon, S., and P. R. Taylor. 2005. Monocyte and macrophage heterogeneity. *Nat Rev Immunol* 5:953-964.
384. Duffield, J. S. 2003. The inflammatory macrophage: a story of Jekyll and Hyde. *Clin Sci (Lond)* 104:27-38.
385. Hogquist, K. A., M. A. Nett, E. R. Unanue, and D. D. Chaplin. 1991. Interleukin 1 is processed and released during apoptosis. *Proc Natl Acad Sci U S A* 88:8485-8489.
386. Shibuya, K., D. Robinson, F. Zonin, S. B. Hartley, S. E. Macatonia, C. Somoza, C. A. Hunter, K. M. Murphy, and A. O'Garra. 1998. IL-1 alpha and TNF-alpha are required for IL-12-induced development of Th1 cells producing high levels of IFN-gamma in BALB/c but not C57BL/6 mice. *J Immunol* 160:1708-1716.

387. Igarashi, K., M. Mitsuyama, K. Muramori, H. Tsukada, and K. Nomoto. 1990. Interleukin-1-induced promotion of T-cell differentiation in mice immunized with killed *Listeria monocytogenes*. *Infect Immun* 58:3973-3979.
388. Labow, M., D. Shuster, M. Zetterstrom, P. Nunes, R. Terry, E. B. Cullinan, T. Bartfai, C. Solorzano, L. L. Moldawer, R. Chizzonite, and K. W. McIntyre. 1997. Absence of IL-1 signaling and reduced inflammatory response in IL-1 type I receptor-deficient mice. *J Immunol* 159:2452-2461.
389. Nambu, A., S. Nakae, and Y. Iwakura. 2006. IL-1beta, but not IL-1alpha, is required for antigen-specific T cell activation and the induction of local inflammation in the delayed-type hypersensitivity responses. *Int Immunol* 18:701-712.
390. Yi, H., L. Zhang, Y. Zhen, X. He, and Y. Zhao. 2007. Dendritic cells induced in the presence of GM-CSF and IL-5. *Cytokine* 37:35-43.
391. Westermann, J., U. Bode, A. Sahle, U. Speck, N. Karin, E. B. Bell, K. Kalies, and A. Gebert. 2005. Naive, effector, and memory T lymphocytes efficiently scan dendritic cells in vivo: contact frequency in T cell zones of secondary lymphoid organs does not depend on LFA-1 expression and facilitates survival of effector T cells. *J Immunol* 174:2517-2524.
392. Shaner, N. C., G. H. Patterson, and M. W. Davidson. 2007. Advances in fluorescent protein technology. *J Cell Sci* 120:4247-4260.
393. Reis e Sousa, C. 2001. Dendritic cells as sensors of infection. *Immunity* 14:495-498.
394. Schmidt, M. R., B. Piekos, M. S. Cabatingan, and R. T. Woodland. 2000. Expression of a human coxsackie/adenovirus receptor transgene permits adenovirus infection of primary lymphocytes. *J Immunol* 165:4112-4119.
395. Hurez, V., R. Dzialo-Hatton, J. Oliver, R. J. Matthews, and C. T. Weaver. 2002. Efficient adenovirus-mediated gene transfer into primary T cells and thymocytes in a new coxsackie/adenovirus receptor transgenic model. *BMC Immunol* 3:4.
396. Hayashi, I., H. Mizuno, K. I. Tong, T. Furuta, F. Tanaka, M. Yoshimura, A. Miyawaki, and M. Ikura. 2007. Crystallographic evidence for water-assisted photo-induced peptide cleavage in the stony coral fluorescent protein Kaede. *J Mol Biol* 372:918-926.
397. Hosoi, H., H. Mizuno, A. Miyawaki, and T. Tahara. 2006. Competition between energy and proton transfer in ultrafast excited-state dynamics of an oligomeric fluorescent protein red Kaede. *J Phys Chem B* 110:22853-22860.
398. Jeltsch, M., A. Kaipainen, V. Joukov, X. Meng, M. Lakso, H. Rauvala, M. Swartz, D. Fukumura, R. K. Jain, and K. Alitalo. 1997. Hyperplasia of lymphatic vessels in VEGF-C transgenic mice. *Science* 276:1423-1425.
399. Achen, M. G., M. Jeltsch, E. Kukk, T. Makinen, A. Vitali, A. F. Wilks, K. Alitalo, and S. A. Stacker. 1998. Vascular endothelial growth factor D (VEGF-D) is a ligand for the tyrosine kinases VEGF receptor 2 (Flk1) and VEGF receptor 3 (Flt4). *Proc Natl Acad Sci U S A* 95:548-553.
400. Boardman, K. C., and M. A. Swartz. 2003. Interstitial flow as a guide for lymphangiogenesis. *Circ Res* 92:801-808.
401. Mackay, C. R., W. L. Marston, and L. Dudler. 1990. Naive and memory T cells show distinct pathways of lymphocyte recirculation. *J Exp Med* 171:801-817.
402. Mackay, C. R., W. Marston, and L. Dudler. 1992. Altered patterns of T cell migration through lymph nodes and skin following antigen challenge. *Eur J Immunol* 22:2205-2210.

403. Mora, J. R., and U. H. von Andrian. 2004. Retinoic acid: an educational "vitamin elixir" for gut-seeking T cells. *Immunity* 21:458-460.
404. Mora, J. R., M. R. Bono, N. Manjunath, W. Weninger, L. L. Cavanagh, M. Roseblatt, and U. H. Von Andrian. 2003. Selective imprinting of gut-homing T cells by Peyer's patch dendritic cells. *Nature* 424:88-93.
405. Barnes, M. J., and F. Powrie. 2009. Regulatory T cells reinforce intestinal homeostasis. *Immunity* 31:401-411.